An Electromagnetic Imaging System for Metallic Object Detection and Classification

By

Abdalrahman Al-qubaa

A thesis submitted to the School of Electrical, Electronic & Computer Engineering
in partial fulfilment of the requirements for the degree of
Doctor of Philosophy

Faculty of Science, Agriculture and Engineering
Newcastle University, December 2012

Abstract

Electromagnetic imaging currently plays a vital role in various disciplines, from engineering to medical applications and is based upon the characteristics of electromagnetic fields and their interaction with the properties of materials. The detection and characterisation of metallic objects which pose a threat to safety is of great interest in relation to public and homeland security worldwide. Inspections are conducted under the prerequisite that is divested of all metallic objects. These inspection conditions are problematic in terms of the disruption of the movement of people and produce a soft target for terrorist attack. Thus, there is a need for a new generation of detection systems and information technologies which can provide an enhanced characterisation and discrimination capabilities.

This thesis proposes an automatic metallic object detection and classification system. Two related topics have been addressed: to design and implement a new metallic object detection system; and to develop an appropriate signal processing algorithm to classify the targeted signatures. The new detection system uses an array of sensors in conjunction with pulsed excitation. The contributions of this research can be summarised as follows: (1) investigating the possibility of using magneto-resistance sensors for metallic object detection; (2) evaluating the proposed system by generating a database consisting of 12 real handguns with more than 20 objects used in daily life; (3) extracted features from the system outcomes using four feature categories referring to the objects' shape, material composition, time-frequency signal analysis and transient pulse response; and (4) applying two classification methods to classify the objects into threats and non-threats, giving a successful classification rate of more than 92% using the feature combination and classification framework of the new system.

The study concludes that novel magnetic field imaging system and their signal outputs can be used to detect, identify and classify metallic objects. In comparison with conventional induction-based walk-through metal detectors, the magneto-resistance sensor array-based system shows great potential for object identification and discrimination. This novel system design and signal processing achievement may be able to produce significant improvements in automatic threat object detection and classification applications.

Declaration

I declare that this thesis is my own work and it has not been previously submitted by me or by anyone else, for a degree or diploma at any educational institute, school or university. To the best of my knowledge, this thesis does not contain any previously published work, except where another person's work used has been cited and included in the list of references.

Acknowledgements

In the name of Allah, the Beneficent, the Merciful. Praise and Gratitude be to Allah for giving me strength and guidance, so that this dissertation can be finished accordingly.

This thesis represents the winning post of a four-year journey to achieve my PhD degree. During this journey, I have been accompanied and supported by many people who deserve to be acknowledged.

The first one I would like to thank is my supervisor: Prof. Gui Yun Tian. Please let me express my deep sense of gratitude and appreciation to you for the knowledge, guidance and unconditional support you have given me. I would like to express my sincere gratitude to Dr. John Wilson for all the helpful assistance. I wish you all the best and further success and achievements in your life.

It is unfair to just say thank you to those who have made many sacrifices to help me: my parents. The only thing I can say to you is that your dream to see me become a scientist will soon be real. I love you from the bottom of my heart.

Grateful thanks to my wife and my three children, who had lived this journey with me, in times of happiness and hardship. Thank you very much for being the motivational factor in my life, supporting me in every possible way and giving me hope after hope to achieve this work successfully. Please forgive me for my shortcomings, which were many, through this journey.

My brothers/sisters and my family in low: thank you very much for your prayers and encouragement. I am really proud of you all. My all team and my friends: thank you very much for what you have done for me. I thank you all for the companionship that made this journey much easier. In fact, I do not need to list your names because I am sure that you know who you are.

Last, but not least, I dedicate this research to my home country (IRAQ). I also thank the Iraqi Cultural Attaché, London for supporting me during my study abroad.

Table of Contents

List of Tables

List of Figures

Abbreviations

ANN:	Artificial Neural Network
BP:	Back-Propagation
CEIA:	Construction Electronics Industrial Automation
CWD:	Concealed Weapon Detection
EC:	Eddy Current
EM:	Electromagnetic
EMR:	EM Reflectometry
ENT:	Entropy
FAST:	Future Attribute Screening Technology
FFT:	Fast Fourier Transform
GMR:	Giant Magneto-Resistance
GUI:	Graphical User Interface
HCR:	Highest Classification Rate
HMF:	Horizontal Magnetic Field
IR:	Infrared
LIBSVM:	Library for SVM
MMW:	Millimetre Waves
MRI:	Magnetic Resonance Imaging
PCA:	Principal Component Analysis
PEC:	Pulsed Eddy Current
QNDE:	Quantitative Non-Destructive Evaluation
RF:	Radio Frequency
RMS:	Root Mean Square Error
SNR:	Signal to Noise Ratio

STD: Standard Deviation

SVM: Support Vector Machine

THz: Terahertz

UXO: Unexploded Ordnance

VLF: Very Low Frequency

WAMD: Wide Area Metal Detection

WD: Weapon Detection

WT: Wavelet Transform

WTMD: Walk Through Metal Detector

3DSMF: 3D Steerable Magnetic Field

Chapter 1: Introduction

This chapter provides a brief background to electromagnetic detection, including an overview of the work undertaken within this thesis. A synopsis of the research objectives is provided and the scope of the work also discussed. Major research achievements are listed and finally the structure of the thesis is laid out.

1.1 Background

In recent years, scientists and engineers have used electromagnetism to invent systems that can detect and locate metallic objects. In many applications, it is desirable to be able to detect metallic objects remotely and automatically. In many security screening scenarios, manual searches and metal detectors are used to find dangerous objects and prevent them from being carried into a controlled area. However, metal detectors cannot provide warnings specifically about threatening objects, and manual searches place security personnel at risk. Imaging technologies such as x-ray and microwave systems are unfavourable in this context owing to the health implications involved, and therefore other imaging techniques that use sensor-arrays exploiting the millimetre wave and terahertz spectra are used. For an application to search for suspicious objects that may be concealed by clothing, while avoiding the health hazards of ionizing radiation, these latter methods can be cost effective. However, another key criterion would be preferable, which is to respect personal privacy [1]. Automatic detection can also increase the throughput of a security checkpoint by expediting decisions or enabling the management of several parallel screening points by fewer personnel.

Currently, there are no reliable metal detector systems that can discriminate between a key chain and a knife using an electromagnetic (EM) method. However, EM methods are preferred for metallic object detection due to the fact that the EM field interacts with metallic objects giving an indication of their presence and electrical properties. Systems and devices that have been built using the principle of EM induction have been prevalent in airports, stations, and stadiums for the detection of suspicious metallic items that are being covertly carried. Inspections are conducted under the prerequisite that a constrained environment should be provided [2]. Here, a constrained environment refers to the following conditions:

- Interrogation of one person at a time.
- Divestment of all metallic objects prior to inspection.
- Detection of one metallic item at a time.

These inspection conditions and detection limitations are problematic in terms of the disruption of the flow of people, the detection and discrimination of multiple metallic objects and false alarms from non-threatening objects. Thus, there is a need for a new generation of detection systems which can operate without the usual constraints and provide enhanced characterisation and discrimination capabilities.

EM methods are one of the most suitable for the inspection and detection of metallic objects in engineering applications involving the petrochemical, aerospace, transportation, energy and nuclear industries. They comprise of a number of techniques that are based upon electromagnetism and the interaction of electromagnetic fields with conductive objects. Such techniques include: beat frequency oscillation, continuous wave metal detection, pulse induction metal detection, and magnetic field gradiometry [3]. Most metal detectors use active EM field techniques to detect and classify metal objects. An active EM field, in this instance, means that the detector sets up a field using a source coil, which is used to probe the environment. The applied (or primary) field induces eddy current (EC) in the metal under inspection, generating a secondary magnetic field that can be sensed by a detector coil. The rate of decay and the spatial behaviour of the secondary field are determined by the target's electrical conductivity, magnetic permeability, shape, and size. Frequency-domain or time-domain analysis is adopted to extract features from the output to obtain information about the object, including its shape, orientation and material [4].

The problem of detecting a concealed object and classifying it using data from the scattered EM field is very difficult to solve, for the following reasons: the scattering mechanism is very complicated, even for simple geometric objects; and also these scattered signals are strongly dependent on the signal polarization and aspect angle of incident and reflection. In fact, the aspect dependency of transient EM fields makes the problem more complicated since it may cause two types of error in the classification. The first relates to the transient response at two different aspects of the same object, which could incorrectly be identified as two different concealed objects. The second problem refers to the transient response of two different concealed objects, which could be classified as one concealed object. An extraction feature which is insensitive to aspect variations is needed to accurately detect and classify concealed objects [5].

In this thesis, the design and implementation of a new metallic object detection and classification system is developed, based on the application of pulsed excitation in conjunction with accurate high spatial-resolution magnetic-field sensing and using giant magneto-resistance (GMR) sensor-arrays. This system uses an ex-service walk-through metal detector (WTMD) as a platform, enabling a two-dimensional image to be constructed from the measured backscattered signals, which can be used later for object identification and classification purposes. System circuit design, WTMD modification, and GMR sensor-array configurations were accomplished as a collaborative process within our team.

An analysis is undertaken of the backscattered transient signal from a range of objects that include real handguns as well as objects that are usually expected to be in the possession of passengers such as mobile phones, keys and wristwatches. Tests focusing on the spatial behaviour of objects are carried out in this research, forming a theoretical framework for the induction detector, and to ascertain which feature extraction methods and classification techniques enable the target to be correctly identified in an effective manner. The signal processing algorithms and software necessary to isolate these signals are developed in order to determine the signatures of threatening and non-threatening objects.

1.2 Motivation

Driven by the need for end-applications and the potential of emerging technologies, there are three major motivations behind this research:

1. Rising passenger numbers at airports and the ever-increasing threat of terrorism in society. Over the last decade events around the world have demonstrated the vulnerabilities of crowded public places to the evils of terror. The need for airport security and safety is now a major concern for all governments around the world. Terrorist activities are increasingly common and an unfortunate reality in today's world.
2. The limited object discrimination and classification capabilities of current security systems cause a lot of false alarms, and passengers are required to remove metallic objects before entering the WTMD implemented in airports. This produces "soft targets" in the form of lengthy queues. These soft targets heighten the risk of a terrorist attack within airport premises that could potentially have the same impact as destroying a commercial flight. Also, composite materials in different objects

give rise to false alarms, where the objects almost made from different material; each material gives a different EM signature. This means that current systems have the ability neither to characterise object shape, size and material type, nor to discriminate between threat and non-threat items using imaging techniques.

3. Limited automatic screening of people for the detection and localisation of threat objects using imaging systems. The traditional screening procedures take a long time to complete for only one scan, furthermore providing only an indication of the existence of a threat item, irrespective of information relating to its shape and location. As such, this can subject operators to various risks and vulnerabilities; hence the need for imaging technology that gives a higher degree of confidence in the automatic scanning and detection of threats.

1.3 Aims and Objectives

The main goal of this work is to design and develop a WTMD and associated signal interpretation algorithms, so that threatening metallic objects can be detected and classified using magnetic field imaging methods.

This goal can be further broken down into the following aims:

1. To design and develop a new WTMD for deployment in unconstrained environments, without necessitating that users divest themselves of metallic items.
2. To improve the characterisation capabilities of such systems, in terms of multiple object separation, object localisation and different object orientations.
3. To automatically recognise and classify threat objects from EM images to achieve rapid inspection at crowded checkpoints.

To pursue these aims the following objectives have been adopted:

- Conducting a literature survey to understand the state-of-the-art of current threat object detection systems.
- To perform an extended experimental study with an existing WTMD, then to investigate the behaviour of GMR sensors in different circumstances in order to design and build a fully functional GMR sensor-array.
- The development of electromagnetic imaging algorithms for the GMR sensor-array to use in the proposed threat object detection and classification system.
- To investigate the system validity and responses relating to size, volume, different orientations, and multiple object discrimination.

- To investigate different feature extraction techniques to find suitable features for threat object identification using the proposed system.
- To investigate suitable machine learning methods and algorithms for automatic threat object detection and classification.

The work outlined in this thesis was carried out at Newcastle University as part of a project entitled "People screening for threats with automatic detection and localisation", which is funded under the Innovative Research Call in Explosives and Weapons Detection 2007, a cross-government funded programme.

1.4 Methodologies

In its combination of theoretical and experimental approaches, the research work includes system design and implementation, data acquisition, feature extraction, data/feature fusion, and object detection and classification. The research work involves three essential stages as shown in Figure 1.1: Stage I: Hardware and software system developing; Stage II: Image processing and feature extraction; and Stage III: Automatic classification. Each stage involves sub-steps that are further described below.

In Stage I, the design methodologies for and configuration of the new system are investigated. The new system is designed with maximum flexibility, with a variable sensor-array pitch and configuration and variable excitation in terms of signal waveform and amplitude. Tests are carried out using pulsed excitation in conjunction with advanced time-frequency analysis and signal shape analysis for object detection, characterisation, localisation and imaging. An EM database is created using real handguns and common metallic objects used in daily life. All acquired data is processed and prepared for better image formation and visualization.

In Stage II, following pre-processing of the EM database, a comprehensive study and investigation of feature extraction tools is carried out. Geometrical shapes, material features, transient response features and time-frequency features are extracted from the EM data. Features are selected and integrated to obtain better object identification and discrimination. Feature vectors are then prepared to feed to the classifiers for the next classification steps.

The final stage employs two different classifier techniques, which are an Artificial Neural Network (ANN) and a Support Vector Machine (SVM), to evaluate all of the proposed features individually and in combination for the accurate automatic classification of objects.

Stage I is covered in Chapters 3 and 4 and Chapter 5 covers Stage II, while Stage III is covered in Chapter 6.

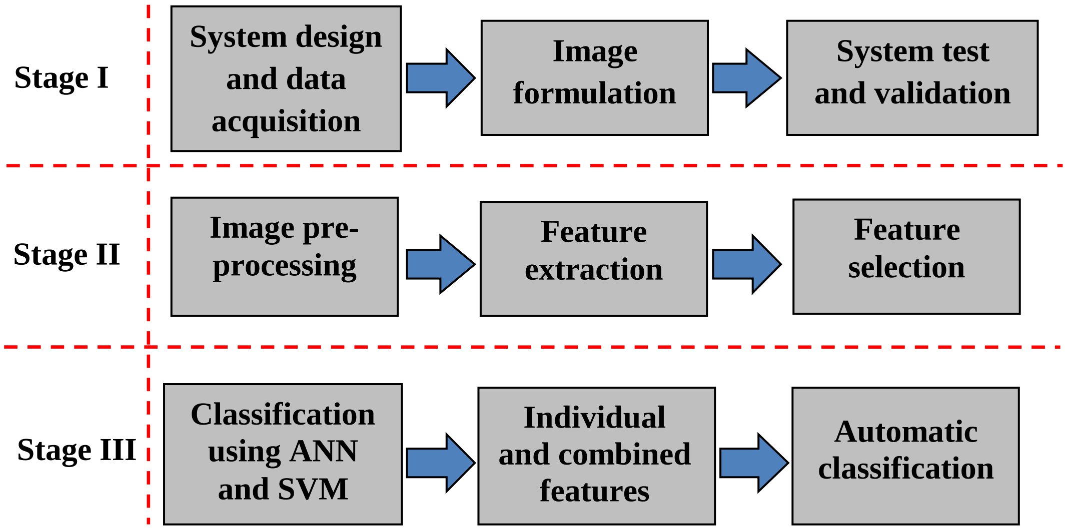

Figure 1.1: Methodology block diagram

1.5 Achievements

The main achievements of this research work include:

1. A literature survey which has brought understanding of and familiarity with electromagnetic gun detection techniques as well as EC research work, and the use of signal processing in metallic object detection and classification.
2. The design and implementation of a new electromagnetic threat object detection system based on the application of pulsed excitation, in conjunction with accurate high spatial resolution magnetic field sensing using GMR sensor-arrays.
3. System validation and experimental testing have been undertaken relating to size, volume, orientation estimation and multiple object discrimination in a single EM image, using a database consisting of EM images derived from the EM pulse response of objects. The database consists of twelve handguns, four knives and approximately twenty other commonly carried objects.
4. An extensive analysis of feature extraction methods to investigate their compatibility for the outcomes of the proposed system. Feature extraction techniques related to object materials, shape, time-frequency, and transient response analysis have been investigated. Based on the test results, these features have been optimised in order to meet the highest classification accuracy.

5. Among the several feature extraction techniques used within this project, a novel time-frequency image correlation method is proposed. This method is a good candidate for numerous applications where time-varying EM field images are encountered pertaining to material discrimination of ferromagnetic and paramagnetic metals.
6. The introduction of a hierarchical framework of automatic object classification techniques in which ANN and SVM classifiers were used and investigated. From this, high classification rates have been achieved.
7. Publications from the work through refereed journals and conferences. In three different conferences and workshop events this work was judged as the best research work presented.

1.6 Thesis Outline

This thesis consists of seven chapters including this introduction. Chapter 2 provides an extensive literature survey of metallic detection systems. Chapters 3 to 6 represent the main contributions of this work, while Chapter 7 summarises the scientific research contributions. Each chapter is outlined below.

A two-part literature review of metal detection systems is provided in Chapter 2. The first part investigates recent sensor technologies used for metal detection, in addition to the physical theories behind these sensors. The second part reviews image processing and classification techniques used in threat object detection systems.

In Chapter 3, the approach to the design and development of a new WTMD system is considered. The theoretical background of EM imaging is reviewed and correlations between measured magnetic properties and objects under test identified. The design and operation of the new metallic object detection system is presented. This system utilises a pulsed excitation coil and an array of GMR sensors for deployment in unconstrained environments. The chapter also describes three configurations of the sensor-array for the system. The signal processing algorithms and the software necessary to isolate EM signals in order to reconstruct a two-dimensional image from the sensor-array outcome are also presented. These are used later for feature extraction and classification purposes.

Chapter 4 provides a study of the capability of the proposed GMR sensor-array in terms of detecting threat and non-threat items. This is accomplished through assessment of the proposed system by considering different characteristics such as: data validation using threat and non-threat objects, repeatability of the same objects, multiple object separation, and response to different object orientations. Simulations where the detection of threat objects are undertaken using data from major tests are included, with results for 12 firearms, 4 knives and around 20 other commonly carried objects. This chapter concludes with the best setup and configuration of the sensor array to reconstruct the EM images of objects.

Several groups of features are investigated and tested in Chapter 5, the aim of which is to find appropriate feature extraction methods with data retrieved from the new EM imaging system for threat object detection and classification. Features have been extracted from the system outcomes using four feature categories, referring to the objects' shape, material composition, time-frequency signal analysis and transient pulse response. After the definition of the proposed feature extraction methods, the effectiveness of individual features is tested and discussed. Based on the results, only features that perform well are selected and used.

Two different types of classification techniques are presented and compared in Chapter 6 to evaluate the features extracted and to adopt an efficient classification technique for automated detection. Classifiers such as ANN and SVM are used and frameworks for these classifiers are presented. A set of training tests are carried out using the groups of features extracted in Chapter 5. Finally, the accuracy for threat object classification of the proposed system is presented for the classifiers.

Finally, Chapter 7 presents the conclusion and major scientific contributions of this work and outlines the achievement of the proposed system for security applications, followed by suggestions for the direction of future work.

1.7 Chapter Summary

This chapter provides an introduction to the thesis and gives a synoptic review of the thesis. An introduction is presented to the research work, which has been conducted on the characterisation of objects using electromagnetic techniques for security purposes, to detect threat and non-threat objects. The current needs and requirements in industry for the development of security systems are generalised and depicted as the background to the on-going study, which is followed by the aims and objectives of the present research. The methodologies used in the research are then presented and the contributions of the work are outlined. Finally, the layout of this thesis and the content of each chapter are summarised.

Chapter 2: Devices and DSP Approaches for Metallic Object Detection

This chapter reviews recent developments in the area of threat object detection and classification. These methods largely use electromagnetic means including: metal detection, magnetic field distortion, electromagnetic resonance, acoustic and ultrasonic inspection, millimetre and terahertz waves, infrared imaging, x-ray imaging... etc. The advantages and disadvantages of these approaches are discussed and research challenges and perspectives are identified. The chapter is organised as follows: Section 2.1 gives a brief introduction about metal detection, sections 2.2 and 2.3 present various underlying phenomena in addition to a comprehensive review of sensor technologies being investigated for the metal detection and EM imaging. Section 2.4 provides a survey of image processing techniques that are being developed to achieve improved threat object detection and classification. The last section summaries the challenges of the current threat object detection area with the proposed technique and the reasons behind that.

2.1 Introduction

Metal detection technology is used in many industries around the world, e.g. detecting metallic foreign bodies in the human body (medical), mine detection (military), screening people for potentially dangerous weapons (security), detection of metallic objects in food products (quality control) and professional treasure hunters.

The goal of automatic detection and recognition of concealed weapons is a technological challenge that requires innovative solutions in sensor technologies and image processing. A number of sensors based on different phenomenology, as well as image processing support, are being developed to observe objects underneath people's clothing. EM methods are preferred for weapon detection (WD) due to the fact that the EM field interacts with metallic objects, giving an indication of the presence and electrical properties of these objects. Systems and devices that are built upon the principle of EM induction have been prevalent in airports, stations, stadiums, etc. for the detection of suspicious metallic items that are being carried covertly. Inspections are conducted under the prerequisite that a constrained environment should be provided. Here, the constrained environment refers to the following conditions: interrogation of one person at a time, divestment of all metallic objects prior to inspection, and detection of one metallic item at a time. These inspection conditions and detection limitations are problematic in terms of the disruption of the flow of people, detection and discrimination of multiple metallic objects and false calls from non-threat objects. Thus, there is a need for a new generation of detection systems which can operate without the usual constraints and provide enhanced characterisation and discrimination capabilities [1].

2.2 Metal Detection Underlying Phenomena

The electromagnetic spectrum defines the range of all possible frequencies of electromagnetic radiation. EM metal detection is based on measuring variations in an EM field caused by an object. The excitation source could be earth gravity field in passive detection system which measure distortion in earth gravity. Alternatively, active detection systems use coils or antennas to generate an EM field, in which objects are detected by measuring reflected or induced signals.

2.2.1 Magnetic field gradiometry

Magnetic field gradiometry [6-10] takes advantage of the interaction between the earth's field (Approx. 0.5G) and metallic objects. It is therefore applicable to the detection and localisation of guns and other ferromagnetic objects, as these materials are magnetically permeable or carry a permanent magnetic moment, and thus distort the earth's field. This field distortion, or gradient, is quantified using a magnetic gradiometer with two field sensors connected in differential configurations to measure the spatial field difference.

Techniques incorporating magnetic field gradiometry have been applied to the development of walk-through systems, using an array of gradiometers aligned vertically at either side of the portal [11]. When a ferromagnetic item passes through the portal, it causes magnetic field distortion, which is sensed by the gradiometer arrays. As the gradiometers are arranged in groups, a degree of localisation of the objects can be achieved. Although gradiometry has been used successfully for some security applications, only ferromagnetic materials can be detected but characterisation of materials is very difficult using this passive technique.

2.2.2 Electromagnetic field induction

EM induction is a common approach for detection of metallic items and Unexploded Ordnance (UXO) [4, 5, 11-27]. Traditional EM induction metal detectors such as walk-through doors and mine detection devices consist of a driver coil and a pickup coil. The driver coil constitutes the generation of the applied/primary magnetic field, which induces EC inside the metal under inspection. In contrast, the pickup coil is used for measuring the net field, which is the superposition of the primary magnetic field and the eddy-current-induced field, i.e. secondary magnetic field. The output from the pickup coil conceives the information of the metal. Either frequency or time-domain analysis is adopted to extract features from the output in an effort to obtain the metallic properties including: shape, orientation, material, etc. The arrangement regarding the configuration of the two coils is dependent on the applications of the detectors. Figure 2.1 shows a diagram of a typical EM induction detector for walk-through application. The configuration of the coils is the transmission setup.

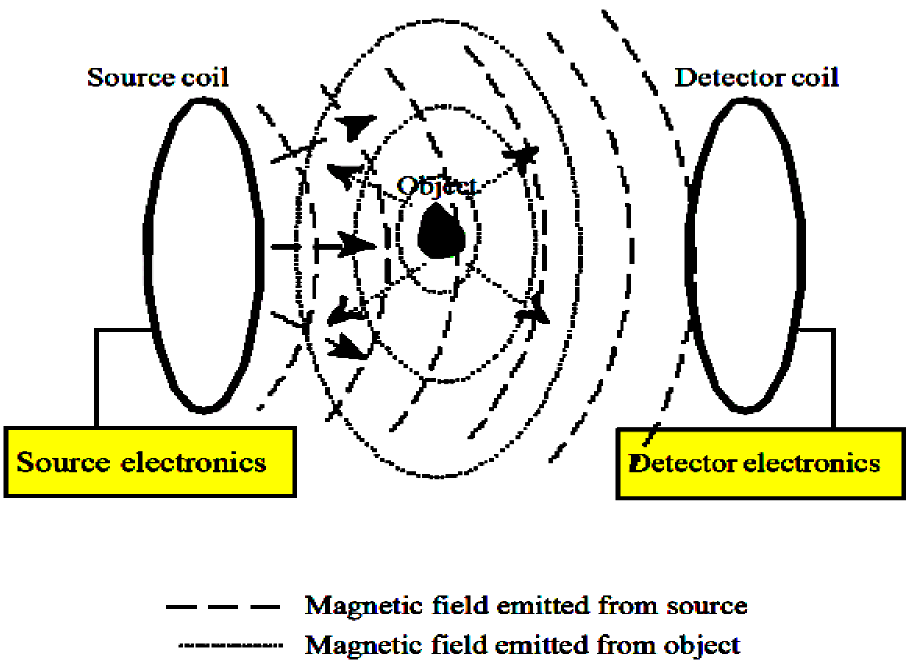

Figure 2.1: Diagram of EM induction metal detectors with coils in Transmission mode [7].

Based on EM induction, several technologies have been proposed and realised for advanced metal detectors, which include: very low frequency, pulse induction, beat frequency oscillation, and 3D steerable magnetic field as explained below.

2.2.2.1 *Very low frequency technology*

Very low frequency (VLF) (3 kHz – 30 kHz) is the most commonly-used method for metal detectors, which uses both driver and pickup coils [21]. By measuring the field response to the primary magnetic field from the metals under inspection, the detection and characterisation of the objects are fulfilled. Compared with EM induction, the pickup coils are shielded from the primary field generated by the driver coils, in a bid to cancel out the mutual inductance between coils and thus improve the detectability.

The signal responses from pickup coils give the implication of the presence of a metallic object. The magnitude of the signal is inversely proportional to the distance between the detector and the object, indicating the location of the object. The characterisation of metals is implemented by looking at the phase shift in the acquired signals. The reasoning behind this is that the inductance and resistance of a metal significantly affects the induced EC in the metal, in terms of amplitude and phase, which gives a distinct field signal with a particular magnitude and phase. During the application, a phase shift level that is determined by using thresholds or notches (phase segments) is employed to discriminate objects above and below the level. The analysis is found limited in object classification, such that just a group of objects in lieu of a particular item can be identified [21].

2.2.2.2 *Pulse induction technology*

The difference between Pulse induction **(**PI) [21, 22] and VLF lies in the type of excitation of current supplied to the driver coil and the subsequent signal processing techniques. PI applies a short but powerful pulse to the driver coils in order to generate the pulsed primary magnetic field. After the pulse collapses, the reflected pulse (over several milliseconds), which travels in the opposite direction of the primary field, appears and results in another current flowing within the driver coil. The duration of the reflected pulse is increased when the PI detector is placed over a metallic object, due to the presence of pulsed EC, which support the reflected pulse and introduces echoes to the signals. In view of the physical background, the PI devices are only able to adopt a single coil for both generating the pulsed field and receiving the reflected pulse. For continuous inspection, PI detectors send the pulses ranging from 25 to 1,000+ pulses per second [23].

The detection of metals is realised by measuring the length of the reflected pulses. The distance between a metal and the PI detector can be estimated by analysing the interval between the driving pulse and the reflected pulse. Features such as pulse decay are found to be effective for object characterisation [25], though the processing is more complicated than VLF. It is noteworthy that the utilisation of pulsed current makes PI capable of efficiently detecting objects at a longer distance, compared with VLF and multi-frequency VLF techniques.

The pulse decay is used for metal detection and characterisation, since the pulse response varies with the properties of different objects, which includes material, shape and orientation. Figure 2.2 shows the pulse decays for different metallic objects. Since unique pulse decays in 3D field signals for a metal can be found. Therefore, the identification of metallic objects can be fulfilled by introducing libraries of target time decay constants.

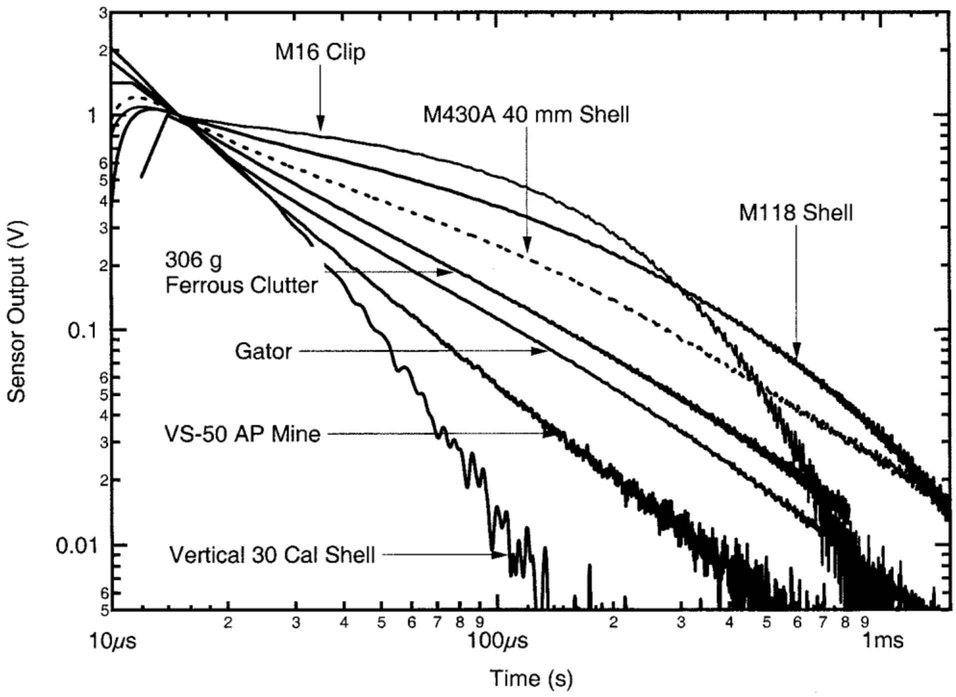

Figure 2.2: The pulse decays for different metal items [24, 25].

2.2.2.3 3D steerable magnetic field

It is relevant that the previous technologies discussed measure the magnetic field in one particular direction, i.e. one-component of magnetic field, which implements the interrogation of metals with one-directional magnetic field vectors. The 3D steerable magnetic field (3DSMF) sensor system improves the traditional EM induction systems by extending one-directional field inspection to three directional inspections [24, 25]. The metals are excited with a 3D pulsed magnetic field, which is relatively uniform over the distance compared to a loop coil. The field vector of the sensor is steered in accordance with the object-body coordinate system, as a result of which, the signal to noise ratio (SNR) is enhanced. The pick-up sensor is also designed to sense the magnetic field in 3D.

The generation of a uniform magnetic field in a particular direction is of great importance. Multiple electrical wires in a 1D linear alignment are used to simulate the sheet current, which generates the uniform Horizontal Magnetic Field (HMF). Figure 2.3a shows the setup for generation of the HMF in the x-direction. A similar setup is used for HMF in the y- and z-directions. Figure 2.3b presents the concept illustration of a 3DSMF transmitter.

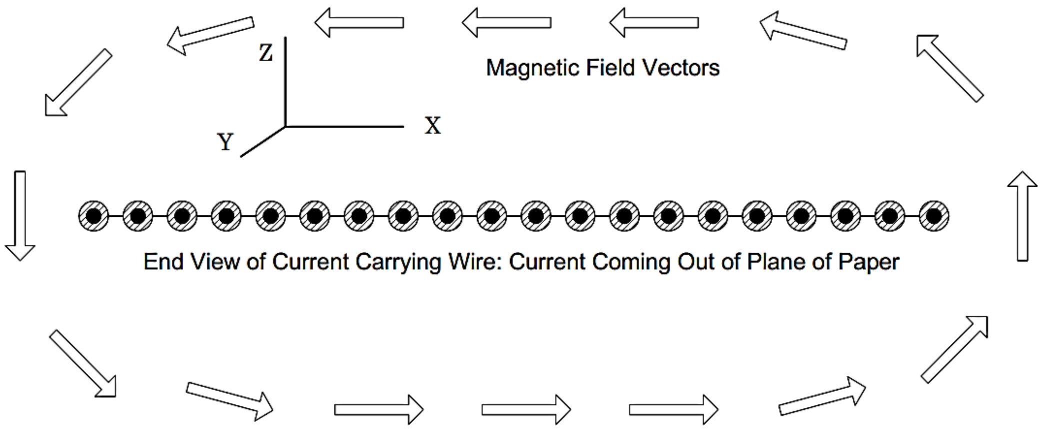

a)

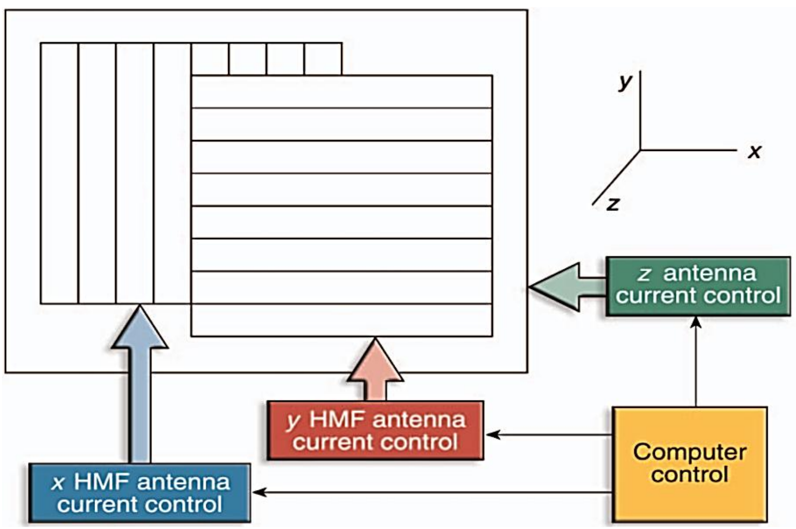

b)

Figure 2.3: a) Electrical wires for generation of uniform HMF in x-direction; b) Concept illustration of 3DSMF transmitter [24, 25].

The parameters of the individual HMF transmitter include: the spatial interval of each pair of electrical wires, the return current path separation distance, and the width and depth (length of wire) of the transmitter. In [25], the suggested value for each parameter via simulations were as follows: spatial interval=2.5 cm, return current path=1 m, width=2 m, and depth=2 m.

The sensing of field, when a target is illuminated by HMF in a particular direction, is achieved by using sensors in differential configuration. The concept illustration of field sensing for HMF in the x-direction is depicted in Figure 2.4. The field response is the superposition of the readings from the left and right sensors, which measure the field in the orthogonal direction, i.e. z-direction, in an effort to decouple the transmitter and the sensors. Since the differential configuration is applied, the noise at two sensor locations is cancelled out, and thus the SNR is improved.

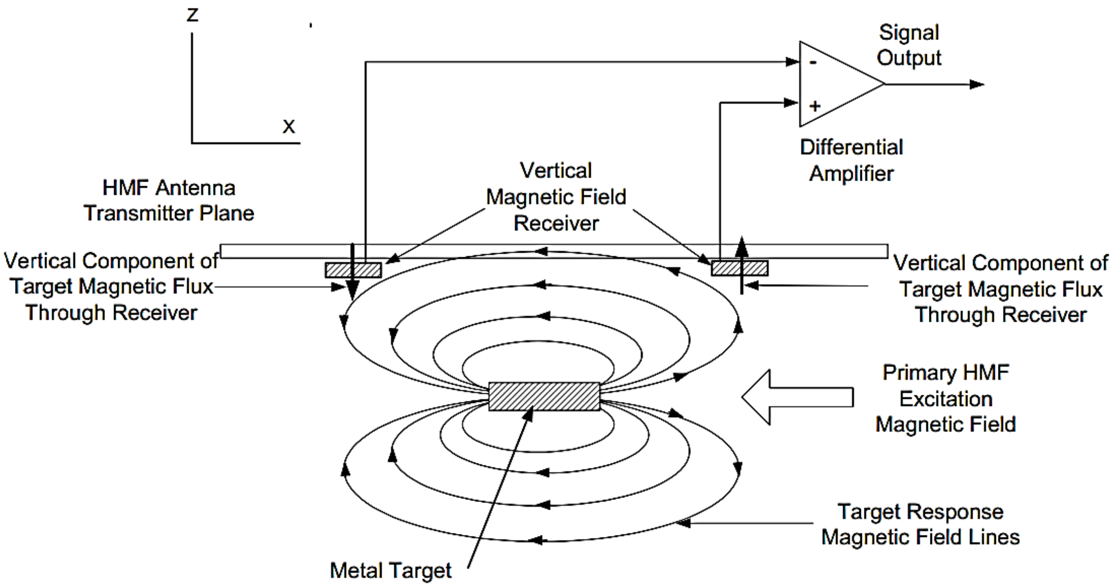

Figure 2.4: Concept illustration of field sensing [25].

Field sensing for the other two HMFs are implemented using the same approach, leading to the construction of the 3D field sensing module.

2.2.3 Electromagnetic wave reflectometry

The difference between EM induction and EM reflectometry (EMR) [28-43] is that EM induction detects the variation in a net magnetic field, or mutual inductance, due to the introduction of metal in the field-illumination region, whilst EMR measures the EM waves reflected from an item in the wave-illumination region. EMR is established based on the wave characteristics of an EM field, with the wave propagation taken into account. In which case, the wavelength of the EM field is comparable with or smaller than the dimension of a detection system. In contrast, the wavelength of EM field used in EM induction is much larger than the system size and thus the displacement current and wave propagation are both neglected.

The frequency range of EMR covers very high frequency (30 MHz– 300 MHz), ultra high frequency (300 MHz – 3 GHz) and super high frequency (3 GHz – 30 GHz). Over such ranges, the EM wave can propagate for a certain distance, which defines the illumination region. When the incident EM wave ‘hits’ an object, it is reflected. The difference between the incident wave and the reflected wave indicates the location of the object, while the amplitude and phase of the reflected wave provides information about the properties of the object, which influences the characteristics of the displacement current within the object. Unlike EM induction, EMR has been found to be sensitive to the permittivity, aside from the conductivity of an object, and capable of inspecting the non-metallic targets such as explosive, plastic knives and liquid. The shape of an object can also be ‘seen’ by EMR. The scattering centres distributing over the object result in the EM resonance [28, 29]. The frequency of EM resonance is found related to the distance between two scattering centres, whilst the amplitude gives an indication regarding the material of the object. EMR normally consists of a transmitter and a receiver [30-34]. The transmitter constitutes the generation of incident EM waves, and the receiver collects the reflected EM waves. The schematic illustration of a reflectometer for detecting and characterising a single metallic object as an example is presented in Figure 2.5a. Figure 2.5b shows the actual dual-polarisation reflectometer (1 GHz - 14 GHz) for object localisation and identification [35, 36].

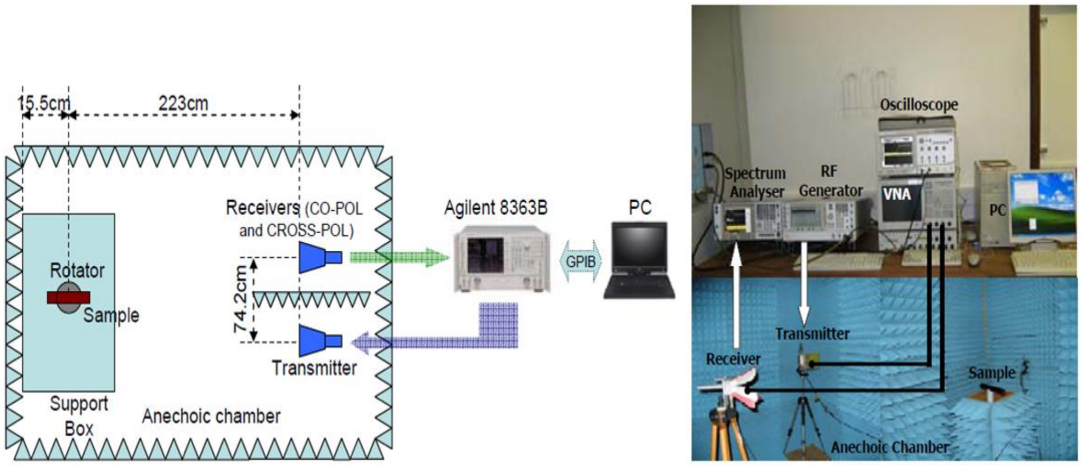

a) b)

Figure 2.5: The schematic illustration of a reflectometer for detecting and characterising a single metallic object: a) Schematic illustration of a dual-polarisation reflectometer, b) the picture of the system.

The reflectometer captures the reflected EM wave in both coherence polarisation and cross polarisation. The cepstrum analysis of the coherence-polarisation wave provides the feature of optical depth, which indicates the location of a metal. The cross correlation between coherence-polarisation and cross-polarisation waves in both time and frequency domains is used as another feature for object identification.

Since only a pair of antennas can be used in construction of the reflectometer, and the antennas stay still (no scan) during the measurement, reflectometers are therefore applicable to gun and knife detection via the acquisition of signals, instead of images. The features extracted from the signals are investigated in order to find the correlation with the location and properties of the objects under EM illumination. So far, reflectometers for security purposes are capable of detecting and identifying a single object from stand-off distance, even though the positions of two metals can be determined via cepstrum analysis.

2.3 EM Imaging for Threat Object Detection

To reliably detect threat and explosives in places like airports, sensitive buildings, and famous constructions, the manual screening procedures do not satisfactory results currently. This is due several reasons, for example the manual screening procedures take a long time to complete only one scan, where it provides only an indication about the existence of the threat item, irrespective of any information relating to its shape and location. As such, this can subject the operator to risks and vulnerabilities, hence the need of imaging technology that has a higher degree of confidence in the automatic scanning and detection of the threat.

This section reviews recent developments in the area of imaging concealed weapon detection (CWD). These methods largely use electromagnetic means, including: microwave imaging, millimetre waves (MMW), terahertz imaging, and infrared imaging. The x-ray imaging has been used for border control and luggage inspections in airports but, because x-ray is harmful to humans, this technique will not be discussed in this review. The advantages and disadvantages of these approaches are discussed and research challenges and perspectives are presented.

2.3.1 Microwave imaging

Microwave imagers are based on the reflectometer principle, but images can be constructed by using the scanning device over the object under inspection, or by using an array of antennas comprising of multiple pairs of transmitters and receivers. The incident EM wave is sent at different angles and positions and the reflected wave is collected by the receivers in the array. Recent advances include the development of security imaging systems, such as those shown in Figure 2.6 [44, 45]. An antenna array is moved around a person by a cylindrical mechanical scanner. The scan takes 4–7 seconds before a 3D cylindrical set of holographic images are produced. The holographic imager can detect threats such as weapons constructed of metal, plastic and ceramic as well as explosive solids and liquids. Although these systems can produce very impressive results, a constrained environment is clearly required [46].

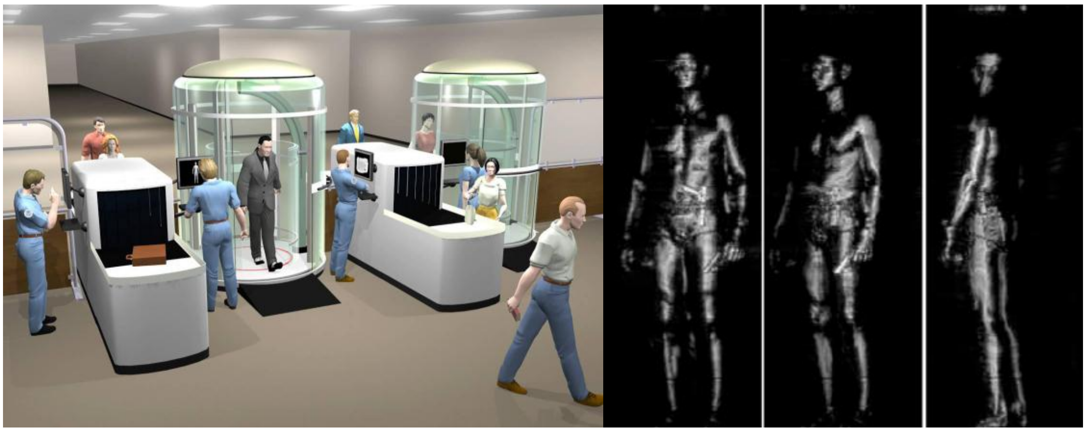

a) b)

Figure 2.6: A Microwave imager for body inspection. a) Conceptual design for entry portal screening using holographic radar imaging [45], b) Microwave images of a person carrying two concealed guns.

Significant research and development activities have been undertaken to enhance the state of the art of holographic radar imaging systems to be installed at security checkpoints, for screening people with concealed threats. Such enhancements include improvements to privacy techniques, by removing human features, but also providing automatic detection of body-worn concealed threats. The imaging techniques include: polarisation-diversity illumination and reception, dual-frequency implementation, and high-frequency imaging at 60 GHz.

In [45] the authors have developed a commercial rapid-throughput, holographic imaging system that has demonstrated the ability of detecting concealed threats. This system is a walk-through system that requires a person to stop for approximately 2-4 seconds, providing a full body scan of the person under surveillance. The operational throughput is on the order of 200 – 400 people per hour. This system has been deployed at security checkpoints throughout the world, including airports in Europe (Amsterdam) and the United States (Phoenix). One of the limitations of this system type is of concern with respect to privacy.

2.3.2 Millimetre waves imaging

MMW based screening systems can be classified into of two types: passive and active. Passive sensors simply observe and report whatever has been detected within the local environment. In the radio frequency (RF) spectral range, natural surfaces will emit different amounts of radiation depending on parameters such as temperature and emissivity. In addition, metals are strongly reflective to RF, which reduces a metal surface's emissivity and allows it to produce reflections of other sources within the scene, the most significant of which being the sky. Passive sensors have the great advantage of producing valuable information without emitting any signals from people [47].

Active sensors typically stimulate the environment by generating and emitting known signals. These signals propagate out to the objects or targets of interest, interact with them, and reflect or scatter energy back to the sensor. Owing that the self-generated signals have known properties, it is often possible to use signal processing to extract very weak emitted target signals from competing sources of noise.

According to safety views, MMW systems utilises very low radiation power to generate detection capability. The system uses a radiation power level approximately 10,000 times less than that of a cell phone (maximum specific absorption rate level of cell phone at 2009 is 1.6~2W/kg depending on region). The use of millimetre wave technology eliminates issues associated with the use of ionising radiation, such as those seen with X-ray systems [48-50].

Figure 2.7 shows how MMW images will look [51]. Passive MMW sensors measure the apparent temperature through the energy that is emitted or reflected by sources. The output of the sensors is a function of the emissivity of the objects in the MMW spectrum as measured by the receiver. Clothing penetration for CWD is made possible by MMW sensors due to the low emissivity and high reflectivity of objects like metallic guns.

Figure 2.7: MMW images (QinetiQ imaging system).

Active MMW imaging systems can be configured as personnel screening portals. It has been developed in a variety of active MMW imaging systems and a technology, including the cylindrical imaging technique that has been successfully commercialised In addition, a three-dimensional imaging technique and prototype that operate close to 350 GHz has been developed. This prototype system uses focusing optics coupled to a high-speed mirror scanning system [52]. In [53], these advanced imaging techniques are described in detail. Figure 2.8a shows a conceptual illustration of this system and experimental imaging results are shown in Figure 2.8b.

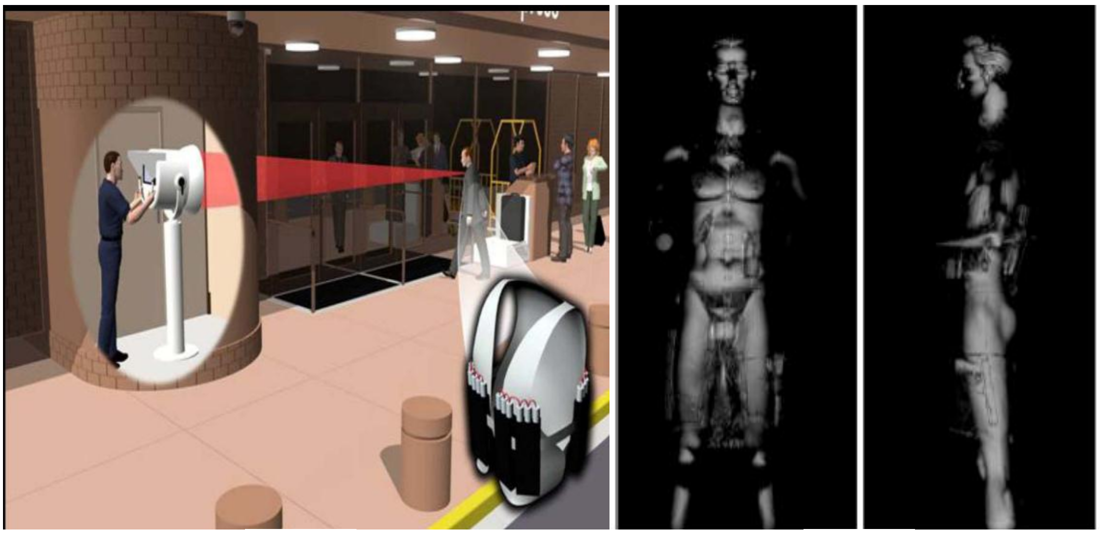

a) b)

Figure 2.8: Three dimensional MMW: a) Conceptual illustration showing a possible deployment of imaging system for personnel screening, b) cylindrical imaging results of a clothed mannequin at 40–60 GHz in [54].

2.3.3 Terahertz imaging

The Terahertz (THz) imaging technique is based on the use of THz electromagnetic waves to spectroscopically detect and identify concealed explosives, chemical or biological agents, and metals through characteristic transmissions or reflectivity spectra in the THz range. Most explosives and related compounds have characteristic absorption and many non-metal and non-polarity materials are transparent to terahertz wave, showing that there is significant potential for safety inspection [54]. Different materials have different effects on the THz wave. Typical clothing items and paper and plastic packaging should appear transparent in the THz system, whereas metals completely block or reflect THz waves. Ceramic guns and knives would partially reflect the THz signal. Skin, because of its high water content, would absorb nearly all T-Rays, with the energy being harmlessly dissipated as heat in the first 100 microns of skin tissue [55]. A THz reflection image of a person as shown in Figure 2.9 would show the outline of clothing and the reflection of objects beneath, such as guns or key chains, but the person's skin would appear substantially dark [56].

Figure 2.9: THz reflection image of a person carrying a gun [58].

There are some advantages of this technique that are attractive for CWD, such as spatial resolution of THz waves that are excellent for CWD; many materials of interest for security applications including explosives, chemical agents, and biological agents have characteristic THz spectra that can be used to fingerprint and thereby identify these concealed materials. THz waves are non-dangerous and totally harmless, as T-rays are non-ionising [56]. However, THz imaging has some issues that will have to be eventually solved, such as the cost and processing complexity because it requires special power sources. The recent introduction of near infrared radiation source, has helped to bring the cost of such systems down below 50K Euros [57]; The most significant limiting factor of the capabilities of THz imaging at stand-off range (3m to 100m) is the atmosphere which causes attenuation and turbulence to the waves [58]. Proper guidelines for using these imaging systems have to be finalised and put into action, as they might be harmful at some specific conditions of exposure [59] or have legal implications; i.e. with respect to the privacy invasion issue because THz can penetrate clothes. In [60], continuous THz wave has also been used in an imaging field. However, the speed of the imaging process requires improvement for security screening applications. To increase the imaging speed, the authors proposed a fast continuous THz imaging system, in which a galvanometer is introduced. The galvanometer makes the beams reflected in different angles by vibrating at a certain frequency, which significantly can decrease the image acquisition time compared to traditional continuous THz imaging system; ideal results of better resolution are obtained too.

2.3.4 Infrared imaging

Infrared (IR) imaging is another commonly used detection system for military purposes. Such applications include target acquisition, surveillance, night-vision, homing and tracking. Human bodies, as well as any other material, emit radiation provided that they are at a temperature above 0 °K. The wavelength of the radiation peak is dependent on the temperature of the body, and the total power emitted from the body is dependent on the size and emissivity of the body. Most infrared sensors are designed to have peak sensitivity near the peak emission wavelength of the human body, which is 10 µm. This technology is normally used for a variety of night-vision applications.

IR radiation emitted by people is absorbed by clothing. This absorbed radiation heats the clothing and is then re-emitted by the clothing. Consequently, the image of a concealed weapon will be blurred, at best, assuming that the clothing is tight and stationary. For normally loose clothing, the emitted infrared radiation will be spread over a larger clothing area, thereby significantly decreasing the ability to image a weapon. The difficulty in observing an infrared signal of a concealed weapon becomes worse as the weapon temperature approaches that of the body [61]. In [62], the researcher used a passive and non-intrusive IR imaging scanning method, combining it with a visual image to devise a scheme that was not only able to highlight sufficiently the presence of a concealed weapon, but also protect the privacy of the person that is being scanned. The work was mainly based on various image processing and computer vision techniques, including image registration and image fusion using the wavelet transform and image segmentation. The experimental results are demonstrating some limitations in terms of hardware used, adopted techniques and implementations. Examples of thermal images are shown in Figure 2.10.

More complete information can be obtained by fusing IR and its corresponding passive MMW image data or electro-optical image, the information can then be utilized to facilitate CWD, as can be seen from more information delivered in the next section.

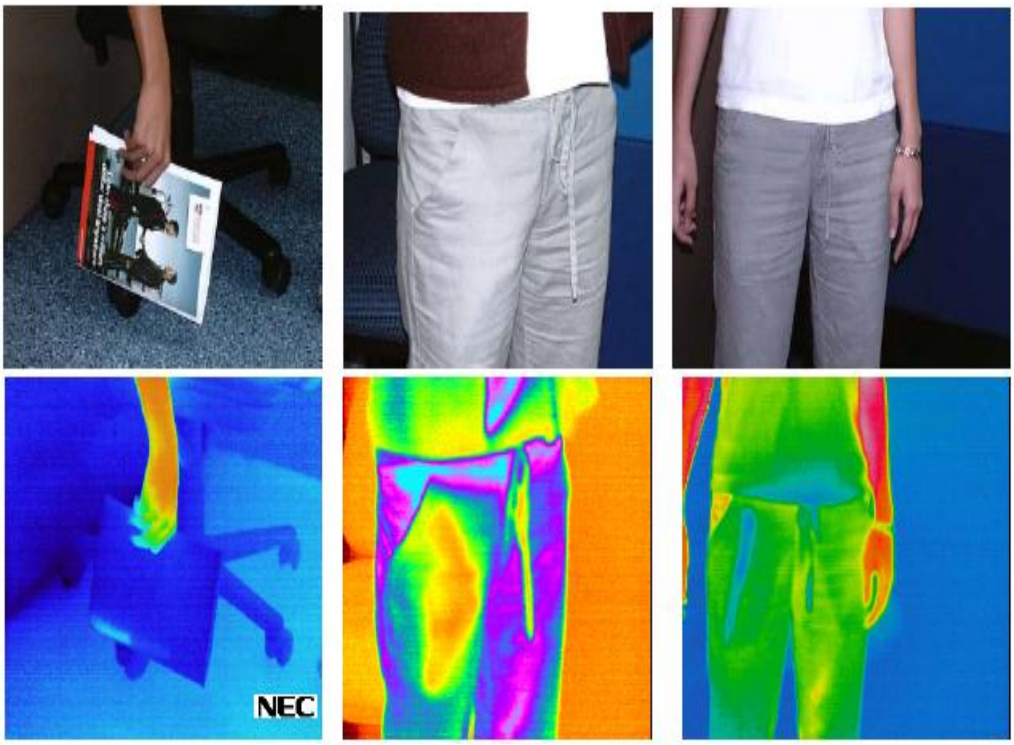

Figure 2.10: Comparison of thermal images and their respective visual images [63].

2.4 Other Metal Detection Approaches

Several technologies are currently used and applied for metal detection in different imaging applications.

2.4.1 Wide area metal detection

Wide area metal detection (WAMD) is the extension of 3DSMF used in applications from UXO detection to crowd screening for gun and knife inspection [26, 27]. The structure of multiple aligned wires simulating the conducting sheet affords the HMF covering a large area. The differential configuration of sensors for field sensing makes the WAMD capable of capturing the field response from metals at larger distances from the transmitters. A concept system is illustrated in Figure 2.11.

Figure 2.11: Concept illustration of the WAMD system [26].

The WAMD system is integrated with CCTV surveillance to monitor a crowd of people in a wide-open area. WAMD constitutes the detection and characterisation of metals carried and concealed in luggage and clothing. In the presence of metallic objects, the WAMD alarm is triggered, when the measured signals or pulse decay match for those weapons within the database. Subsequently, CCTV surveillance localises and tracks the suspect for further interrogation.

2.4.2 Magnetic resonance imaging

Magnetic resonance imaging (MRI) has been used as a powerful inspection tool in medical science. The MRI system normally consists of three gradient coils for the generation of a 3D magnetic field (up to several Tesla) in the body. This magnetic field interacts with the nucleus of atoms in the body, which is in turn detected by a microwave probe using pulse microwave excitation scanning over the body. Different nuclei behave differently when exposed to the pulsed 3D magnetic field and thus produce various resonances (energy absorbance), which produces a distinct output from the microwave probe. Even though in medical surgery MRI is conducted in the absence of any metals for health and safety issues, it can be seen that MRI can be used for weapon detection, especially those that are concealed on the body. A metallic weapon results in a void in the MRI images. Figure 2.12a exhibits a typical MRI system in medical science. Figure 2.12b shows an MRI image containing a metallic item in the brain, the metallic item causes void in the MRI image, which indicates that the use of MRI for the detection of weapons is achievable [11, 43].

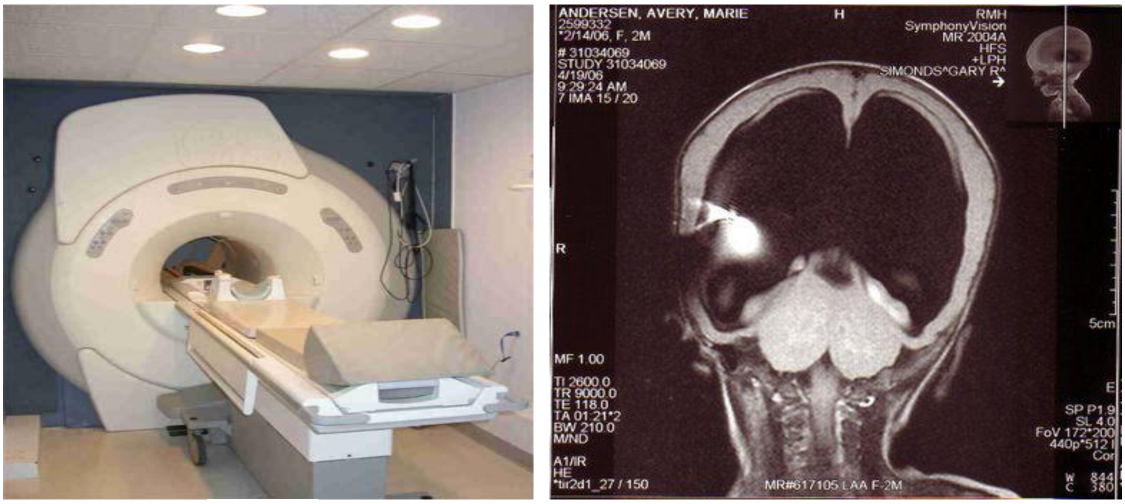

a) b)

Figure 2.12: a) picture of an MRI system; b) an MRI image showing a metal implant (white void) in the brain [11, 43].

2.4.3 Acoustic and ultrasonic detection

The detection of weapons using acoustic and ultrasonic detectors is dependent on the acoustic/ultrasonic reflectivity of materials that make up an object, as well as the shape and orientation of the object. Hard objects provide a high acoustic/ultrasonic reflectivity, while soft objects provide small reflectivity. The important detection parameters for these technologies are size of the target, diameter of the detector antenna, wavelength of the wave emitted, and the emitted power. Ultrasonic detectors operate from 40 kHz to frequencies well below 1 MHz, because of the increasing attenuation at higher frequencies.

Ultrasonic (high frequency) detectors [63] have problems penetrating thick clothing, whereas acoustic (low frequency) detectors can propagate more easily through clothing and “see” a concealed object. Conventional acoustic and ultrasonic based detectors are sensitive to hard objects in general, and therefore they cannot differentiate between weapons and harmless objects. Consequently, devices based on these technologies produce many false-positive detections. From the combination of the ultrasonic/acoustic approach, a nonlinear acoustic method for WD has been developed [64]. Figure 2.13

shows the principle of the ultrasonic/acoustic technique. This technology uses the ultrasonic beams of frequencies *f1* and *f2* to project sound onto a small area of a person at a distance and converts the energy probed from ultrasound into audio frequencies. The nonlinear interaction in the mix zone produces the frequencies: *f*1, *f*2, *f*1-*f*2, and *f*1+*f*2. The frequency difference *f*1-*f*2, tuned in the audio range, is used to interrogate the subject with a beam that is able to penetrate clothing. Parametric acoustic arrays [65] can be used to produce nonlinear acoustic effects where the detection of a concealed weapon can be based on signatures. The nonlinear acoustic method for WD uses correlation algorithms to perform pattern matching and classification techniques to display the nature of a hidden weapon. In general, this technique is harmless because: it does not involve ionising radiation, it is sensitive to metals and non-metals, and it is able to penetrate clothing [63]. However, fast scanning is required for ultrasonic beams in order to find and focus on a target.

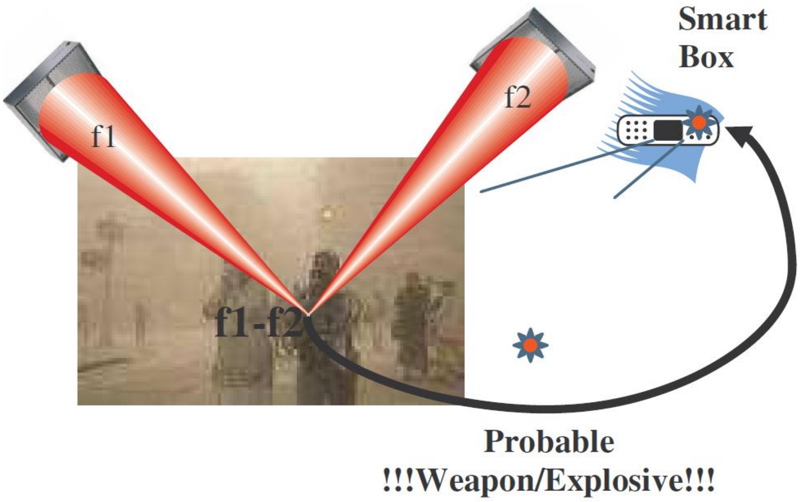

Figure 2.13: Concept showing crossed beam ultrasonic nonlinear acoustic generator for the CWD. Practical design considerations include parametric or crossbeam mixing to generate the acoustic probe [65].

2.4.4 Electromagnetic resonances

This is an active technique that uses EM resonance as a fingerprints or signature to distinguish weapons and nuisance objects. EM resonances in the objects are determined by its size, shape, physical composition. These resonances occur over the range between 200 MHz and 2 GHz. The detector uses radar to sweep through this range of frequencies and record the resonant response. The radar return, or resonance based scattering, exhibits some features that make it attractive for object identification schemes such as: scattering return, which is larger in the resonance region; natural resonances, as seen in the scattered return, which are independent of the orientation of the object; some natural resonances can characterise an object over a large frequency band; an object's resonance pattern can uniquely identify it within a class of objects.

To induce a resonant response in an object, it is necessary to illuminate it in the frequency band of the natural resonances [66]. Figure 2.14 shows the radar cross section of a sphere, where the radius as a function of its circumference is measured in wavelengths. The figure shows that radar cross section increases as a fourth power of frequency and sixth power of radius. When the circumference length is between 1 and 10, the wavelengths in the radar cross section exhibit oscillatory behaviour with several peaks, which correspond to the natural electromagnetic resonance of the sphere [29].

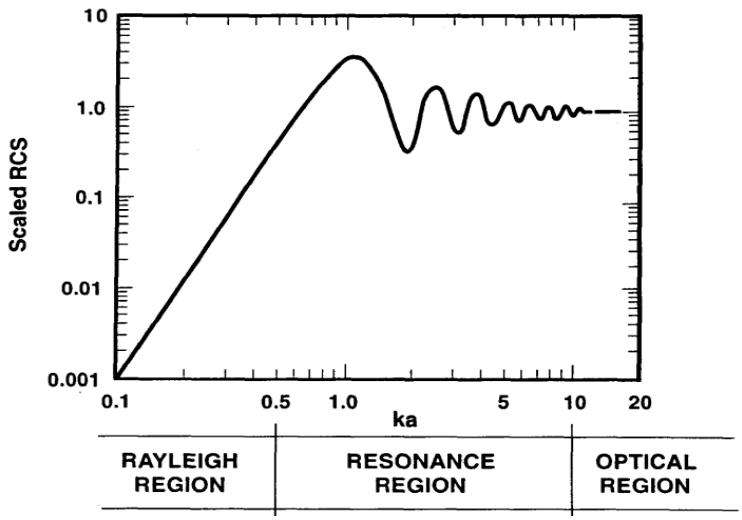

Figure 2.14: Enhancement of radar cross section in the resonance region [29].

The theory of operation of this method begins with the target space illuminated by either a pulse or swept frequency source. The signal reflected by objects in the target space provide an electromagnetic signature (EM resonance), a unique spectrum for each object. The object signatures are then compared to known signatures so as to determine whether or not any of the objects within the target space are threat items [11]. Neural network processing is used to classify the difference between weapons and harmless objects [67]. The person carrying the object will also exhibit a unique electromagnetic signature, which must be subtracted from the composite person-object signature. Benefits of this method include: an operational approximate range of 6 m, allowing the detection of concealed weapons, even if they are behind a human body, operational power that is at a safe limit power for human exposure, and does not invade the privacy of individuals. The problem found with this technique is the noise corresponding to the signature of people. Signatures of individuals vary from one person to another and also, they vary when a weapon is present. Unfortunately, the signature of an individual with a weapon is very similar to one without a weapon, and so there is a problem with classification and a high rate of false alarms.

2.4.5 Combining different sensors for security monitoring

Imaging techniques based on a combination of sensor technologies and processing will potentially play a key role in addressing the problem of threat object detection. The combination or fusion between multiple EM sensors is essential for the improvement of weapon and gun detection. Throughout the literature, different EM sensors have been combined over the past 10 years [11, 43, 50, 62, 68, 69]. The technology of sensor fusion is a research area that is growing rapidly due to the fact that it provides means for combining pieces of information coming from different sources/sensors, resulting in enhanced overall system performance (improved decision making, increased detection capabilities, diminished number of false alarms, improved reliability in various situations at hand) with respect to separate sensors/sources. As an example, by fusing passive MMW image data and its corresponding IR or electro-optical image using CCD camera, more complete information can be obtained; the information can then be utilized to facilitate concealed weapon detection. In [43], fusion of an IR image revealing a concealed weapon and its corresponding MMW image has been shown to facilitate extraction of the concealed weapon. In addition, fusion of a CCD image and its corresponding MMW image facilitate recognition of a concealed weapon by locating the person hiding the object. If either one of these two images alone is presented to a human operator, it is difficult to recognize the weapon concealed underneath the clothing. If a fused image is presented, a human operator is able to respond with higher accuracy. This demonstrates the benefit of sensor fusion for the CWD application, which integrates complementary information from multiple types of sensors.

Recently, a new system has been tested in a US laboratory called Future Attribute Screening Technology (FAST). FAST relies on non-contact sensors, so it can measure attributes as someone walks through a corridor at an airport. Also, it does not depend on active questioning of the subject. The system measures pulse rate, skin temperature, breathing, facial expression, body movement, pupil dilation, and other psycho physiological/behavioural patterns to stop unknown terrorists [70].

The system, based on: a remote cardiovascular and respiratory sensor to measure heart rate and respiration, a remote eye tracker, thermal cameras that provide information on the temperature of the skin in the face, a high resolution video for assessing facial expressions and body movements, and an audio system for analysing changes in voice. This system is expected to scour crowds looking for unusual behaviour. These techniques are deployed with the aim of identifying people who should be approached and quizzed by security staff, as can be seen in Figure 2.15.

Figure 2.15: Concept illustration of a FAST system [71].

The project hopes to advance a security system that monitors people for unintentional facial twitches, called "micro-expressions", which can suggest someone is lying or trying to conceal information. The new mobile units transmit data to analysts, who then use a system to recognise, define and measure seven primary emotions and emotional cues that are reflected in contractions of facial muscles. The results are then transmitted back to the screeners. The FAST system has been installed and tested at an airport and has shown to be 78% successful [70]. Figure 2.16 shows a snapshot from the new FAST system.

Figure 2.16: Snapshot from the new FAST system

2.5 EM Signal and Image Processing for Threat Object Detection

Manual screening procedures for detecting concealed weapons such as handguns, knives and explosives are common in controlled access settings such as airports, entrances to sensitive buildings and public events. It is sometimes desirable to be able to detect concealed weapons from a standoff distance, especially when it is impossible to arrange the flow of people through a controlled procedure. The development of automatic detection and recognition of concealed weapons systems is a technological challenge, which will require innovative solutions in sensor technologies and image processing. This problem also presents challenges in the legal field that, a number of sensors based on different phenomenology, as well as image processing support, are needed to observe objects underneath people's clothing. Before an image or video sequence is presented to a human observer for operator-assisted weapon detection or fed into an automatic weapon detection algorithm, it is desirable to pre-process the images or video data to maximize their exploitation.

The image processing procedures that have been investigated for CWD applications range from simple de-noising and feature extraction, to automatic pattern recognition and classification [71]. An image processing architecture for CWD is shown in Figure 2.17.

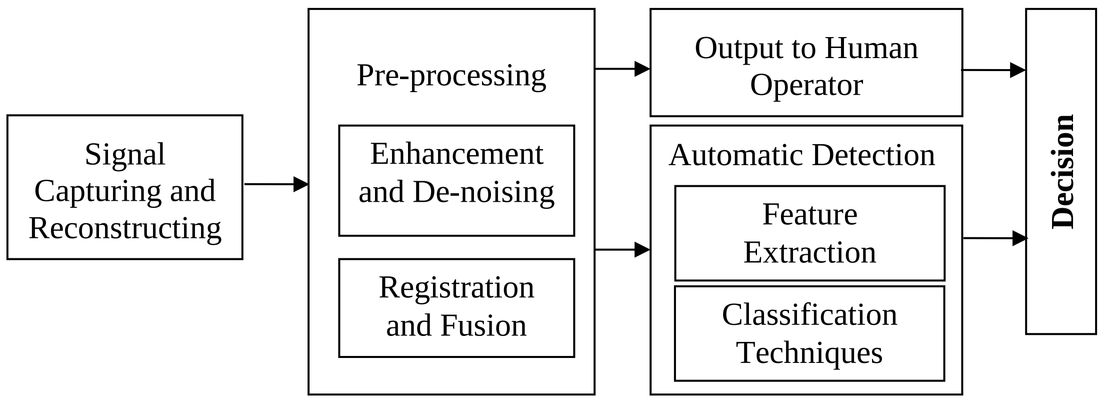

Figure 2.17: Image processing architecture for CWD.

It would be impossible to discuss the entire signal processing techniques for weapon detection, because the processing algorithms vary according to the detection techniques and the applications. However, this section provides a general picture of what has been achieved within this research field.

2.5.1 Threat object detection signal processing

WD images come with background noise and clutter, which directly lower the probability of detection. The sources of noise can be divided into two categories: inherent and environmental. Inherent noise includes such things as sensor electronic offsets. Environmental noise includes induced electrical noise and stray dynamic magnetic fields caused by nearby moving objects. Digital filters with proprietary pole and response functions are used to further condition the raw data [72]. Lee et al. [73] proposed a method to simultaneously suppress noise and enhance objects for passive MMW video sequences. They adopted an un-decimated wavelet transform to achieve enhancement via multi-scale edge representation. A motion compensated filtering was applied for temporal de-noising.

Ramac et al. [74] employed the grayscale morphologic filtering technique to remove the clutter and spots in IR and MMW images. This clutter refers to the irrelevant details such as shadows, wrinkles, and artefacts. Xilin et al. [75] used the NL-means algorithm to remove the noise from THz images, because it is asymptotically optimal under a generic statistical image model. In addition, they found the anisotropic diffusion algorithm to perform very similarly for terahertz images. The results of the two de-noising algorithms are provided in the research. Slamani et al. [76] proposed a mapping procedure consisting of three stages. The first stage is threshold computation, which segments the original image into a number of binary scenes. A low-pass filer and a high-pass filter are used to group pixels and detect edges for each scene in the second stage. At the third stage, a composite is obtained by summing all the processed sub-images together. This procedure actually accomplishes a clustering of pixels with common features that will directly affect the systematic performance.

Image fusion techniques have also been used to combine more than one EM sensor for CWD purposes [43, 68]. The pixel-level image fusion will retain salient features, irrespective if these features are relevant or not. Such prominence will be presented in the final fusion result. Another critical issue that should be addressed is image registration which aims to ensure that each pixel from different images corresponds to the same physical point on the object so that the images can be compared or operated upon the original images.

2.5.2 Feature extraction techniques for threat object detection

Feature extraction is a general term for the process of transforming a large input data set into a reduced representational set of features, which are still able to describe the input data with sufficient accuracy. In order to achieve effective pattern recognition, two types of features are normally required: features having physical meaning and features without physical meaning [77]. For example, geometric features such as shape, size and position of the pattern are considered to be features with physical meaning. Features extracted from the same image, but based on the statistical understanding of the image fall into the second category.

Advanced signal processing algorithms have been used to analyse changes in the magnetic field change that are generated when a person passes through a portal. Pattern recognition and classification techniques can calculate the probability that the acquired magnetic signature correlates to a known database of weapon versus non-weapon responses. Also, extracting distinctive features from the EM signal is imperative for the proper classification of these signals [78, 79]. Feature extraction techniques involve the transformation of the input image into a set of features. In other words, feature extraction is the use of a reduced representation and not the full representation of an image, in order to solve pattern recognition problems with sufficient accuracy.

One common method for metal detection and classification is to extract or generate features from the EM signal to represent the possible targets of interest. Feature extraction using time-frequency analysis has been used for stationary targets of backscattered signals, where features are extracted from the scattered field of a given candidate target, from the joint time-frequency plane. These features are then fused using the Principal Component Analysis (PCA) to obtain a single characteristic feature vector that can effectively represent the target of concern [80]. Joint time frequency analysis was used to overcome the limitation of using the Fourier series to represent the EM signals, which requires an extremely high number of sinusoid functions. The sinusoid function provides a feasible way of computing the power spectrum for an EM signal, which serves as a unique fingerprint for the CWD response to various targets (such as weapons and cell phones) [72].

Time-frequency analysis using Fourier and wavelet transforms (WT) have been used extensively for signal representation. The WT has been used to represent time series data, such as ECG waveforms and mine signal detection [81-83], and can be thought of as an extension of the classic Fourier transform, except operating on a multi-resolution basis. The results obtained from [84] verify that the continuous wavelet transform based technique produces features that are suitable to detect and identify signal data of metallic targets in laterite soil environments.

Shape is one of the most prominent features of any object. Many researchers have tackled the problem of object detection and classification using object shape features with different tools such as invariant moments, Fourier descriptors, Hough transform and shape matrices to extract shape characteristics [85, 86]. The invariant moment's method is widely used in feature extraction, since it is rotation, scale, and translation invariant. Objects can be detected with a classification of over 90% accuracy, after producing a set of invariant moments feature vectors in certain systems [87]. In [88] invariant moments have been used to identify the shape of a hand gun to classify objects into weapon and non-weapon objects, in which the researchers obtained an accuracy rate of up to 96%. In [89], the author reported three different shape recognition methods: invariant moments, Fourier descriptors and compactness (which is provides a measure of contour complexity versus area enclosed). In the first stage, several shapes are extracted from known weapon and non-weapon images. Each shape is run through the three algorithms and three dimensional numbers are obtained, such that each shape is represented by a three dimensional vector. The vectors that were obtained from the eight known weapons are grouped in one reference named as *Libarary1*, which is shown in Figure 2.18, and the other shapes (squares and circles) are grouped as *Labrary2*. During the second stage of a newly extracted shape image with unknown origin, the three algorithms are executed and the shape is characterised by a three dimensional vector. The Euclidean distances between the new sample and each sample of the reference libraries are computed, where the shortest distance determines the class of the new image.

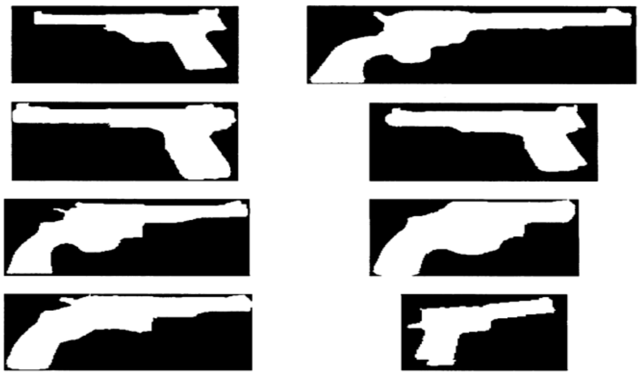

Figure 2.18: Typical shape in the weapon library.

Statistical techniques have been used as feature extraction methods to detect and classify metal objects. Throughout the literature, PCA has been used as a feature extraction tool [80, 90]. PCA is a multivariate statistical analysis method that transforms data into uncorrelated eigenvectors, or principal components, corresponding to the maximum variability within the data. PCA is also used to optimise and reduce the amount of redundant data, providing a convenient way to normalise the object in terms of translation and rotation [77]. In [91], PCA was used to propose detection and recognition in real-time of a concealed object with passive MMW imaging. A feature vector is extracted after PCA, which is invariant to scale and orientation, and tolerant to distortion. The decision rule is based upon the feature vectors and Euclidean distance technique to classify between handguns and steel plate. Edge chain code is used as a reinforcement feature technique for edge detection in the image field [92]. It can also be applied to features for representing objects in images [93].

Cross correlation techniques can be used as useful features for metallic object detection and characterisation. In [36] the authors designed a system working within a range of 1 to 14 GHz for gun detection, using this portion of the microwave frequency spectrum. The cross correlation between coherence polarisation and cross-polarisation RF returns are used to distinguish between different objects. Cross correlation techniques haves been applied from [94] [95], where the authors of EM signal transient responses derive their work from a series of EM images based upon defect characterisation and metallic object classification respectively.

Examples of other features extracted from a metal detector include: the signal amplitude that represents a material feature in order to obtain the properties of the objects under test [79], the key model parameters associated with fitting a Gaussian approximation to the input data [69], and the morphological / statistical properties and significant raw data values of target signatures in the input data [96]. Some extraction techniques that do not produce a set of features but instead attempt to model the input data associated with target signatures, are methods such as: electromagnetic induction spectroscopy [97], Kalman transform based using data array [98] and the phase loop representation [99].

2.5.3 Threat object classification techniques

After pre-processing, the images can be displayed for operator-assisted weapon detection, or they can be analysed with a weapon detection module for automated detection and classification. Artificial neural networks (ANN) are widely used in pattern recognition and classification, since they do not require neither any information about the probability distribution nor a priori probability of different classes [100]. ANNs have applications in distributed information storage, parallel processing, reasoning, and self-organization. They also have the capability of rapid fitting of nonlinear data, so they can solve many problems that are difficult for other methods [101]. In [102], the authors presented a neural-network-based scheme for metal target detection and classification. A single-layer network trained using the recursive least square learning rule was employed in six different optical bands for performing feature extraction and detection/classification tasks. Simulation results on six different optical bands were provided, which indicated the effectiveness of the proposed schemes. It was shown that the use of a neural network in multispectral wavelengths provided a useful tool for target detection and classification. In [78], a case study to classify a metal detector signal for automated target discrimination was conducted. Two different network strategies were applied to classify metallic object signal data with ANN. These results indicated that ANNs provide a vital role for improving the performance of the classification. In [88], probabilistic an ANN classifier was used to classify the extracted weapons candidate regions into threat and non-threat objects. The proposed framework was evaluated against a database consisting of real images and data of various weapons, with different sizes and types of gun, where a high accuracy rate was achieved. In [103], an ANN was used to differentiate between different target types of handguns in MMW images. A combination of techniques was presented that enabled handguns to be effectively detected at standoff distances. The using of late time responses allows non-threat objects to be distinguished from handguns. Information regarding the optical depth separation of the scattering corners, as well as the degree and shape of the cross polarisation, enable a neural network to successfully detect concealed handguns in the research.

In [91], the author used a simple classification procedure to detect and classifay hidden objects from MMW images based on Euclidean distance. A decision rule classified an unknown object into one of trained classes. The decision rule is based upon the Euclidean distance between feature vectors. Andrews et al. [104] have presented a technique of sweeping using MMW to detect concealed items, where ANNs have been used with the extracted information to detect conceald objects.

Recently, other machine learning methods have been used, such as the support vector machine (SVM). The SVM is a concept in statistics and computer science to derive a set of related supervised learning methods, which analyse data and recognise patterns used for classification and regression analysis [105]. In [106], the authors revisit an attractively simple model for EM induction response of a metallic object using SVM, to train and produce reliable gross characterisation of objects based on the inferred tensor elements as discriminators. The researchers are focusing on shape and size to evaluate the classification success of different SVM formulations for different types of objects. Consequently, they noticed that SVM has an inherent limitation, in that it takes a very long time to determine an answer in some instances. The other limitation is that the capacity of the SVM and the width of its kernel are adjustable parameters, which should be fixed in certain scenarios. In [107], the problem of classification metallic objects using their EM induction response was proposed, by decomposing that response into coefficients and then using an SVM and an ANN to process these coefficients. The performance of each method was also compared, since it demonstrated that there was no simple relationship between the size of the objects and the overall magnitude of their coefficients, so learning algorithms were necessary for the classification of these objects. When trained with all types of objects, both the ANN and the SVM were able to classify all of the objects with a reasonable degree of accuracy. In [108], SVM was used to detect and classify metallic UXO. The classifier ran by itself and did not require any human intervention. The SVM can be trained very quickly, even when the feature space has more than 20 dimensions, and it was a simple matter to add more training data on-the-fly. The authors stress that none of the classifications yielded false negatives: all UXO were identified correctly in every instance.

2.6 Summary and Problems Identified

The first part of this chapter reviews the sensor technologies currently being used for the metal and weapon detection application. Several of the systems are based upon electromagnetic, acoustic or ultrasonic-wave technologies. A critical issue raised is the challenge of performing detection and classification at a close distance with high probability of detection and low probability of false alarm. Also, the systems performance relies highly on the operator decision. All approaches show the advantages and disadvantage in the operating range, material composition of the weapon, penetrability, and attenuation factors. It is clear that no single technology can meet all the requirements for a comprehensive CWD system.

The second part of this chapter provide a survey of the previous image processing techniques being developed to achieve better weapon detection. Specifically, topics such as image enhancement, feature extraction and fusion, and classification methods were reviewed. The progresses in signal processing and artificial intelligence techniques have allowed the object classification to be carried out precisely, which automate the process and make it more reliable, as it is not a subjective analysis.

Through literature survey, the high risk aspects of the problem have been identified as: 1) Detection sensitivity in unconstrained environments; 2) Metallic object identification; 3) Multiple object separation; 4) Signal processing and feature extraction and; 5) Automatic object classification.

To minimise the risks, proposed mitigation methods can be summarised as follows

- The new system should provide accurate detection results not only in the lab, but also in noisy, real world environments (with electronic devices, metallic structural components, surrounding buildings, etc.); the system should quickly make decisions with low false-alarm rate, and be capable of discriminating and identifying multiple objects in close proximity.
- The system should have no 'side-effects' regarding health and safety issues. Among all of the pervious methods, we choose to develop a detection system based upon induction phenomena, since it is safe to human body and require cheap equipment, albeit that it provides imprecise detection and it is hard to handle.
- To improve the detection sensitivity and signal-to-noise ratio, a high current, narrow pulse excitation source should be used. The narrow pulse excitation source will allow a high peak field value while retaining a comparable RMS field strength to current designs. Unlike current pulsed metal detection systems, where only the decay time of the signal is measured, the developed system will take advantage of more sophisticated signal analysis techniques extended from our team pulsed EC work.
- The system should be able to; detect non-stationary and small objects; discriminate threat objects (e.g. guns and knives) from non-threat objects (e.g. keys, drinks cans and mobile phones); be capable of decision making for different object combinations with threat and non-threat items (e.g. mobile phones close to guns).

- A rich metallic object database and their characteristics will be established and analysed for our feature extraction, selection and system evaluation, in collaboration with London Metropolitan Police.
- The project aims also to build an open platform, which can integrate other modality sensing and imaging e.g. CCTV, thermal and radar images to overcome the fact that current approaches are more sensitive to magnetic volumes than fine structural and material characteristics due to limitations of detection distance.
- To address the issue of multiple object separation and different object orientation, the following techniques will be applied: (1) optimisation of sensor array specification involving sensor sensitivity and spatial resolution; (2) correlation of amplitude and time features of pulse field responses; (3) use invariant feature extraction techniques, e. g. invariant moments.
- To address the automatic object classification issue, several feature extraction techniques will be applied and investigated to select proper features to use them with classifiers for a best classification rate can be achieved.

In the following chapter, new system designs and signal processing methodologies are investigated in relation to these challenges.

Chapter 3: GMR Electromagnetic Imaging System: Design and Implementation

The comprehensive literature survey carried out suggests that more research work on threat object detection systems and their signal analysis are still required in the field of security applications. This chapter details the design and implementation of a new metallic object detection system, utilising an array of GMR sensors in conjunction with pulsed excitation to develop a new WTMD for deployment in unconstrained environments, i.e. without users divesting themselves of metallic items. System hardware was supported with a graphical user interface (GUI), which enabled a two-dimensional image to be constructed from measured backscattered signals, to be used later in image processing for object identification and classification purposes are developed.

This chapter is organised as follows: section 3.1 discusses the fundamentals of a WTMD. Section 3.2 presents the new system design and the underlying development steps. Data acquisition and pre-processing is detailed in section 3.3, with the formation of the two-dimensional image. Section 3.4 explains the GUI development for the system, while section 3.5 summarises the chapter.

3.1 Fundamentals of Walk-Through Metal Detector

WTMDs are an integral part of airport security surveillance systems and government buildings. Most of these metal detectors use the EM signal variations as a mean to detect metal. Any modern WTMD comprises mainly of a transmit panel (transmit coil), a receive panel (receive coil), and an excitation method. The magnetic field produced by a source will interact with a nearby object. The type and strength of these interactions depends on:

- Type of material that the object is made of
- Size and shape of the object
- Orientation of the object in the magnetic field
- Speed of the object through the magnetic field.

Most WTMD units use active EM techniques to detect and classify metal objects. An active EM field, in this instance, means that the detector sets up a field using a source coil, where the field is used to probe the environment. The primary (applied) field induces EC in the metal under inspection, which in turn generates a secondary magnetic field that can be sensed by a detector coil. The rate of decay and the spatial behaviour of the secondary field are determined by the target's electrical conductivity, magnetic permeability, shape, and size. Sets of these measurements can be then taken and used to identify the objects.

The following subsections discuss the basics of electromagnetic imaging and specification used in WTMD.

3.1.1 Theory of Electromagnetic Imaging Systems

The EM response of a material can be obtained by solving Eq. 3.1:

$$\nabla \times E = \frac{\partial \mathrm{B}}{\partial \mathrm{t}} \tag{3.1}$$

where $\nabla \times E$ is the curl of electric field, t is time, and B is the magnetic flux density. The electric displacement and magnetic field are introduced solely as a matter of convenience when considering polarisable and magnetisable materials. The magnetic field H is related to B through the magnetisation M (Eq. 3.2):

$$H = \frac{1}{\mu_0} B - M(H) \tag{3.2}$$

In this equation, μ_0 is the permeability of vacuum and M is explicitly written as a function of H. In the material, the magnetization vector M is defined as the average magnetic moment per unit volume. It is thus suitable to visualise the magnetisation of a material as being from an assembly of magnetic dipoles. If these dipoles are distributed evenly throughout the material, the material is consistently magnetised. For a nonmagnetic material, such as copper, there is no magnetisation (M=0) and thus, the magnetic flux density and the magnetic field are related by Eq.3.3.

$$B = \mu_r \mu_0 H \tag{3.3}$$

where μ_r is the relative magnetic permeability of the target and μ_0 is the permeability of vacuum.

The functional relationship of the magnetisation with the magnetic field, *M (H)*, helps classify the three main classes of magnetic materials: diamagnetic, paramagnetic and ferromagnetic. The magnetic field at any point around the magnetic source is governed by the Eq. 3.4, 3.5 and 3.6 [109]:

$$B_x(x, y, z) = \frac{\mu_0}{4\pi} 3\mu \frac{xz}{(x^2+y^2+z^2)^{5/2}} \tag{3.4}$$

$$B_y(x, y, z) = \frac{\mu_0}{4\pi} 3\mu \frac{yz}{(x^2+y^2+z^2)^{5/2}} \tag{3.5}$$

$$B_z(x,y,z) = \frac{\mu_0}{4\pi} 3\mu \frac{z^2 - \frac{1}{3}(x^2+y^2+z^2)}{(x^2+y^2+z^2)^{5/2}} \qquad 3.6$$

The magnetic field produced from the objects will use the same equation but with equations 3.4, 3.5 and 3.6 multiplied by the relative permeability μ_r .

The type of magnetic field generated by an excitation coil is that of a pulse induction field. Pulse induction detectors typically produce a transmitter current, which is turned on for a time and then turned off. The decaying field generates pulsed ECs in the target, which are then detected by analysing the decay of the pulse induced in the receiver coil. Conductive objects show a unique time-decay response. The pulse induction technique detects metal objects by calculating the time-decay response of the pulse induced in the receiver coil [26].

Figure 3.1 illustrates the concept of magnetic inductive metal detection methods, using the received signals for each position. The figure shows a change in decay rate of the signal received by the pulse induction detector with respect to the reference signal when passing over a metal object at position 10. The magnetic field produced by a source interacts with a nearby conductive object. The type and strength of this interaction depends on several parameters such as: the type of material that the object is made of, the size and shape of the object, the orientation of the object in the magnetic field, the speed of the object through the magnetic field, and the distance between the sensors and the object. All of these parameters should be taken into account when designing a system, so as to detect and discriminate between threat items [11].

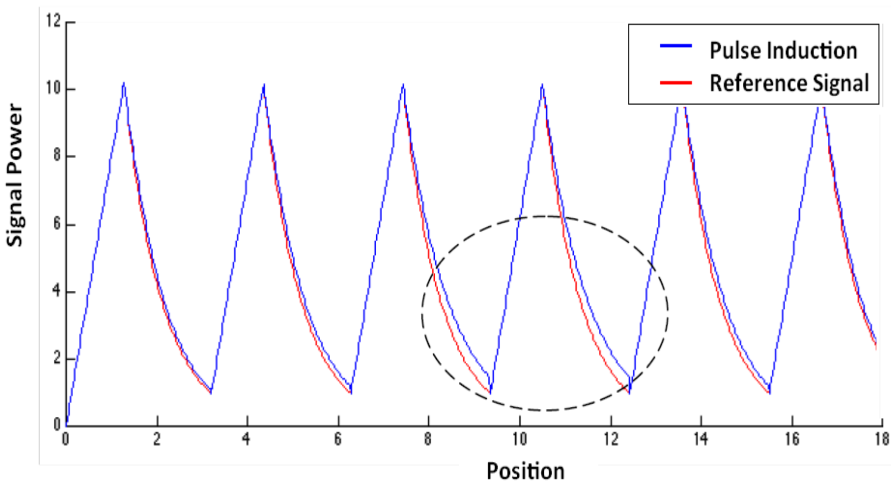

Figure 3.1: Pulse induction metal detection.

In this work, a WTMD from CEIA Company was used, which is widely used in UK airports. Details of this device will be presented in next section.

3.1.2 Specifications of CEIA System

A thorough investigation of the *Construction Electronics Industrial Automation* (CEIA) walkthrough arch, donated by the London metropolitan police (shown in Figure 3.2) has been undertaken to ascertain: the mode of operation, the excitation and pickup coil configuration, and the signal processing techniques. The operation of the CEIA arch is simplistic in terms of object detection, as the arch simply beeps when a metallic material passes through it; there is no indication of the type of metal or location of the metal.

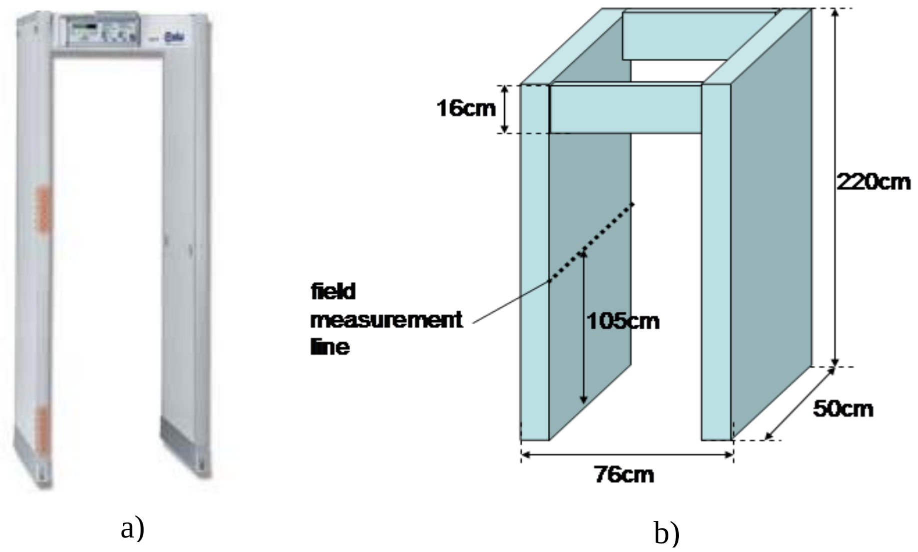

Figure 3.2: a) CEIA walk through metal detection arch [4], b) Measurements of CEIA arch in the laboratory.

In order to ascertain and understand the coil configuration, electromagnetic and X-ray investigations of the arch panels were carried out, yielding the result shown in Figure 3.3. It can be seen from the X-ray image in Figure 3.3a and b that there is a network of coils, criss-crossing the panel, measurements with a magnetic field sensor indicated that the wires were organised as two coils with current flow shown in Figure 3.3c. The use of multiple, overlapping trapezoid (parallelogram) shaped excitation and receive coils are described in a number of metal detection patents. The advantages of such coil configurations are described as [110, 111]: 1) They allow detection of objects orientated in any direction through a multi-axis excitation field, unlike loop coils, where excitation is predominantly along one field axis. 2) The design of the coils can be configured to vary sensitivity along the height of the detector to optimise sensitivity in the most security aware areas. 3) The interaction of the coils can be designed to maximise sensitivity to the horizontal field component. This can be achieved by reinforcing fields in the horizontal plane and partially cancelling fields in the vertical plane, helping to cancel potential sources of noise from underneath the detector.

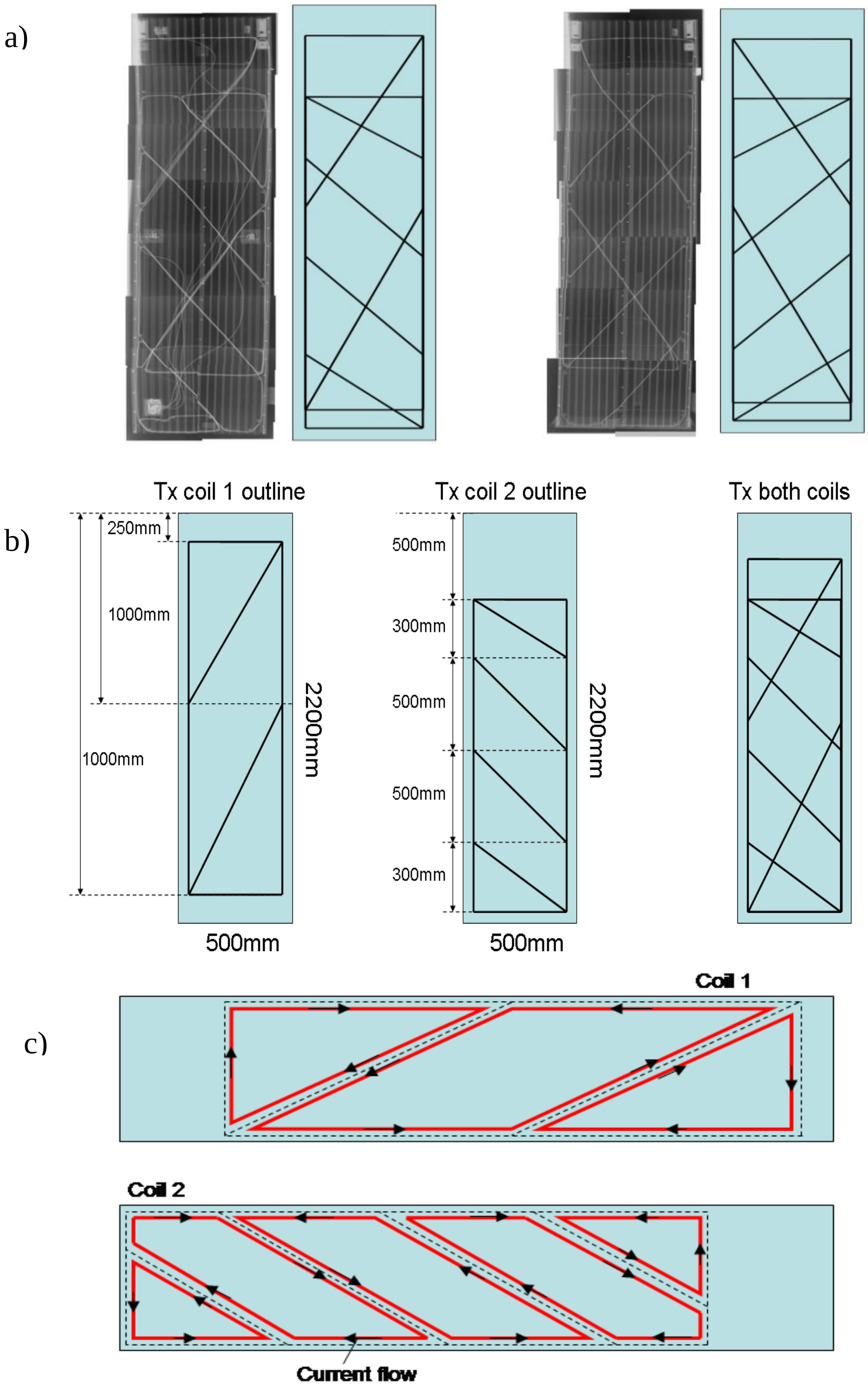

Figure 3.3 : X-ray image and predicted configuration of: a) Tx and Rx panel, b) Panel's measurements, and c) Coil configuration deduced from EM measurements.

Further investigation of the arches revealed that they operate in a transmit-receive configuration, with two overlapping transmit coils in the left panel and two mirror image receive coils in the right panel. The two transmit coils operate at different frequencies, 3.42 kHz and 3.72 kHz. The primary purpose of the coil configuration suggest that the two mirror image pairs of coils are coupled by differing excitation frequencies, thus the sensitivity of the arch to objects in different positions can be tailored to the desired application. Object detection is accomplished through the integration of the signals from the two receive coils, leading to an increase in amplitude at the integrator output when an object passes through the arch. Simple thresholding is applied to the integrated signals to trigger the alarm.

The strengths of the CEIA system include the ability to vary sensitivity to objects in different human body parts. The major limitation of the system is its inability to discriminate between different materials or provide any kind of identification or characterisation of the objects detected.

3.2 Proposed System Design and Principles of Operation

In this section, a description of the detection system will be detailed with their capturing condition.

3.2.1 Giant magneto-resistance sensor

The GMR is one of the most fascinating discoveries in thin-film magnetism, which combines both technological potential and deep fundamental physics. In 1988, Baibich et al. discovered giant negative magneto-resistance in Fe/Cr multilayers, in which the interlayer exchange interaction causes antiferromagnetic alignment of adjacent Fe layers [112]. Like other magneto-resistance effects, GMR is the change in electrical resistance in response to an applied magnetic field. Baibich's group discovered that the application of a magnetic field to a Fe/Cr multilayer resulted in a significant reduction of the electrical resistance of the multilayer. In fact, the resistivity changed by as much as a factor of two. This effect was found to be much larger than either ordinary or anisotropic magneto-resistance, earning the new title "giant magneto-resistance" or GMR.

The use of GMR technology for magnetic sensing appears promising due to the fact that it has a high sensitivity within a wide frequency range while an extremely low power and cost, and a collective manufacturing process, which facilitates the construction of large array probes [113]. The GMR sensor, which is one of the families of solid state magnetic field sensors, is made of several ferromagnetic metallic thin films that are separated by thin nonmagnetic layers. When these layers are subjected to a magnetic field, the resistance can be reduced significantly (see Figure 3.4). The wide spectrum response and high sensitivity of these GMR sensors are of particular interest in EC inspection. With its small dimensions, the usage of GMR sensors can also give a high spatial resolution for defect detection. Smith et al. reported the technology of fabricating GMR sensor-arrays that are promising for EC testing [114]. A 2D array of GMR sensors can be built to form a magnetic imaging plane [115], which would provide an image of a relatively large area in a single sweep, with high resolution and without the need to scan the probe. The potential of using sensor-arrays for pulsed EC (PEC) imaging provides ways to obtain more information about defect location and geometry, in addition to rich depth information. With the construction of more sophisticated array arrangements, the imaging technique can provide more reliable and faster inspection results for defect characterisation, assessment and reconstruction of 3D defects [116].

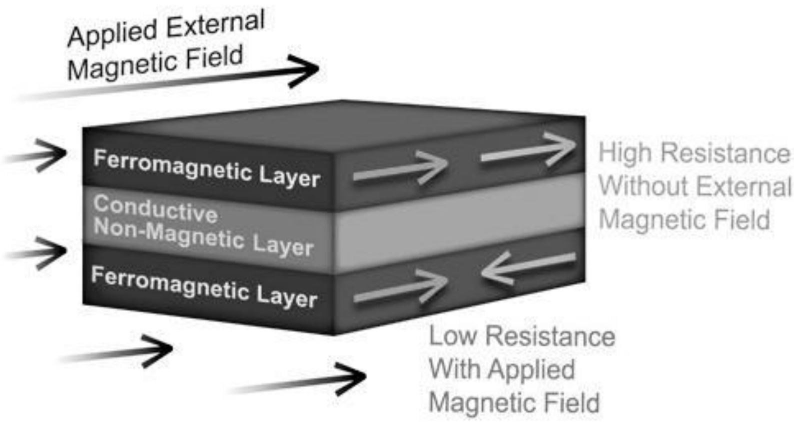

Figure 3.4: GMR senor layers

3.2.2 Pulsed excitation current

The EC technique has been shown to be one of the most effective techniques for the detection and characterisation of conductive samples. This technique is based on inducing electric currents in the material being inspected and observing the interaction between those currents and the material. The induced ECs are essentially a circulating current generated by the electromagnetic coils and monitored simultaneously by measuring the electrical impedance of the coil. When an alternating current is applied to the test coil, a primary magnetic field is established in an axial direction around the coil.

As the coil approaches an electrically conductive material, the alternating magnetic field interacts with the test object material, causing a circular electrical current to flow in the object as predicted by Faraday's law. This electrical current then creates its own secondary magnetic field, which is at all times, opposite in direction and opposing the coil's magnetic field, in accordance to Lenz's law. The interaction between the magnetic field generated by the coil and the magnetic field generated by the ECs, is monitored by pick up coils to give an indication of objects size, shape, or any variations in the material's properties [117].

The excitation frequency for EC testing is selected based on the material of each object to be detected. In obtaining the best sensor response, the sensor must induce the greatest EC density in the sample to be tested [118]. The oscillation is sinusoidal and may range from several Hz up to several MHz. The effectiveness of conventional single frequency EC is limited to the identification of only one or two test conditions [119].

In order to counteract some of the limitations of single frequency EC, the pulsed EC (PEC) technique has been introduced. PEC is currently an emerging technology in EC. This technology is based upon pulsed excitation current, providing new perspectives for the detection and the characterisation of the test sample. It measures the transient response of the magnetic field instead of the impedance and reactance of coils used in conventional EC testing [120]. In recent years, PEC has gained attention in different application [118] and extensive research has been performed in the area thanks to its wideband spectrum excitation that is an improvement to the multi-frequency techniques.

3.2.3 GMR sensors with PEC excitation feasibility study

An initial study was carried out to verify the suitability of the use of pulsed excitation in conjunction with NVE GMR sensors for the work, where NVE is the name of the company, to optimise signal conditioning circuitry and to select the appropriate GMR sensor package (different packages have different sensitivities and field ranges) for the full array. In order to accomplish this, a small 8-element array was constructed and interfaced to an array of instrumentation amplifiers with an existing data acquisition system, which is used to collect readings from the sensors and using pulse excitation mode. Figure 3.5 shows the measured field for three different objects; an Aluminium block, a Stanley knife and a set of keys, in reflection mode. It can be seen from the plot that each object invokes its own characteristic signature in terms of signal amplitude, signal shape and time based features, such as time to-peak. It is these characteristics that can be used to characterise and classify different objects passing through the arch.

Figure 3.5c shows results of a test using the 1x8 array to image aluminium step shaped sample, where the sample gets thicker towards the right hand side of the plot. A 2D interpolation of the image has been used to increase the resolution of the image. Although the array is rather sparse at a 20mm pitch, the results show the potential of the technique for object imaging.

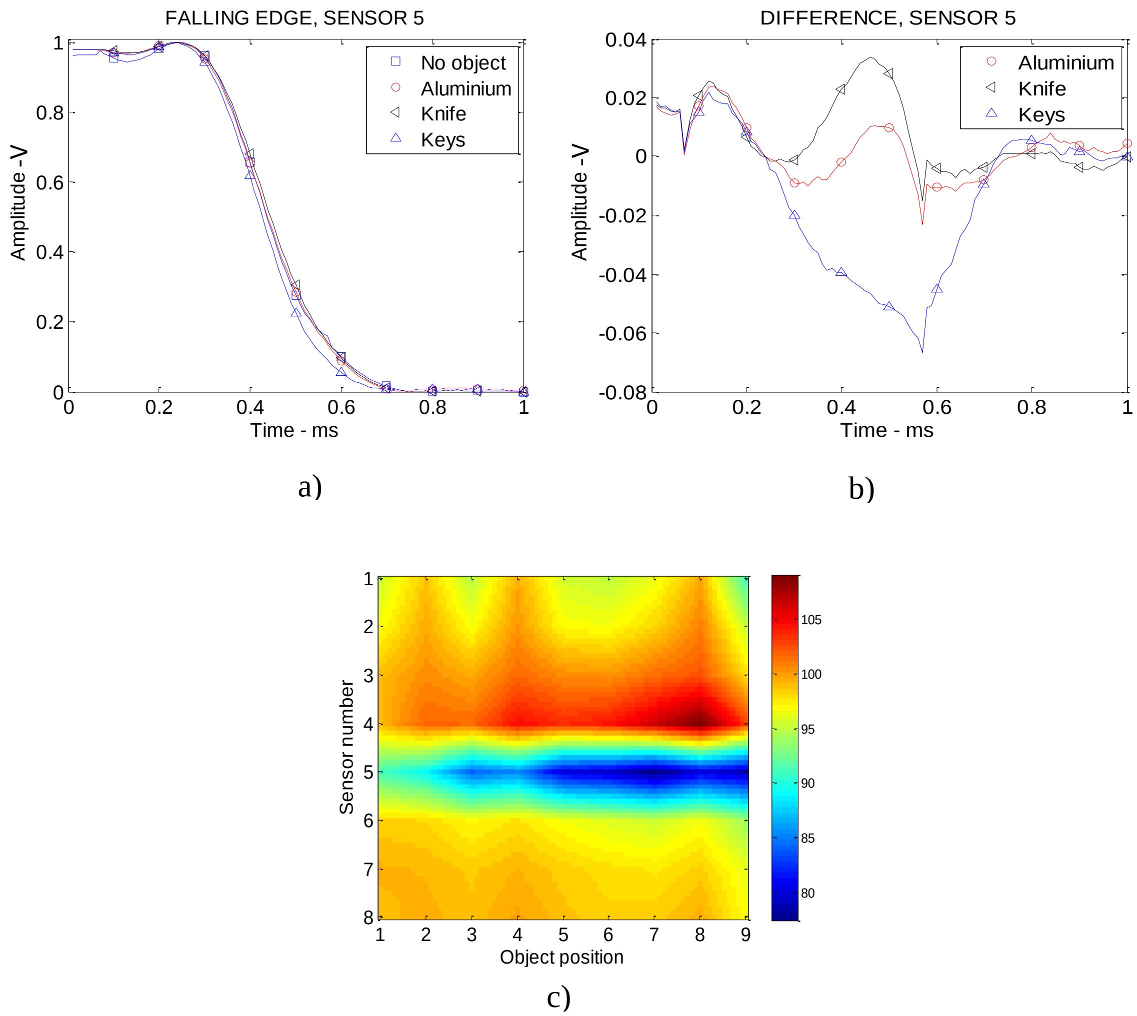

Figure 3.5: EM measured field. a) Normalised falling edge of measured field with three different objects present, b) Normalised difference signal for three different objects, c) Percentage change in amplitude for aluminium step sample.

These preliminary results show that the use of pulsed excitation in conjunction with a sensor-array has the potential to: match the capabilities of current detector to detect the presence of an object and identify the object position though simple thresholding of the response signal, characterise the object material through time-frequency analysis and extraction of signal features such as time to peak, and finally provide an image of the object through tomography techniques in conjunction with real time interpolation to improve image resolution.

3.2.4 Sensor-array configuration

Different configurations of the sensor-array have been investigated. First, a 2D sensor-array has been formulated. Second, one column was then selected from the whole array to form 1D array. Finally, two diagonal 1D arrays that cover whole person body were used and also aligned directly above the excitation coil.

As a result of the successful completion of the feasibility of the GMR array test outlined in the previous section, a full array was designed for the system. The array was designed with maximum flexibility in order to fully assess optimal sensor spacing for the system. Figure 3.6 shows the first array design; the pitch of the array in the horizontal direction is fixed at 7.75mm, but the vertical pitch is variable, with a minimum pitch of 3.5mm. The sensor and the amplifier are built on separate boards, with the signal lines as close as possible and a twisted pair cable between the two boards in order to optimise common mode rejection and reduce pickup noise.

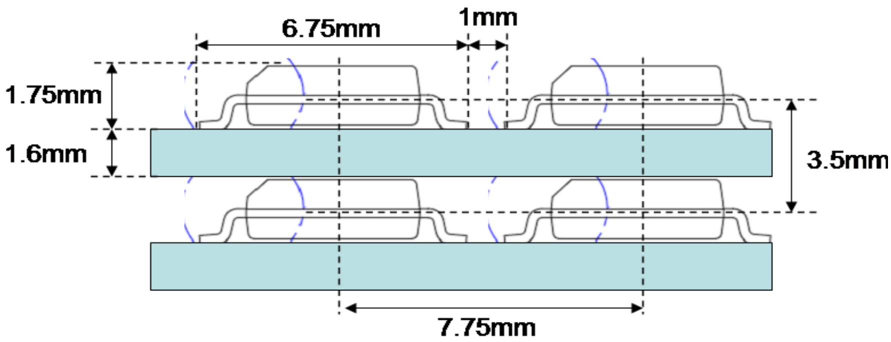

a)

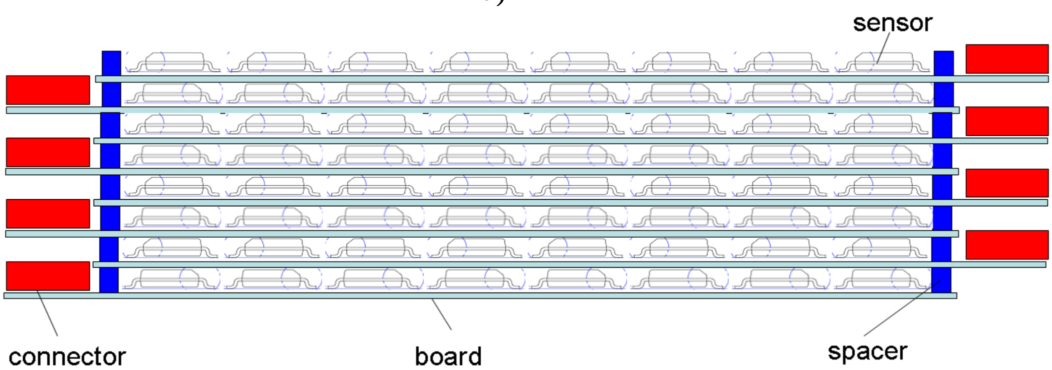

b)

Figure 3.6: a) Minimum sensor pitch is 7.75mm x 3.5mm, b) Stacked sensor-array design configurable as two 8 x 8 arrays, one 16 x 8 array, one 40 x 1 array, or two 40 x 1, all with variable vertical pitch.

A single column in the array provides a more coherent result than using the full array because the relationship between the sensors used to create the image and the excitation field remains constant, whereas for the full array, the relationship between the sensors and the excitation field varies between columns of sensors. On the other hand, using less number of sensors will reduce hardware costs and processing time.

Uniform pulsed excitation response have been achieved by employing a linear array aligned with the coil, as shown in Figure 3.7a. By aligning the array in this way, the pulse measured at each sensor is close to identical (Figure 3.7b and c); any variation in the pulse amplitude is due to small errors in sensor positioning, with respect to the coil. The local magnetic field distribution for each sensor is almost identical, as shown in Figure 3.7c. As such, the change in response to the presence of a given object is uniform for the whole array and the models for EM excitation, resulting in a greatly simplified magnetic field distribution. Therefore, the diagonal sensor-array setup will be considered for the rest of this study.

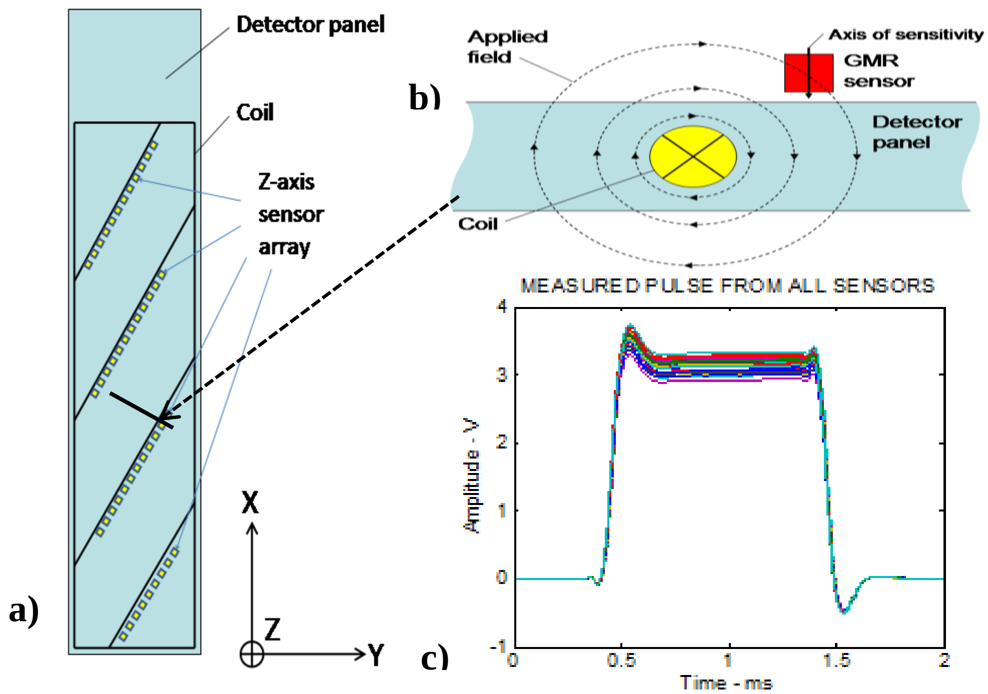

Figure 3.7: Uniform pulse excitation response. a) Sensor-array positioning with respect to coil, b) Interaction of applied field and GMR sensor, c) Uniform pulse response from a group of sensors.

Restricted by the: width of the WTMD panel, the coil position, and the separation between each two consecutive sensors, it was not possible to place more than 40 sensors onto the coil. This would make the proposed system able to examine only a portion of the individual body. To overcome this pitfall, another configuration was adopted where two sensor-arrays, each with 40 sensors, was placed onto two adjacent coils. This allowed the system to cover a whole individual body. All three different types of configuration are shown in Figure 3.8.

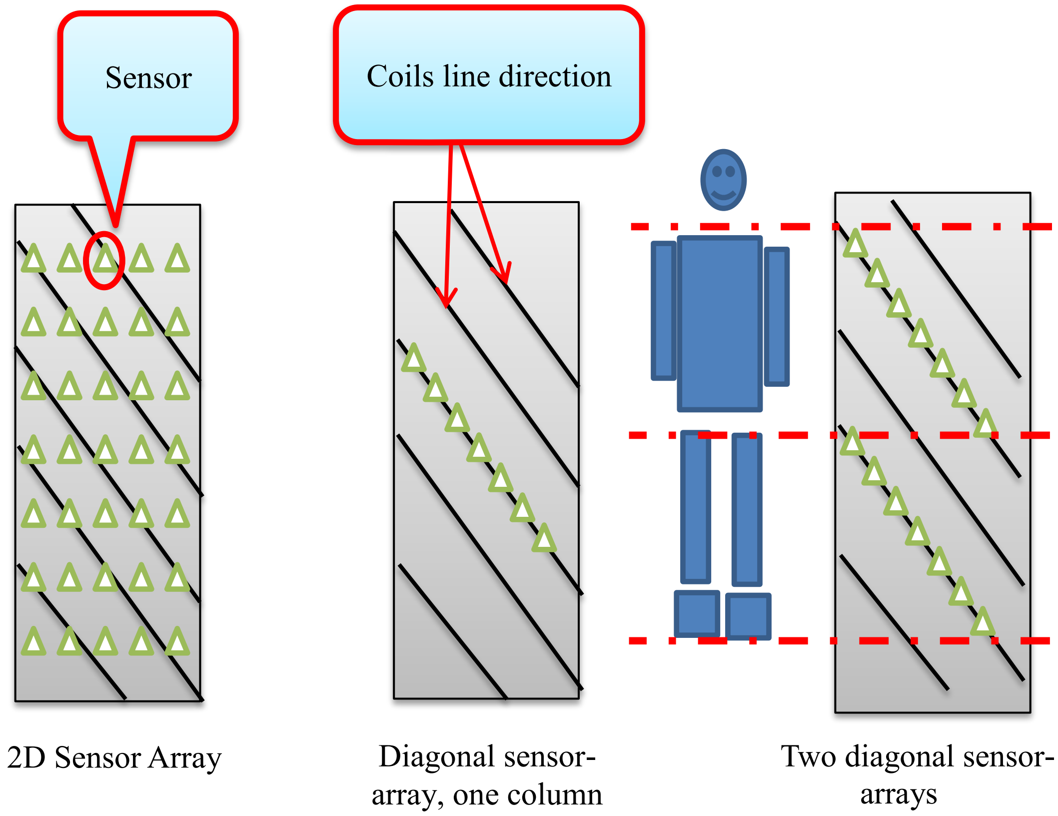

Figure 3.8: Different sensor-array configurations

The spacing or separation between the sensors (Figure 3.9a) has a large impact on the overall design of the system; the smaller the spacing, the greater the number of sensors that are needed and the greater the complexity and cost of the system. Four different sensor spacing were trialled during the tests: 7.5mm, 10mm, 15mm and 42mm. After an analysis of the results was completed, the 15mm spacing was found to be a good compromise between spatial resolution and system complexity (Figure 3.9b). The exaggeration of field distribution for smaller objects works to compensate for the sensor separation. Although the chosen sensor separation means that the vertical accuracy can only be guaranteed to be within 15mm, tests have shown that the measurement of the actual position of the distribution is not particularly useful in object characterisation, and analysis of other aspects of the EM signature are more reliable for object discrimination. Figure 3.9c show the two sensor boards fitting together to form a continuous linear array.

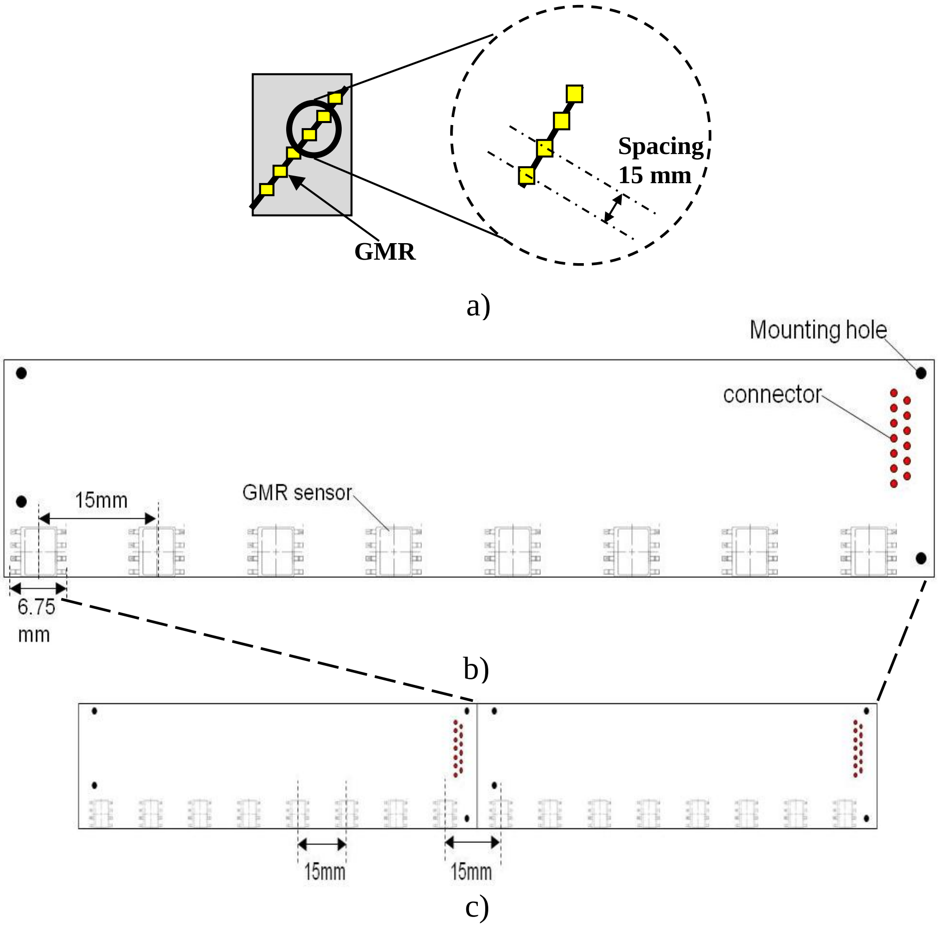

Figure 3.9 : The spacing between the sensors: a) The array spacing, b) Single GMR sensor board layout, and c) Two sensor boards fitting together to form a continuous linear array.

3.2.5 Magnetic sensor-array specifications

NVE GMR sensors were chosen for the array, primarily because NVE company offers a number of sensors with varying magnetic field ranges. After initial tests and the feasibility study with Hall sensors, which offer a wide magnetic field range but with low sensitivity, the AAL002-02 [121-123] low hysteresis GMR sensor was chosen for the array, according to its highest sensitivity compared with the other NVE GMR sensors. These selections of sensors are shown in Figure 3.10, where the sensitivity to the magnetic field is indicated by the slope of each line. The AAL002-02 sensor has a linear magnetic field range of 1.5 - 10.5 mT and a sensitivity of 4.5 - 63µ V/T at a supply voltage of 15V. The “L” in the sensor model name indicates that a low hysteresis (maximum 2%) GMR material has been used to fabricate the sensor. This characteristic was chosen because it was initially intended to utilise an applied magnetic field, varying from zero to a maximum value, where the lower hysteresis value would minimise the error at low field strengths. However, after initial testing, it was found that a more stable signal could be achieved by biasing the sensor response into its linear region using a DC offset superimposed on the excitation signal.

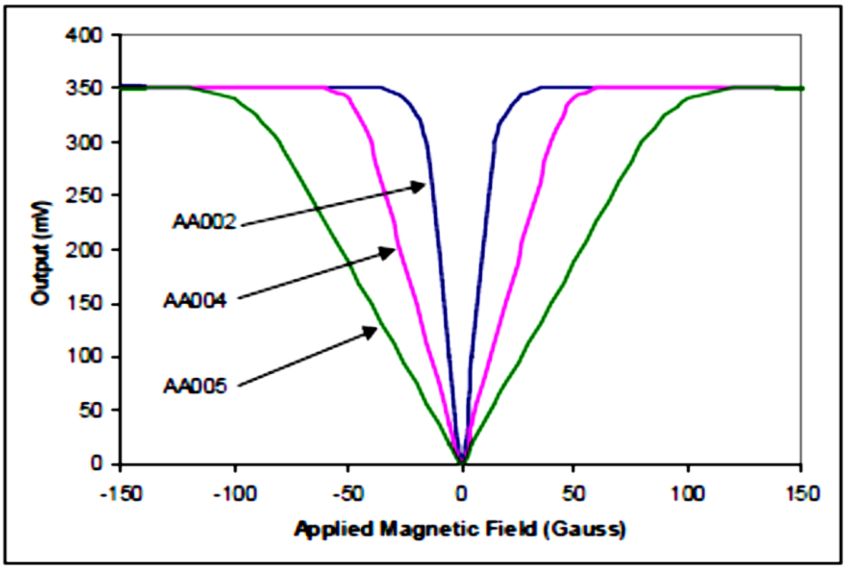

Figure 3.10: Sensitivity of the different NVE GMR sensors [121]

As mentioned in 3.2.4, the sensor and the amplifier are built on separate boards as shown Figure 3.11, with signal lines as close as possible and a twisted pair cable between the two boards as in order to optimise common mode rejection and reduce pickup noise.

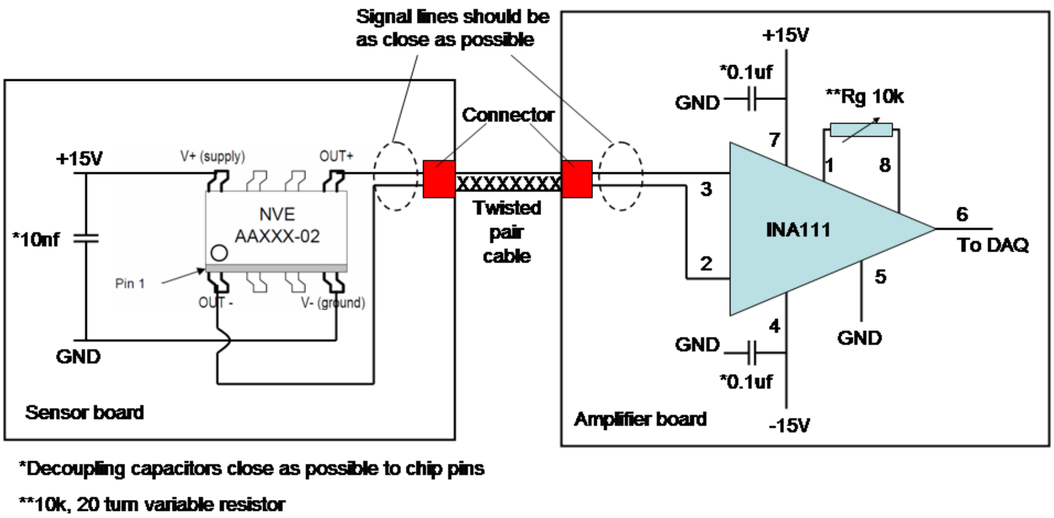

Figure 3.11: GMR measurement circuit

3.2.6 Magnetic sensor-array excitation response

In this system, a pulsed excitation is applied to the coil. Pulsed excitation provides opportunities to apply an interrogating field with rich frequency components in a single waveform. In the tests detailed in this work, a pulse repetition frequency of 500Hz is used with a square wave pulse width of 1ms and an applied current of 0.5A – 1.5A.

Figure 3.12 shows the pulse response for a steel object and an aluminium object, measured using a single GMR sensor. It can be seen from the plots that the change in pulse response from the presence of an object (steel or aluminium) is actually very small. Computing the difference between the signal with and without an object present, as shown in Figure 3.12b and Figure 3.12d (amplification x200), allows us to accentuate the difference between the two signals. It can be seen that a peak in the signal difference can be observed during the rising/transient part of the signal; the time and amplitude characteristics of this signal can be used to extract information about the object under inspection.

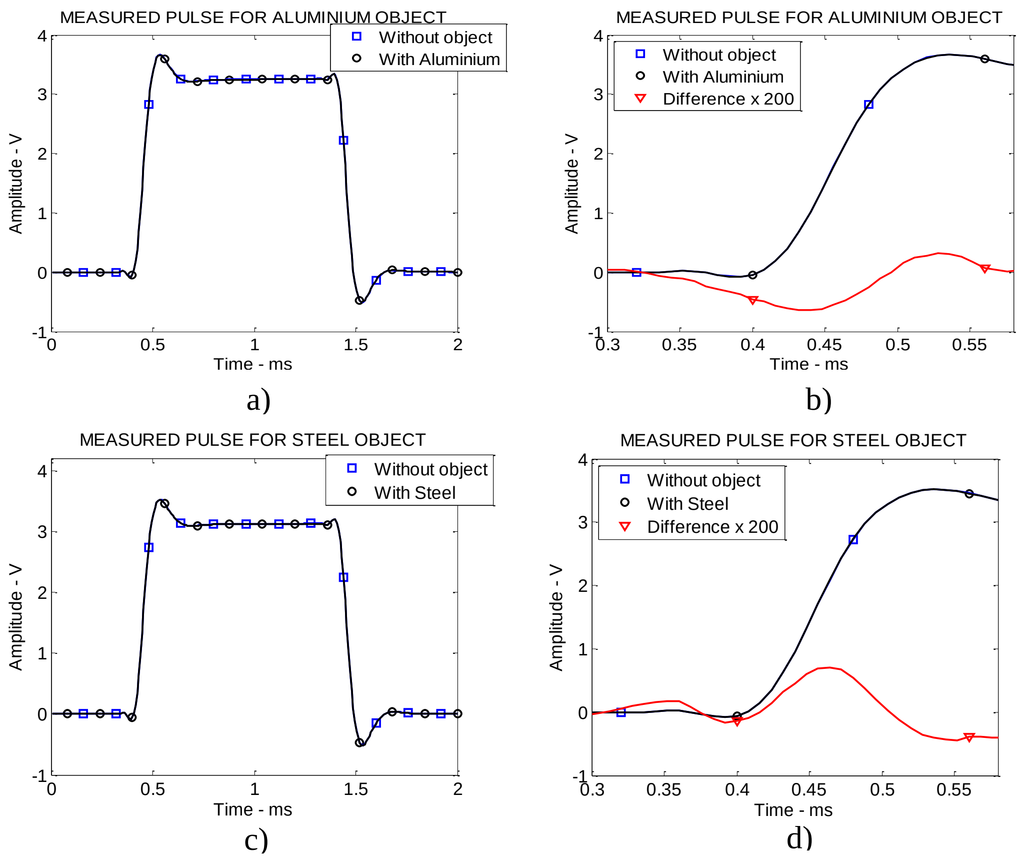

Figure 3.12: a) Pulse response of one sensor in a diagonal array in the presence of an aluminium object, b) Rising edge of the pulse response for an aluminium object with the difference calculated, c) Pulse response from the presence of a steel object, and d) Rising edge of the pulse response for a steel object with the difference calculated.

3.2.7 System blocks and connection diagram

A connection diagram of the system is shown in Figure 3.13. The upper part (Capturing the signal part) of the diagram is duplicated five times to make 80 channels (16 channels on each of the five cards). Two 8-channel sensor boards are connected to each of the 16-channel amplifier boards via a 20-core ribbon cable. The input instrumentation amplifier INA111 provides differential termination and amplification for the sensor outputs. The amplifier circuits are powered by a +/-15V power supply. The outputs from the amplifier boards are connected to the data acquisition boards in the PC via the breakout boxes. An additional connection is established to the data acquisition board from the function generator. This allows the data acquisition to be synchronised to the excitation waveform.

A function generator supplies the excitation waveform in the excitation part as showed in the lower part in Figure 3.13. The Bipolar power amplifier is set to produce an output current that is proportional to the input voltage supplied by the function generator. The output from the function generator must be connected to the current programming input on the amplifier for this to be achieved. The output from the power amplifier is connected to the coil in the excitation board via the arch control box. None of the electronics in the control box are used in the test; it is just there to establish a connection to the excitation panel. A list of the equipment used is shown in Table 3.1, while the overall system set up in the laboratory is depicted in Figure 3.14.

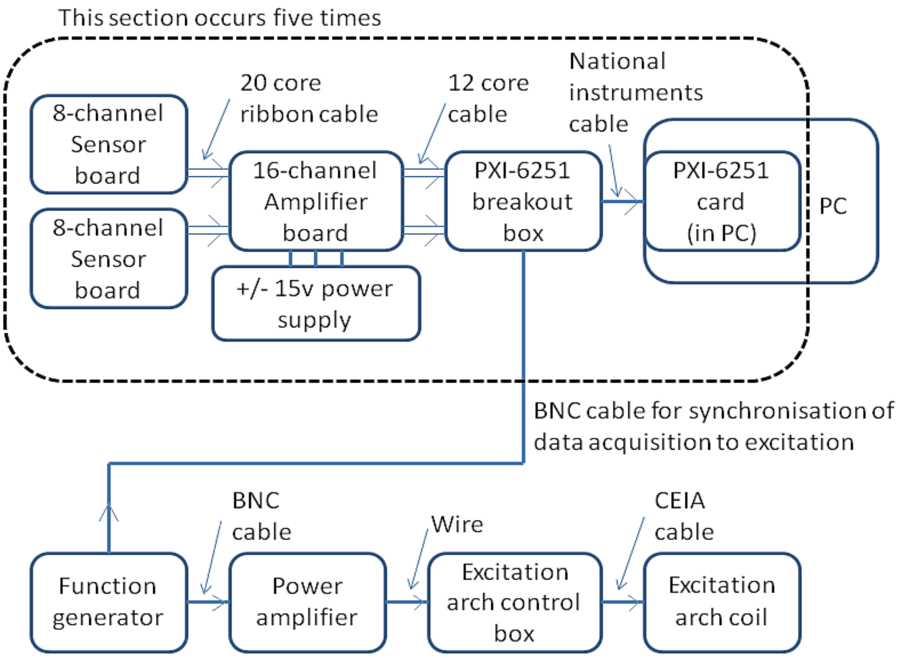

Figure 3.13: Proposed system diagram.

Table 3.1: Equipment list

Equipment Name	Description
Agilent 33250A function generator [124]	Provides the excitation waveform to power amplifier.
Kepco BOP 36-12ML bipolar power amplifier [125]	Provides the excitation to the coil, where the excitation current is proportional to the excitation voltage from the function generator.
National instruments data acquisition system:	PC equipped with a PXI bus to accommodate multiple data acquisition cards [126].
	5 x NI PXI-6251, 16 input data acquisition cards. Allows acquisition of 80 channels of data at a sample rate of 125kHz [127].
	5x breakout boxes and cables to allow us to establish a connection to the data acquisition cards.
Sensor boards	Each board contains 8 x NVE AAL002-02 GMR sensors [121].
Amplifier boards	Each board contains 16 circuits based on the INA111 instrumentation amplifier [128], to allow connections from two 8-channel sensor boards.
CEIA walk-through metal detector and control box	We provide our own pulsed excitation to the coils in the metal detector panel via a connection in the control box.

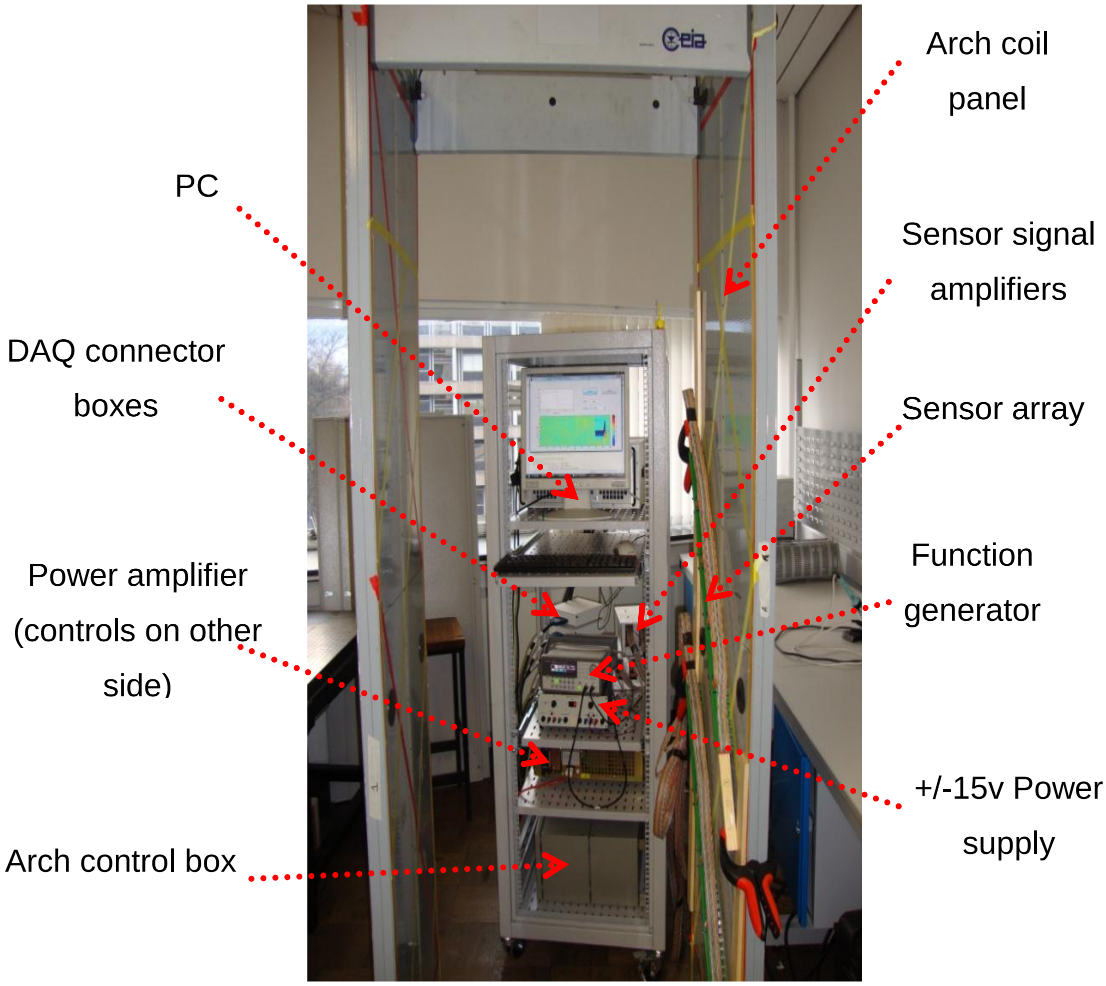

Figure 3.14: System set up in the Lab.

3.3 Electromagnetic Signal and Data Processing

Different metallic objects were used during the conduction of the experiment, observing the reaction of the system to a threat items (i.e. guns and knives) and non-threat items (i.e. mobile phone, keys, etc.). The resultant EM signals measured by GMR sensors during the presence of object in the system are organized as a two-dimensional array to be used for image processing purposes. In order to detect the response of any concealed weapons, powerful signal processing algorithms that accurately extract the target signature are required. The proposed system configuration consists of the existing walk-through system with a sensor-array consisting of 80 sensors, connected to the data acquisition hardware. Signal processing scripts have been written in MATLAB and integrated into GUI, in order to develop the prototype system towards a fully operational system. The following subsections discuss the processing of the received EM signal, as well as the GUI specification.

3.3.1 Investigation of selected feature maps

Different EM field visualisation techniques in conjunction with pulsed excitation have been studied. The minimum value of each sensor response is considered as an offset. Figure 3.15 shows the typical sensor response, both with and without this offset. The mean signal level (V_{DC}) is calculated with the offset included as shown in Figure 3.15a. This method of quantification is affected by both static fields, as well as the variation in pulse amplitude. Alternatively, the offset value requires to be removed before calculating V_{PEAK} and $V_{RMS,}$ in order to obtain the equivalent responses from all sensors, as shown in Figure 3.15b.

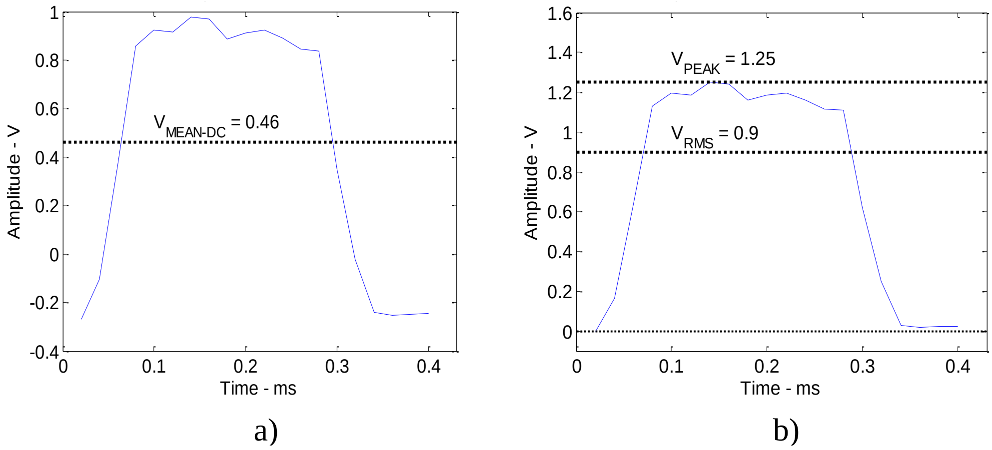

Figure 3.15: Quantification of signal level for: a) Offset-included *mean* calculation, and b) Offset-removed *peak* and *RMS* calculation

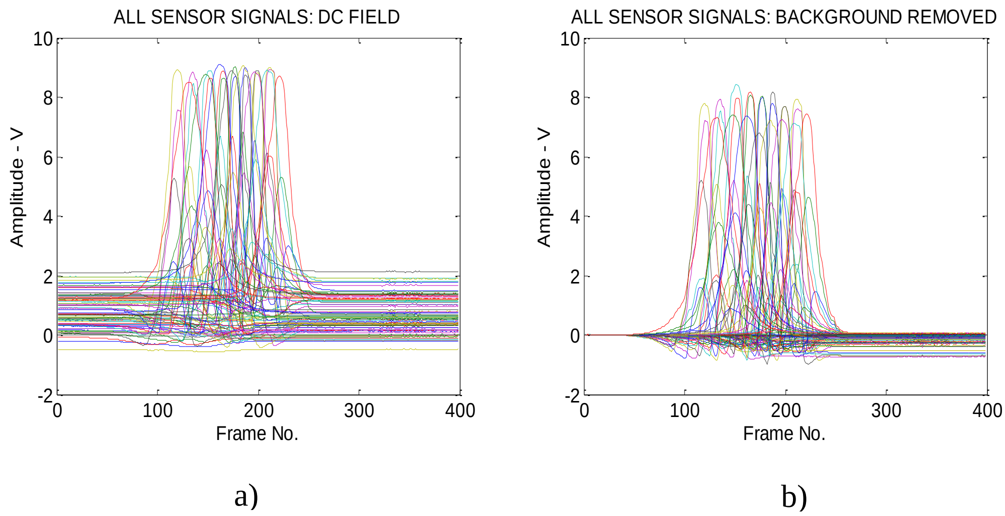

Figure 3.16: V_{DC} feature signals: a) Raw signals for all 80 sensors, and b) Signals for all 80 sensors with background field subtracted

The process shown in Figure 3.15 produces a matrix with 40 or 80 channels (depending if 40 or 80 sensors are used), with one sample (V_{DC}, V_{RMS} and V_{PEAK}) for each pulse. The result of V_{DC} feature is shown in Figure 3.16a. In order to obtain only the back-scattered field of the object being detected, the back-scattered field response without the target presence is subtracted from the responses obtained when the target is presented. This method cancels out most of the effects of the surroundings, which makes way for the next stage where the background field is subtracted from the result. As no object is in the array at the start of the test, the first few readings are taken as the background field. The average value of these first few readings for each sensor is subtracted from the signal, resulting in the signal shown in Figure 3.16b.

The 2D array sensor configuration for the initial test required that the signals to be reorganised, forming a series of images (one image for each of the original pulse repetitions) and a 2D spline interpolation of the image was used to increase the resolution of the image. It was observed during the comprehensive test for the system that the (V_{DC}) feature map produces the lowest noiseless signature results of objects. Figure 3.17 shows the three feature map images for the keys sample. The location of the object under test is marked in the figure with a black rectangular frame.

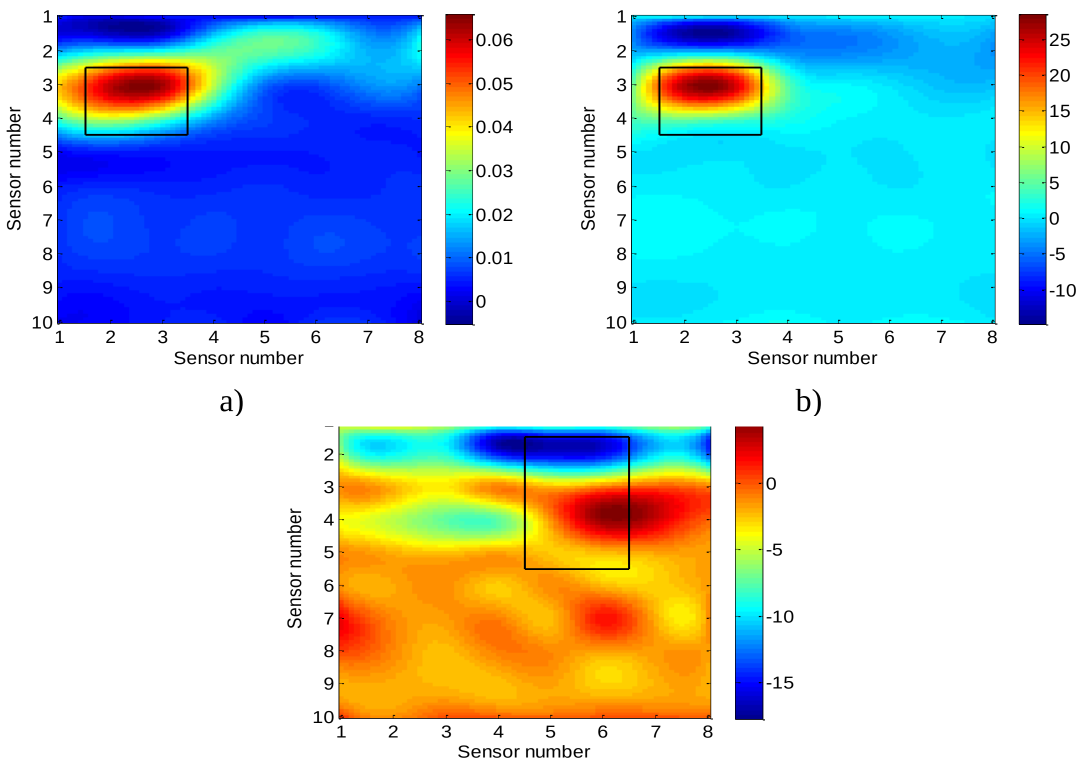

Figure 3.17: Three feature map images for keys sample only: a) V_{DC} image, b) V_{RMS} image, and c) V_{PEAK} image.

3.3.2 Max-value image formation

After the single column sensor-array configuration was adopted, a new feature map for image formation method was used. In this type of image construction, the maximum value of each signal measured by the GMR sensors during the presence of object in the system was captured and recorded (versus time) as follows:

1. The object under inspection is moved through the detector with data being acquired at 125000 sample/sec and an excitation pulse repetition rate of 500Hz (Figure 3.18a).
2. Sets of 10 pulse responses are averaged to produce a single pulse response signal (Figure 3.18b). (Each pulse response equivalent to 250 samples, so 10 pulse responses equivalent to 2500 sample).
3. A single value is computed from each previously computed pulse response signal (Figure 3.18b). The maximum value of the difference signal (with and without object) was used.
4. Each of these single values corresponds to a single pixel in the final image (Figure 3.18c).

Over the time, the EM field distribution of the object can be determined, as the object moves through the array, and consequently the object can be identified. When 40 sensors were used, the EM images dimensions will be 40*140 pixels. The 140 reading-values were found to be enough to capture the response of an object that passes through the proposed system.

Figure 3.19 shows some samples used to test the system and their constructed max-value images using the 40 diagonal sensor-arrays. The images were scaled for the display to show the details, the colour scale represents the change in magnetic field intensity. It was also observed that there was alternate dipole colour orientation in constructed image so that the red colour represents the positive increase and the blue represents the negative increase.

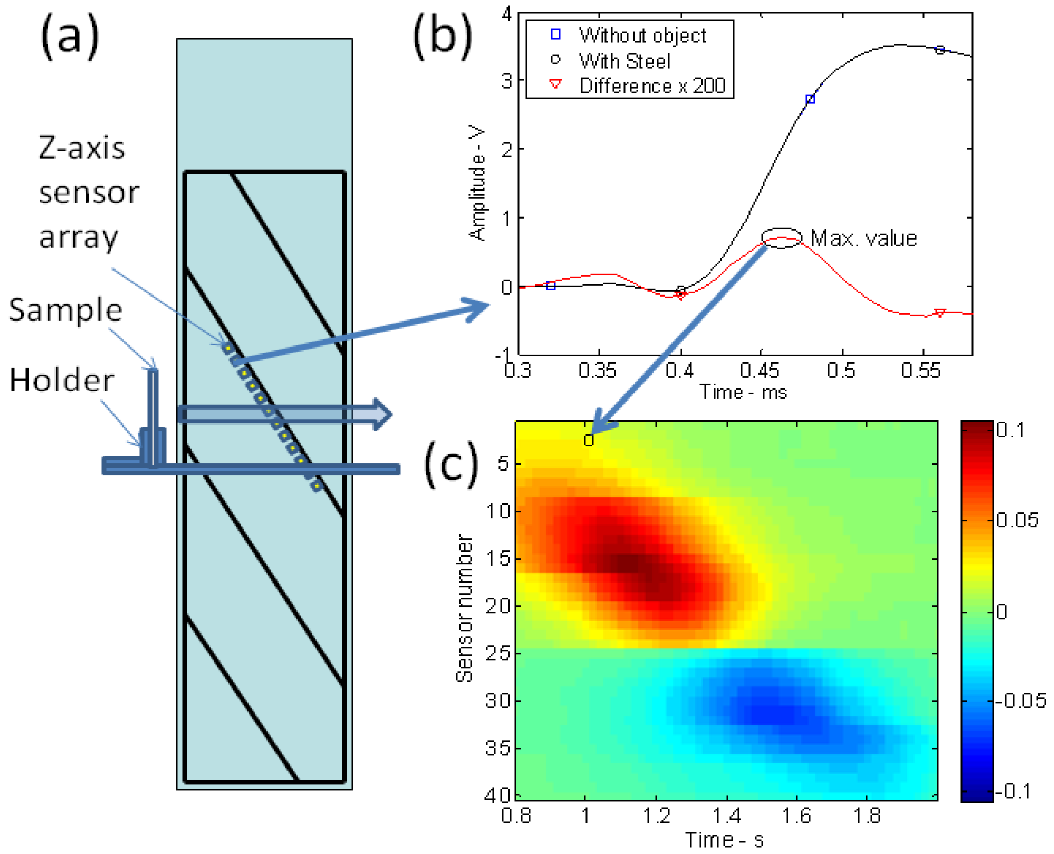

Figure 3.18: EM image constructed from data acquired from line array over time.

Replica Gun	Kitchen Knife	Hunting Knife	Mobile Phone	House Key	Scissors

(a)

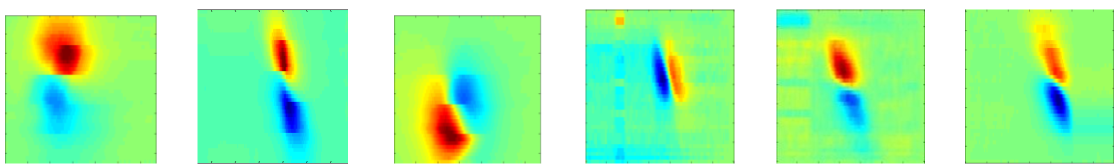

(b)

Figure 3.19: Some samples used to test the system and their constructed max-value images using the 1D diagonal sensors array: a) Samples in the holder. b) The equivalent EM images formed using 40 sensors.

3.3.3 Transient response images formation

In order to extract more information about the objects in the WTMD from the test results, a form of transient analysis was employed. It has been observed that aluminium objects exhibit a tendency for the EM signature to appear later in the image sequence, increasing in intensity over time. In contrast, the EM signatures corresponding predominantly to ferromagnetic objects (such as the hunting knife used in our database) have a tendency to appear earlier in the sequence, peak in amplitude at a particular point and to change in distribution field over time.

In this formed transient EM imaging technique, the pulse response from each sensor is analysed and chopped into sections, or time slots, as shown in Figure 3.20a. The values of the samples in each time slot are averaged using the data from all sensors for the whole test. Finally, an image is built up for each time slot using the average value of each slot, instead of the maximum values, and represented as pixels in the final images.

This procedure can be summarised as follows:

1. The object under inspection is moved through the detector with data being acquired at 125000 sample/sec and an excitation pulse repetition rate of 500Hz.
2. Sets of 10 pulse responses are averaged to produce a single pulse response.
3. The averaged pulse response from each sensor is analysed and chopped into sections, or time slots, as shown in Figure 3.20a.
   It was observed that the pulse rising edge is enclosed between the 44th and 72nd samples, distributed over 28 samples. Each time slot was chosen to be two samples, therefore 14 time-slots were made.
4. A single value was computed from each pulse response, which was the average of the samples in each slot of the difference signal, with and without the object.
5. Each of these single values corresponds to a single pixel in the final image for a particular time slot. Fourteen images were made for the fourteen time-slots values of all sensors as shown in Figure 3.20b.

Figure 3.20b shows a sequence of these transient images for the hunting knife. Analysis of the transient image sequence can be used to extract more information about the object under examination.

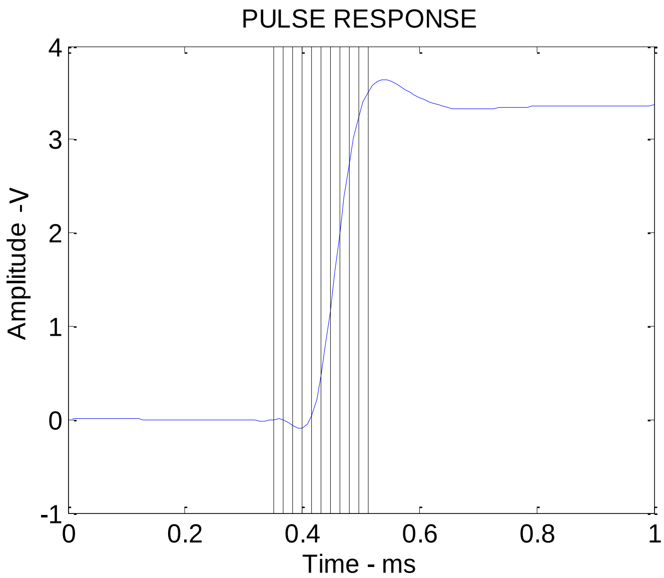

a)

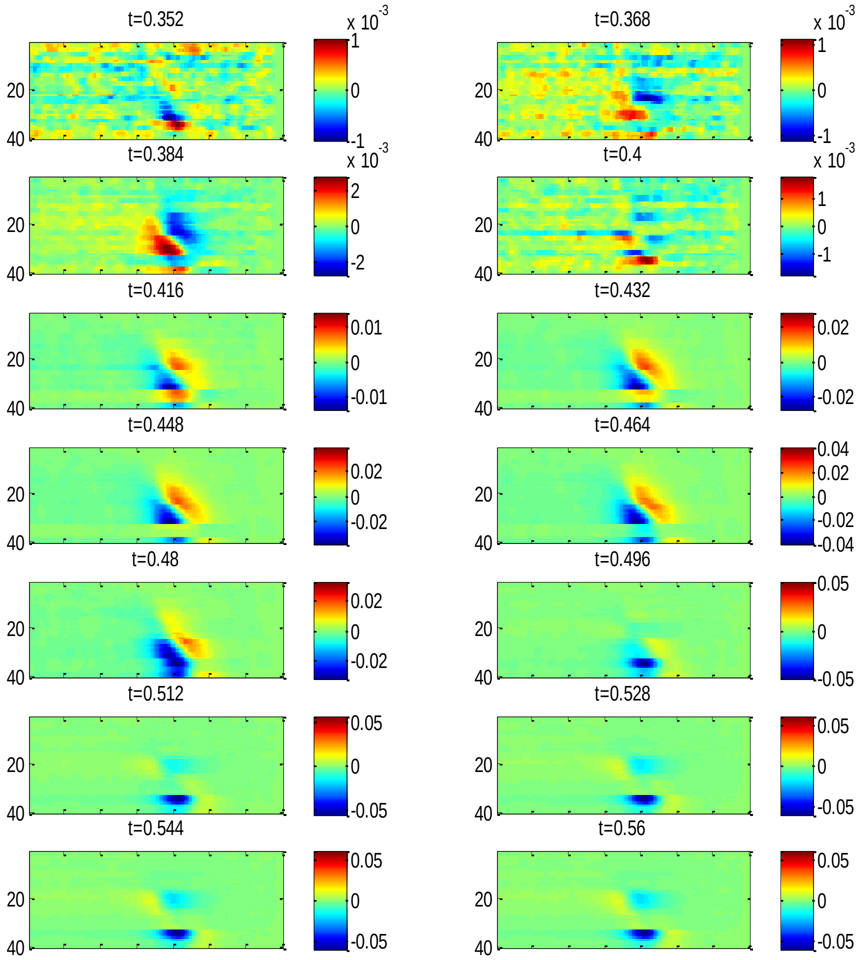

b)

Figure 3.20: A sequence of transient images for the hunting knife sample: a) Pulse response with time slots marked, b) Transient response imaging result.

3.4 Guide User Interface of the System

The basic GUI shown in Figure 3.21 has been developed to ease: data acquisition, response viewing, and parameter settings for the threat object detection system. It features:

1. First axis showing the raw signal from one of the sensors.
2. Second axis showing the processed image from the array.
3. A place to enter the desired gain of the system (i.e. sensitivity adjustment that should be fixed for certain system setup and coil power).
4. A drop-down menu to determine the type of analysis to apply to the raw data to produce the image, i.e. DC, Peak, and RMS.
5. A start button; initialises the data acquisition routine and starts acquisition.
6. A stop button; stops data acquisition and clears all the active data acquisition objects.

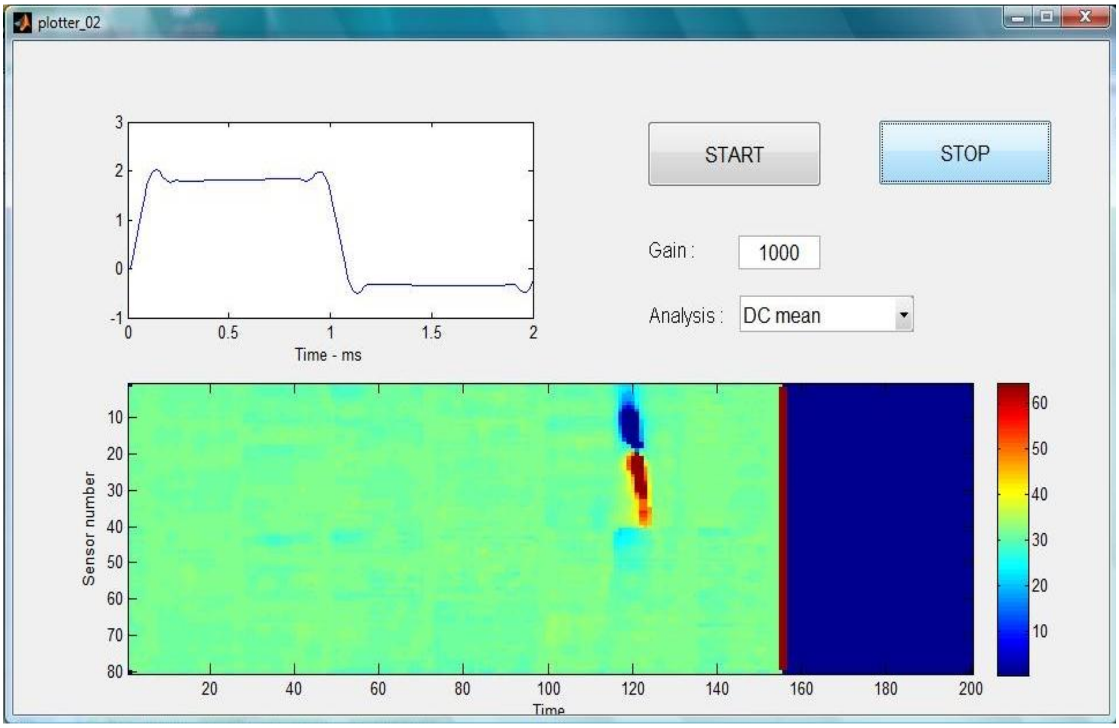

Figure 3.21: The basic GUI for the system

The second axis were set to suppress noise data, until the user press the START button (show as dark blue part in Figure 3.21). When START is pressed, a red line is drawn vertical along the x-axis to indicate the start of recording pass. The recording pass involves a short period of signal recording, prior to the introduction of the object, to estimate the background noise when then object is moved through the system. The object moves through the system over a period of 1~3 seconds, which is equivalent to pedestrian normal walking speed [129]. As the object moves through the system, the second axes begins appending new information to the left of image, removing the oldest information from right so that only the recent 200 program iterations are displayed. The captured image will appear sliding from left to right. As previously highlighted, 140 iterations were found enough to cover the object response, so generated images of 140*N pixels will be used in subsequent image processing in the next chapters, where N is the number of sensors used. For further details refer to the system manual in Appendix A.

3.5 Summary

The design methodology and configuration of the new system have been presented in in this chapter. The new system has been designed with maximum flexibility, with a variable sensor-array pitch and configuration and variable excitation in terms of signal waveform and amplitude. Tests have been carried out using pulsed excitation and it has been concluded that pulsed excitation in conjunction with advanced time-frequency analysis and signal shape analysis has the greatest potential for object detection, characterisation, localisation and imaging.

The CEIA walkthrough arch, donated by the London Metropolitan Police, was used to form the infrastructure of our new design. A thorough investigation of this arch has been undertaken, to ascertain: the mode of operation, excitation and pickup coil configuration and signal processing techniques. The new system has been designed around the use of GMR sensor (AAL002-02 NVE) arrays in conjunction with pulsed excitation.

An optimum sensor-array design is achieved by the adjustment of: 1) number of the sensors which is either one sensor-array consist of 40 sensors or two sensor-arrays consist of 80 sensors; 2) space between these sensors which is 15mm sensor spacing in the array that gave the best balance between spatial resolution and system complexity; 3) position and direction of the sensor-array in terms of the coils or pulse excitation, the diagonal sensor-array that is aligned above the coil configuration was found to give better results. Pulsed excitation is applied to the coil, owing that the pulsed excitation provides the opportunity to apply an interrogating field with a rich frequency components in a single waveform.

To achieve the best visual detection of the object, different statistical characteristics of the response signals were studied. A novel formation of reconstructed images has been developed and called: max-value image formation which use a simple average and select the maximum value techniques, and transient response images formation which involving the generation of a transient image sequence, which is used to extract further information about the object under examination. When 40 sensors were used, the 140 reading-values were found to be enough to capture the response of an object that passes through the proposed system therefore; the dimensions of the reconstructed images will be 40*140 pixels.

A prototype user interface was developed, encompassing: signal pre-processing, the necessary software to isolate the response signals, management of the data acquisition, parameter setting, and image reconstruction. The chapter conclude that magnetic field imaging could be used to detect and identify a metallic objects. In comparison with conventional induction based WTMDs, the GMR array based system has shown great potential in object identification and discrimination.

Chapter 4: System Validation and Experimental Testing for Threat Object Detection

The key to a successful detection of threat objects, such as guns and knives, is an effective detection system with high resolution and high dynamic range. The detection system should be efficient and safe for human as possible, having less distortion in the pulse transmission/ reception, and be directive with high-radiation efficiency. The previous chapter detailed the proposed EM imaging system according to: GMR sensor fusibility study, design and implementation of the proposed system, and the use of different signal and data processing methods on the resultant signal from the system. In order to validate the system for detection, characterisation and classification of objects using EM signatures, this chapter aims to study the capability of the new system in terms of detection and identification of threat and non-threat items. Tests are carried out within a controlled environment (object placed in sample holder) and uncontrolled environment (an object concealed in clothes of a person passing through the WTMD). The following sections also discuss the data validation and repeatability of the similar type objects, robustness against object orientation, and system capability for multiple object separation.

4.1 Real Handgun Detection

A selection of six handguns was borrowed from the London Metropolitan Police to investigate the EM response from a variety of real threat items. The specifications of the handgun samples are listed in Table 4.1 and pictured in Figure 4.1

Table 4.1: Specification of the real handguns used

Sample #	Description
1	Small revolver – 0.38” Smith & Wesson – Deactivated.
2	Revolver – 0.38” Enfield service revolver – Deactivated.
3	Large automatic – 9mm Glock G17 – Live.
4	Large automatic – 0.45 Colt M1911 – Replica.
5	Small revolver – Brocock Puma air pistol – Live.
6	Small automatic – 7.65mm Walther – Deactivated.

The test samples are representative of a range of weapons which would be of interest for detection. The composition of the weapons includes steel, zinc alloy, aluminum, and polymers. A single diagonal sensor-array configuration (as explained in Chapter 3) was adopted for the tests. Experimental setups and follow-on results with the real handguns are detailed in the following subsections.

Sample 1 Sample 2

Sample 3 Sample 4

Sample 5 Sample 6

Figure 4.1: The six samples used in the tests

4.1.1 Controlled/uncontrolled experiments setup

Controlled experiments tests were carried out using the apparatus depicted in Figure 4.2. The apparatus consists of:

- The holder (see Figure 4.2a) that holds each sample in a constant position as it is moved past the array.
- The platform, which is fixed between the panels to ensure that the sample maintains a constant horizontal position with respect to the array and the panel.
- The ramp (see Figure 4.2c), where the sample is moved down the ramp (in the holder) past the array.

Figure 4.2a shows the array configuration and the relationship between the array and the samples, while Figure 4.2b shows the weapons in the sample holder constructed for the tests. The holder is configured to ensure that the samples retain a constant and comparable distance and orientation with respect to the array during each pass through the system. Figure 4.2c shows the ramp position in respect to the sensor-array, which will allow the sliding of the holder with the sample to be passed through the WTMD. The apparatus is designed so the sample can move past the array in 10cm increments with respect to the panel as shown in Figure 4.2d.

Additionally, uncontrolled tests were carried out by concealing object within clothes of an individual. The individual was then directed to walk at normal walking speed through the arch of the proposed system. Figure 4.3 depicts the uncontrolled test with an object being concealed under raincoat jacket.

To emulate the situation in a secure area like an airport, the following procedure was adopted in subsequent tests:

1. No restriction to the distance of the object from the sensor-array was imposed. However, the distance would be less than 1.0 meter, as this is the width of the WTMD.
2. The individual was carrying the samples in different bodily locations, i.e. upper and lower body.
3. Another important aspect was that the walking speed of the individual was neither restricted nor measured. However, as stated previously, the individual was allowed to walk freely.

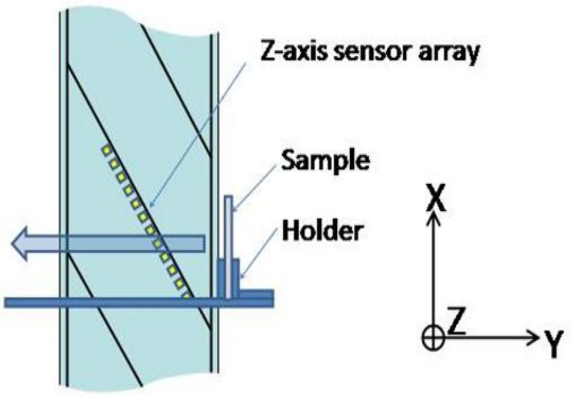

a) b)

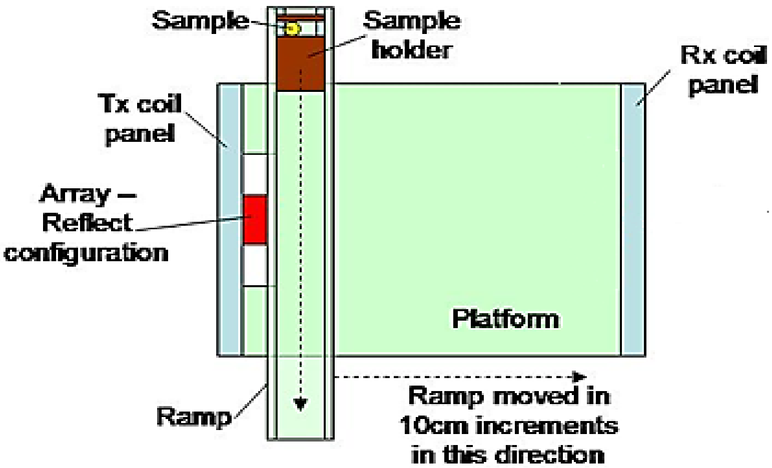

c)

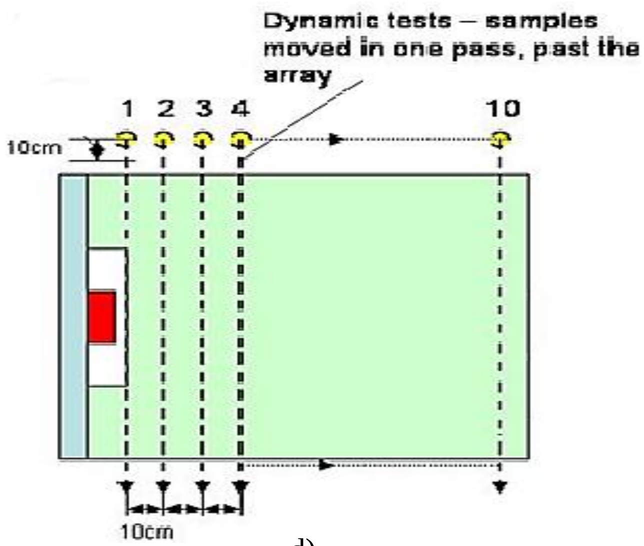

d)

Figure 4.2: Controlled experiments test set-up: a) Sensor array configuration, b) The handgun in the sample holder, c) Schematic top view of the WTMD with holder, and d) without holder showing the selected separation distances between the sensor-array and the object.

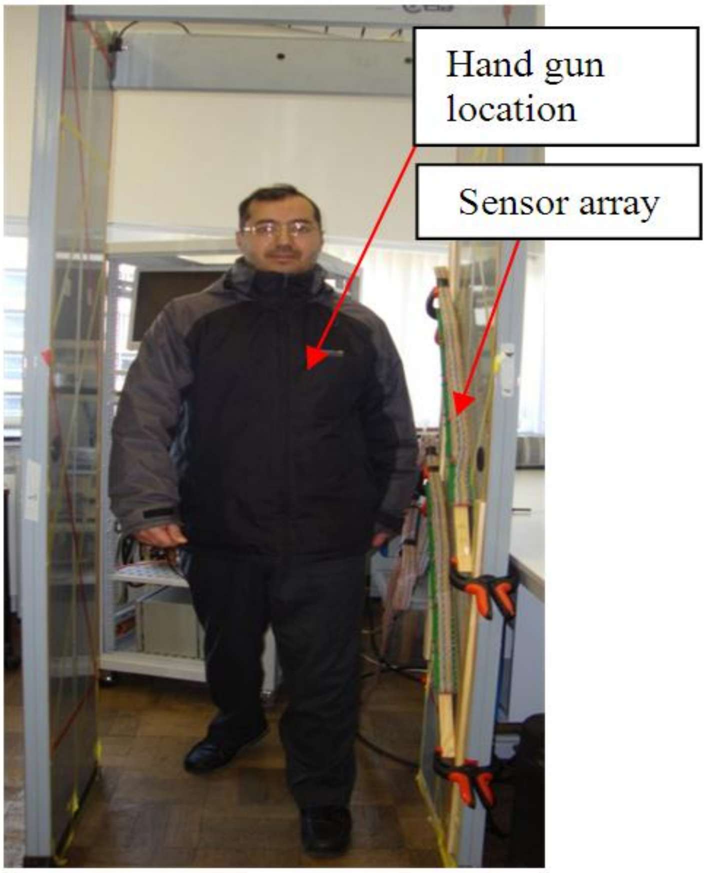

Figure 4.3: Walking through the proposed system arch in an uncontrolled test.

4.1.2 Handgun detection in controlled environment

Using the gun samples previously highlighted, several tests were undertaken with objects being placed at distances of: 100mm, 150mm, 200mm, 250mm, 300mm and 350mm from the excitation panel.

Results for the 100mm test are shown in Figure 4.4 and appear to set an acceptable baseline, as would be expected for the controlled test set-up, with a characteristic “dipole” signature being evident in most cases for a metal mass. The one exception is sample 4, the replica gun, which is very difficult to locate from the test results, having the lowest amplitude response and therefore the poorest signal to noise ratio. It is notable that samples 2 and 3 give similar results, responding with a type of dipole distribution, indicative of a ferromagnetic object made predominantly from a single type of metal. The simple form of the distribution also indicates that there is a very little metal in the handle of these objects, and the array sees them as a simple tube/block of metal.

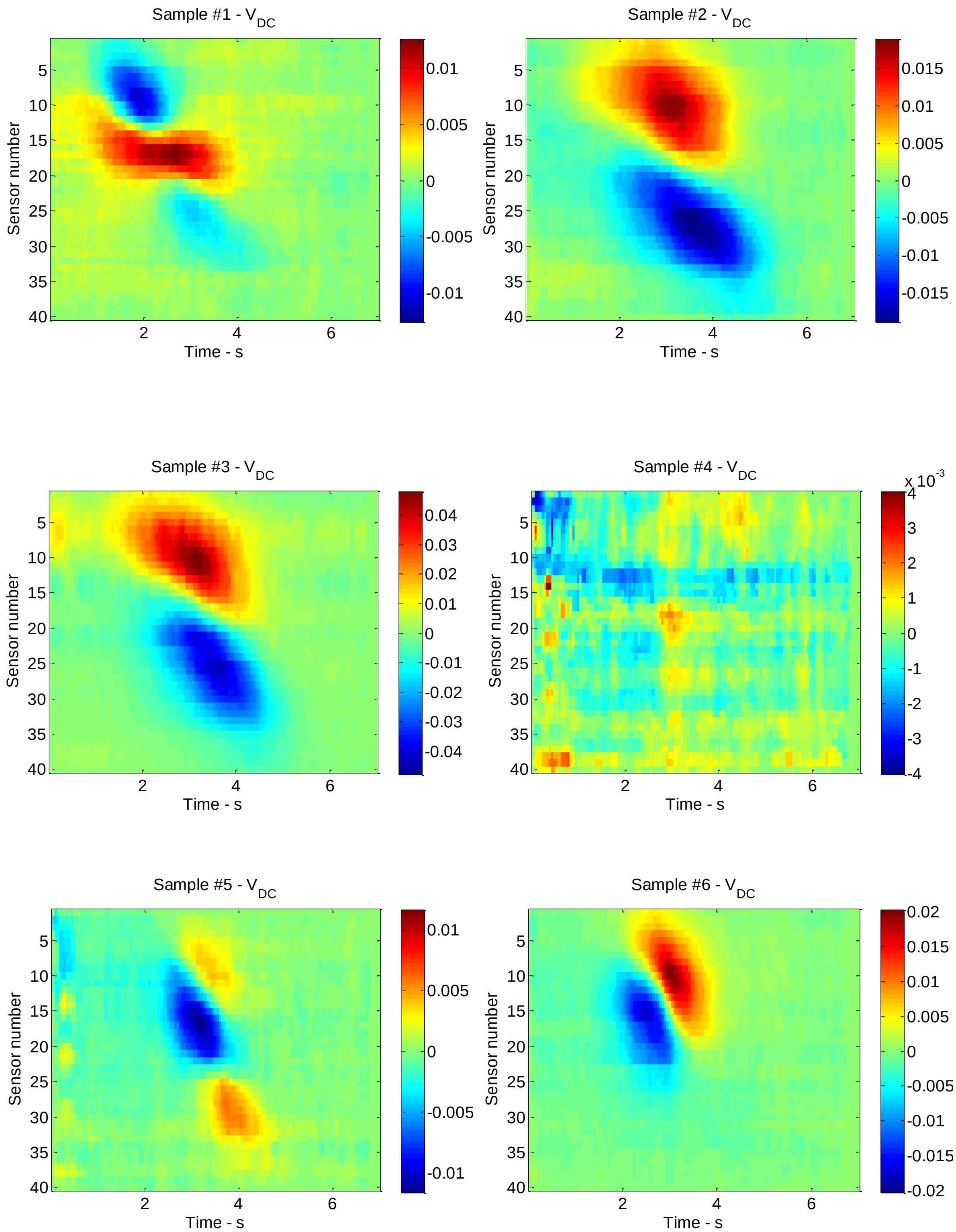

Figure 4.4: Feature maps (EM images results) for all samples, for tests using the sample holder.

4.1.3 Handgun detection in uncontrolled environment (walk-through tests)

Another set of tests for the uncontrolled walk-through simulations, using the same real handguns as used in the previous section. The guns in this test are carried in the inside jacket pocket of an individual walking through the arch, as shown in Figure 4.3 with test results provided in Figure 4.6. The EM images for the objects are clearly compressed along the x-axis in comparison to the controlled tests. This is due to the object moving through the arch at a greater speed, albeit the actual distributions remain very similar.

4.1.4 Difference between controlled and uncontrolled test

To give clear view in respect of the differences between the two previous cases, Figure 4.5 shows EM images for sample 3 for the controlled and walk-through tests using a sensor-array with 40 sensors. The results from the walk-through test have been expanded along the horizontal axis and compared to sample 3, as shown in Figure 4.5 to aid in comparison. The comparison of the plots show that although the controlled and walk-through tests do not give identical results, the general form of the EM signatures are very similar. Thus, using appropriate analysis techniques, it could be ascertained that the signatures are from similar, if not the same object.

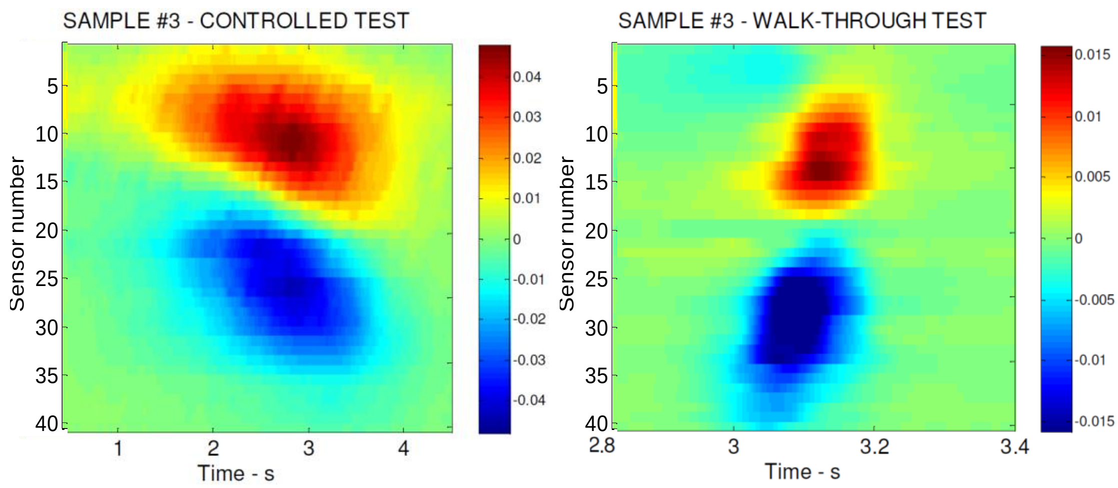

a) b)

Figure 4.5: EM images for Sample #3: a) controlled and b) Non-controlled tests.

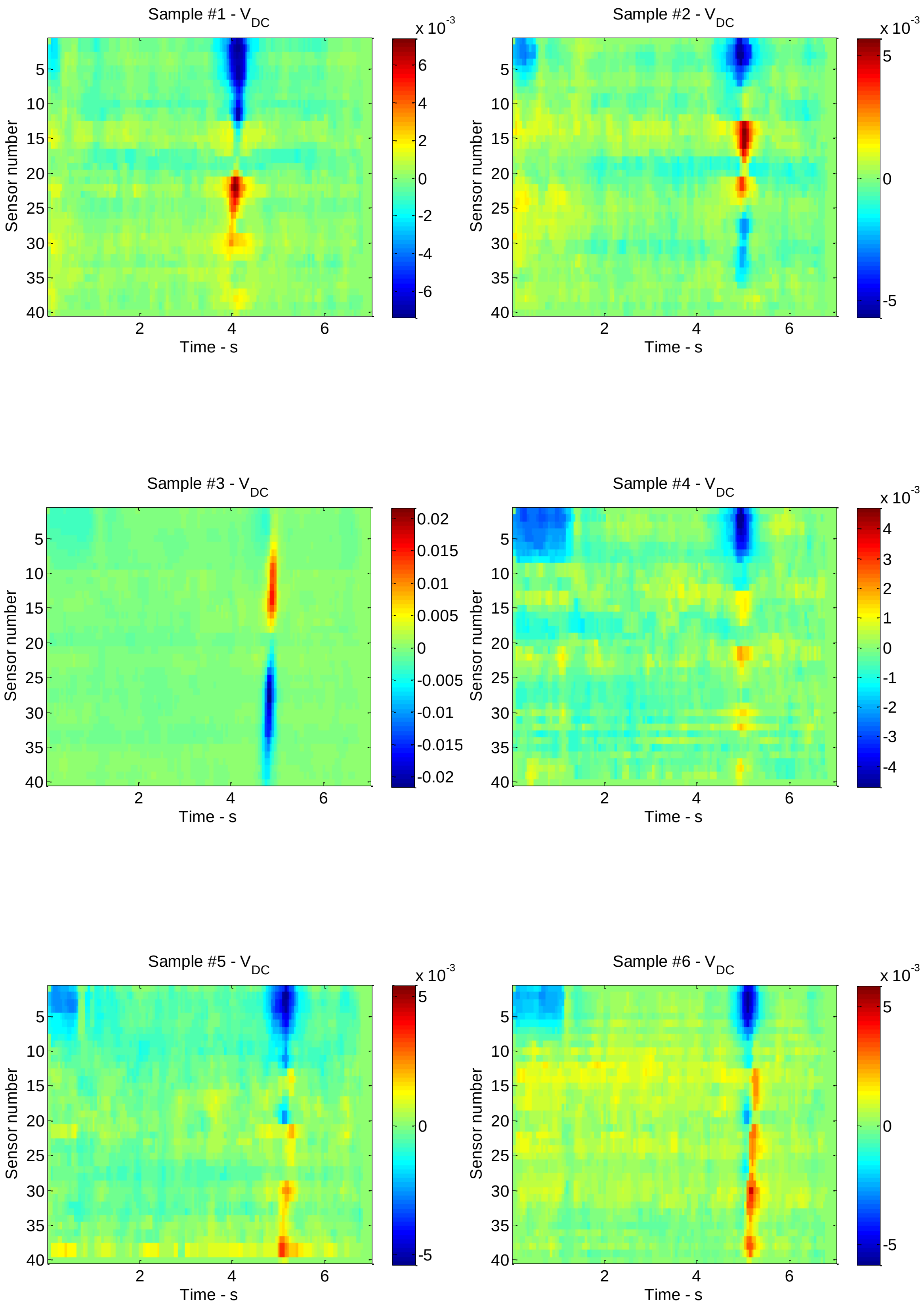

Figure 4.6: Results for all handguns, from the non-controlled walk-through test.

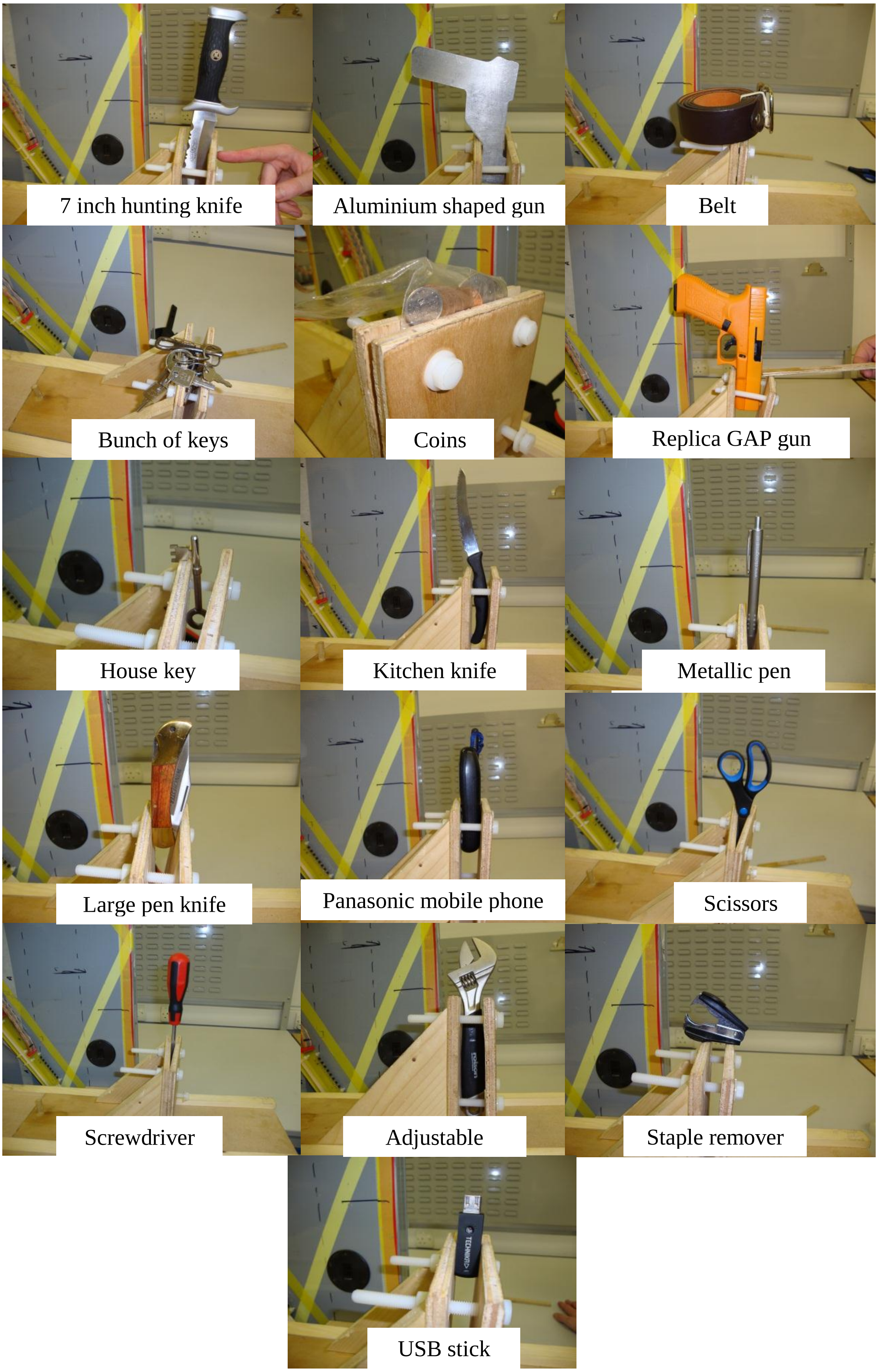

Figure 4.7: Threat and Non-Threat objects used.

4.2 Daily used Objects Detection

In order to examine the new system upon other objects, including items normally carried by members of the public, a series of tests were set up using the same diagonal array configuration. More than 16 common daily used items have been investigated. Figure 4.7 shows the objects that were used in this test.

The objects represent a combination of small objects typically carried by members of the public (coins, USB stick, mobile phone, etc.), larger ferromagnetic objects which may possibly be carried by members of the public and have the potential to be identified as threat objects (screwdriver, spanner, large bunch of keys) and actual threat objects (kitchen knife, pen knife, 7″ hunting knife).

The objects are moved past the array dynamically and data acquired with the object inside a holder. The tests were repeated for controlled and uncontrolled environments, as discussed in previous section.

4.2.1 Daily used objects in controlled environment

The test was done using the same set up for the handguns. Some of the resulting EM images are shown in Figure 4.8.

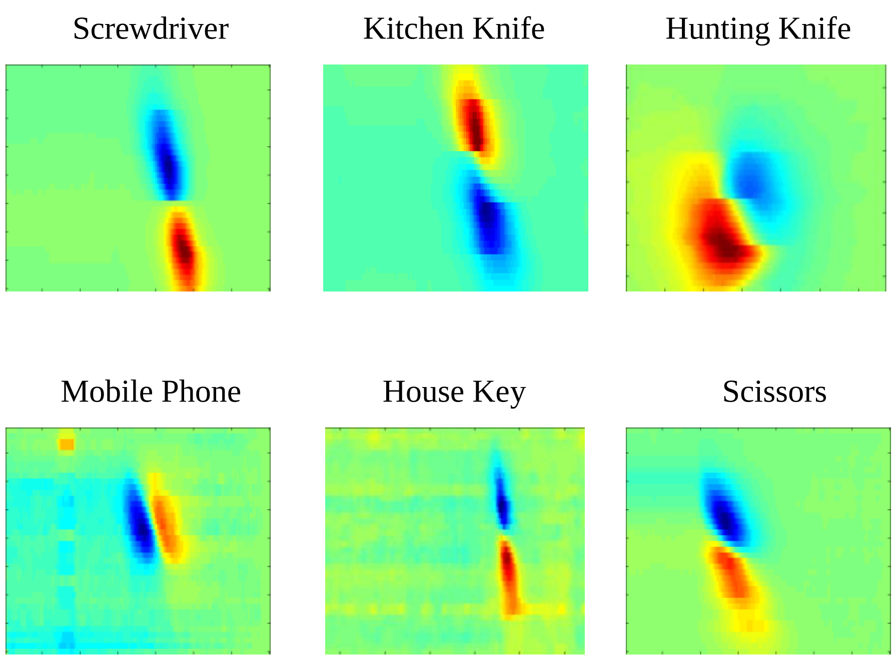

Figure 4.8: EM images results for some daily used items.

Calculations of feature amplitude have been undertaken. Figure 4.9 presents plots of the peak-to-peak amplitude of the three feature maps processing (as detailed in Chapter 3, section 3.3), corresponding to the objects.

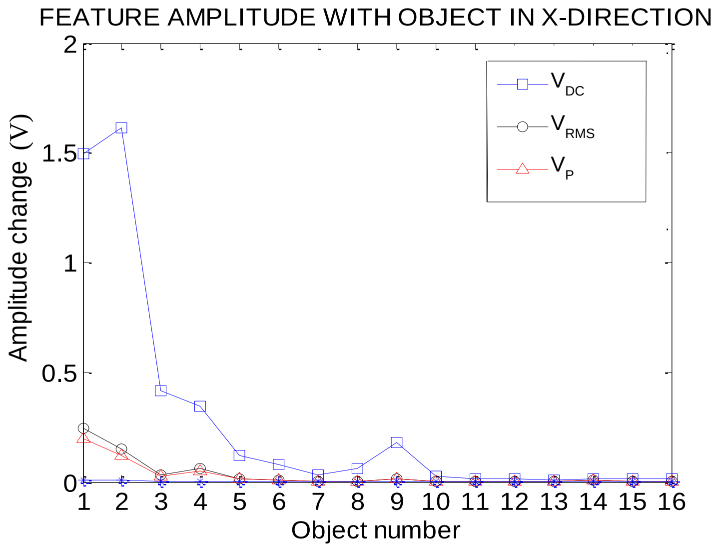

Figure 4.9: The peak-to-peak amplitude for the three feature maps

The objects are numbered in descending order according to the peak-to-peak amplitude as follows:

1. Kitchen knife
2. Screwdriver
3. Large pen knife
4. 7 inch hunting knife
5. Replica GAP gun
6. Single house key
7. Adjustable spanner
8. Scissors,
9. Panasonic mobile phone
10. Bunch of keys
11. Pen
12. Small bag of coins
13. Belt
14. Staple remover
15. Gun shaped aluminium
16. USB stick

It is interesting to note that the "threat objects", i.e. the knives and the replica GAP gun are within the highest amplitude objects, as are the larger other daily used objects, i.e. the screwdriver, spanner and scissors.

4.2.2 Daily used objects in uncontrolled environment (walk-through tests)

In order to assess the capabilities of the system for the detection of items in an unconstrained environment, a test was configured in the lab, where the objects were carried in the jacket pocket of an individual walking through the array, rather than mounted within the sample holder.

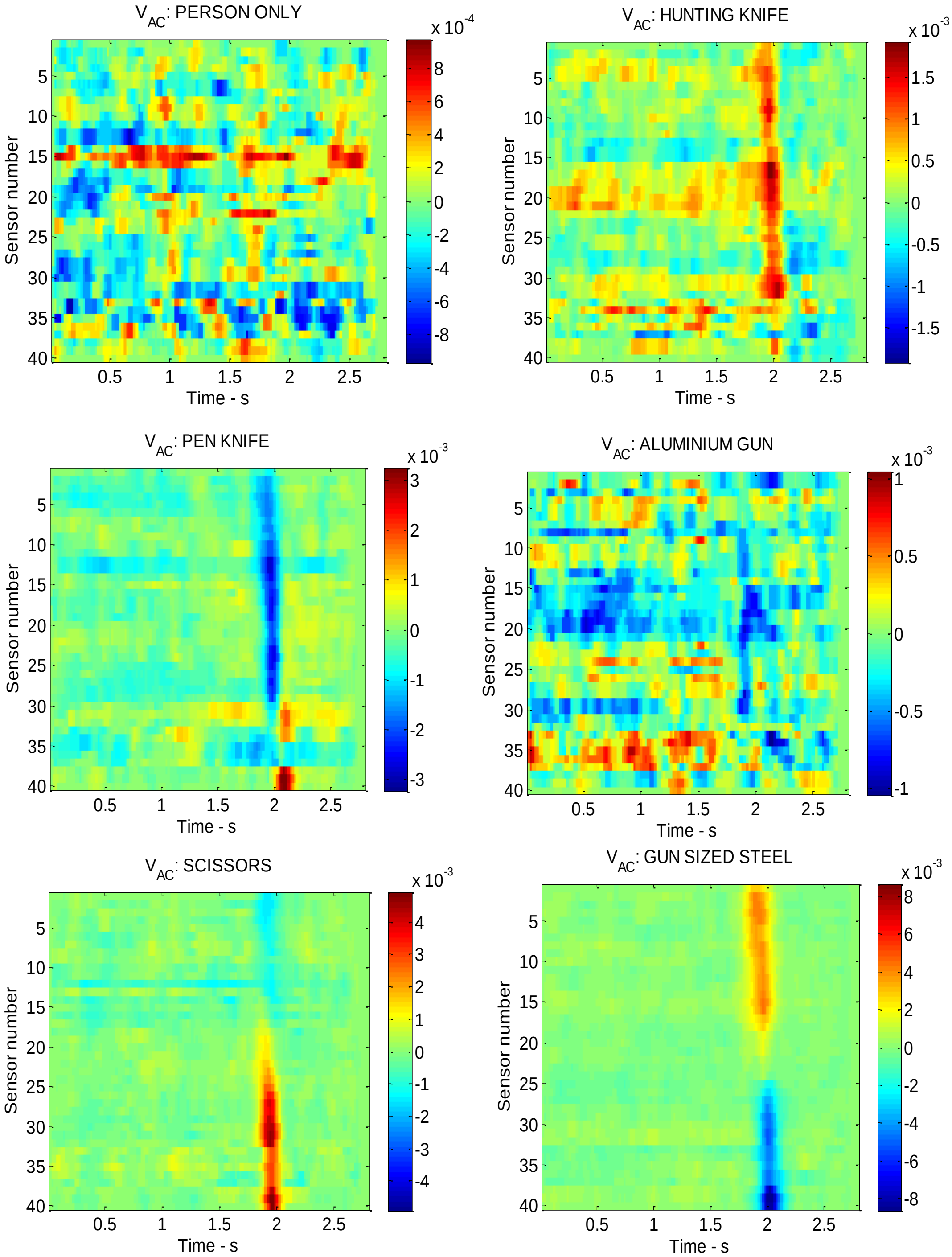

Figure 4.10: Results of tests for various objects passing through the system in an unconstrained environment.

In addition to previous items, a steel block with approximately the same size and weight as a real handgun was used in order to provide an object that would respond in a similar way to a real firearm. Figure 4.10 shows the results of the tests for a selection of objects. It can be seen from the test results that similar to previous tests, the ferromagnetic objects give the strongest signature.

Using a simple amplitude measurement for objects in an unconstrained environment, show that similar to the tests using the sample holder, the larger ferromagnetic objects give the strongest response, with the smaller non-threat objects and the predominantly aluminium objects giving a very low amplitude response as in Figure 4.11.

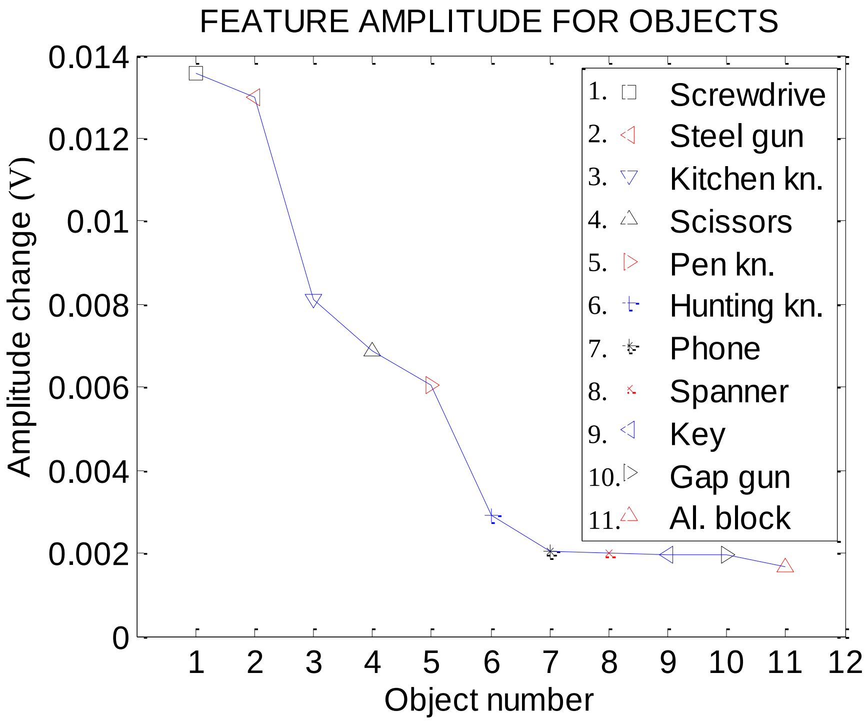

Figure 4.11: Feature amplitude for the unconstrained test

4.2.3 Difference between the controlled and uncontrolled tests

The results for the hunting knife and the scissors are shown in Figure 4.12, along with the results from the previous tests that were carried out with the objects in the sample holder for comparison. It can be seen from the plots that the EM signatures for the objects in an unconstrained environment remain very similar, i.e. strong a dipole distribution for the hunting knife and a single area with an increase in amplitude for the scissors.

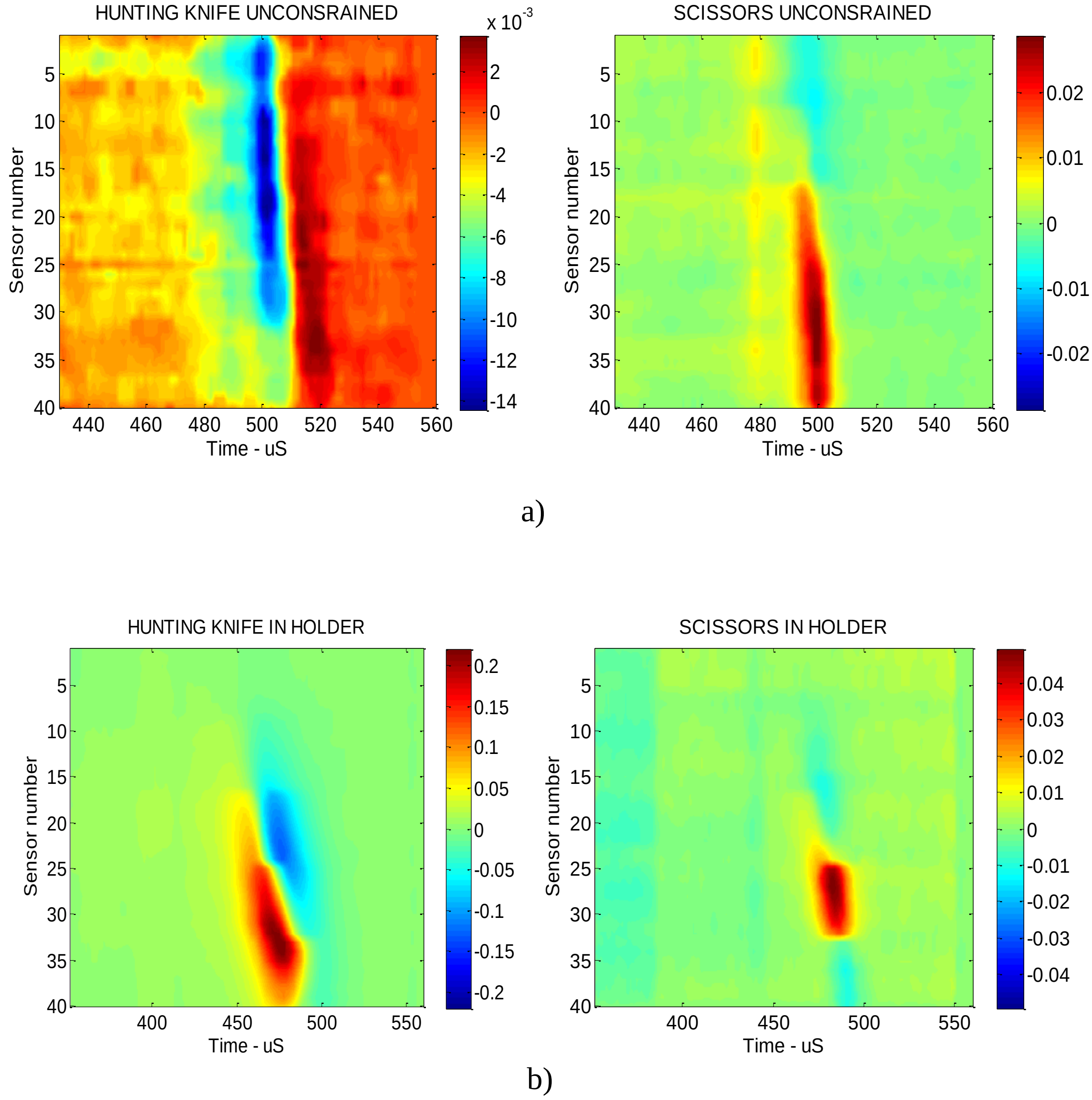

Figure 4.12: Results of tests for various objects passing through the system in: a) an uncontrolled (Walk-through) environment, and b) a controlled environment.

4.3 Sensitivity Measurements

Sensitivity of the proposed system to each object was measured as the peak to peak amplitude change of the resultant feature map. Figure 4.13 shows a plot of the sensitivity of the system to different samples. The sensitivity in respect of each object will always decrease with an increase of distance to the excitation unit. This effect needs to be quantified in order to ascertain the useful range of the system. It can be seen from Figure 4.13 that for sample 3, the object can still be detected at a distance of 60cm. It is also apparent that some of the other samples do not give such a good response and that maximising the detection range for these objects will require collaborating efforts from more than one sensor, in addition to appropriate signal processing algorithm to distinguish trivial changes in different responses, hence 40 or 80 sensors were used.

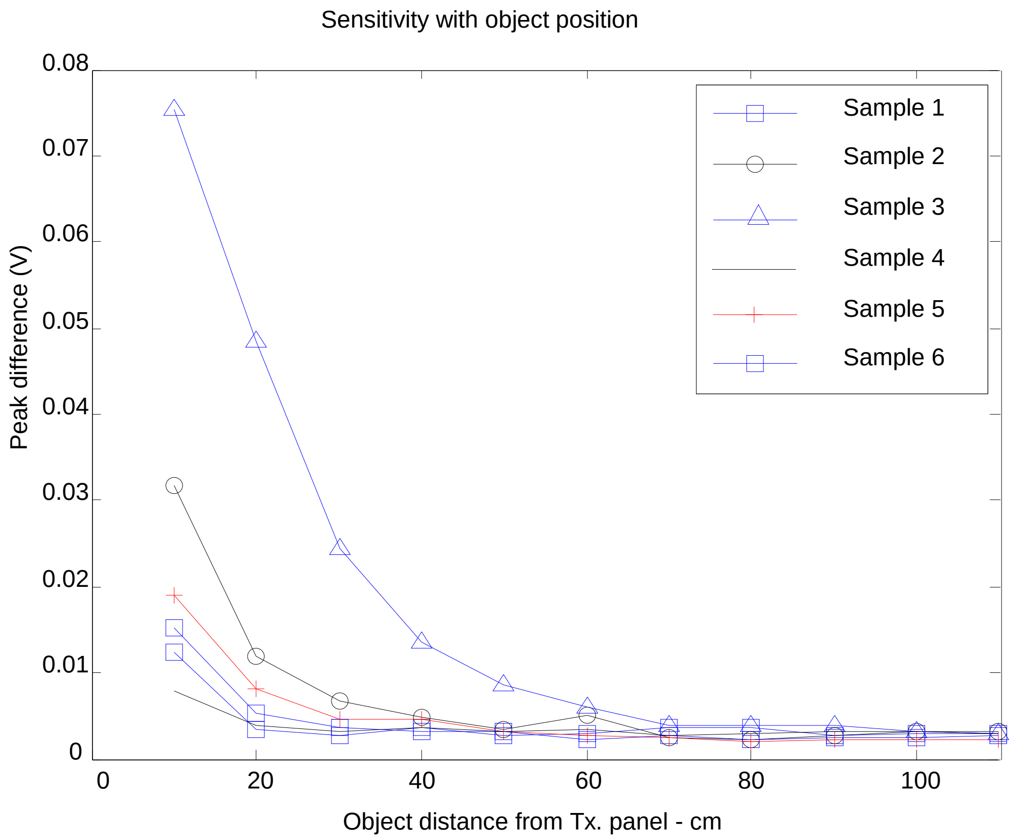

Figure 4.13: Sensitivity plot of variation in response with increasing distance.

4.4 Repeatability Measurements

Simple repeatability tests for the six handgun samples were carried out, where each sample was tested several times to check data validity, prior to the results being plotted. Figure 4.14 shows the amplitude change of the GMR signals for five repetitions (Rep.1 to Rep.5) of the test for all six handguns samples. It can be seen from Figure 4.14a that the controlled test has the greatest repeatability, yet the data trend is similar for the walk-through test also in Figure 4.14b, as would be expected.

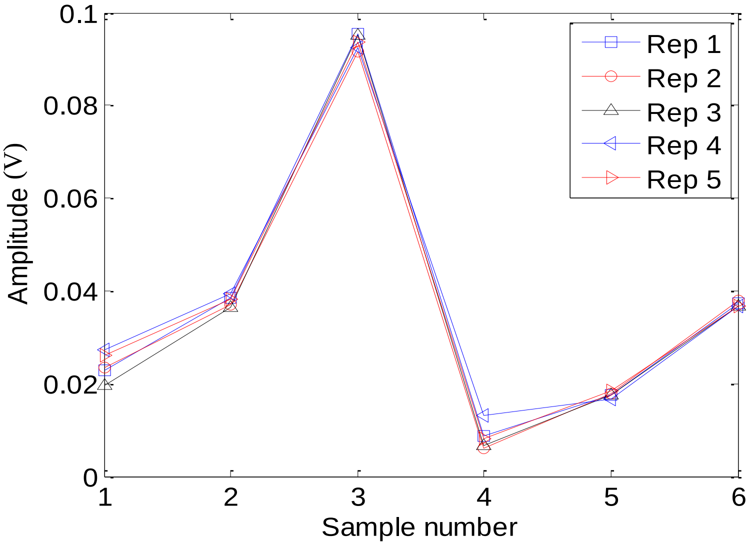

a) Controlled test

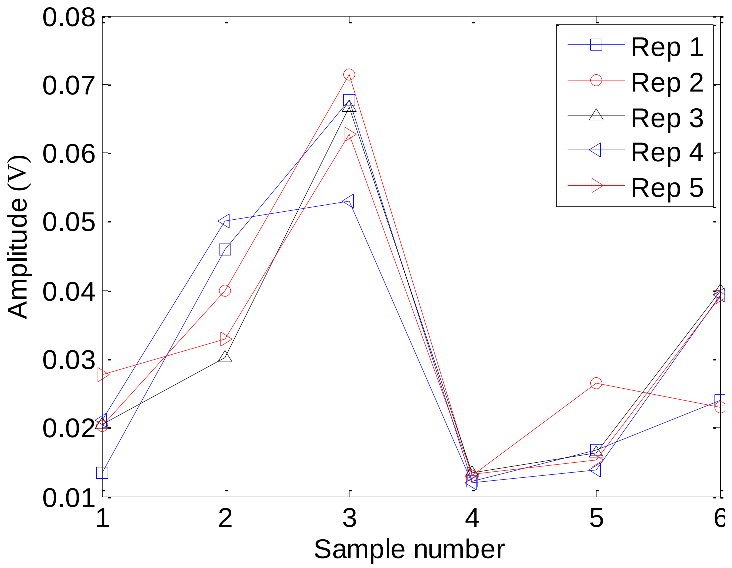

b) Walk-through test

Figure 4.14: Amplitude difference for five repetitions (Rep) of the test for the real handgun samples for: a) Controlled test, and b) Walk-through test.

4.5 Robustness Against Object Orientation

Another set of experiments were carried out to study the reflected signals from objects under different orientations, to check the validity of the proposed system. Figure 4.15a illustrates the test set-up for different orientations. The objects were moved past the array dynamically and data was acquired with the object moving. Data acquisition was undertaken with the samples orientated in three directions.

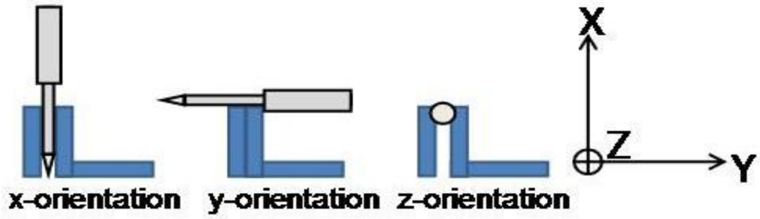

a)

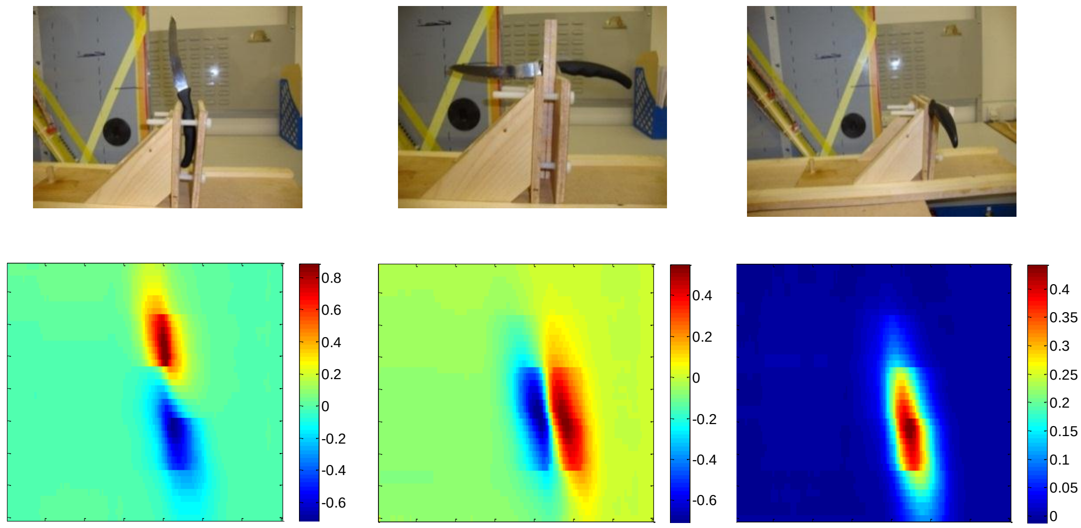

x-direction y-direction z-direction

b)

Figure 4.15: a) Test set-up for sample orientations. b) Kitchen knife sample in the holder along with their corresponding EM results.

The results for the kitchen knife are shown in Figure 4.15b. It can be seen from these images that the feature map follows a fairly predictable evolution with the rotation of the object; in the x-direction and y-direction the object appears as a dipole distribution, yet with the rotation of the distribution correlating to the rotation of the object. In the z-direction, only one end of the "dipole" is presented to the array, so a uni-polar distribution is observed.

A similar trend is followed by all of the objects, where the object appears as two peaks in the feature map. As the object is rotated, this distribution is also rotated from the x-directional image to the y-directional image. However, the z-directional image exhibits a clear uni-polar distribution.

Figure 4.16 presents the peak-to-peak amplitude of the feature maps, while Figure 4.17 presents the same information, but normalised for ease of comparison. It is interesting to note from the two figures, that the trend of the data is similar, irrespective of the orientation of the object, when 16 samples were used and numbered in descending order (as in subsection 4.2.1) according to the peak-to-peak amplitude, as the amplitude measurement is invariant of the object rotation/orientation.

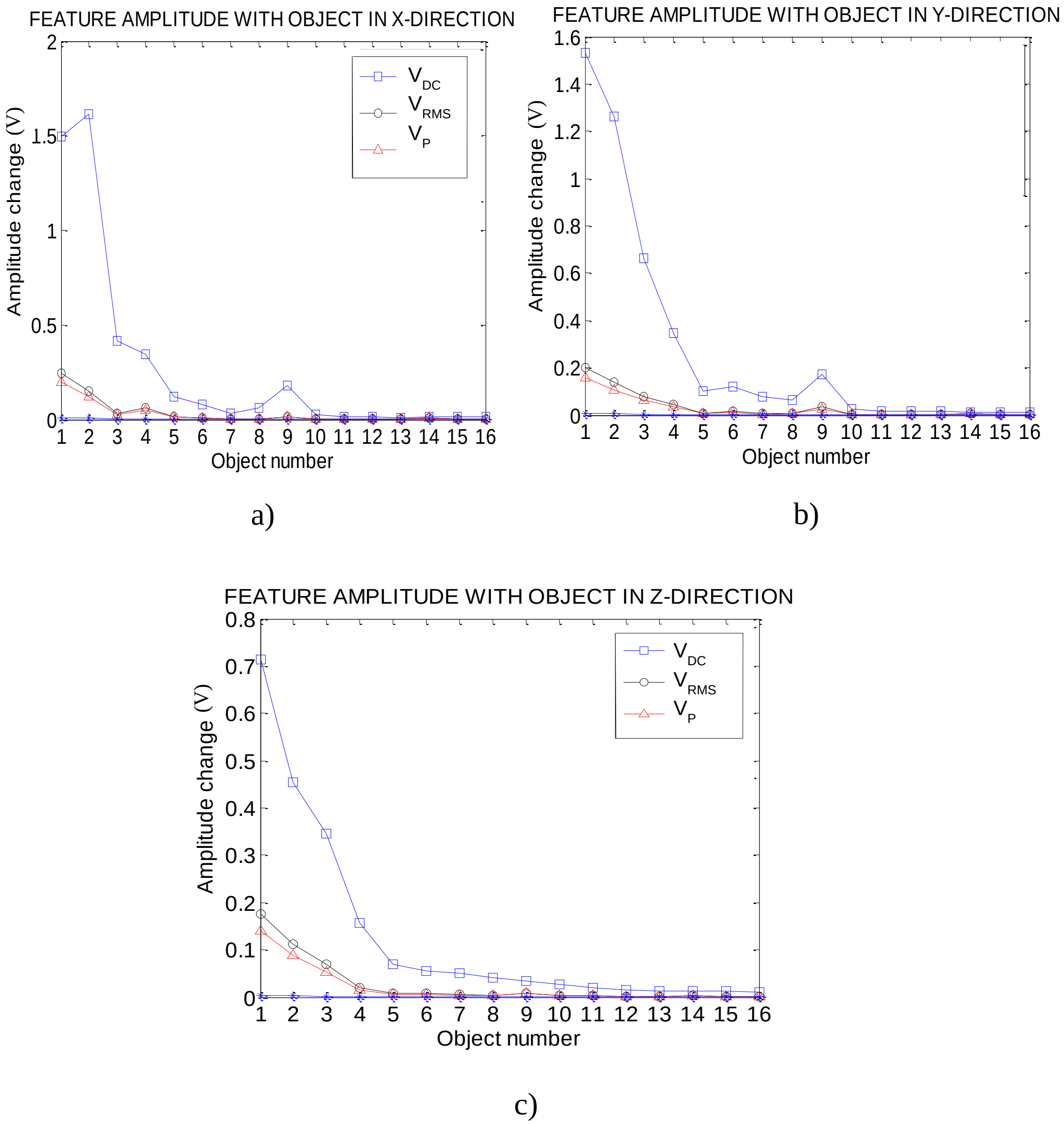

Figure 4.16: Peak to peak amplitude for feature maps for: a) x-direction, b) y-direction, and c) z-direction. (The x-axis represents the sample number as identified in section 4.2.1).

From the amplitude plot, the following observations can be deduced:

- Because the minimum (rather than the mean) distance between the array and object was kept constant during the tests, the z-directional plots are generally lower in amplitude.

- The system shows that it is least sensitive to objects that are either very small (USB) or non-ferromagnetic. The problem with the non-ferromagnetic objects may be addressed by an improved signal processing routine.
- It should also be noted that the gun and knifes provide the highest amplitudes of the objects across all three features. Also large size daily used item, e.g., screwdriver, spanner and scissors gives also higher amplitude response compared to other small size items.

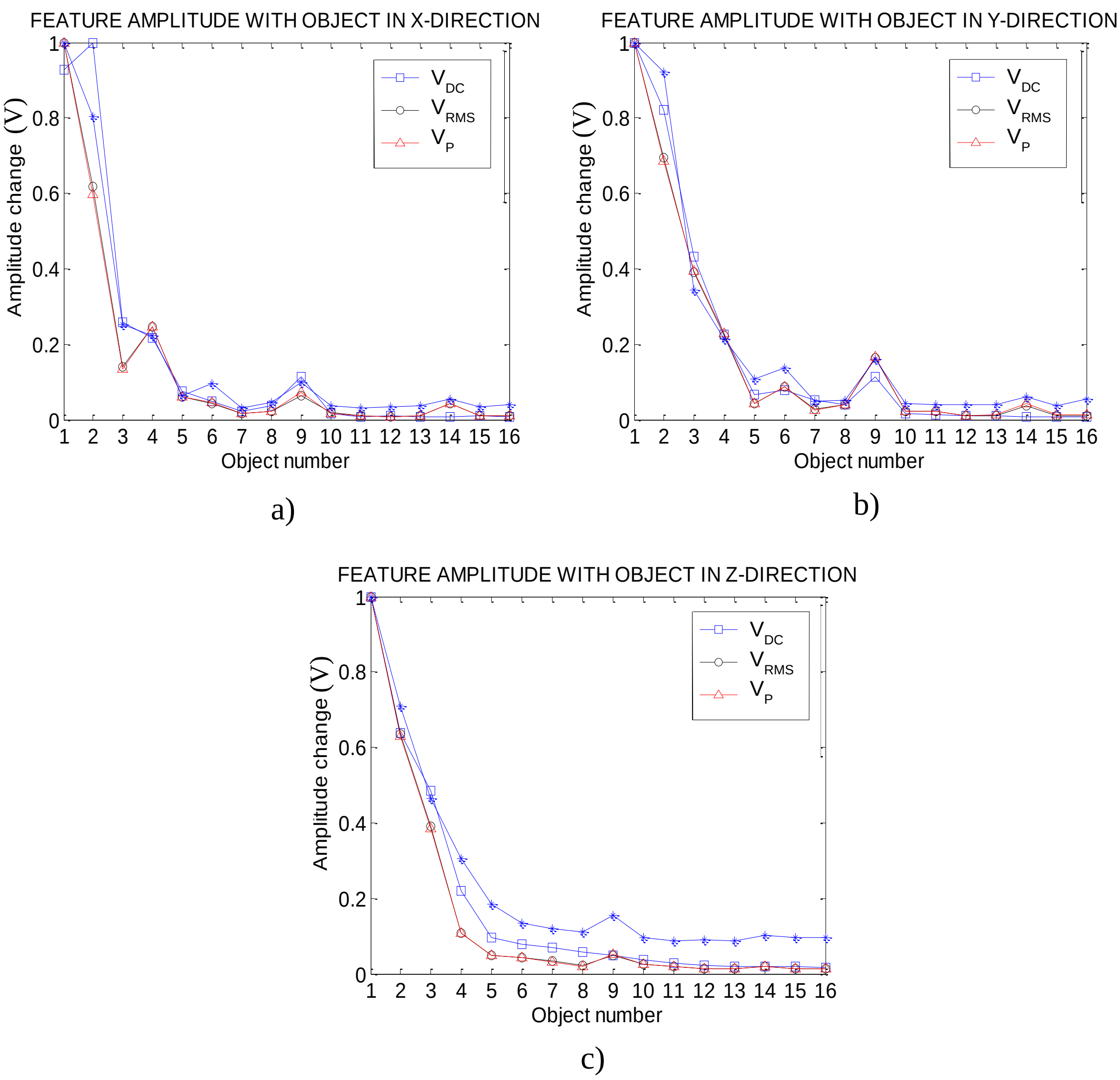

Figure 4.17: Normalised peak to peak amplitude for feature maps for: a) x-direction, b) y-direction, and c) z-direction

The test was repeated using the handgun samples also. Figure 4.18 shows the results for sample #1, parallel to the panel and rotated by 90°. The result is similar to the daily used items, in which only one end of the dipole is presented to the array in the z-direction, so a uni-polar distribution is observed. It can be seen from the plot that for this sample at least, the signature is not rotation invariant.

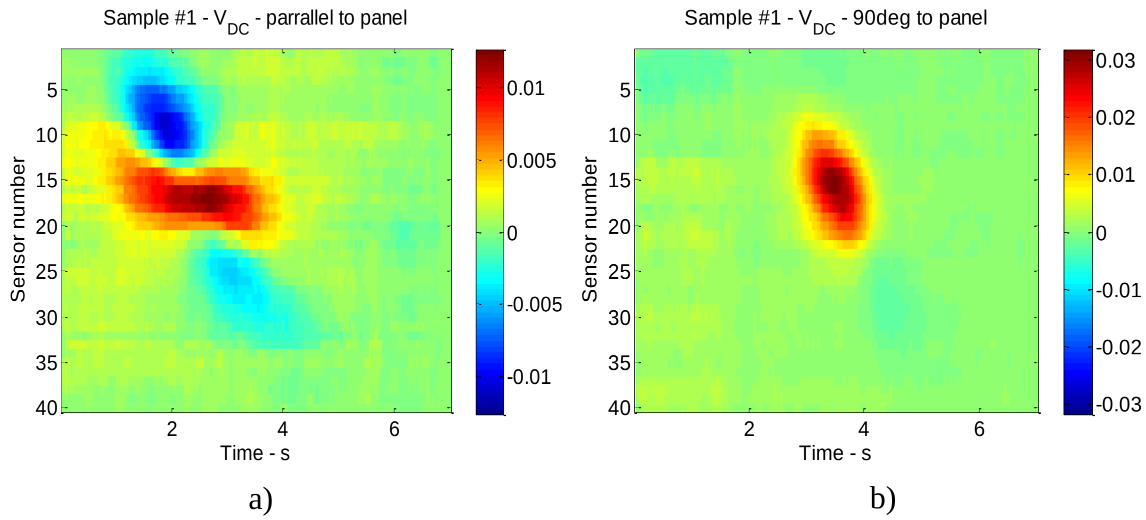

Figure 4.18: Feature map for rotation of object: a) Sample 1 parallel to panel, and b) Sample 1 rotated 90° to panel (z-direction).

4.6 Multiple Object Detection

Two experiment configurations used to measure the capabilities of the proposed system in order to discriminate multiple objects will be discussed in this section.

Firstly, in the early stage of the developing system, tests were undertaken using the 2D sensors array configuration, with 80 sensors to test two different samples: a standard set of keys and a Stanley knife arranged side by side. The results of the test are presented in Figure 4.19, where it is shown the feature maps for combinations of the two objects. It can be seen from Figure 4.19a, and Figure 4.19b, the presence of these objects individually can easily be identified from the EM images. The signatures from these two objects are distinctive and comply with previous observations from different materials; the Stanley knife consisting predominantly of aluminium, causes a strong reduction in EM images; the set of keys consisting predominantly of steel causes a switch in polarity of the EM image, i.e. a strong increase in image in the object position and a strong reduction outside this position. Figure 4.19c shows the EM image for both objects (keys and Stanley knife) positioned in the system, with a separation of approximately 30mm. It can be seen from Figure 4.19c that the signatures for both objects are preserved in this image, thus the objects can still be identified and consequently, the proposed GMR sensor can be used for this purpose.

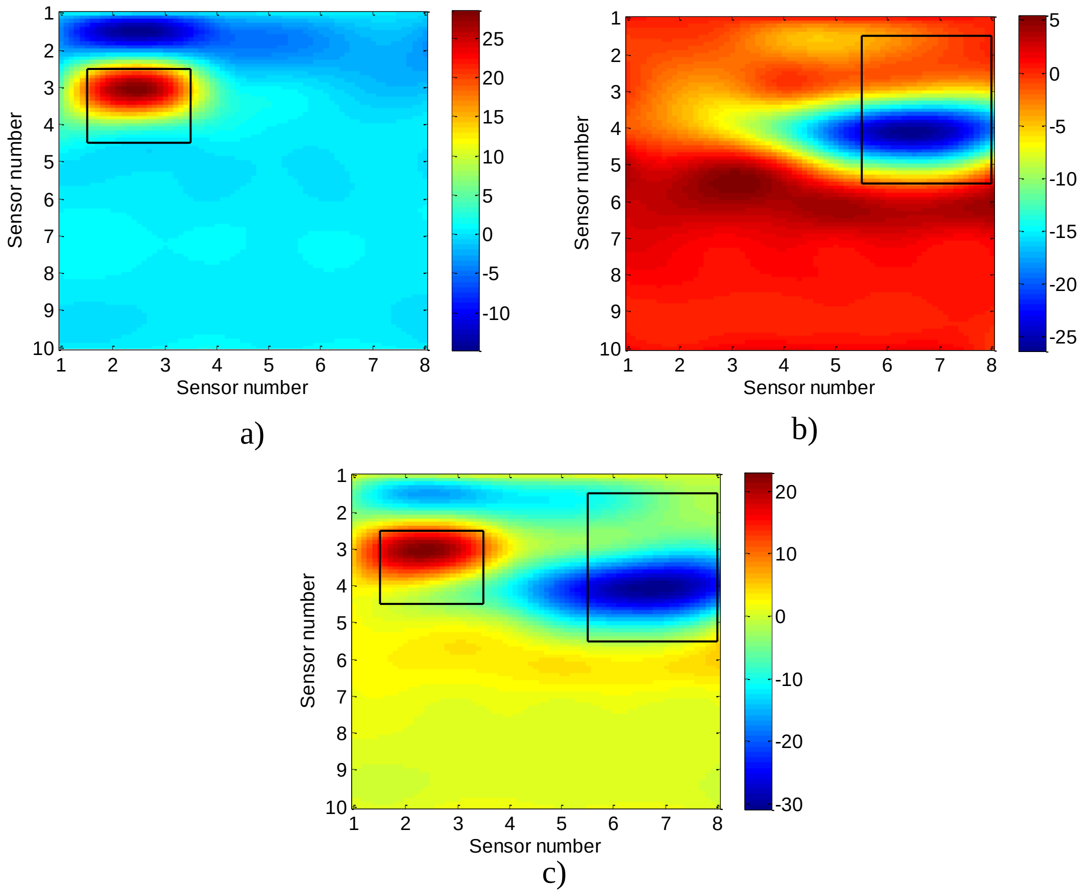

Figure 4.19: Images of V_{RMS} with: a) Keys only, b) Stanley knife only, and c) Combinations of keys, and Stanley knife (boxes indicate the approximate position of the objects).

Secondly, an additional test was conducted to assess the capabilities of the system using the last 1D sensor-array configuration with a sensor-array consisting of 40 sensors, to detect multiple objects and to determine the optimal object separation distance for accurate object detection and discrimination. The test shown in Figure 4.20 was performed with a replica GAP gun (sample #5) and a phone. In this test, the sample holder was employed to move the objects through the WTMD in a controlled manner. The replica gun was clamped within the sample holder and the mobile phone was hung next to it at three separation distances: 0mm, 60mm, and 120mm.

It can be seen from Figure 4.20b, that the presence of the gun by itself causes a typical dipole distribution, with one negative and one positive peak. Adding the phone at a separation distance of 0mm simply increases the intensity of the negative peak; thus in this position, the two objects are virtually indistinguishable from one larger object. Only at a separation distance of 60mm do we start to be able to distinguish the two objects. This discrimination of object signatures can be further enhanced by employing a simple processing technique, through taking absolute values of the measurements and then suppressing the values to less than a certain threshold, as shown in Figure 4.21, where a clear object discrimination can be achieved at 60mm and greater.

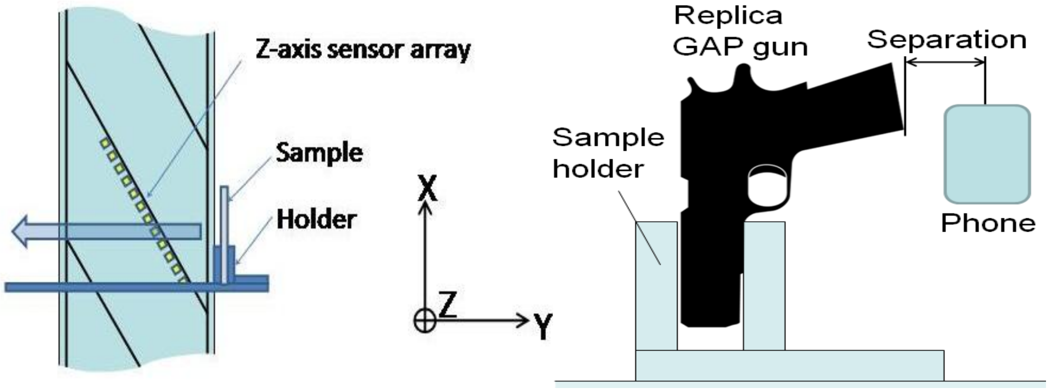

a)

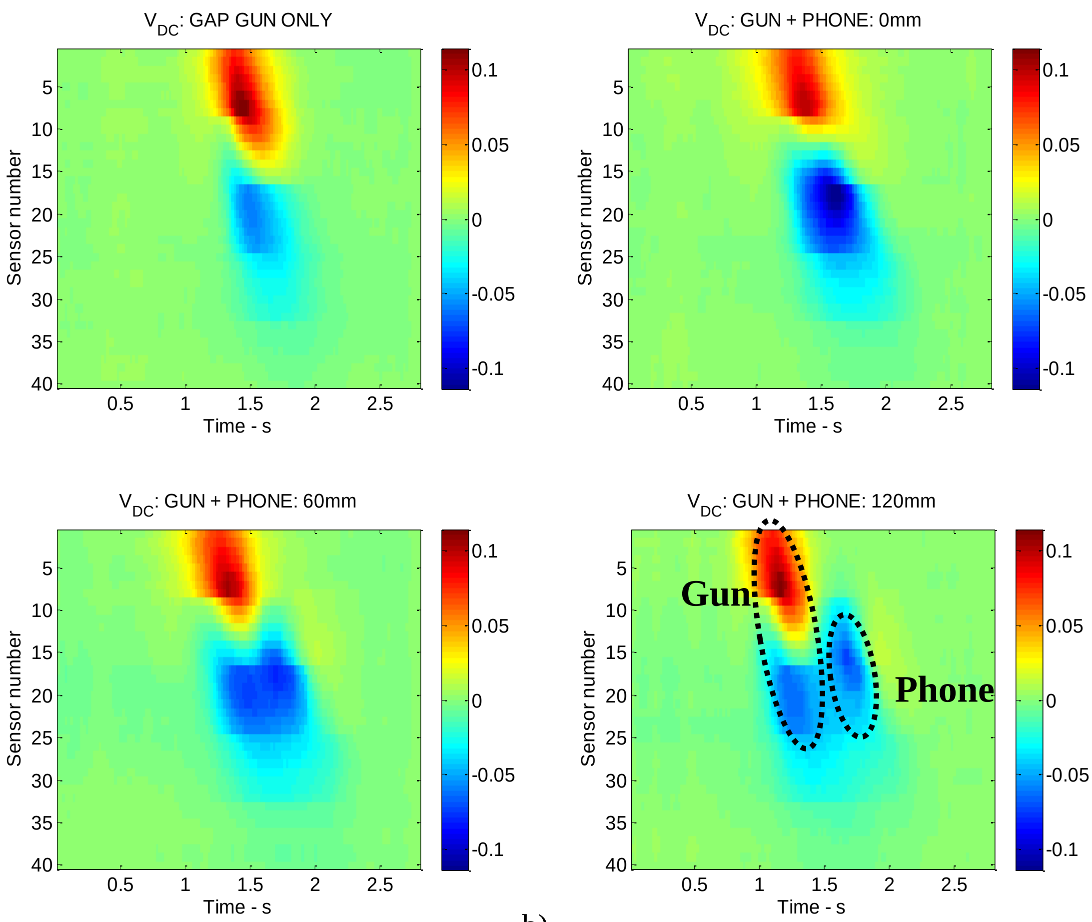

b)

Figure 4.20: Multiple object tests: a) Test set-up, and b) Result images for gun alone and gun with phone for a separation distance of 0mm, 60mm, and 120mm.

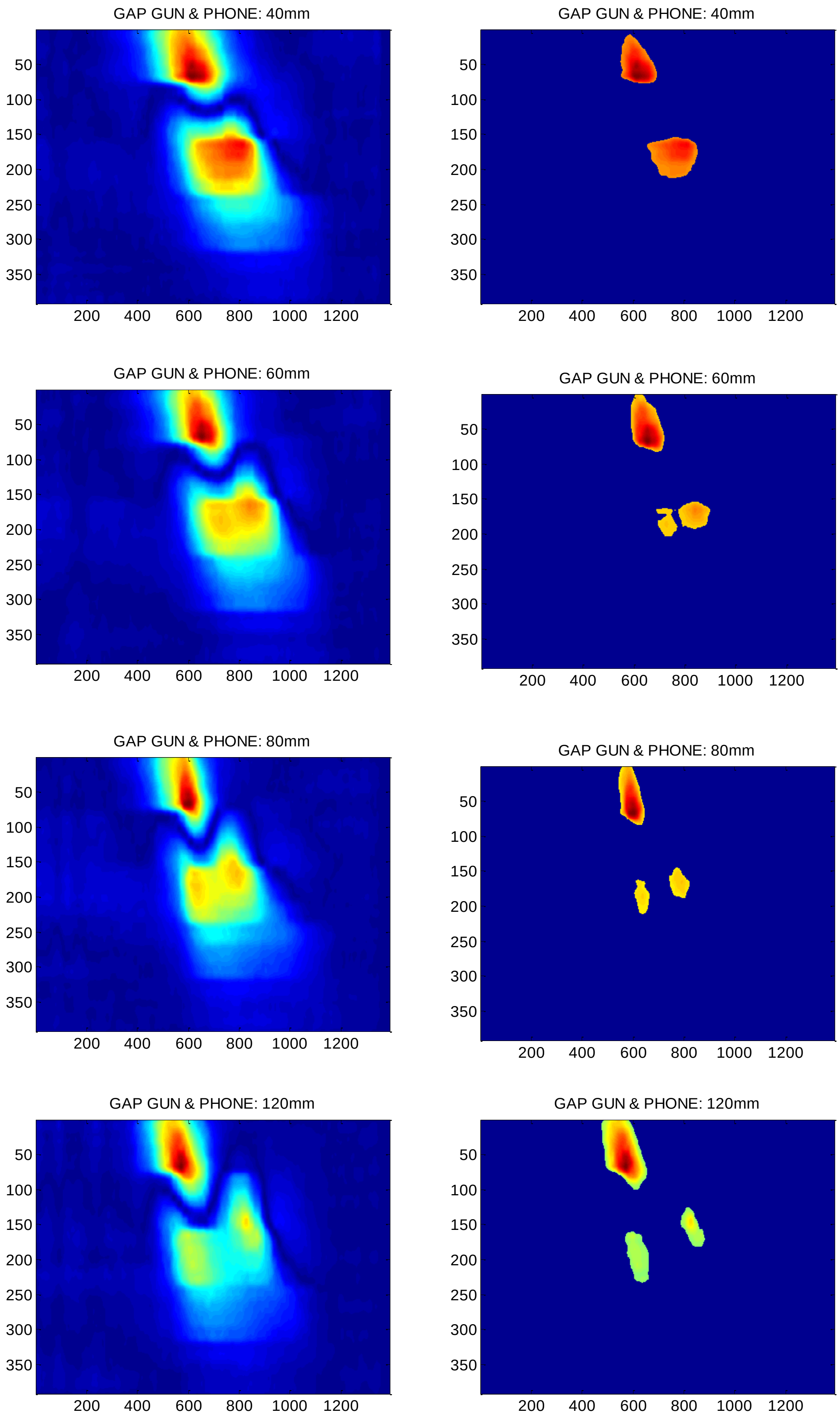

Figure 4.21: Thresholding techniques applied to discriminate between the two objects

4.7 Using Full-Body Array (Two Sensor-arrays)

Another group of tests was undertaken to verify the proposed system using two sensor-arrays, each using 40 sensors (totalling 80 GMR sensors). Items were placed in different pockets of a person walking through the arch, as shown in Figure 4.22. The following group of tests were carried out:

1. Gun in inside trouser pocket.
2. Gun in inside jacket pocket.
3. Gun in inside jacket pocket & phone in trouser pocket.
4. Gun in trouser pocket & phone with keys in jacket inside pocket.

Due to data acquisition card requirements, the sampling rate was reduced from 125 kHz to 62.5 kHz in order to maintain the same memory space, while introducing the new sensor-array. Figure 4.23 shows the results for this test. In general the results of this test are poor, possibly due to the decreased tolerance to noise from the lower sample rate.

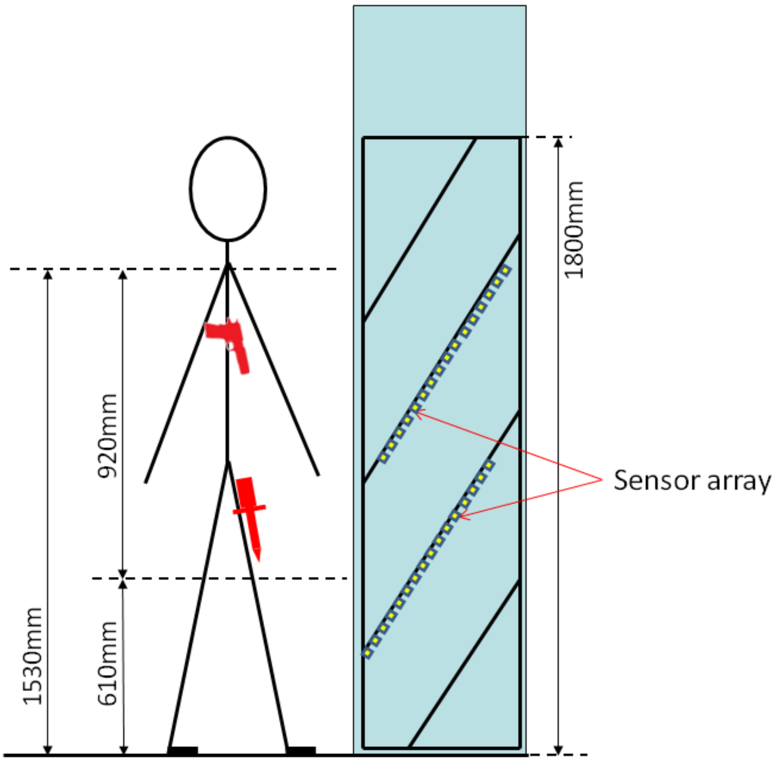

Figure 4.22: Walk through test set-up with full array.

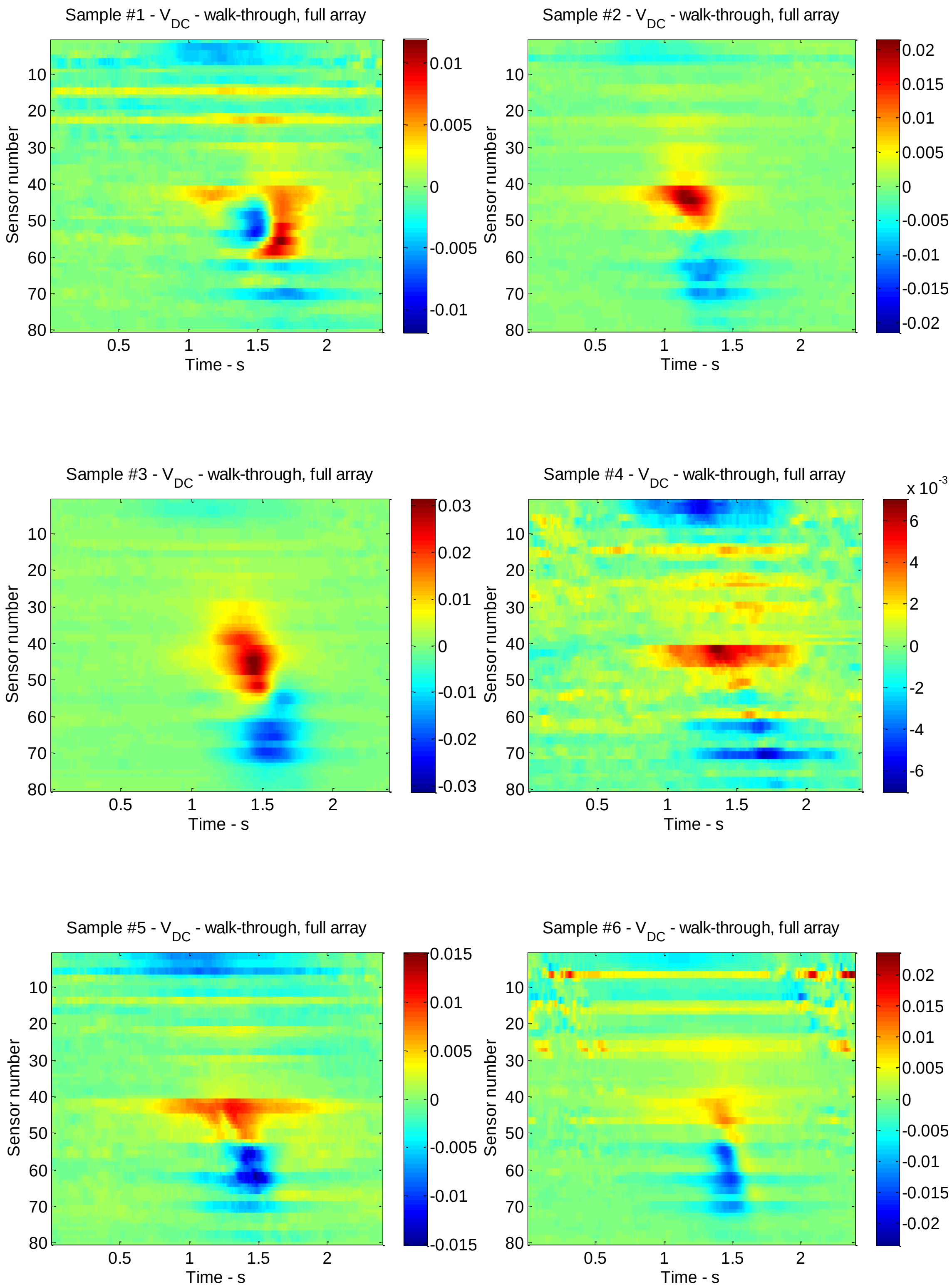

Figure 4.23: Test results with full array for test #1, gun in trouser pocket.

4.8 Summary

Different experimental tests have been carried out to assess the new system in respect to object detection and classification. The tests included a variety of threat and non-threat items, either in sample holders or carried by an individual through the system in typical places on the body, i.e. jacket and trouser pockets.

The sensitivity of the system to evaluate the object detection distance was investigated. The test results showed that for good resolution the distance from the panel should be less than 60cm for all objects and that sensitivity decreases substantially as the distance from the arch panel increases. The test results show that when the metallic object is far from the sensors, both in theory as well as in the experiments, the image of the object is not the same size as the original object, due to the amplitudes becoming smaller. To overcome this problem, ideally a relationship should be determined between the distance and amplitude.

To check data validity, simple repeatability tests were also carried out. Each sample was tested several times and the results were then plotted for all objects, where the initial results show the validation of the system in terms of repeatability in both controlled and walk-through test.

Different tests have been investigated to determine the validity of the different object orientations. The test results show that, in the x-direction and y-direction the object appears as a dipole distribution, yet with the rotation of the distribution correlating to the rotation of the object. In the z-direction, only one end of the “dipole” is presented to the array, so a uni-polar distribution is observed. It has been observed also that the trend of the data is similar, irrespective of the orientation of the object, when 16 samples were used and numbered according to the peak-to-peak amplitude.

A small set of tests incorporating multiple objects was also carried out. The results show that using a simple analysis of the feature map with thresholding applied, in order to discriminate objects, can yield some useful information such that at object separation distances < 30mm, the system only see objects as one composite item, thus not distinguishing between them as separate items. While at object separation distances > 60mm the system can distinguish between the two targets. However, sampling objects that are in close proximity to each other may appear as one large object.

The tests where an individual walked through the arch carrying the objects, rather than objects moved through on the sample holder represents a move towards the application of the equipment in an unconstrained environment.

It has been shown that some basic real-time imaging of EM signatures from objects may be possible. It is clear from the experiments conducted that magnetic field imaging could be used to detect and identify a metallic object. In comparison with conventional induction based WTMDs, the GMR array based system has shown great potential in material discrimination, as samples are made from mixed materials are clearly distinguished. Whereas with currently induction based WTMD, only discrimination between metal and non-metal is possible, our novel system has taken previous possibilities a step further. The proposed EM system technique is more advanced in object characterisation as it depends on the amplitude of the EM field making training possible using a database of objects; unlike traditional thresholding adopted in the traditional induction based system, which largely depends on material volume.

The data collected will be applied for offline processing, investigating of different feature extraction methods and training of algorithms for object classification for both detection and classification, which will be discussed in the next chapters.

Chapter 5: Feature Extraction and Combination

The feature extraction work presented in this chapter is the second major part of the proposed system for automatic detection and classification using EM images. The aim of this chapter is to find appropriate feature extraction techniques for the data retrieved from the new EM imaging system. Several groups of features such as *shape*, *material*, *time-frequency analysis* and *transient response* features are investigated, developed and tested. These methods have been proposed in order to provide complementary information about the threat object signature. A novel time-frequency image correlation method was successfully proposed pertaining to the discrimination of ferromagnetic and non-ferromagnetic metallic materials. In the following sections, a brief background is given of each feature extraction technique along with the motivation behind its use, in addition to detailing the feature extraction approach involved. The effectiveness of individual features is then tested and discussed. Based on the results for individual feature characters, only features that perform well are selected for feature fusion and then for object classification.

5.1 Introduction

For image pattern recognition, feature extraction is a special tool to reduce the dimensionality of a large set of data. When the input image is too large to be processed using an algorithm, it needs to be transformed into a representative set of features. The process of transforming the input image into a set of features is called feature extraction. In other words, feature extraction is the use of a reduced representation of an image to solve pattern recognition problems with sufficient accuracy, instead of using the image at full size. Following the feature extraction step, feature selection and optimisation are considered to be complementary steps. Feature optimisation helps to improve the performance of learning models, such as training using a neural network, by removing the least relevant features from the data. Feature optimisation also improves the understanding of extracted features by identifying the important features and determining how they are related to each other. Therefore, extracting distinctive and distinguishable features from EM signals is imperative for their proper classification [77-79].

In this work, four main groups of features have been extracted from the EM signal. These groups are categorized as: *shape*, *material*, *time-frequency analysis* and *transient response*. The shape groups consist of edge chain codes and invariant moments features [130, 131], while the material groups are inferred from both the change in amplitude [79] and PCA [90] of the EM signal. The time-frequency analysis categories consist of the use of Fourier and Wavelet transform techniques [78, 132]. The transient response category applies cross-correlation techniques [80, 94, 133] to the novel EM transient response images developed in Chapter 3. These features are considered as object signatures, both individually and when combined, and are processed by a classifier. Two types of classifier were used, ANN and SVM, both of which are discussed in the following chapter. Figure 5.1 below shows the proposed feature extraction and classification plan for the detection and classification of threat objects.

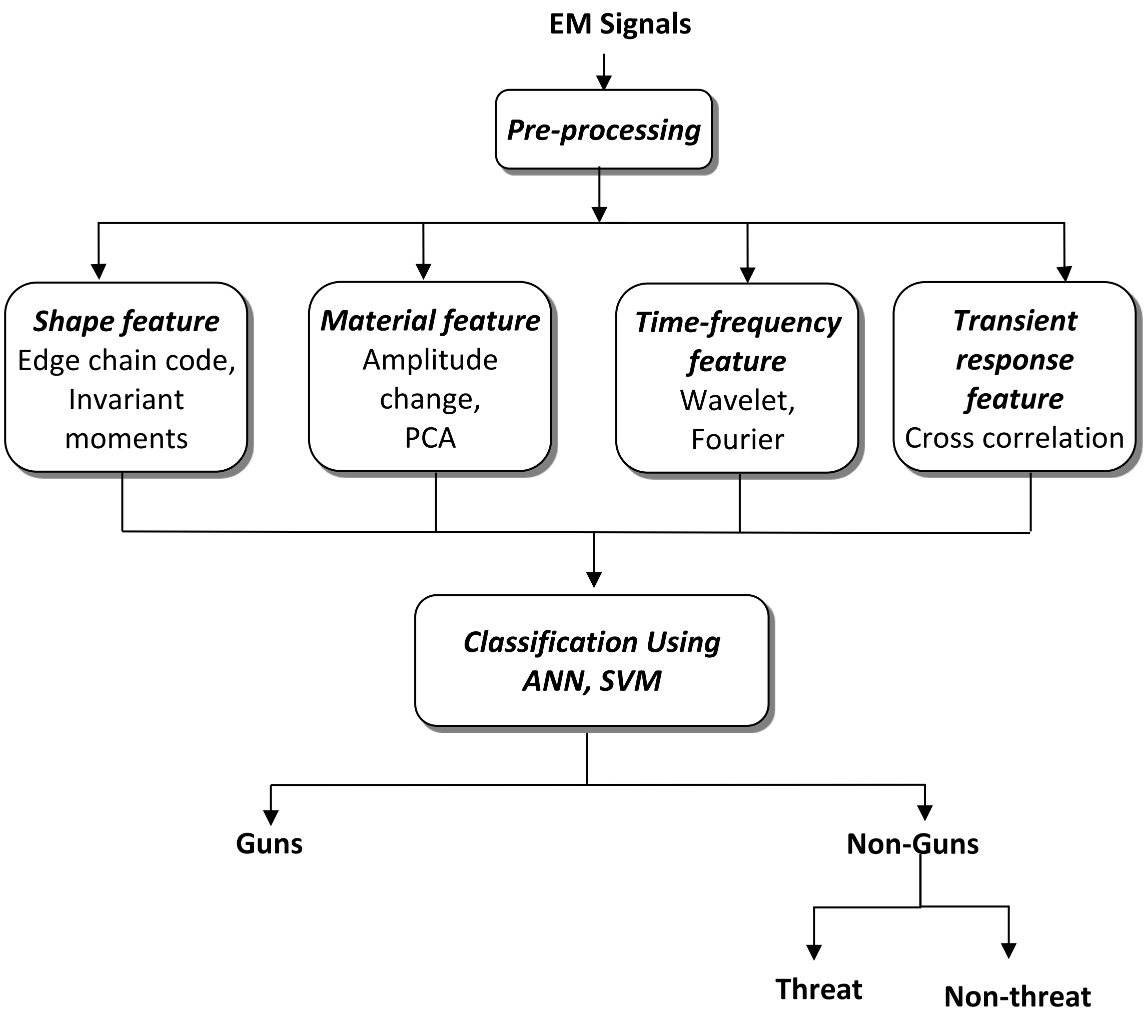

Figure 5.1: Hierarchical Classification Methodology

5.2 Image pre-processing

Various methods are introduced for the processing of EM images in order to detect objects and prepare the images for subsequent feature extraction and classification. These techniques are applied to the results obtained from the three configurations of the sensor-array.

The final EM response data arranged from the final system configuration consists of 40*140 values, as explained previously in Chapter 3. These datasets were interpreted as 2D greyscale images (as shown in Figure 5.2a) for the feature extraction process. However, coloured images (as shown in Figure 5.2b) were presented throughout this thesis for better viewing. The Matlab image functions *mat2gray* and *imagesc* were used for these purposes.

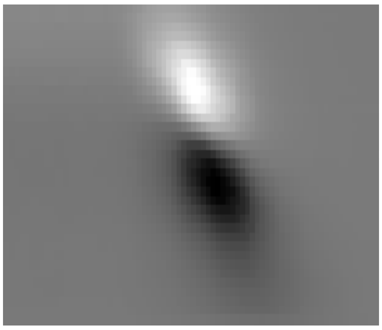

a)

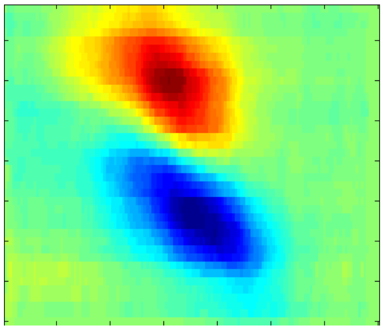

b)

Figure 5.2: Data received from the system for the handguns sample #2: a) Greyscale image. b) Colour scale image.

5.2.1 EM image enhancement

Different operations were undertaken for the receiving of the EM data from the acquisition card and the display of the EM images, and enhancement processes were used for viewing the images with optimal resolution and adequate noise reduction. In addition to averaging the data, the first 5 seconds was marked as a background period and subsequently subtracted from the rest of data.

A smoothing filter was also used, namely Savitzky–Golay filter. This filter more effectively preserves the high-frequency content of the desired signal, by performing a local polynomial regression (of degree k) on a series of values (of at least k+1 points, which are treated as being equally spaced in the series) to determine the smoothed value for each point. The main advantage of this approach is that it tends to preserve characteristics of distribution, such as relative maxima, minima and width, which are usually "flattened" by other adjacent averaging techniques, such as moving averages for an example [134, 135]. All of these operations have consequently contributed to the enhancement of the image outcome from the system.

5.2.2 EM image segmentation

In computer vision, segmentation refers to the process of partitioning a digital image into multiple sets of pixels, by assigning individual pixels to classes. Image segmentation is typically used to locate objects and boundaries in images. The goal of segmentation is to simplify or change the representation of an image into something that is more meaningful and easier to analyse, and therefore image segmentation is an important step towards pattern detection and recognition [77].

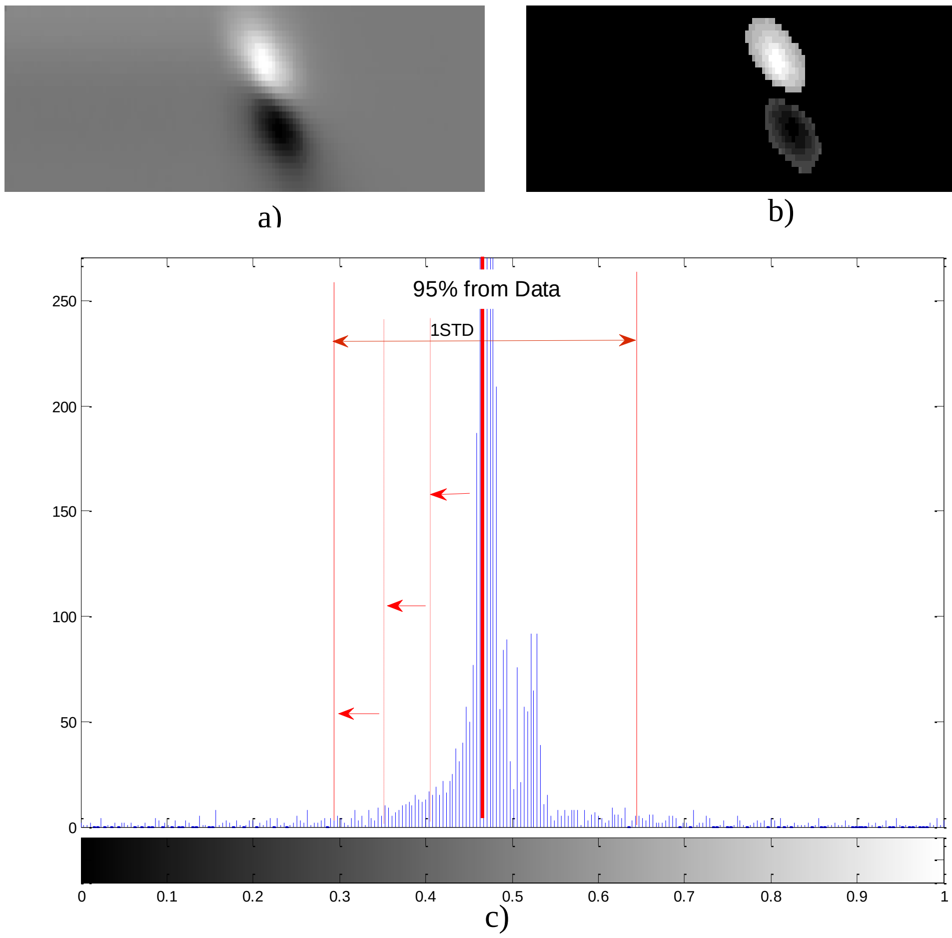

Figure 5.3: Segmentation process for the kitchen-knife sample using image histogram. a) Original image, b) Segmented image, and c) Original image histogram.

In this work, histogram-based segmentation has been developed for the specific automatic segmentation of the EM images. The image segmentation used here consists of the following steps:

1. Normalise the data to values between [0 1].
2. Compute the image histogram.
3. Extract 95% of the values from the histogram that represents the background.
4. The remaining data represents the object effect.

Looking at the grey-level histograms of our database, two thresholds are needed to extract the object from background. These thresholds were chosen to comply with the 95% confidence interval rule [77]. In other words, the thresholds are chosen to be ±3 STDs away from the mean of the background cluster in the histogram. This process obtains the region of interest from the EM signal. Figure 5.3 shows the kitchen-knife sample segmentation process.

5.3 Proposed Feature Extraction

Four categories of features have been extracted from the EM signal. These are: object shape features; object material features; time-frequency features; and the transient feature response, which are explained next.

5.3.1 Shape categories

Shape is one of the most prominent features of any object. As reviewed in chapter two, geometrical shape features are the most widely used features for weapon detection and classification. This is because the shape of the threat items is the first and major factor analysed by experts during manual interpretation. Many researchers have tackled the problem of object classification based on feature extraction techniques using the object shape descriptor by employing different tools such as edge chain codes, invariant moments, Fourier descriptors, Hough transform and shape matrices in order to extract shape characteristics [85].

5.3.1.1 Edge chain code feature

The edge chain code is mostly used as a reinforcement technique for edge detection in the image segmentation field [92]. It can also be applied to features representing objects in images [93]. It is a type of representation that consists of a series of numbers. These numbers represent the direction from one pixel to the next, which can be used to represent the shape and input format for numerous shape analysis algorithms [136]. In this work, the edge chain code is implemented for the first time in the area of weapon detection and classification. The edge chain code consists of a list of codes ranging from zero to seven in an anticlockwise direction. These codes represent the direction of the next pixel connected in a 3*3 window, as shown in Figure 5.4a. For example, in Figure 5.4b we start at the first edge on the top left and go clockwise around the edge. The code for each edge has been listed, resulting in the chain code: 00117600665566644333222.

Statistical moments were applied to the EM images. Based on the understanding of moments and considering the object edge chain code as a distribution, the seven features shown in Table 5.1 can be defined and described to analyse the sample's edge [137, 138].

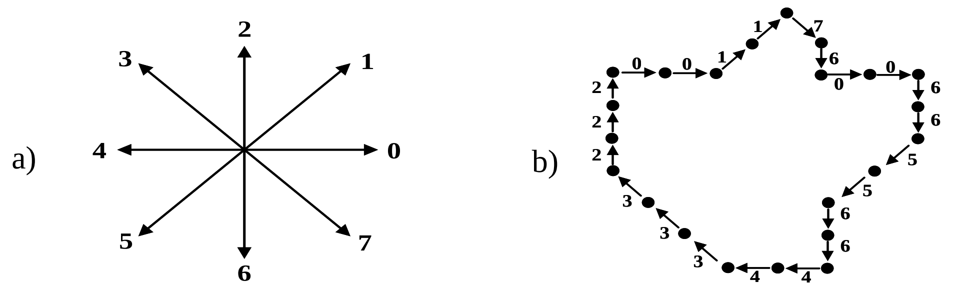

Figure 5.4: Calculation of the 8-directional chain code: a) 8-directional chain code, and b) Chain code sample.

Table 5.1: Statistical moments and their explanations in respect to physics

Feature	Equation	Physics Description
1. mean^{1st}	$X = \frac{1}{N}\sum_{j=1}^{N} X_j$	Estimates that value around which central clustering occurs
2. var^{2nd}	$\overline{Var(X_1 ... X_N)} = \frac{1}{N-1}\sum_{j=1}^{N}(X_j - \overline{X})^2$	Having characterised a distribution's central value, it is possible to characterise its width or variability around that value.
3. STD^{2nd}	$\sigma(X_1 ... X_N) = \sqrt{Var(X_1 ... X_N)}$	var_2nd's square root
4. ADev^{2nd}	$ADev(X_1 ... X_N) = \frac{1}{N}\sum_{j=1}^{N}\left\lvert X_j - \overline{X}\right\rvert$	A more robust estimator of width
5. Skew^{3rd}	$Skew(X_1 ... X_N) = \frac{1}{N}\sum_{j=1}^{N}\left[\frac{X_j - \overline{X}}{\sigma}\right]^3$	Characterises the degree of asymmetry of a distribution around its mean.
6. Kurt^{4th}	$Kurt(X_1 ... X_N) = \left\{\frac{1}{N}\sum_{j=1}^{N}\left[\frac{X_j - \overline{X}}{\sigma}\right]^4\right\} - 3$	Measures the relative peakedness or flatness of a distribution.
7. Rv	$R_v = \frac{\sum_{i=0}^{N-1} \Delta r_i}{N-1}$	Measures the average change ratio

The first six features are used to analyse the chain code as a distribution. In addition, the code for each pixel represents the change in direction from the last pixel. All those codes together represent the change for the entire edge. Therefore, the chain code change from one pixel to the next can be determined as $\Delta r_i = |r_{i+1} - r_i|$, so that it is possible to evaluate whether or not the edge is smooth by measuring the average chain code change. Based on this technique, the last edge chain code feature Rv is defined.

To prepare the EM images for the edge chain code process, several image pre-processing steps were taken. Firstly, the optical and EM images were converted to black and white scale images. Secondly, Otsa and Kubur threshold techniques were applied [77]. Then fill the unwanted hole followed the threshold techniques. Finally, the removal of very small objects was undertaken, such as the effects that appear under the platform of the EM images. Figure 5.5 shows the results for handgun 6. The six real handgun samples (the same samples as were used in Chapter 4) have been tested using the first sensor-array configuration and the relationship between the features derived from the resulting optical images and the EM images can be seen in Figure 5.6.

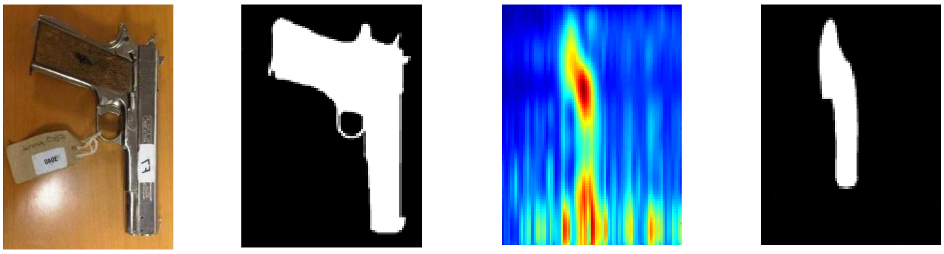

a) b) c) d)

Figure 5.5: Image pre-processing of handgun sample #6: a) Optical image, b) Black and white image, c) EM image, and d) EM black and white image.

It can be seen from Figure 5.6 that there is a relationship between the threshold real optical image and the threshold EM images. Therefore, the edge chain code features could be considered as a feature to represent the objects' signature. However, this method was applicable only to the two dimensional sensor-array results, and consequently is not discussed further or used in the classifiers in the following chapter. Further investigation of this technique for use in automatic classification will be a task for future work. For further details refer to Appendices B and C.

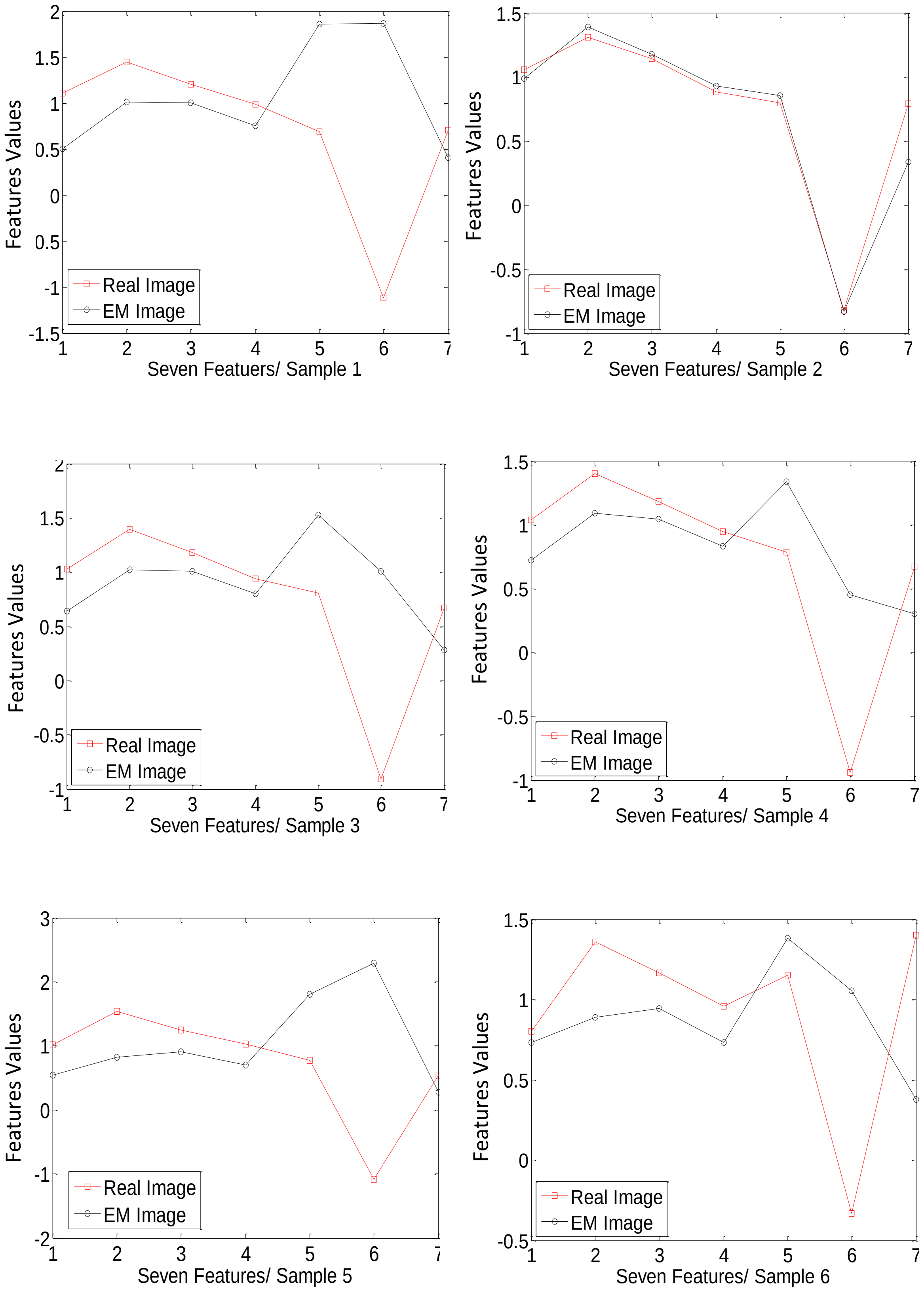

Figure 5.6: The relationship between the features obtained from the real image samples and the EM images.

5.3.1.2 Invariant moments

The moment invariant technique has been used since the early 1960s [86]. It was an essential development, since many problems in image processing and recognition focus on classifying an image. The method used to determine the invariant moment is also widely used in feature extraction, since it is invariant to rotation, scale, and translation. The fact that invariant moment can be used to describe the geometric behaviour of image intensity distribution yields the benefit that its values can be used as tools in recognition, identification and verification processes. In certain systems [87], objects can be detected with a classification accuracy of over a 90%, after a set of invariant moment feature vectors have been produced. Invariant moments have also been used [88] to identify the shape of a handgun and to classify objects into weapon and non-weapon objects, where the researchers obtained an accuracy rate up to 96%. Three different shape recognition methods have been reported [89]. One of these was an invariant moment technique used to build a feature vector for the classification of eight types of handguns.

In this work, shape features were extracted from the EM images using the invariant moments introduced in a previous study [86]. Two-dimensional moments of a digitally sampled $M \times M$ image that has grey function $f(x,y)$, $(x, y=0,\ldots M-1)$ is given as Eq. 5.1:

$$m_{pq} = \sum_{x=0}^{x=M-1} \sum_{y=0}^{y=M-1} x^p . y^q f(x,y) \tag{5.1}$$

where p, $q=0,1,2,3\ldots..$

Based on the second and third moments from the general moment in Eq. 5.1, eight moments ($\emptyset_n$) Where n=1, 2..., 8 are derived (Eq. 5.2) and applied to grey images converted from the original data. The resultant eight moments are grouped into a feature vector called an *f-Moment*, which is considered as a signature for each individual object based on the characteristics of its EM image shape.

Figure 5.7 shows the 8 moments for the ten objects, the six handgun samples and the other four are non-threat items (mobile phone, USB, pen and belt). It can be concluded that the moments of the handgun samples are higher than those of the other objects in this test. It is noteworthy that the results will not be affected by the orientation of the object, as the invariant moment does not vary with rotation.

$$\phi_1 = m_{20} + m_{02}$$

$$\phi_2 = (m_{20} - m_{02})^2 + 4m_{11}^2$$

$$\phi_3 = (m_{30} - m_{02})^2 + (3m_{21}^2 - m_{03})^2$$

$$\phi_4 = (m_{30} + m_{12})^2 + (m_{21} + m_{03})^2$$

$$\phi_5 = (m_{30} - 3m_{12})(m_{30} + m_{12})[(m_{30} + m_{12})^2 - 3(m_{21} + m_{03})^2] + (3m_{21} - m_{03})(m_{21} + m_{03})[3(m_{30} + m_{12})^2 - (m_{21} + m_{03})^2]$$

$$\phi_6 = (m_{30} - 2m_{02})[(m_{30} + m_{12})^2 - (m_{21} + m_{03})^2] + 4m_{11}(m_{30} - m_{12})(m_{21} + m_{03})$$

$$\phi_7 = (3m_{21} - m_{03})(m_{30} + m_{12})[(m_{30} + m_{12})^2 - 3(m_{21} + m_{03})^2] - (m_{30} - 3m_{12})(m_{21} + m_{03})[3(m_{30} + m_{12})^2 - (m_{21} + m_{03})^2]$$

$$\phi_8 = (m_{20} + m_{02}) - 4m_{11}^2 \qquad 5.2$$

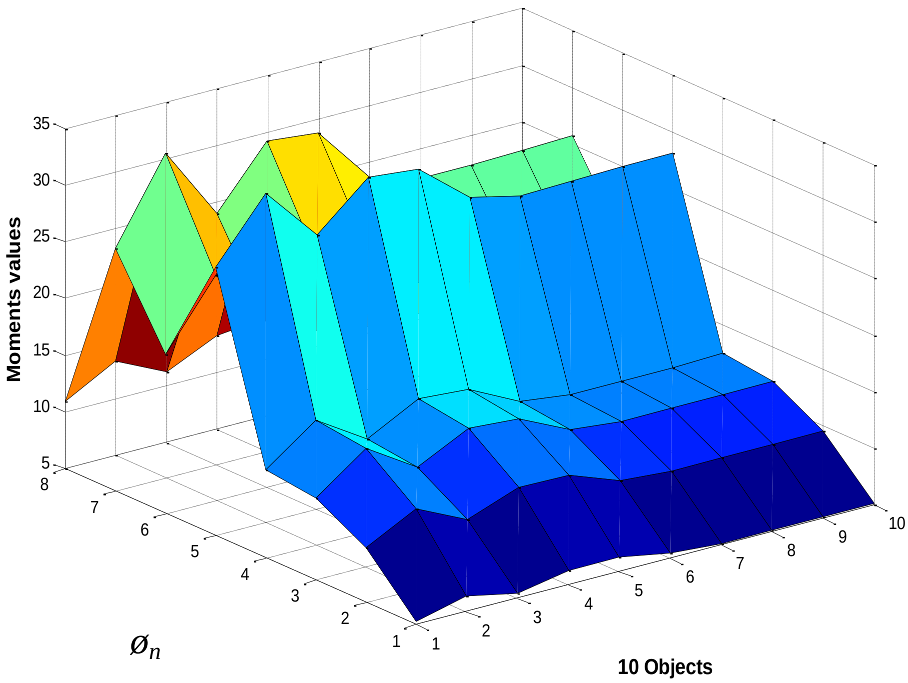

Figure 5.7: Eight moments $\o_n$ for 10 different objects, six handgun samples (#1- #6) and four non-threat metallic items (#7- #10) samples respectively.

5.3.2 Material categories

Since the EM signal represents the EM reflection of samples sensed by a GMR sensor, this signal shows primarily the material properties of an object. Each sample has a different EM field, because these fields are typical for different objects. Reasons for these differences include size, electrical and magnetic material properties and also the metal distribution in the object. The proposed material features were deduced from the EM image using two techniques as follows.

5.3.2.1 Maximum EM field change features

Signal amplitude represents a material feature used to obtain the properties of the objects under test. Each object generates an overall variation in EM signal amplitude according to the EM reflectivity of the material it is constructed from [79]. As an example, Figure 5.8 shows an initial field test measured using a GMR sensor for three different objects: an aluminium block, a Stanley knife, and a set of keys. To alleviate the error in this test, samples were chosen of approximately equal sizes and positioned at the same distance from the sensor. It can be seen from the plots that each object yields its own characteristic signature in terms of signal amplitude. The aluminium object produces a smaller amplitude variation than those made of steel. The test reveals that objects made of different materials produce different amplitude variations.

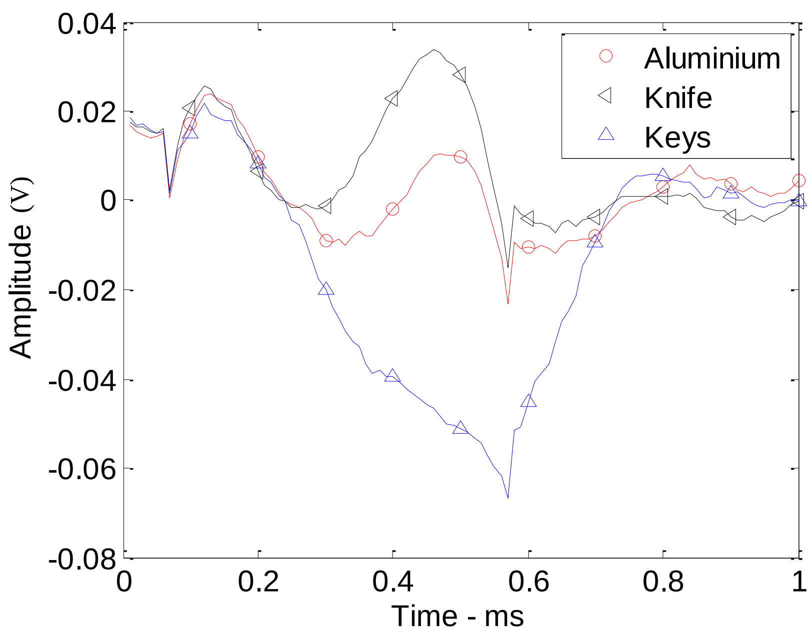

Figure 5.8: Electromagnetic signals for three different objects from one GMR sensor.

The proposed amplitude variation feature (AMP_{change}) is calculated as the difference between the maximum ($Max(EM_{signal})$) and the minimum ($Min(EM_{signal})$) values from the received signal, as shown in Eq. (5.3):

$$AMP_{change}=Max(EM_{signal})- Min(EM_{signal}) \qquad 5.3$$

AMP_{change} is directly related to the EM field intensity of the object's material. This new feature is formed in a feature vector called *f-Max-Min* which is used by the classifier. Figure 5.9 shows the maximum amplitude change for the samples used. Generally, the handguns have the highest amplitude change, except that the mobile phone (#7 in the figure) gives a higher amplitude change than some of them. This is because its battery cell returns a high EM response, especially when it is fully charged, and so the system will give a positive false alarm when classifying the mobile phone.

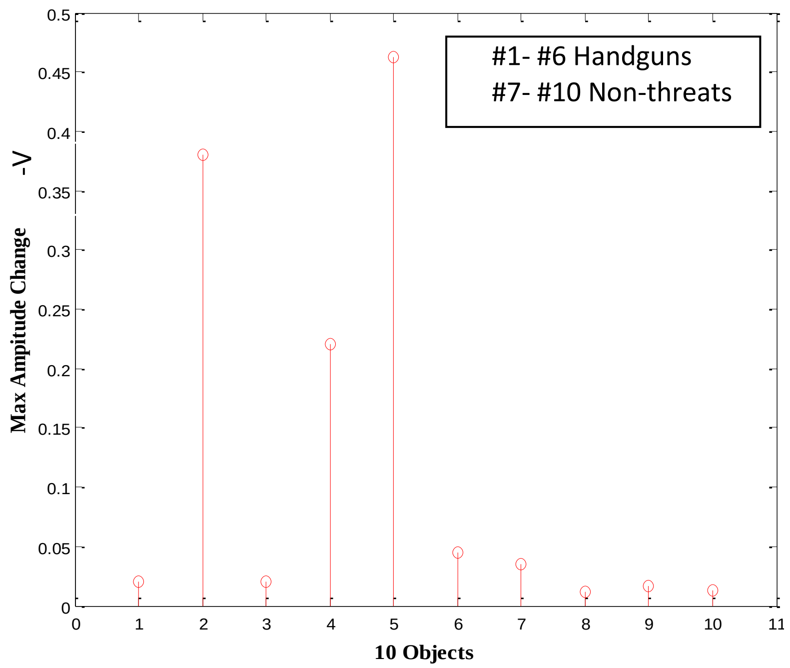

Figure 5.9: Maximum amplitude change for ten objects, six handgun samples (#1-#6) and four non-threat metallic items (#7- #10).

5.3.2.2 *PCA-based feature*

In pattern recognition, PCA is commonly used for pattern classification and identification. It involves a mathematical procedure that transforms a number of possibly correlated variables into a smaller number of uncorrelated variables called *principal components*. The first principal component accounts for as much of the variability in the data as possible, and each succeeding component accounts for as much of the remaining variability as possible. This technique is a popular statistical method which tries to explain the covariance structure of data by means of a small number of components. These are calculated based on maximizing variance and decomposing covariance. Usually, two or three PCs provide a good summary of all of the original variation. The PCA approuch has two most significant goals. Firstly, it reduces the dimensions of the data; Secondly, it can also reveal those underlying factors or combinations of the original variables that principally determine the structure of the data distribution. Therefore it can be used to provide the features of this data. PCA has been widely used as a feature extraction tool [80, 90] which transforms data into uncorrelated eigenvectors or principal components (PCs) corresponding to the maximum variability within the data. Therefore, it is used to optimise and reduce the amount of redundant data and provides a convenient way to normalize objects in terms of translation and rotation [77]. From PCA a feature vector is extracted, which is invariant to scale and orientation, and tolerant to distortion. Concealed object detection and recognition in real-time has been proposed using PCA with passive millimeter wave imaging [91]. The detailed steps of PCA [80, 90, 102] are summarised as follows: 1) organisation of the dataset; 2) calculation of the mean along each dimension; 3) calculation of the deviation; 4) determination of the covariance matrix; 5) calculating the eigenvectors and eigenvalues of the covariance matrix; 6) sorting the eigenvectors and eigenvalues; 7) computing the cumulative energy content for each eigenvector; and finally, 8) selecting a subset of the eigenvectors as the basis vectors such that the k eigenvectors correspond to the maximum k of eigenvalues.

In this work, PCA is applied to each EM signal to derive its eigenvector. The covariance of input data (Σx) is calculated as follows (Eq. 5.4):

$$\sum_{x} = E\left((x - \mu_x)(x - \mu_x)^T\right) \tag{5.4}$$

Eigenvalues λ and Eigenvectors W_i are identified using covariance Σx (Eq. 5.5).

$$(\lambda I - \Sigma_x) = 0\,; \qquad (\lambda I - \Sigma_x)W_i = 0 \tag{5.5}$$

where, I is an identity matrix of the same order as Σ_x and μ_x is the mean.

To identify between the objects, the PCA technique was applied to a sample of a range of 14 commonly used items in addition to the six handguns in a separate test. The

PCA components were integrated together and the relationship between the PCA1 and PCA2 are plotted in two dimension feature space which represents the correlation between the PCA components as shown in Figure 5.10. It was found that PCA method has the potential to discriminate between handguns and other objects, where objects are clearly classified into two non-overlapping clusters based on their two PCA components.

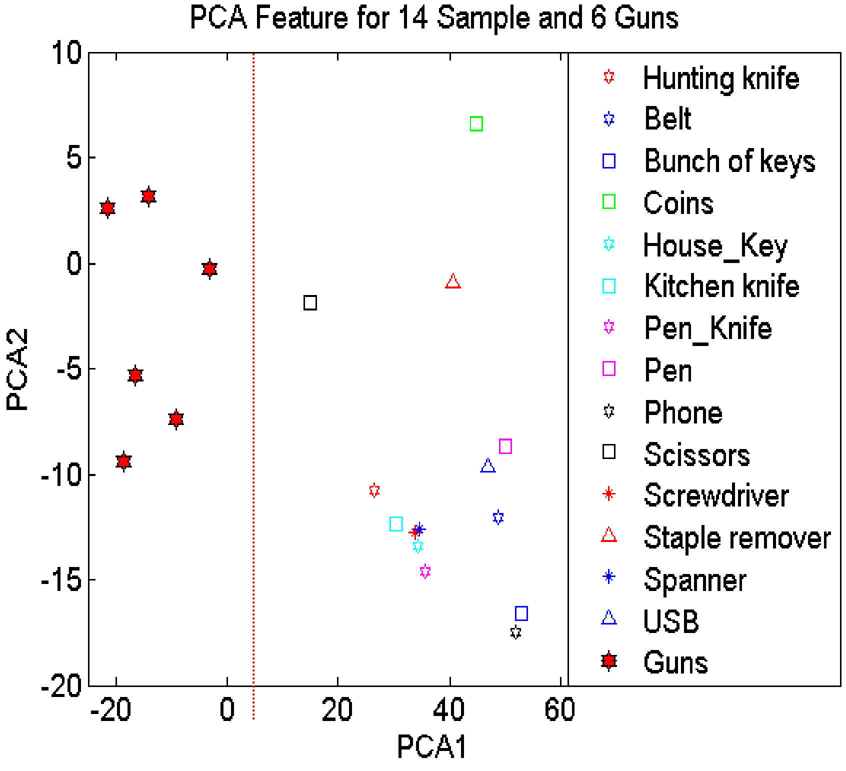

Figure 5.10: PCA discrimination between handguns and other commonly used items.

A further test was carried out using the handgun samples only. The first two components, PCA1 and PCA2, have been plotted in a 2D space. The test was repeated five times with the handgun in the holder being moved through the WTMD, and the results are shown in Figure 5.11. Likewise, the results for five other uncontrolled tests of a person walking through the system with a handgun concealed inside his jacket pocket are shown in Figure 5.12.

It can be seen from Figures 5.11 and 5.12 that, in general, the objects can easily be separated and that each object correlates to a specific grouping.

The results of the uncontrolled tests in Figure 5.12 show some fluctuations; however, items can still be discriminated when using three PCA components. So, in order to ensure more accurate classification results, the third component is also proposed in addition to the first and second components as an input for the classifier. These three components are grouped in a feature vector named f-PCA for each sample and are then supplied to the classifier, as explained in the next chapter.

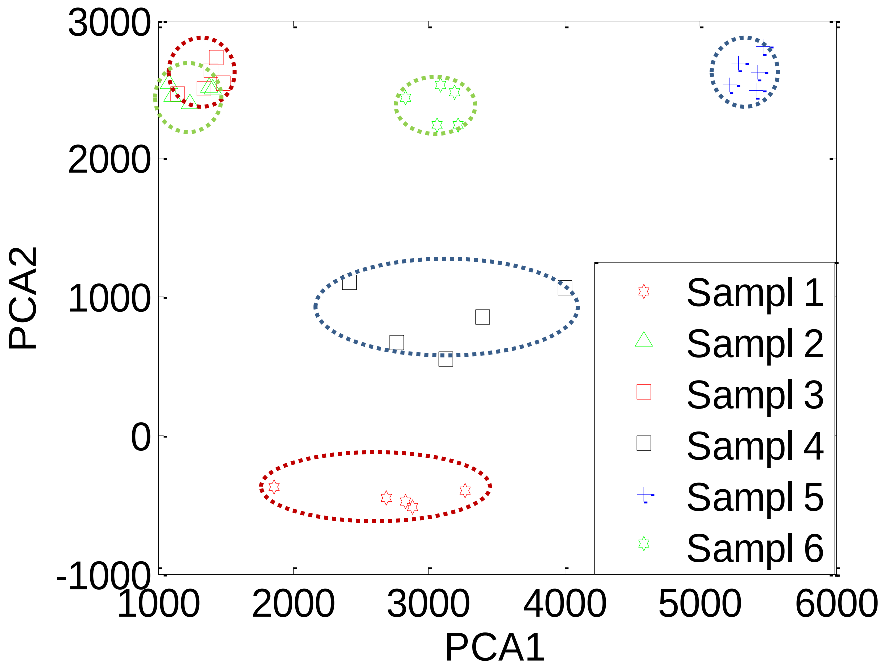

a)

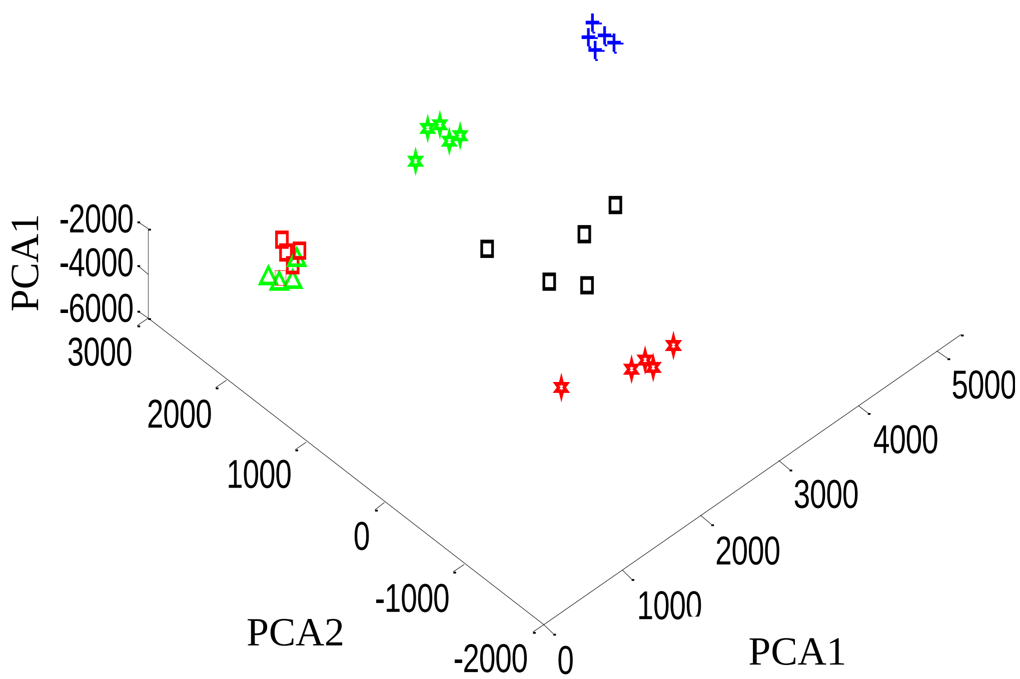

b)

Figure 5.11: Discrimination using PCA for six handguns in the holder using: a) Two PCA components, and b) Three PCA components.

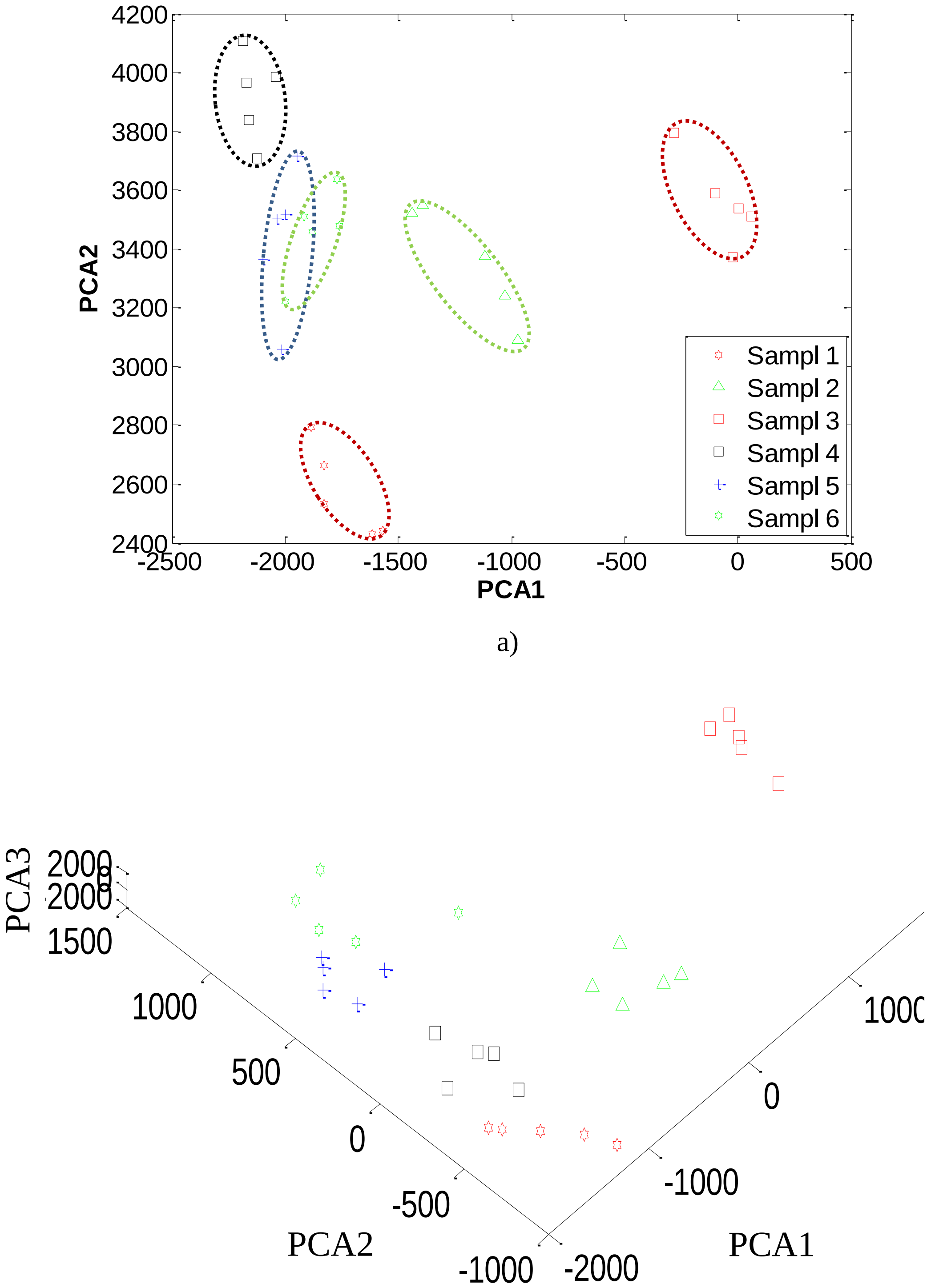

a)

b)

Figure 5.12: Discrimination using PCA for six handguns concealed inside a person jacket pocket using: a) Two PCA components, and b) Three PCA components.

5.3.3 Time-frequency based features

Feature extraction using time-frequency analysis has been used for study of EM response signal. Features are extracted from the scattered field of a given candidate target from the time-frequency plane to obtain a single characteristic feature vector that can effectively represent the target of concern [80].

In this work the feasibility is investigated of using the time-frequency domain as a feature extraction technique in terms of its outcomes in improving detection and classification capability of the new system. Two different features were extracted using two different techniques, which are the Fast FT (FFT) and WT. Brief backgrounds of FFT and WT are given below along with the motivation behind their use, and the feature extraction approaches employed are detailed in subsequent sections.

5.3.3.1 Fast Fourier transform

The Fourier series provides an alternative way of representing data. Instead of representing the signal amplitude as a function of time, the signal represents how much information is contained at different frequencies. This technique is important in data acquisition, just as it is in stereos that allow you to isolate certain frequency ranges. In general the FFT is a better way to compute the Fourier transform of discrete data [72].

The signal can be decomposed as a weighted sum of sinusoid functions. This provides a feasible way of computing the power spectrum for a signal. The power spectrum then allows to be computed the Fourier coefficients more rapidly. The power spectrum serves as the fingerprint of the analysed signal and can be used for the detection and classification of concealed weapon [72]. Researchers usually only care how much information is contained at a particular frequency, irrespective of whether it is part of a sine or cosine series. Therefore, they are interested in the absolute values of the FFT coefficients. The absolute value of FFT for an EM signal provides the total amount of information contained at a given frequency, where the square of the absolute value is considered to be the power of the signal [139].

In this work, the power spectrum (PS) at each frequency for each object signal is used as a feature vector to discriminate between different objects, where each object gives a different PS. Examples are shown in Figure 5.13, where the FFT was applied and the absolute value of the result was squared to obtain the PS.

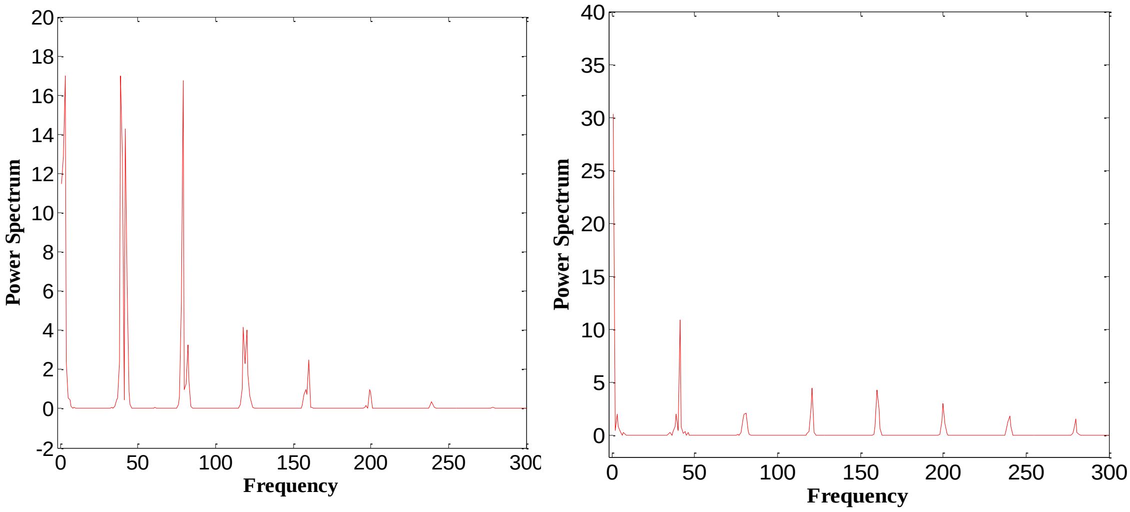

a) b)

Figure 5.13: Part of the power spectra of: a) Handgun, and b) Mobile Phone.

The PS results will be (40*140), so to reduce the size of data before being sent to the classifier, PCA techniques were applied and the first three PCA components were selected since these accounted for 99.6% of the variance. Subsequently, the data is subjected to PCA and the data is approximated using a limited number of the most significant eigenvectors. So, at the end, each object has 3 features delivered from the FFT process, as summarised in Figure 5.14. These are fed to the classifier method, named *f-FFT* as detailed in the next chapter.

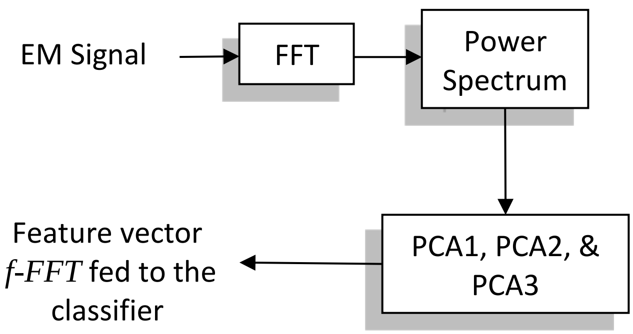

Figure 5.14: FFT feature extracted steps.

Figure 5.15 shows the behaviour of the PCA feature vector extracted from the FFT process. The test was conducted using the six handguns along with the different non-threat objects. It is clear from Figure 5.15that handgun #4 gives a very low response because it consists of plastic material, and the mobile phone gives a high response because it is fully charged, as mentioned previously. Therefore, these features alone cannot discriminate between the different samples and they should be fused or combined with other features for accurate classification.

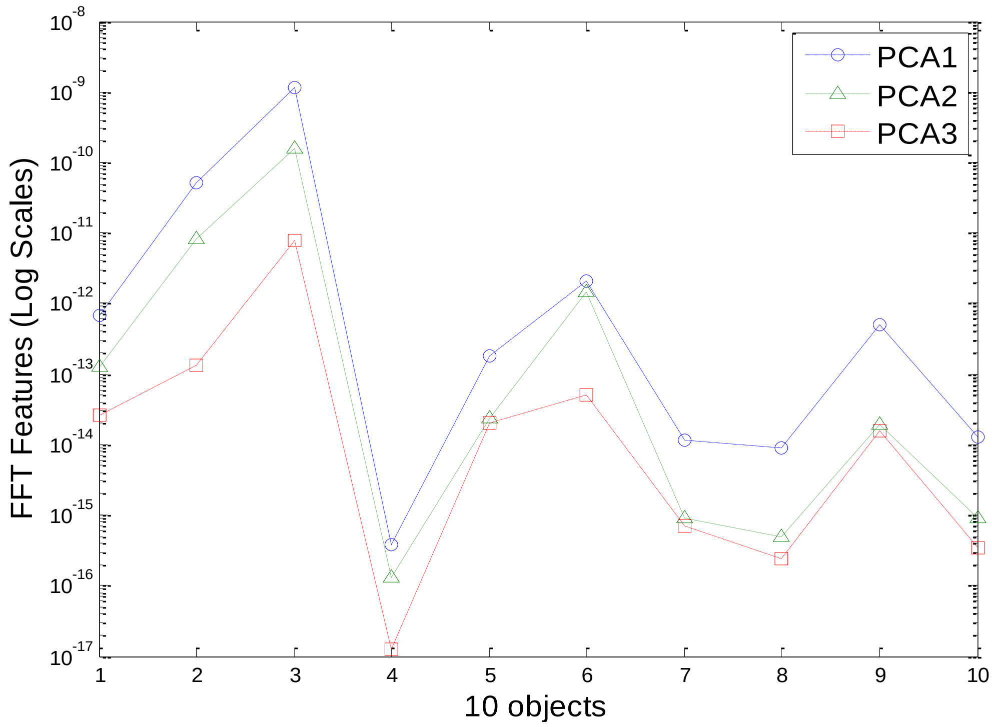

Figure 5.15: Feature vector extracted from the FFT process for 10 objects, #1-#6 are threat items (handgun samples) and the others (#7-#10) are non-threat items (camera, house key, mobile phone and pen).

5.3.3.2 Wavelet transform

In contrast to the FFT, wavelet transform (WT) analysis is useful in decomposing a time series into simultaneous time-frequency space. The analysis provides information about both the amplitude of any "periodic" signals within the series, and how this amplitude varies with time. The origins of wavelet analysis dates back to the mid-1980s and it was originally driven by the need for applications to analyse seismic signals more sensitively than with Fourier techniques [140]. This method has been used to represent time series data such as ECG waveforms and mine signal detection [81-83], and it can be thought of as an extension of the classic Fourier transform except that it operates on a multi-resolution basis. The multiresolution feature of the WT enables a signal to be decomposed into a number of resolutions (also called scales) via the dilation and translation of a specified analysing (also called a “mother” wavelet). Each resolution represents a particular level of coarseness of the signal. The preservation of spatial information after the transformation is another feature of the wavelet transform [140].

This enables the identification of areas in the original signal that correspond to particular object characteristics present in the wavelet transform data. An example of this is its application to electrocardiogram signals, which in some respects resemble metal detector signals [141]. Previous researchers have also verified that the WT can be used to produce features from metal detector data suitable for target classification [78, 84].

In this study, the discrete wavelet transform has been used. Since the target responses consists of early and late time responses, the multiresolution property of the WT is well suited for analysing such data. The term “discrete” here refers to discrete sets of dilation and translation factors, and discrete sampling of the signal. At a given scale, J, a finite number of translations is used in applying multiresolution analysis to obtain a finite number of scaling and wavelet coefficients. The signal can be represented in terms of the following coefficients (Eq.5.6) [31]:

$$f(x,y) = \sum_k C_{JK} \ \varphi_{JK}(x) + \sum_{j=1}^{J} \sum_k d_{jk} \psi_{jk}(x) \qquad 5.6$$

where φ_{JK} are the scaling functions, C_{Jk} are the scaling coefficients, ψ_{jk} are the mother wavelets and d_{jk} are the wavelet coefficients. The first term in Eq.5.6 gives the low resolution approximation of the signal, while the second term gives the detailed information at resolutions from the original down to the current resolution J. Daubechies order 4 has been selected from the wavelet family, due to its similarity to the waveforms generated by metal detection target signals [84, 142], and three resolution levels of wavelet decomposition have been implemented to encapsulate the majority of the significant wavelet behaviour, and to eliminate most of the significant wavelet behaviour which corresponds to background noise in the signal. Three types of statistical operation were applied to the wavelet approximation coefficients as a unique fingerprint for each object. These statistical operations are entropy (ENT), standard deviation (STD) and root mean square (RMS). As a result, each EM image has three types of features with three levels of decompositions. Thus, a feature vector was generated named *f-WT* consisting of 9 values to be fed to the classifiers. Figure 5.16 shows the flowchart diagram of the classification procedure using WT.

Figure 5.17 shows the resulting features of ENT, STD and RMSE for the three WT levels using the same 10 handguns and non-threat objects as in the previous test. It can be seen from this figure that these feature give good indications to discriminate between the handguns and the other objects. However, some of the non-threat objects have features close to those of the handguns, such as the entropy of the house key for instance. This leads to the need to combine wavelet features with the other features in order to improve the classification results.

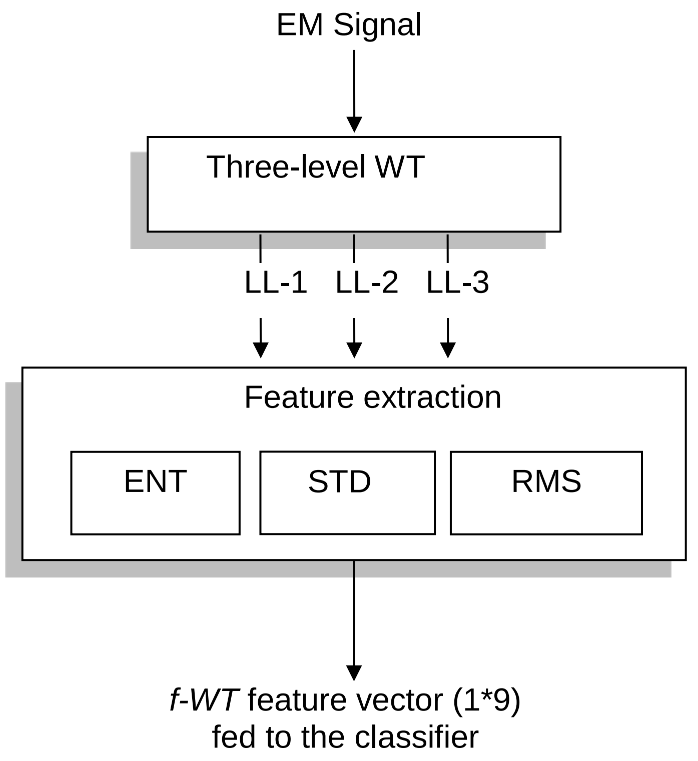

Figure 5.16: Flowcharts of the gun classification procedure using discrete wavelet transform features.

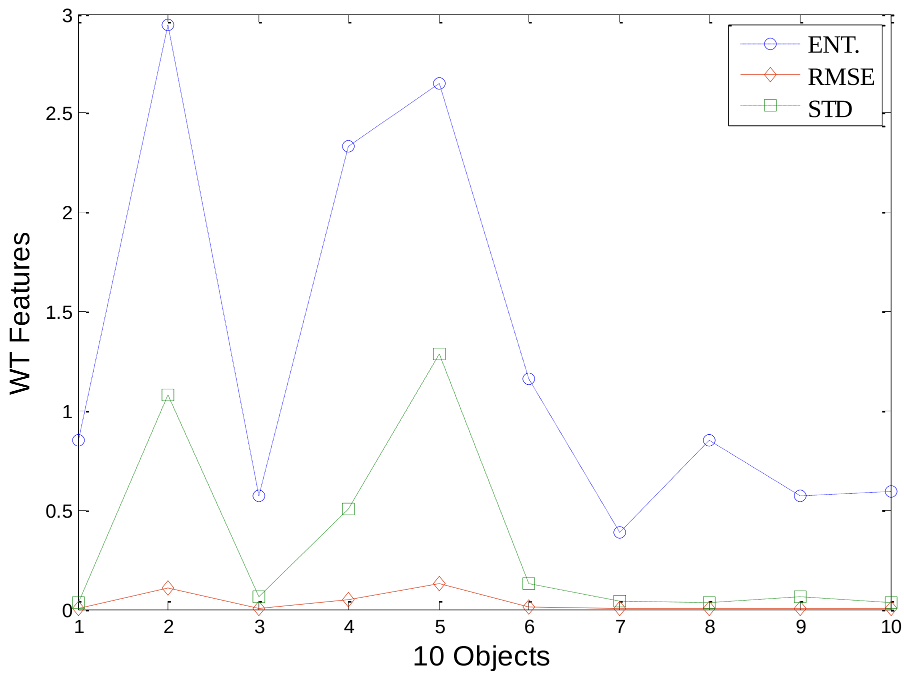

Figure 5.17: Wavelet feature for 10 objects, #1-#6 are threat items (handgun samples) and the others (#7-#10) are non-threat items (camera, house key, mobile phone and pen), for the one-level WT analysis.

5.3.4 Transient analysis features

Analysis of the transient image sequence can be used to obtain more information about the object under examination, and is especially useful for object classification. In this work, a cross-correlation technique is used to obtain signatures for the objects under test using the sequences of 14 images generated by the new system as detailed in Chapter 3.

Cross-correlation techniques can be used to generate useful features for metallic object detection and characterisation. Young [36] designed a system for gun detection using a portion of the microwave frequency spectrum. In his work, the cross-correlation between coherence polarisation and cross-polarisation RF returns was used to distinguish between different threat objects. Normalized cross-correlation has also been implemented in our previous work [94], using the EM transient response signal obtained from a sequence of EM images to detect different angular defects (this technique is detailed in Appendix D).

In our work [95] a novel cross-correlation technique was used to classify different objects into a number of groups such that: paramagnetic, ferromagnetic and combinations of both depending on the transient analysis features. The EM images were generated using the pulse response from the material in the handguns and other daily used objects under inspection. The cross-correlation for each two successive images *f(s,t)* and *g(x,y)* in this sequence is calculated using Eq.5.7. Then the maximum value of each cross-correlation result is aggregated for all of the 14 images pairs to create a 13-value feature vector, to be used as a unique fingerprint for each sample under test [77].

$$C(x,y) = \sum_s \sum_t f(s,t)\, g(x+s, y+t) \tag{5.7}$$

for x=0,1,2,…,M-1, y=0,1,2,….,N-1, and the summation is taken over the image region where *g* and *f* overlap.

The whole cross-correlation analysis procedure is summarized in Figure 5.18.

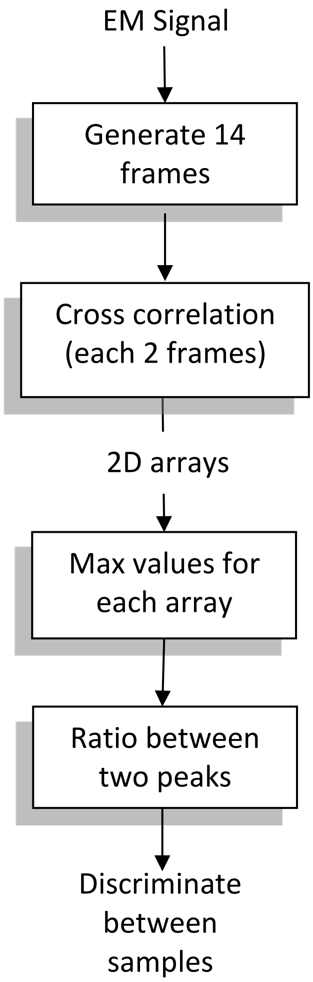

Figure 5.18: Cross correlation analysis steps

An example is shown in Figure 5.19, where a cross-correlation technique has been applied to the transient image sequence obtained from the new system and processed to classify the objects into paramagnetic, ferromagnetic, and combinations of both. Figure 5.19a represents maximum cross-correlation values between each two frames for 20 different items. Figure 5.19b shows the results of computing the ratio between two peaks which are evident in the cross-correlation plot shown in Figure 5.19a, where different objects have unique transient features reflecting materials and geometrical characteristics. The results can be applied for object discrimination and are sorted according to ascending amplitude. It can be seen from Table 5.2 that a clear distinction can be made between paramagnetic, ferromagnetic and mixed objects, thus allowing very good discrimination.

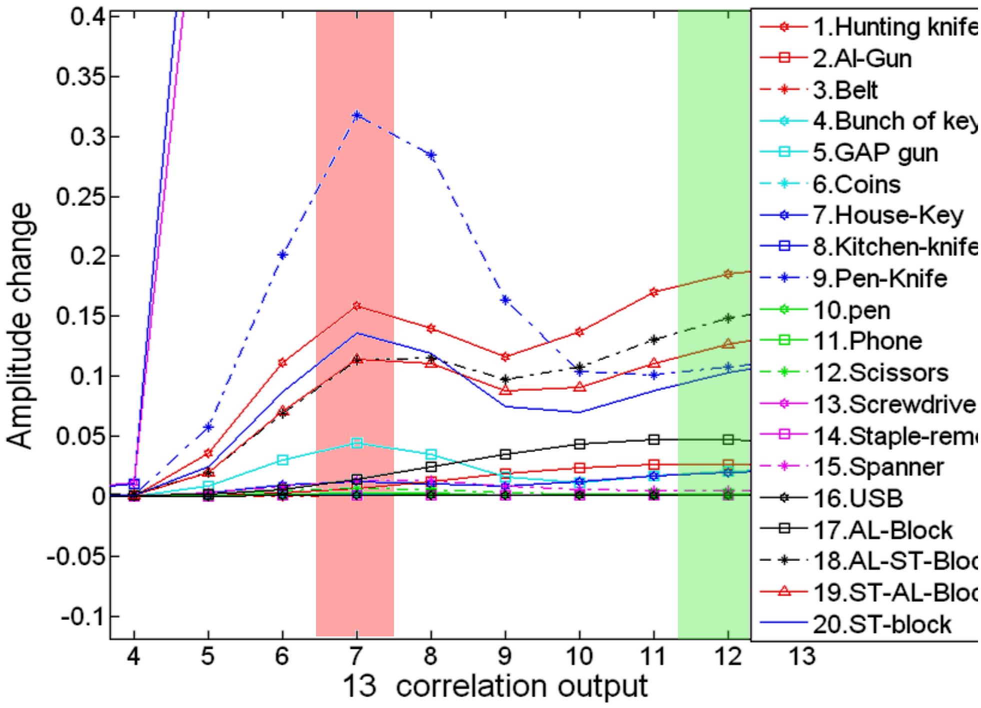

a)

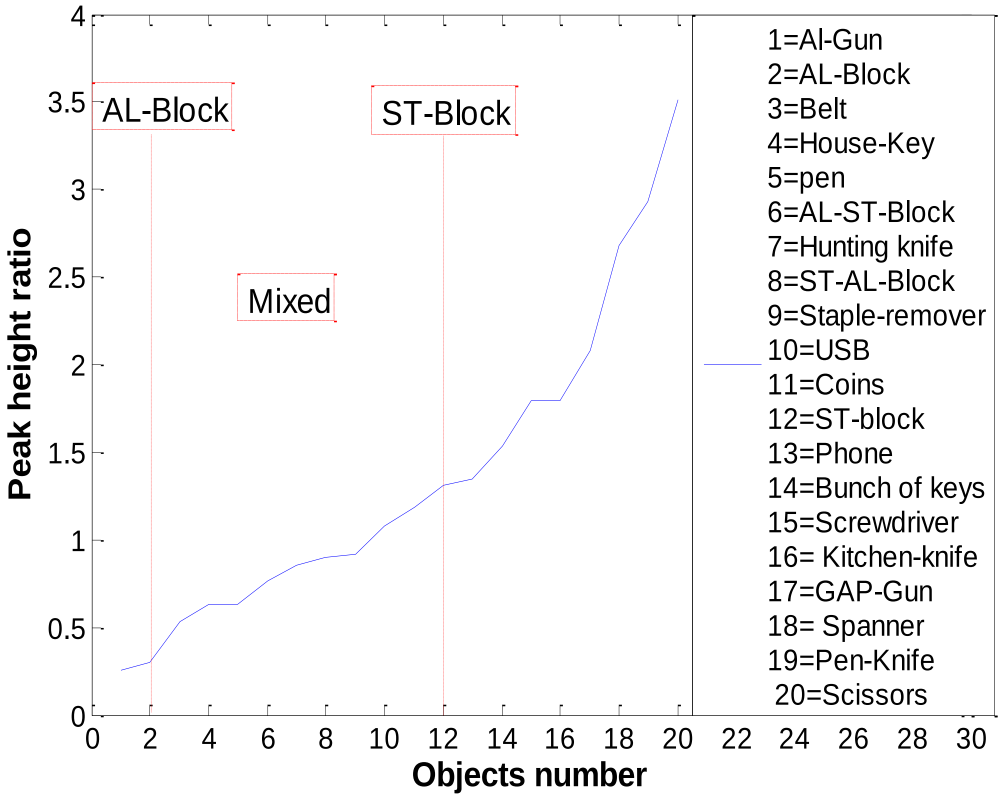

b)

Figure 5.19: Material determination through transient analysis: a) Maximum cross-correlation between each two successive images in transient sequences for 20 different objects, and b) Ratio of highest two peaks of each curve in (a). (AL=aluminium, ST= steel)

Table 5.2: Cross correlation results (AL=aluminium, ST= steel)

Class 1 Para-magnetic	Class 2 Mixed	Class 3 Ferro-magnetic
AL-Block	ST-AL-Block	ST-Block
Gun shaped AL-Block	AL-ST-Block	Screwdriver
	Hunting-Knife	Kitchen Knife
	House-key	Pen-Knife
	Belt	Gap-gun
	Staple-remover	Scissors
	Coins	Spanner
	USB	Bunch of keys
	Pen	Phone

The validity of the maximum cross-correlation value has been proved in previous tests in that each sample has a different signature from the transient response analysis, and so each cross-correlation is aggregated for all the 14 images pairs to create a 13-value feature vector to be used as an input for the automatic classification purposes described in the next chapter.

5.4 Feature Combination

Several attempts at feature fusion were conducted in order to identify and discriminate between real handguns and items in daily use based on combinations of the feature categories described above. Some of these attempts are explained in this section, and have been discussed in more detail elsewhere [143, 144].

5.4.1 Feature combination for handgun identification

To distinguish between the various handgun samples two features are used. In the first attempt, edge chain features are combined with maximum amplitude change features. To select the best feature from the seven edge chain features, minimum Euclidian distances between the two edge chain code feature vectors in the optical and EM images using the six handguns have been obtained and the results are shown in Table 5.3. It is clear that the STD^{2nd} feature has the lowest Euclidian distance, and so it is the best one to represent the handgun samples. Figure 5.20 illustrates the feature space plot for the discrimination and identification of the six handguns using STD^{2nd} and PCA features.

Table 5.3: Minimum Euclidian distance between two feature vectors

Features	**Mean^{1sr}**	**Var^{2nd}**	**STD^{2nd}**	**ADev^{2nd}**	**Skew^{3nd}**	**Kurt^{4nd}**	**R_v**
Euclidian D.	0.7	0.8	0.3	0.5	1.3	3.2	1.1

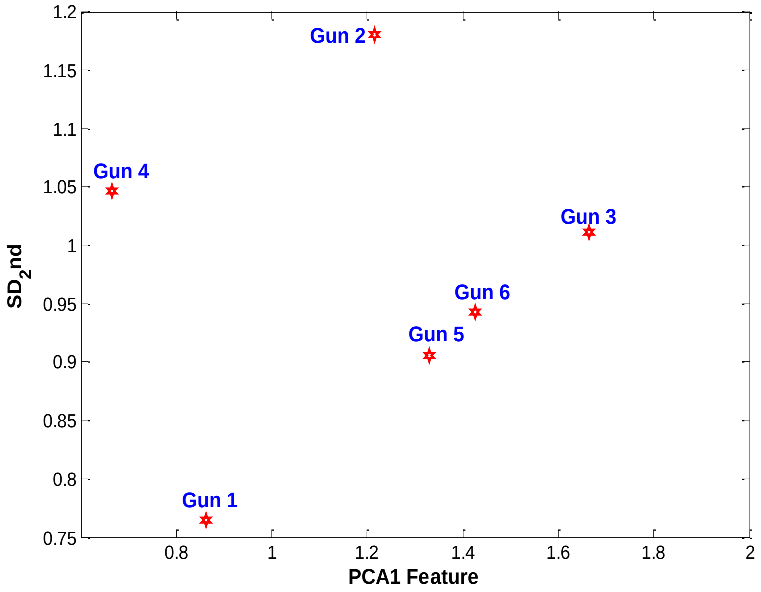

Figure 5.20: Handgun identification using PCA and edge chain code features.

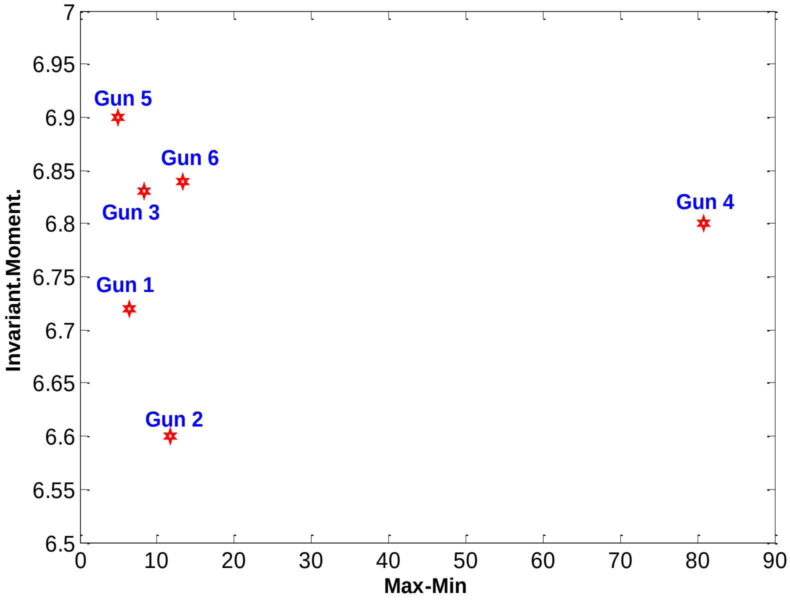

Figure 5.21: Handgun identification using maximum amplitude change and first invariant moments features.

In another attempt a different combination of the features of maximum amplitude change (*f-Max-Min*) and invariant moment was tested and the results are illustrated in Figure 5.21. It is worth mentioning that all of the other seven moments yield results very close to that of the first moment. In Figure 5.20 and Figure 5.21 the different samples can be identified. The six handgun samples are made from different combinations of materials, and sample 4 which was a Glock pistol can be easily discriminated. This could be because this sample is made from ordnance grade steel material and also contains a lot of plastic polymer. The results for samples 1 and 2 also allow relatively good discrimination. Samples 3, 5 and 6 are nearest to each other, from which it may be infer that they are made from very similar materials, and they also have high weights (937g, 800g, 1140g respectively), compared to samples 1, 2 and 4 (which weigh 516g, 637g, and 689g respectively). Using this identification approach, promising results for clustering and classification are expected.

5.4.2 Feature combination for daily used items

Different combinations of features using EM images have been investigated to discriminate between other objects which are not handguns (the database for such objects was detailed in Chapter 3). One of these tests is shown in this subsection, where the relationship between the first invariant moment and maximum amplitude change features are plotted in Figure 5.22.

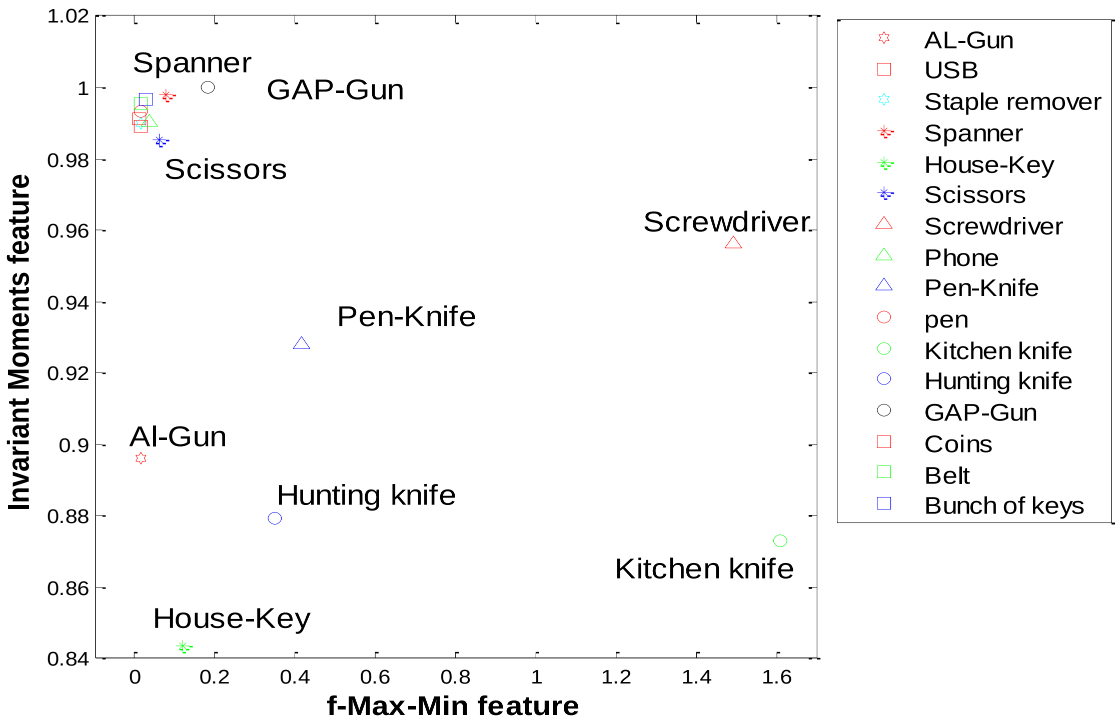

Figure 5.22: Object identification using invariant moment and maximum amplitude change features

It can be seen from Figure 5.22 that some of the threat objects, i.e. the kitchen knife, hunting knife, pen-knife, GAP gun, Al-Gun, screwdriver, spanner and scissors, can be discriminated from the other objects, which are the USB stick, staple remover, mobile phone, pen, coins, belt, and bunch of keys. Most of the non-threat items are clustered in the top-left corner of the figure, while the threat items are scattered throughout the feature space. Hence, discrimination using the invariant moment and maximum amplitude change features is used to classify daily used items (non-handguns) in the next chapter.

5.5 Summary

New approaches to weapon detection have been successfully tested based on features extracted from the EM response signal of a target. A comprehensive study and investigation of feature extraction tools has been carried out in this chapter. Geometrical shapes, material features, transient response features and time-frequency features were extracted from the EM data. Features were selected and integrated to obtain better object identification and discrimination. Feature vectors were prepared to feed to the classifiers for the next classification steps.

A novel time-frequency image correlation method is proposed and successfully tested. This method is a good candidate for numerous applications where time-varying EM field images are encountered, pertaining to material discrimination among ferromagnetic and non-ferromagnetic metals. The PCA features have shown promising results. The PCA1 and PCA2 components can discriminate between handguns and other commonly used items very clearly, whereas PCA3 has been found to be able to discriminate among members of the handgun group when plotted together with PCA1 and PCA2. On the other hand, edge chain code features have been neglected in this analysis because the configuration of the sensor-array adopted did not provide EM images corresponding to the actual sample shape.

Several attempts were conducted in this chapter to determine the possibility of identifying and discriminating between real handguns and daily used items based on combinations of feature categories. Several feature combination tests have been carried out using feature clustering in two- or three-dimensional feature space. These combinations showed the feasibility of identifying different handguns as well as non-threat objects.

The proposed feature extraction techniques have achieved good object detection and identification performance using the new data system. Some promising results indicating the feasibility of using these data to characterise and classify objects have been produced. Table 5.4 shows a comparison of the extracted features with the numbers of features in each feature vector.

In the next chapter the prepared feature vectors from this chapter will be the input for techniques for automatic threat object classification.

Table 5.4: Comparison of the extracted features

Technique	**Purposes**	**Limitation**	**No.**
Edge chain code	Shape descriptor	Only binary data and EM images equivalent to the optical images	7
Invariant moments	Describe the geometric behaviours of the image intensity distribution	Preferable to use the 8 moments together	8
Principal component analysis	Preserves the total variance of the images in the first few components	Neglects redundant information and small data variations	3
Maximum-minimum	Finds amplitude range of each image - directly related to EM intensity	Only measures the maximum EM field change – no information on distribution, etc.	1
Fast Fourier transform	The signal will be represented in frequency domain	Could not represent the data in the time domain	3
Wavelet transform	The signal will be represented in time-frequency domain.	Adjustment needed to select mother wavelets and the number of levels analysis	9
Cross correlation	Track the correlation between transient images	Only applicable to transient data	13

Chapter 6: Automatic Classification of Threat Objects

In threat object detection applications the EM images can be displayed after pre-processing for operator-assisted weapon detection or fed into a weapon detection module for automated weapon detection and classification. Automatic or machine recognition and classification are important, since the images obtained from the EM fields provide mostly ghost imaging which is not directly related to the object's properties and so is very difficult to interpret. Among the various frameworks in which pattern recognition has been traditionally formulated, the statistical approach has been most intensively studied and widely used in metal detection and classification. More recently, artificial neural networks (ANN) and support vector machines (SVM) imported from statistical learning theory have been receiving increasing attention.

In this chapter, two different types of classification techniques are investigated and compared, in order to identify an efficient technique for an automated classification process that suits the proposed system, and to evaluate the appropriate feature or feature combinations extracted from the EM response signature detailed in Chapter 5. The two classification methods are the ANN and SVM, both of which are supervised learning classifiers. The architecture and design of the classifiers are then presented. A set of training tests were carried out using the feature vectors prepared in Chapter 5 with a proposed feature combination framework. Classification methodology and test bed setup are explained, and two groups of objects representing threats and non-threats were used. Finally, the results are presented and the accuracy of each classifier for the identification of threat objects using the proposed system is discussed.

6.1 Pattern Recognition Methods for Object Classification

Pattern recognition and classification aims to classify objects based either on a priori knowledge or on special information extracted from the pattern. The objective of this process is to classify the patterns of objects based on the feature extracted from them. Four classification methods are widely used for object classification. Decision tree classification is a technique for object classification based on a tree-like model, using decision tree learning. This classification method is very simple for people to understand and interpret. However, the decision has to be generated in advance based on expert knowledge and descriptions of the object. The K-nearest neighbour (KNN) classification method is a type of instance-based learning method that classifies unlabelled objects based on their similarity to examples in the training set. This method is analytically tractable and simple to implement. The biggest advantage of using KNN is that it is a method using highly adaptive local information. However, this method is also very susceptible to high dimensionality [100]. Alternatively, ANN and SVM methods are implemented in this work because of the capability of these methods to perform parallel processing on large input data sets simultaneously. They are good at classifying patterns when the training data is complex and noisy [145], which is more like the situation in this work.

6.2 Artificial Neural Network Classifier

Among pattern recognition techniques, ANNs have been increasingly used as an alternative way to implement basic pattern classifiers such as KNN classifiers [146]. ANNs can be viewed as systems inspired by the operation of biological neural networks. An ANN consists of an interconnected group of artificial neurons which process information based on their self-learning ability. The main characteristics of neural networks are that they have the ability to learn complex nonlinear input-output relationships, use sequential training procedures, and adapt themselves to the data [145]. This method is used in pattern recognition and classification since it does not need any information about probability distributions or the priori probabilities of different classes [100]. In addition, ANNs have the capacity for distributed information storage, parallel processing, reasoning, and self-organization. They also have the capability of the rapid fitting of nonlinear data, and can thus solve many problems which are difficult when using other methods [101].

The three major advantages of using ANNs are that: (1) they can perform classification work that a linear classifier cannot; (2) when one element of an ANN fails in operation, the network can continue based on their parallel nature; and (3) the way ANNs learn does not need to be reprogrammed. However, there are two major drawbacks of ANNs: (1) every ANN needs to be trained before use; and (2) a long processing time is needed for a large neural network [146].

ANNs have been used widely in metal object detection and classification [78, 88, 91, 102-104, 147], as reported in Chapter 2. Two major types of ANN have been developed for detection and classification: feed-forward neural networks [148-150] and recurrent neural networks [151]. Among several ANN applications, it has been concluded that feed-forward neural networks are used in most applications [100, 152].

6.2.1 Neural network selection for threat object detection

In pattern recognition there are many ways to develop classifiers, and methods which follow the neural networks paradigm have been among the most successful [100]. A number of neural networks have been developed based on different applications. Based on the learning algorithm, the feed-forward back-propagation neural network (BP neural network) is considered the simplest and most successful neural network for pattern recognition. This is because the information moves in only one direction in this network, forward from the input nodes, then through the hidden nodes and to the output nodes. There are no cycles or loops in the network [146]. This characteristic makes BP neural networks more robust in solving the metallic object classification problem effectively when the input data (features) contain overlapping information. So, in this work, a feed-forward BP neural network is selected as the classifier used for the proposed system.

Each input into the neuron has its own weight associated with it. A weight is simply a floating point number and it's these adjust when eventually come to train the network. The weights in most ANN can be both negative and positive, therefore providing influences to each input. As each input enters the node it's multiplied by its weight. The node then sums all these new input values which gives the activation (again a floating point number which can be negative or positive). If the activation is greater than a threshold value, number 1 as an example, the neuron outputs a signal. If the activation is less than 1 the neuron outputs zero..

A neuron can have any number of inputs from *1…n*, where *n* is the total number of inputs. The inputs may be represented as x_1, x_2, x_3... x_n, and the corresponding weights for the inputs as w_1, w_2, w_3... w_n. The summation of the weights multiplied by the inputs is typically called a step function as in Eq. 6.1 [153].

$$A = \sum_{i=0}^{i=n} w_i x_i \tag{6.1}$$

Feed-forward BP neural networks allow signals to travel one way only; from input to output with no feedback. The output of any layer does not affect that same layer. Feed-forward BP neural networks tend to be straightforward networks that associate inputs with outputs. The architecture of a three layer feed-forward BP neural network is shown in Figure 6.1. This network consists of the input layer, hidden layer and output layer. There can be multiple hidden layers, so the feed-forward BP neural network is also called a multilayer perceptron [146].

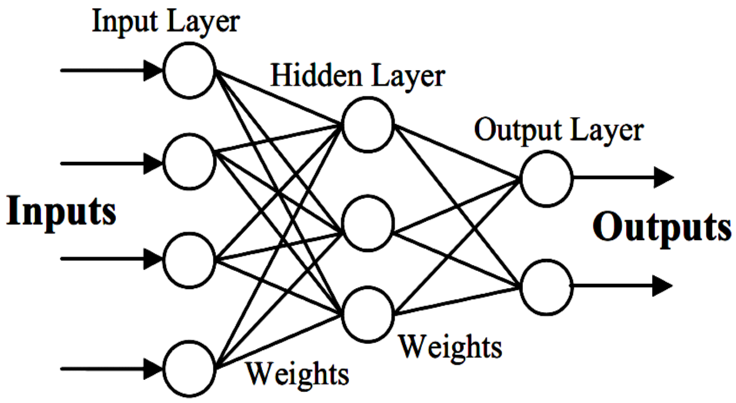

Figure 6.1: Architecture of a three layer feed-forward neural network

6.2.2 Feed-forward BP neural network learning

When the training of feed-forward neural network is being undertaken, the weights of each neuron are adjusted in such a way that the error between the expected output and the actual output is decreased. This process requires that the neural network computes the error derivatives of the weights. In other words, it must calculate how the error changes as each weight is slightly increased or decreased. The back propagation algorithm is a very typical supervised learning method for determining these weights. For example, when a data set is applied to the neural network, the network produces some output based on the current weights. This output is compared with the expected output, and a mean-squared error value is calculated. The error value is then propagated backwards through the network, and small changes are made to the weights in each layer. The weight changes are calculated in order to reduce the error signal for the case in question. The whole process is repeated for each of the example cases, and then reiterated with the first case again, and so on. The cycle is repeated until the overall error value drops below some pre-determined threshold. Mathematical presentations of the BP algorithm can be found in [145, 153].

The architecture of the proposed feed-forward BP neural network can directly influence the speed of convergence of network training and the accuracy of object classification. The design of BP neural network architecture mostly refers to the numbers of layers and neurons in each layer.

6.2.2.1 Number of layers

The BP neural network designed in this work for metallic object classification has one input layer and one output layer. The number of hidden layers needs to be decided prudently as it may directly influence the results. Cybenko pointed out in the Cybenko theorem (1989) that, with respect to a data set which can be classified using a linear classifier, the hidden layer is not necessary [154]. It may complicate the network and even degrade the results. Therefore, a feed forward neural network with one single hidden layer is capable of approximating any continuous, multivariate function to any expected degree of accuracy. Technically, increasing the number of hidden layers can enhance the processing capabilities of neurons. However, it also makes the network far more complicated and will rapidly increase the time needed for the training process. Based on the reasons outlined above, in this work one hidden layer is believed to be sufficient to solve the object classification problem.

6.2.2.2 Number of neurons in each layer

The number of neurons in the input layer is totally dependent on the dimensions of the input data. For example, in this work the number of input neurons is eight when *f-moment* feature vectors are used as an input. On other hand, the number of neurons in the output layer is equal to the number of categories desired. So, the number of neurons in the output layer in this work is one, for guns or non-guns. The non-guns objects are further classified as threats or non-threats at the second stage.

The decision about the number of neurons in the hidden layer is always a complicated issue and has been discussed by many researchers. It is normally decided based upon the application concerned, although it does not have to be a certain number for any specific application. Hecht-Nielsen [155] suggested that the number of neurons in the hidden layer for a neural network with one hidden layer should be smaller than $2N+1$, where N is the number of neurons in the input layer, in order to insure that the neural network is able to approximate any continuous function. In another method [156] it is suggested that the number of neurons should be equal to $\sqrt{M+N}+i$, where M is the number of output neurons, N is the number of input neurons and i is varied from one to ten.

6.2.3 ANN specifications used for threat object detection

Table 6.1 summarizes the BP ANN specifications used in this study. Feature vectors generated in Chapter 5 are used as input to the ANN classifier. A three-layered ANN classifier was used. The number of nodes in the hidden layer was selected to be 2N nodes based on [155] with the sigmoid activation function. Sigmoid functions are commonly used in ANNs because of their special mathematical properties. These properties include continuity, differentiability at all points and monotonicity (i.e. monotonically increasing within a finite range). Among several types of sigmoid functions, the "*logsig*" function *S(t)* was used for the hidden layer in this work as in Eq. 6.2 [153]:

$$S(t) = \frac{1}{1 + e^{-t}} \tag{6.2}$$

The output layer consists of a single output neuron to provide the classification of the target (1= gun, 0= non-gun in the first stage, and 1= threat, 0=non-threat in the second stage) with a linear activation function. The ANN classifier was trained using the BP learning rule with the Levenberg-Marquardt algorithm. This algorithm appears to be the one of the fastest methods for training moderate-sized feed-forward neural networks [132].

Table 6.1: Artificial Neural Network Parameters (as used in MATLAB)

No. of nodes in Input layer	:	Same no. of feature vector elements used (N).
No of nodes in Hidden layer	:	Double no. of used features (2N).
No of nodes in Output layer	:	One node (gun or not).
Transfer function	:	'logsig' for hidden layer, 'purelin' for output layer
Training function	:	'trainlm'
Max number of Epochs	:	10000
Min performance gradient	:	1e-10

6.3 Support Vector Machine Classifier

Recently SVM has attracted considerable interest in the classification field area. Although the subject can be said to have originated in the late 1970s [129], it is only in the past decade has it received close attention. The SVM is a concept in statistics and computer science which involves a set of related supervised learning methods that analyse data and recognize patterns, and used is for classification and in regression analysis [157]. The SVM runs by itself and does not require any human intervention, and it can also be trained very quickly, even when the feature space has more than 20 dimensions. In this work, the SVM based method is used as a second classification method to classify EM signals since it is good at classifying patterns when the training data is complex and noisy [145], which is the case in the presented context. A comparison of the SVM with the ANN results was made to determine which method is most suitable for the proposed system.

6.3.1 The principles of SVM

The SVM is a binary classification method that takes as input labelled data from two classes, and then outputs a model file for classifying new unlabelled or labelled data into one of two classes. The basic objective of an SVM is to find the optimal hyper-plane that correctly separates the data of the two classes as completely as possible (see Figure 6.2). This method maximizes the margin between the classes by selecting a minimum number of support vectors. Non-linear SVM classifiers operate in two stages: first they perform a non-linear mapping of the feature vector onto a high-dimensional space that is hidden from the inputs and outputs, and then they construct an optimal separating hyper-plane in the high-dimensional space [158].

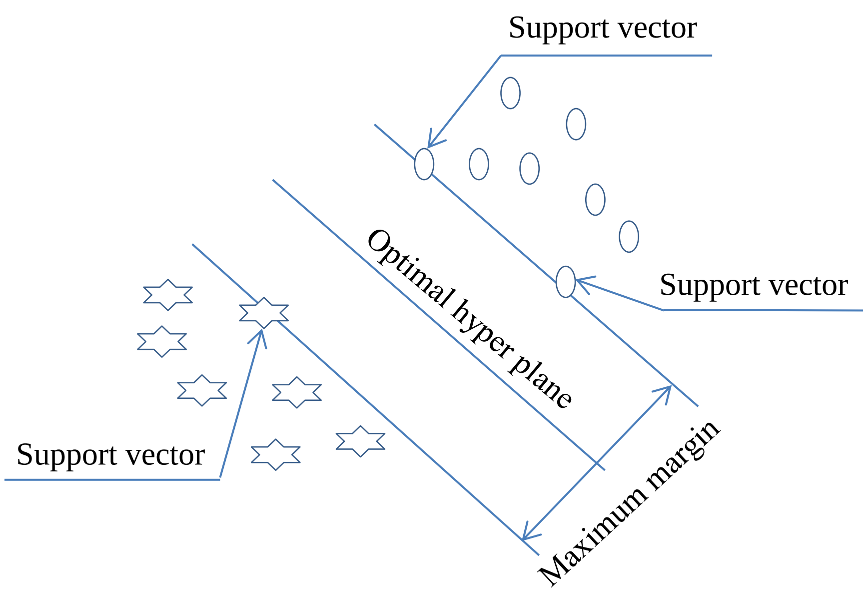

Figure 6.2: Classification of data by SVM

The SVM abstracts a decision boundary in multi-dimensional space using an appropriate sub-set of the training set of vectors; and the elements of this sub-set are the support vectors. Geometrically, support vectors are those training patterns that are closest to the decision boundary. This method is based on the idea of mapping the data x into a higher-dimensional feature space via a nonlinear mapping ϕ, and linear regression is then worked out in this space. The general regression problem can be described as follows: given a group of training samples, and learn machines (training) study the relationship among the input-output variables. Assuming the given training data ((x_i, x_j), i = 1,2, ... ,l), in which $x_i \in R_n$ is the i^{th} point of a study sample of n-dimensional input values, $x_j \in R$ is the corresponding target value, and $_j$ is the number of training samples. The goal is to find a function *f(x)* which can make a good approximation to all the sample points. In general, the support vector machine estimating function is (Eq.6.3) [159]:

$$f(x)=<\boldsymbol{\omega}^T.\ \phi\ (x)>+b \tag{6.3}$$

where, *f(x)* is the regression function; $\boldsymbol{\omega}$ is the normal vector; *b* is the offset; and ϕ (x) is the feature mapping function.

6.3.2 Kernel selection

The standard support vector regression algorithm at the same time needs a kernel function to be introduced, such as Eq.6.4:

$$\mathrm{K}(x_i; x_j)= \phi\ (x_i)^{\mathrm{T}}\ \phi\ (x_j) \tag{6.4}$$

Though new kernels have been proposed by researchers, four main types could be used: linear, polynomial, sigmoid and radial basis functions.

In this work, the radial basis function (RBF) is used as a kernel (K), as in Eq.6.5 [105]:

$$K(x_i, x_j) = \exp(-\gamma \|x_i - x_j\|^2), \gamma > 0 \tag{6.5}$$

Here γ is a kernel parameter. The RBF kernel was selected for two reasons. Firstly, it maps samples nonlinearly into a higher dimensional space so that, unlike the linear kernel, it can handle cases when the relationship between class labels and attributes is nonlinear. Secondly, the number of hyper-parameters influences the complexity of model selection, and the RBF kernel has less hyper-parameters than the polynomial kernel. Hence the RBF kernel is associated with fewer numerical difficulties [160].

There are two parameters for an RBF kernel: C and γ. C > 0 is the penalty parameter of the error term and γ is the kernel parameter of the RBF. It is not known beforehand which C and γ is best for a given problem; consequently some kind of model selection or parameter search must be conducted. The goal is to identify a good (C; γ) so that the classifier can accurately predict unknown data. The LIBSVM, is a library for SVM developed by Chang and Lin [105] and is used in this work. Chang and Lin developed an improved procedure known as cross-validation to find the best (C; γ) and embed it in the LIBSVM library core.

As specified by [105], all the feature vectors are normalised to the range [-1, +1] in each column as a preliminary step in applying SVM. The advantages of scaling are to avoid attributes in greater numeric ranges dominating those in small numeric ranges and to avoid numerical difficulties during calculation. After training using the SVM, the model is obtained for the prediction of unknown objects.

6.4 Classification Strategy

Features extracted from EM response signals were applied, individually and in combination, to the ANN and SVM classifiers through two major stages in order to categorise the objects under test into *Gun* and *Non-gun* in stage one, and in a second stage the *Non-gun* were categorised into *Threat* and *Non-threat* items, *Threat* items here refers to the any common daily used objects which have the ability to directly injure a human body or are otherwise considered to be harmful objects. Based on the initial classification results, the features with the highest classification rates (*Hcr*) were selected to be combined with the other features in order to gain higher classification accuracy. If the new classification rate is less than the previously achieved classification rate or when 100% is achieved then the combination process is halted. The block diagram of the classification strategy is explained in Figure 6.3.

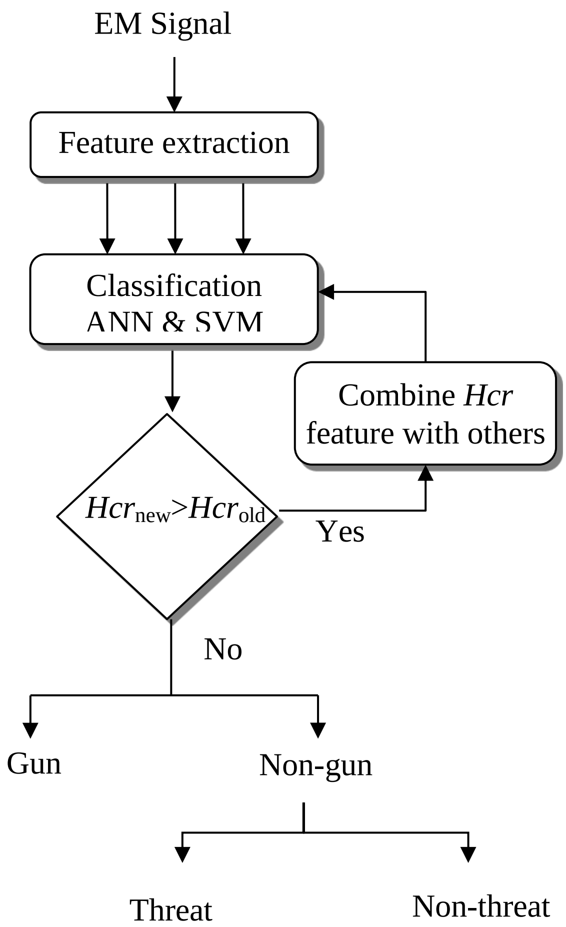

Figure 6.3: Classification strategy block diagram.

6.5 Classification Test Bed Setup

Experiments were conducted using the proposed system with two groups of objects. The first group (*GROUP_1*) consisted of twelve different objects: six of these objects were handguns which are called "*Gun*", while the others were daily used objects that contain metallic parts which are called "*Non-gun"*. The second group (*GROUP_2*) consisted of ten daily used objects, five of which contained a bulky amount of steel (such as knives, scissors and screwdrivers) that may be considered as threats and were named "*Threat"* and the rest are considered as non-threatening and are named "*Non-threat*" (such as cameras, mobile phones, and keys).

Table 6.2 describes the specifications of the *GROUP_1* objects, where Table 6.2a represents the handgun types and weights and Table 6.2b represents the non-guns objects. The handgun samples represent the most common weapons seized by the police; of particular interest are sample #5, which is blank firer that has been converted so as to fire live ammunition through the welding of another barrel to the existing mechanism, and a replica handgun (sample #6) which is commonly used by armed robbers.

Table 6.2: *GROUP_1* objects used in experimental test.

(a) Guns		**(b) Non-Guns**	
#1	Small revolver 0.516g	**#7**	Panasonic mobile phone
#2	Small semi-automatic revolver 0.637g	**#8**	Wrist watch
#3	Medium revolver 0.937g	**#9**	House Key
#4	Medium semi-automatic revolver 0.689g	**#10**	Screwdriver
#5	Converted blank firer 0.800g	**#11**	Scissors
#6	Replica 1.140g	**#12**	Kitchen knife

Figure 6.4 shows *GROUP_1* samples in the sample holder constructed for the tests, where Figure 6.4a represents the gun samples and Figure 6.4b represents the non-gun samples. The composition of all of the weapon samples commonly includes steel, with several other materials being incorporated such as zinc alloy, aluminium, and polymers.

GROUP_2 samples are shown in Figure 6.5, where Figure 6.5a represents samples that are usually considered harmless, or "*Non-threat*", and Figure 6.5b represents samples that are usually considered harmful, or *"Threat"*, similar configuration was used to set up the two groups of samples in the system.

During the tests, the sensitivity of the proposed system to each gun sample was measured in terms of the peak to peak amplitude change of the resultant response signal at different distances from the sensor-array.

Figure 6.6 shows a plot of the system sensitivity to different samples. It is clear that the differences between average peaks are extremely small. This was also found to be true for several tests using the same gun.

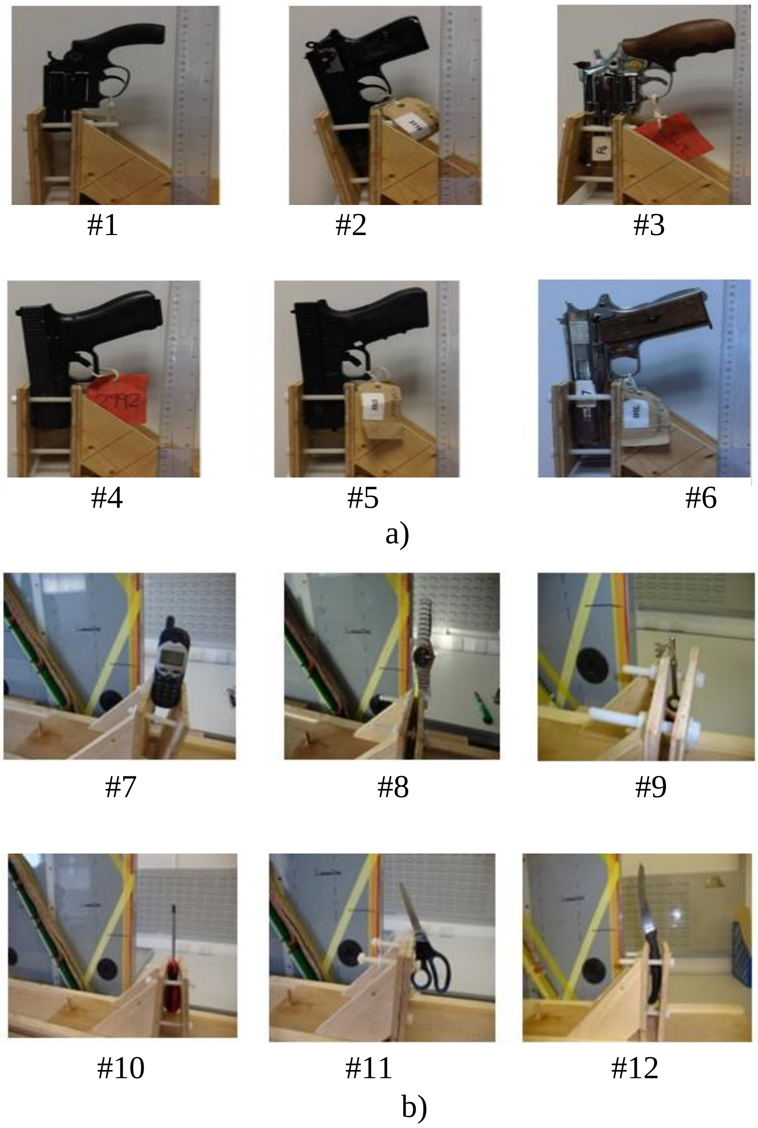

Figure 6.4: *GROUP_1* samples utilized in the test: a) gun samples, and b) non-gun samples.

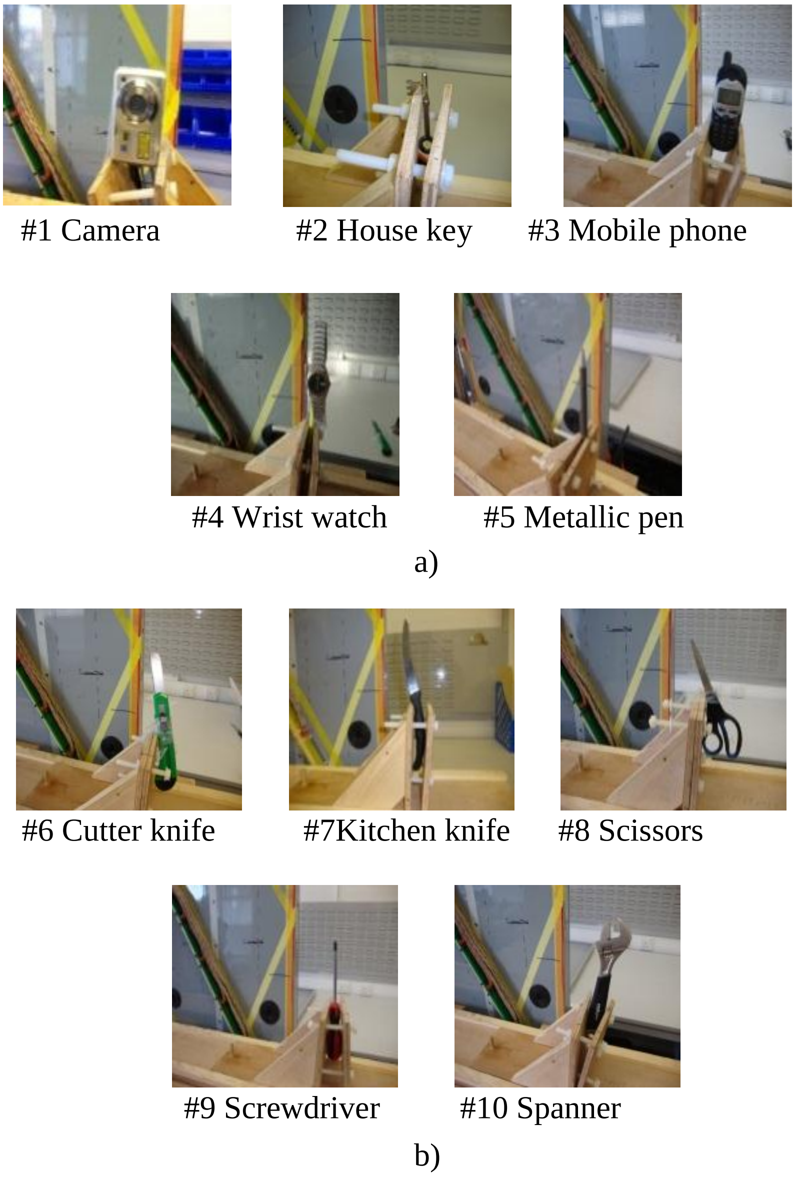

Figure 6.5: *GROUP_2* samples utilized in the test: a) non-threat samples, and b) threat samples.

The results of the sensitivity test were used to solve the data shortage problem and to increase the number of items. Each object was tested five times using the proposed system to generate five samples for the same object. Hence, for the twelve objects under test (six being guns and the other six not), 60 EM signal samples were generated. Based on this, the ANN classifier was trained using 48 EM signals for all of the objects (four for each object), while the remaining 12 EM signals were used as test samples. In terms of *GROUP_2*, five threats and five non-threat samples were used, so 50 EM signals were generated; 40 EM of which were used for training and the rest for testing, as shown in Table 6.3.

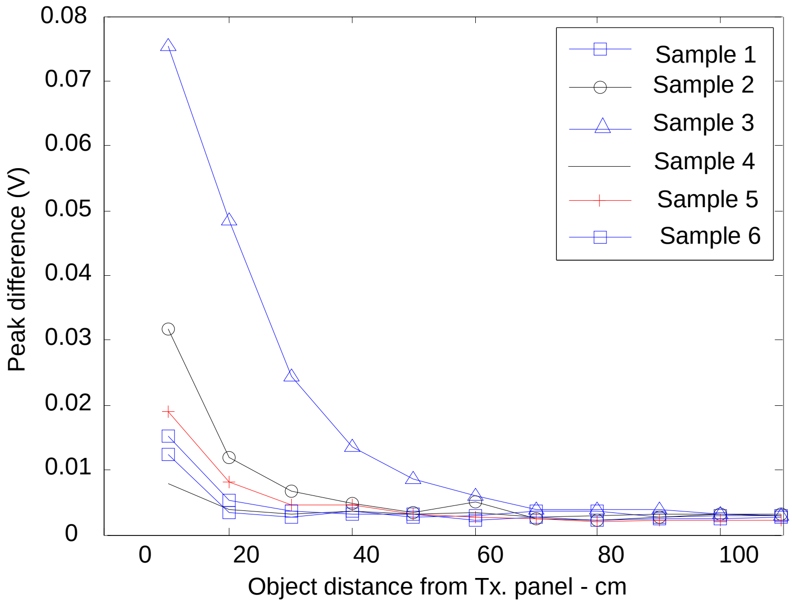

Figure 6.6: Sensitivity plot of variation in response for the six guns.

Table 6.3: Data set of the work

GROUP_1	***Total No. of Images used= 60***			
	No. of training images = 48		No. of testing images = 12	
	Guns 24	Non-guns 24	Guns 6	Non-guns 6
GROUP_2	***Total No. of Images used= 50***			
	No. of training images = 40		No. of testing images= 10	
	Threat 20	Non-threat 20	Threat 5	Non-threat 5

6.6 ANN Classification Performance

In this section, the results of the proposed features for object classification are presented. The results of *GROUP_1* are discussed first, followed by discussion of the results of *GROUP_2*.

6.6.1 GROUP_1 ANN classification results

For *GROUP_1*, each type of feature vector was individually provided as the input for the ANN. The results are shown in Table 6.4.

Table 6.4: Results for each feature vector using ANN with *GROUP_1* objects.

Feature vector	Hidden layer neurons	Objects	Correctly classified	Incorrectly classified	Classification rate
f-Moment	16	Gun	6	0	100%
		Non-gun	3	3	50%
			9	3	**75%**
f-Max-Min	2	Gun	5	1	83%
		Non-gun	4	2	67%
			9	3	**75%**
f-PCA	6	Gun	4	2	67%
		Non-gun	5	1	83%
			9	3	**75%**
f-Corr	26	Gun	5	1	83%
		Non-gun	5	1	83%
			10	2	**83%**
f-WT	18	Gun	5	1	83%
		Non-gun	5	1	83%
			10	2	**83%**
f-FFT	6	Gun	5	1	83%
		Non-gun	3	3	50%
			8	4	**67%**
f-All	74	Gun	6	0	100%
		Non-gun	4	2	67%
			10	2	**83%**

In addition to the features obtained in Chapter 5, another feature set named *f-All* was formed from all the individual features combined to enhance the classification rate. The features were normalised before combination to avoid any misclassification. The results are also shown in Table 6.5 . However, the *f-All* feature vector did not achieve a higher classification rate compared to those with the individual features alone.

Taking it a step further, combinations of *Hcr* features and other features were then adopted. The highest classification rates were achieved from *f-Corr* and *f-WT* features. Therefore, the combination of *f-Corr with the each of other features* was selected as it yielded one of the two highest classification rates. The selected combination is illustrated below:

- *Comb.1: f-Corr* with *f-Moment* features.
- *Comb.2: f-Corr* with *f-PCA* features.
- *Comb.3: f-Corr* with *f-Max-Min* features.
- *Comb.4: f-Corr* with *f-WT* features.

- *Comb.5: f-Corr* with *f-FFT* features.

The classification rates of these combinations are displayed in Table 6.5.

Table 6.5: Results for different feature combinations using ANN with *GROUP_1* objects.

Feature vector	Hidden layer neurons	Objects	Correctly classified	Incorrectly classified	Classification rate
Comb.1	42	Gun	2	4	33%
		Non-gun	6	0	100%
			8	4	**67%**
Comb.2	32	Gun	5	1	83%
		Non-gun	5	1	83%
			10	2	**83%**
Comb.3	28	Gun	6	0	100%
		Non-gun	5	1	83%
			11	1	**92%**
Comb.4	34	Gun	5	1	83%
		Non-gun	6	0	100%
			11	1	**92%**
Comb.5	34	Gun	5	1	83%
		Non-gun	4	2	67%
			9	3	**75%**

The results in Table 6.5 show an improvement in the classification rates, for example when the *f-Corr* features were combined with the *f-Max-Min* and *f-WT* features (*Comb.3* and *Comb.4*) where both achieved 92% classification rates. Based on these results, a new combination (*Comb.6*) was created. Since *Comb.6* did not achieve a 100% classification rate, a new combination (*Comb.7*) between *Comb.2* and *Comb.3* was then created. Thus, the last two new combinations were as follows:

- *Comb.6: f-Corr, f-Max-Min* and *f-WT* features.
- *Comb.7: f-Corr*, *f-Max-Min* and *f-PCA* features

The results of the final two combinations are shown in Table 6.6. The classification rate of *Comb.7* reached 100%, it should be mentioned here that this ideal classification rate could have been obtained due to the limited number of handgun samples. Generally, the results give an indication that the transient features show better results than other features when used together for the classification of the EM signals. Figure 6.7 shows the classification rates of all of the individual and combined features using the ANN with *GROUP_1* objects. No further combinations were tried as a 100% classification rate had been achieved.

Table 6.6: Results for further features combinations using ANN with *GROUP_1* objects.

Feature vector	Hidden layer neurons	Objects	Correctly classified	Incorrectly classified	Classification rate
Comb.6	34	Gun	5	1	83%
		Non-gun	6	0	100%
			10	2	**92%**
Comb.7	34	Gun	6	0	100%
		Non-gun	6	0	100%
			12	0	**100%**

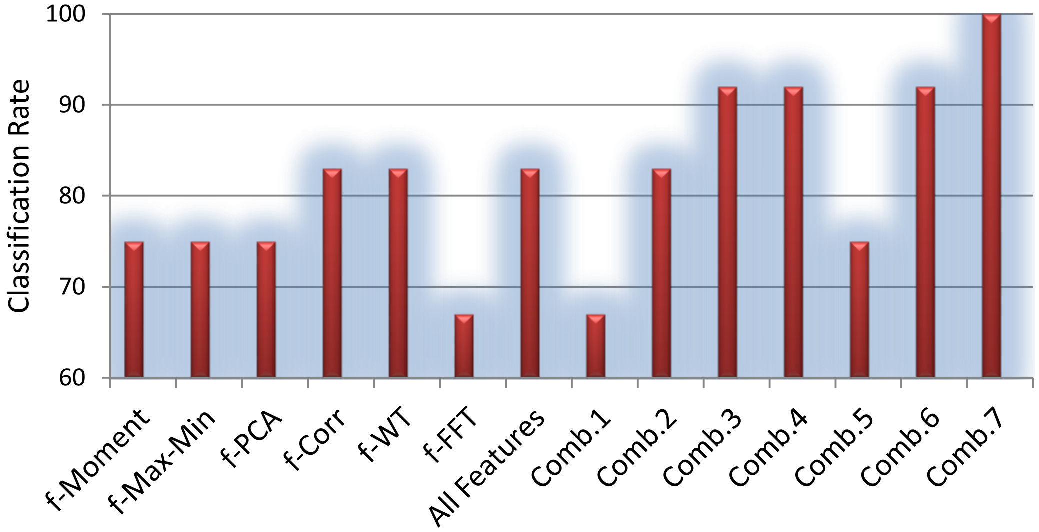

Figure 6.7: Classification rate of the features extracted from the EM system using ANN with *GROUP_1* objects.

6.6.2 GROUP_2 ANN classification results

As a second stage after the handguns were detected, the non-gun items were further classified into threat and non-threat items. For this purpose, *GROUP_2* was used. Tests were carried out using each of the feature vectors individually as the input for the ANN. The classification results for *GROUP_2* are presented in Table 6.7. From this table, the results for the *f-Corr* features reached a 100% classification rate, indicating also that the transient response feature through time is the best feature for discriminating between the everyday items using an ANN. Hence, no further combined features were investigated.

Furthermore, the results show a 0% misdetection rate for the threat objects when using *f-Moment*, *F-WT* and *f-Max-Min* features.

Figure 6.8 shows the classification rates of the features extracted from the EM detection system using ANN with the *GROUP_2* objects.

Table 6.7: Results of each feature vectors using ANN with *GROUP_2* objects.

Feature vector	Hidden layer neurons	Objects	Correctly classified	Incorrectly classified	Classification rate
f-Corr	26	Threat	5	0	100%
		Non-threat	5	0	100%
			10	0	**100%**
f-Moment	16	Threat	5	0	100%
		Non-threat	4	1	80%
			9	1	**90%**
f-PCA	6	Threat	1	5	80%
		Non-threat	5	0	100%
			6	5	**90%**
f-WT	18	Threat	5	0	100%
		Non-threat	4	1	80%
			9	1	**90%**
f-FFT	6	Threat	3	2	60%
		Non-threat	5	0	100%
			8	2	**80%**
f-Max-Min	2	Threat	5	0	100%
		Non-threat	3	2	60%
			8	2	**80%**

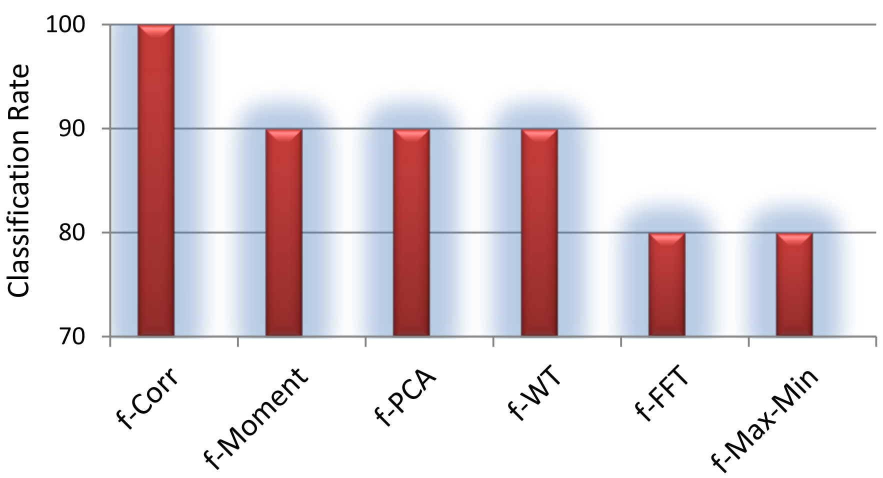

Figure 6.8: Classification rate of the features extracted from the EM detection system using ANN with the *GROUP_2* objects.

6.7 SVM Classification Performance

In this section, the results for the features proposed for object classification using the SVM method are displayed. This method was used as a second classifier method to evaluate the features extracted from the new system and to adopt an efficient classification technique for an automated process. The same methodology as that shown in Figure 6.3 is used to classify the objects, but this time using the SVM. Firstly, the results of *GROUP_1* are discussed, and then results of *GROUP_2* are presented.

6.7.1 GROUP_1 SVM classification results

Each type of feature vector was individually provided to the SVM as the input. Also, another feature set named *f-All* was formed from all the individual features combined to enhance the classification rate. However, the *f-All* feature vector did not achieve a higher classification rate compared to the individual features alone. The results are shown in Table 6.8.

Table 6.8: Results for each feature vector using SVM with *GROUP_1* objects.

Feature vector	Objects	Correctly classified	Incorrectly classified	Classification rate
f-Moment	Gun	6	0	100%
	Non-gun	3	3	50%
		9	3	**75%**
f-Max-Min	Gun	6	0	100%
	Non-gun	2	4	33%
		8	4	**67%**
f-WT	Gun	6	0	100%
	Non-gun	2	4	33%
		8	4	**67%**
f-PCA	Gun	6	0	100%
	Non-gun	1	5	16%
		7	5	**58%**
f-FFT	Gun	6	0	100%
	Non-gun	1	5	16%
		7	5	**58%**
f-Corr	Gun	6	0	100%
	Non-gun	0	6	0%
		6	6	**50%**
f-All	Gun	1	5	16%
	Non-gun	6	0	100%
		7	5	**58%**

Also, combinations of the feature vector with the highest classification rate and the other features were tested, as illustrated below:

- *Comb.1: f-Moment* with *f-Max-Min* features.
- *Comb.2: f-Moment* with *f-WT* features.
- *Comb.3: f-Moment* with *f-PCA* features.
- *Comb.4: f-Moment* with *f-FFT* features
- *Comb.5: f-Moment* with *f-Corr* features.

The classification rates for these combinations are shown in Table 6.9, and it is clear that there is an improvement in the classification rates compared to when using individual features. All other possible combinations were tried, however no further improvements were achieved.

Table 6.9: Results of different feature combinations using SVM with *GROUP_1* objects.

Feature vector	Objects	Correct classified	Incorrect classified	Classification rate
Comb.1	Gun	6	0	100%
	Non-gun	3	3	50%
		9	3	**75%**
Comb.2	Gun	6	0	100%
	Non-gun	2	4	33%
		8	4	**67%**
Comb.3	Gun	6	0	100%
	Non-gun	3	3	50.%
		9	3	**75%**
Comb.4	Gun	6	0	100%
	Non-gun	3	3	50%
		9	3	**75%**
Comb.5	Gun	6	0	100%
	Non-gun	2	4	33%
		8	4	**67%**

The SVM classifier shows 0% misdetection in all combinations of features, as shown in Table 6.9. (Again, this ideal result may have been due to the use of limited numbers of samples).

The classification rates of the features individually and in combination extracted from the EM detection system using the SVM with *GROUP_1* objects are summarised in Figure 6.9.

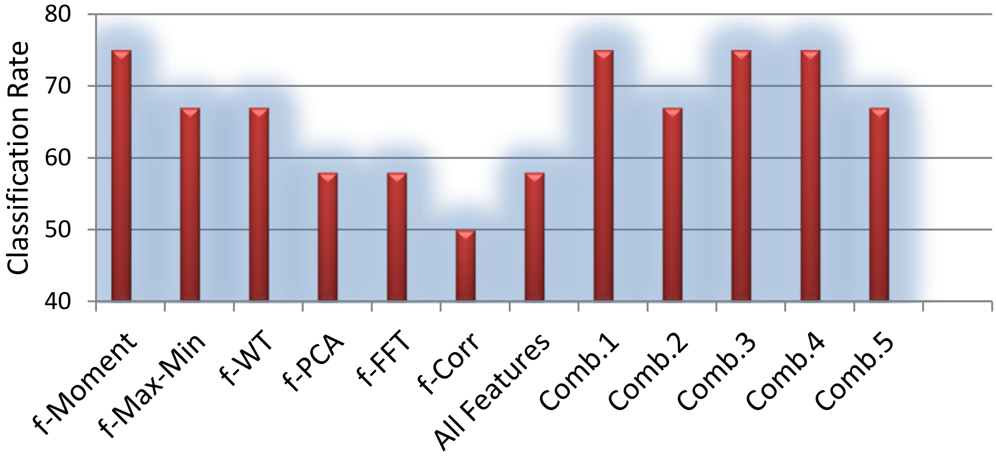

Figure 6.9: Classification rates of the features extracted from the proposed system using SVM with *GROUP_1* objects.

6.7.2 GROUP_2 SVM classification results

The results for *GROUP_2* are presented in Table 6.10 classifying threat and non-threat items from among the everyday used objects.

Table 6.10: Results for each feature vector using SVM with *GROUP_2* objects.

Feature vector	**Objects**	**Correctly classified**	**Incorrectly classified**	**Classification rate**
f-Corr	Threat	1	4	20%
	Non-threat	5	0	100%
		6	4	**60%**
f-FFT	Threat	4	1	80%
	Non-threat	0	5	0%
		4	6	**40%**
f-PCA	Threat	3	2	60%
	Non-threat	1	4	20%
		4	6	**40%**
f-Max-Min	Threat	3	2	60%
	Non-threat	0	5	0%
		3	7	**30%**
f-WT	Threat	3	2	60%
	Non-threat	0	5	0%
		3	7	**30%**
f-Moment	Threat	2	3	40%
	Non-threat	0	5	0%
		2	8	**20%**

Table 6.10 shows that when using the SVM classifier the transient features (*f-Corr*) gave the best results in classifying the everyday items.

Combinations between the highest scoring feature (*f-Corr*) and all other features yielded the same results as using *f-Corr* alone. It is noted that all combination results will give the same result as that for the highest individual feature. Figure 6.10 shows the classification rates of the features extracted from the EM detection system using the SVM with *GROUP_2* objects.

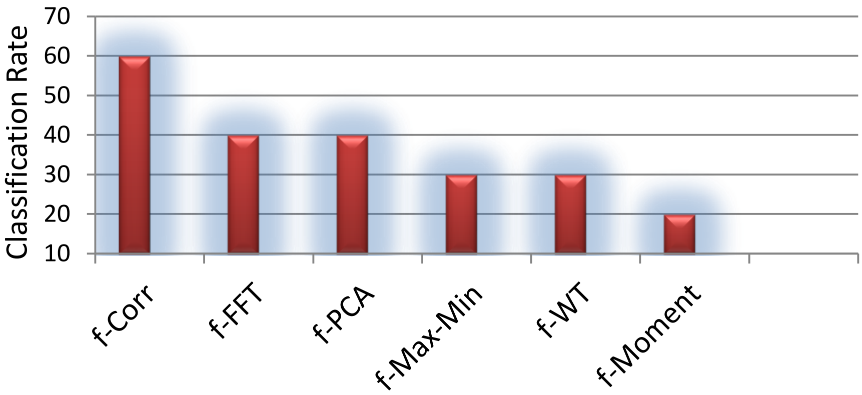

Figure 6.10: Classification rates of the features extracted from the proposed system using SVM with *GROUP_2* objects.

6.8 Comparison of the SVM and ANN

In this work, the performance of each classification method was compared in terms of threat object detection and classification using the new system. To highlight the differences between the SVM and ANN, the ANN training phase employs an empirical risk minimization principle which minimizes the error in the training data, whereas the SVM adopts a structural risk minimization principle which minimizes the upper bound of the generalization error. There are, therefore, a number of difficulties inherent to ANN design, namely model selection and parameter settings (and generally, the choices made are a result of the designer's experience and empirical considerations) [108]. The SVM, is instead trained by solving a constrained quadratic optimization problem, and in order to identify the optimal architecture as well as evaluate the influence on performance of various design parameters, several SVM setups have to be tested [161]. This problem was solved by developing an improved procedure known as cross-validation to find the best parameters, and to embed this procedure in the LIBSVM library core. Also, unlike with ANNs, the computational complexity of SVMs does not depend on the dimensionality of the input space [162].

Based on our study, both algorithms are capable of classifying objects when trained on the features extracted from the EM objects' responses. The classification process using the SVM was faster than that of the ANN because, when a test vector is presented, a trained SVM only has to determine on which side of the hyper-plane the new point falls in order to determine its class, while the ANN uses different functions through its layers.

In general, ANN classification rates proved superior to those of the SVM. On the other hand, all handgun samples were accurately identified using the SVM algorithm. This is due to its use of the LIBSVM model which represents an improved procedure to find the best kernel parameter of the function.

Although both classification methods gives good classification rates in terms of *GROUP_1* objects, the ANN method yielded superior results for *GROUP_2* objects. This is because the SVM is more sensitive, and training on these objects is not so efficient due to the diversity in their sizes and materials.

A closer look at the *GROUP_1* results for both classifiers show that, although both classification methods give high classification rates for most features, especially in terms of handgun objects, the ANN classifier gives low of false alarms rates compared to the SVM for non-gun items. Furthermore, the SVM classifier yields no false alarms for handgun objects when using all features both individually and in combination.

In terms of feature combinations, the classification rates using the ANN are became higher, whereas the classification rates stay the same or are less than those for each feature individually when using the SVM.

In comparison with the other EM classification algorithms reported in the literature [78, 88, 91, 103, 104, 105, 107-109], our algorithm shows superior results in terms of the variety of object tested, algorithm complexity and the accuracy of results.

As a final recommendation, it is suggested that LIBSVM should be used in the first stage, as it has the capability to detect the handgun samples with higher classification rates using all feature types. In the second stage, the ANN is better for discriminating between the threat and non-threat objects because it has the highest classification rate using also all of the feature types.

6.9 Summary

In this chapter, the problem of metallic object classification using their EM induction responses is solved using an ANN and an SVM to process features extracted from these responses. The performance of each method has been compared. In brief, the high classification accuracies obtained show that the feature extraction technique is capable of generating features that are adequate for representing the targets uniquely by target type. Hence, the proposed methodologies for feature extraction and the classifier techniques are suitable for the task of metallic threat object classification.

The two classification methods, ANN and SVM, were used for threat object classification. They are implemented due to their capability for parallel processing on large input data sets simultaneously as well as because they are good at classifying patterns when the training data is complex and noisy, which is the case in the context investigated. The characteristics of the BP neural network make it more robust than other ANN algorithms, and it solves the object classification problem effectively when the input data of features contain overlapping information. A feed-forward BP neural network with one hidden layer was chosen, because it is capable of approximating any continuous, multivariate function to a great degree of accuracy. The number of neurons in the hidden layer was decided to be double the number of input vectors. In the SVM, LIBSVM was chosen for use because it is an improved procedure to find the best RBF kernel parameter.

Several experimental tests have been carried out using six types of features. These features were utilized to classify 22 objects, six of which are real handguns and the others are different metallic items used in daily life. Several feature combination tests have been carried out in order to achieve the highest possible classification accuracy and these combinations showed better results than with each feature tested alone. The results show that transient response features are particularly good for classifying metallic items among other features used individually and in combination with other features, especially when using the ANN classifier.

The majority of the results showed that more than 92% of the objects can be correctly classified using the ANN, while in feature combination cases classification rates of 100% were achieved so that all the samples used were correctly classified. On the other hand, the SVM gave a 100% classification rate in terms of the detection of all handguns in the sample using all features with or without combinations. The SVM also had a faster processing time, which would be important in easing flows in any crowded secure area.

Based on these studies, the use of the SVM in the first classification stage should be recommended to classify handgun samples, while the ANN is suitable for use to discriminate between threatening and non-threatening objects in the second classification stage.

Table 6.11 summarises the characteristics of the proposed system in comparison with other available WTMD systems. It can be seen from the table that, although microwave imaging has excellent capabilities in terms of imaging and localisation, the costs are high and the technique is highly constrained in application, since subjects must stand still for inspection. Both magnetic field gradiometry and EM induction have reasonable detection capabilities and low cost, but localisation and characterisation are limited and imaging is not possible. The proposed system offers a good compromise between the constraint of the non-divestment of metal objects, imaging, characterisation, and classification capabilities. As a number of sensors are used in the system, the cost will be acceptable compared to current walk through systems, but the gains in imaging and the discrimination of multiple objects as well as classification will justify the cost.

It can be concluded that magnetic field imaging could be used to detect and identify metallic objects. In comparison with conventional induction based WTMDs, the GMR array based system has shown great potential in object identification, discrimination and classification.

Table 6.11: Summary of techniques used in walkthrough metal detectors

	Active excitation	**Detection of non-metals**	**Localisation**	**Imaging**	**Constraints**	**Cost**
Microwave imaging [163, 164]	Yes	Yes	Excellent	Yes	Stand still, time consuming	High
EM Induction [4, 24]	Yes	No	Poor: limited by size of coils	No	Divestment of metallic objects, limited area	Low
Magnetic field gradiometry [8, 10]	No	Ferromagnetic only	Good: limited by sensor pitch	No	Divestment of metallic objects, limited area	Low
Proposed system	Yes	No	Good: limited by array pitch	Yes, limited by array pitch	Limited area	Low

Chapter 7: Conclusions and Further Work

This chapter summarises the research work presented in the thesis. Conclusions are drawn and the contributions of the work to the field of EM metal detection and classification are highlighted. Finally, potential future directions for research are outlined in terms of improving the existing system, such as extending it to build an EM threat item database and developing image processing software to detect and classify threat items.

7.1 Conclusions and Major Contributions

A system for the automatic detection and classification of threat objects based upon the responses of objects to EM fields has been developed in this thesis. The heart of the method is to use pulse excitation to generate an EM field induced inside the object body, and then to receive the secondary EM field reflected from the object after disturbing this field. Features were extracted from the received signal to represent a unique signature in classifying each object. There were two main objectives for this thesis. The first was to design and implement a new metallic object detection system that could identify a metallic object based on the object's response to EM fields using magnetic field imaging methods. The second was to develop a suitable signal processing algorithm to classify the targeted signatures.

The proposed system uses an array of GMR sensors in conjunction with pulsed excitation to develop a new WTMD for deployment in unconstrained environments where users need not divest themselves of metallic items in any secured area. This system enables a two-dimensional image to be constructed and used in later image processing for object identification and classification purposes.

In the development and investigation of the new system, four major parts were undertaken: to design and implement an EM sensor-array system; to test and evaluate this system in terms of detecting different threat and non-threat objects; image pre-processing and feature extraction from the system outcome; and finally automatic threat object classification. All of these parts have been investigated, discussed and developed in chapters 3 to 6 of this thesis.

The main scientific findings of this work are as follows:

- The new system has been designed around the use of AAL002-02 NVE GMR sensor-arrays. This sensor type was chosen for the array due to its highest sensitivity compared with the other NVE GMR sensors. Tests have been carried out using pulsed excitation and it has been concluded that pulsed excitation in conjunction with advanced time-frequency analysis has the greatest potential for object detection, characterisation, localisation and imaging.

  An optimum sensor-array design is achieved by the adjustment of following:

  1) The number of sensors, which is even one array units, consists of 40 sensors or two arrays units consisting of 80 sensors.
  2) The space between these sensors in the array, which at 15mm gave the best balance between spatial resolution and system complexity.
  3) The position and direction of the sensor-array in terms of the coils or pulse excitation which is slanted in the sensor-array directly above the coil.
- A novel formation of reconstructed images has been developed and is called max-value image formation. This technique uses simple averaging and chooses the maximum value. Transient response image formation then involves the generation of a transient image sequence which is used to extract further information about the object under examination.
- A prototype user interface was developed, which included signal pre-processing, the software necessary to isolate the response signals, management of data acquisition, parameter setting, and image reconstruction.
- The capability of the proposed system to detect threat and non-threat items was tested. Twelve real handguns were tested along with more than twenty other items commonly used in daily life. Tests were undertaken using a holder as well as an individual walking through the system arch carrying the objects in typical sites on the body such as in jacket and trouser pockets.
- The new system was evaluated in terms of the following:
  1) Repeatability: the test results showed that the control and walk-through tests have the greatest repeatability.
  2) Orientation robustness: it is concluded from the test results that the images follow a fairly predictable evolution with the rotation of the object. The

trends in the data were observed to be similar irrespective of the orientation of the object.

3) Distance sensitivity: The test results showed that, for good resolution, the distance from the panel to the object should be less than 60cm and that sensitivity decreases substantially as the distance from the arch panel increases.

4) Multiple object detection: the test results show that, at object separation distances greater than 0.6 cm the system can easily distinguish between two target objects.

- Features which reflect the objects' shape, material properties, time-frequency, and transient response analysis have been extracted and integrated to obtain better object identification and discrimination. A novel time-frequency image correlation method was successfully proposed, pertaining to the discrimination of material into ferromagnetic and non-ferromagnetic metals. The results show that the transient response features are most suitable for threat object classification and deliver a high classification rate individually or when combined with other features when used with the two proposed classifiers.
- The two classifiers, ANN and SVM, were selected to find an efficient technique for an automated classification process which best suits the proposed system, and to evaluate the features suitable for threat object classification. Several feature combination tests have been carried out. The results showed that the SVM can recognise all the handgun samples correctly and it has faster processing time which is an important issue in easing the flow of people in any crowded secure area. On the other hand, the majority of results showed that more than 92% of the objects can be correctly classified using the ANN, while in feature combination cases it achieved 100% classification where all of the samples used were correctly classified.
- Based on the study' results, the SVM should be recommended in the first classification stage as it has the capability to detect all of the handgun samples used in this research, while ANN is suitable to be used to discriminate between threat and non-threat objects in the second classification stage since it has the highest classification rates for these types of objects.

7.2 Further work

Following the research outcomes achieved in this work, several directions for further work are suggested in terms of improving the existing techniques. A stand-alone walk-through system with superior object discrimination and localisation capabilities is envisaged for future exploitation. It is thought that the discrimination capabilities of the system could be developed to the point that an individual could pass through the system without removing metallic objects. This would be realised through "training" the system to identify threat objects by presenting it with a wide variety of threat and non-threat objects and programming responses accordingly.

The next section presents a proposal for a new route to design an EM detection and imaging system, while the subsequent lists suggestions to enhance specific areas of our proposed system.

7.2.1 Design of a new prototype of the EM detection and imaging system

A new EM imaging prototype system has been proposed. Figure 7.1 shows the overall prototype system design proposed for future work. Pulsed excitation is provided to the two excitation coils via a switching circuit controlled by the PC. A GMR sensor-array is used to measure the field in both *transmit-receive* and *reflection* modes, with a multiplexer used to switch between groups of sensors to reduce the data acquisition requirements of the system. Although the system is designed to work as a stand-alone detector, the configuration will be flexible enough to accommodate other sensing modes such as CCTV or thermal imaging. The prototype system will utilise the existing CEIA arch coils, but a new coil can also be designed and constructed at a later date.

Figure 7.2 shows the proposed operation of the system. Step 1; a line of sensors at each side operate as regional metal detectors; the presence of a metallic object is detected through simple thresholding of the signal, with decision making informed by the parameters of the measured signal such as shape and material which can be used to identify the material and calculate the approximate volume of the object. Steps 2; if the object is identified as a potential threat, a set of sensors near to the object are activated for data acquisition. Step 3; the result of this data acquisition can be used for object imaging, further discrimination of the object's material and volume and fitting to known patterns for classification and categorisation in discriminating, for example, between guns, knives and non-threat objects such as keys and mobile phones.

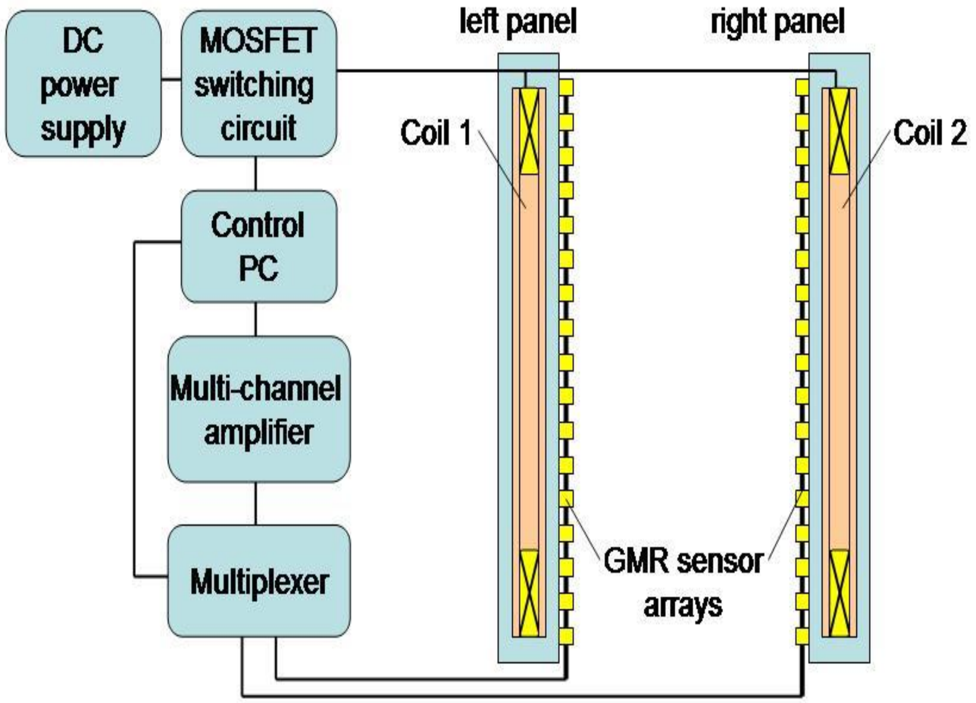

Figure 7.1: System diagram for the new prototype pulsed electromagnetic threat detection and imaging system.

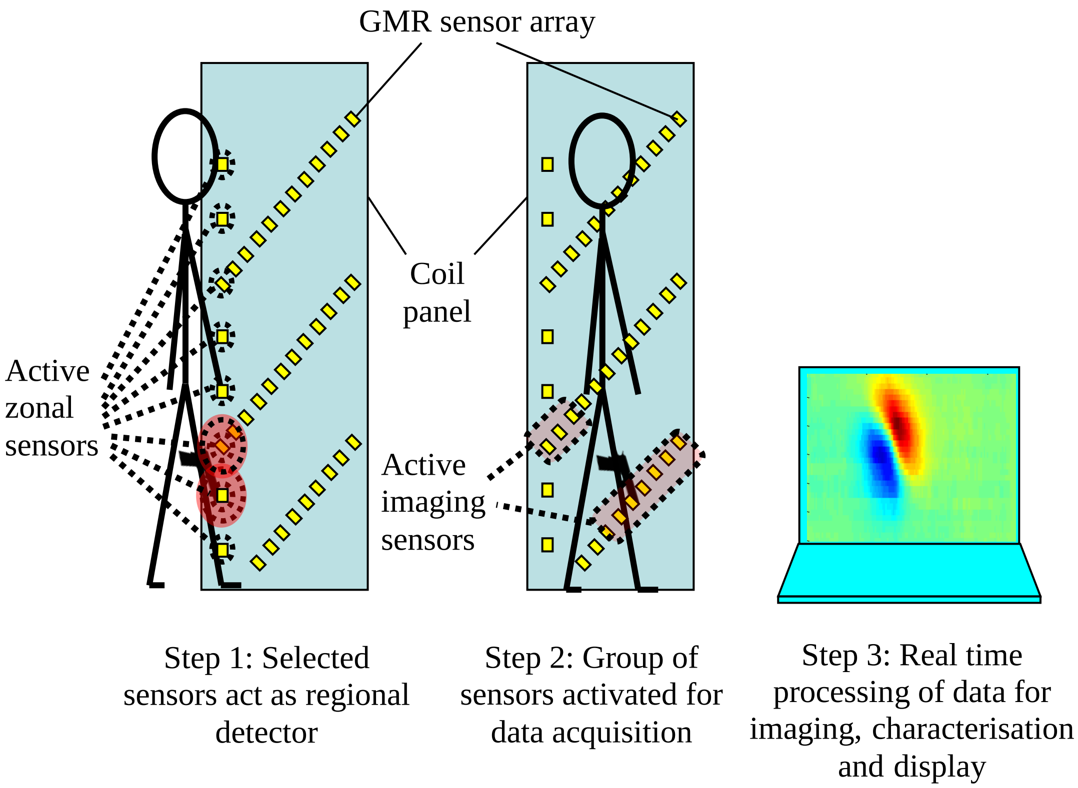

Figure 7.2: Proposed system operation.

7.2.2 Suggested enhancements for the proposed system

In order to bring the system to a point where a fully operational prototype could be realised, the following issues would need to be resolved:

- Hardware integration; the current system is built around a number of discrete devices. For prototyping, the system would need to be integrated into a single control box. Also, the current system is built around a CEIA arch, with our own excitation system attached. Although this works well, there are obvious issues with this arrangement. The design of a customised WTMD will enhance the system.
- There are some noise and cross interference issues when a magneto-resistive array of large area is deployed in this type of application. Noise reduction techniques such as EM shielding need to be investigated.
- The system could be built for 3D imaging to enhance its sensitivity by adding a sensor array in the roof of the WTMD panel in order to visualize in the third dimension. This will help much in the recognition of actual shape and size as well as the orientation and localisation of the object.
- Large sample size and real application tests are needed. The collection of signal responses of different classes of guns, knives and other threatening metallic objects are vital in the development of a comprehensive signature database.
- New research looking at optical magnetometers could be applied to this work in order to compensate for some of the current system's shortcomings, including further improvements in spatial resolution for magnetic field measurement. These qualities have made such technology valuable in the medical field, and its introduction into this system would certainly enhance object identification and classification.
- The project was also built as an open platform, which can integrate other modalities of sensing and imaging such as CCTV, thermal and radar images in order to overcome the fact that current approaches are more sensitive to magnetic volumes than fine-structural and material characteristics due to the limitations of detection distance.

References

[1] D. Daniels, *EM Detection of Concealed Targets*. Inc Hoboken, New Jersey: John Wiley & Sons, 2010.

[2] F. Sadjadi and B. Javidi, *Physics of Automatic Target Recognition*: Springer, USA, 2007.

[3] B. Javidi, *Optical Imaging Sensors and Systems for Homeland Security Applications*. USA: Springer, 2006.

[4] N. G. Paulter, "Users’ Guide for Hand-Held and Walk-Through Metal Detectors," *NIJ Guide 600-00, NCJ 184433, Office of Science and Technology, U.S. Department of Justice, DC 20531*, 2001.

[5] A. Agurto, Y. Li, G. Tian, N. Bowring, and S. Lockwood, "A Review of Concealed Weapon Detection and Research in Perspective," presented at the IEEE Proceedings of International Conference on Networking, Sensing and Control, 2007.

[6] Honeywell. *Simple Magnetic gradiometer*. Available: http://www.magneticsensors.com/applications/gradiometer.html

[7] R. Koch and G. Keefe, "Room temperature three sensor magnetic field gradiometer," *Review of Scientific Instruments*, vol. 67, pp. 230-235, 1996.

[8] L. Roybal, P. Rice, and J. Manhardt, "New approach for detecting and classifying concealed weapons," in *SPIE Proceeding on Surveillance and Assessment Technologies for Law Enforcement*, pp. 96-107, 1997.

[9] P. Czipott, "stand-off detection and tracking of concealed weapons using magnetic tensor tracking:Final activities report," National Institute of Justice, US Dept Justice, United States, 2001.

[10] S. Kumar, R. Perry, R. Moeller, C. Skvoretz, J. Ebbert, K. Ostrom, L. Bennett, and V. Czipott, "Real-time tracking magnetic gradiometer for underwater mine detection," in *IEEE Techno-Oceans '04*, pp. 874-878 Vol.2, 2004.

[11] N. G. Paulter, "Guide to the technologies of concealed weapon and contraband imaging and detection," NIJ Guide 602-00, 2001.

[12] R. Jia and R. Groom, "On inversion of gradient magnetic data for detection of multiple buried metallic objectives," in *Symposium on the Application of Geophysics to Engineering and Environmental Problems*, pp. 1772-1778, 2004.

[13] S. Singh and M. Singh, "Explosives detection systems (EDS) for aviation security," *Signal Processing*, vol. 83, pp. 31-55, 2003.

[14] E. Gasperikova, "A new-generation EM system for the detection and classification of buried metallic objects," *Lawrence Berkeley National Laboratory. Paper LBNL-53963*, 2003.

[15] K. Davis, Y. Li, and M. Nabighian, "Automatic detection of UXO magnetic anomalies using extended Euler deconvolution," *GEOPHYSICS*, vol. 24, pp. 1133-1136, 2005.

[16] R. International. (2011). *EM61 electro-magnetic metal detection*. Available: http://www.reynolds-international.co.uk/uploads/files/07tssem61.pdf

[17] C. Bruschini, "Evaluation of a commercial visualising metal detector for UXO/mine detection: the HILTI Ferroscan system," *International Workshop on Sustainable Humanitarian Demining*, 1997.

[18] N. Goldfine, A. Washabaugh, D. Schlicker, and I. Shay, "High-resolution inductive sensor arrays for UXO detection, identification, and clutter

suppression," *SPIE Proceedings on Detection and Remediation Technologies for Mines and Minelike Targets VIII*, vol. 5089, pp. 1-12, 2003.

[19] D. He and M. Yoshizawa, "Metal detector based on high-Tc RF SQUID," *Physica C*, vol. 378-381, pp. 1404-1407, 2002.

[20] W. Dagang, Q. Rui, C. Ji, W. Kainz, and S. Seidman, "Safety evaluation of walk-through metal detectors," in *Electromagnetic Compatibility, 2005. EMC 2005. 2005 International Symposium on*, vol. 3, pp. 796-800, 2005.

[21] J. Tyson. (2002). *How Metal Detectors Work*. Available: http://electronics.howstuffworks.com/metal-detector.htm

[22] A. Agurto and M. Sibley, "New proposal for the detection of concealed weapons," *Proceedings of Researchers' conference at Huddersfield University,* 2007.

[23] Y. Tiejun and L. Carin, "Analysis of the electromagnetic inductive response of a void in a conducting-soil background," *IEEE Transactions on Geoscience and Remote Sensing*, vol. 38, pp. 1320-1327, 2000.

[24] C. Nelson, C. Cooperman, W. Schneider, D. Wenstrand, and D. Smith, "Wide bandwidth time-domain electromagnetic sensor for metal target classification," *IEEE Transactions on Geoscience and Remote Sensing,* vol. 39, pp. 1129-1138, 2001.

[25] C. Nelson, D. Mendat, T. Huynh, L. Thomas, J. Beaty, and J. Craig, "Three-dimensional steerable magnetic field (3DSMF) sensor system for classification of buried metal targets," *SERDP Project MM-1314 Final Technical Report*, 2006.

[26] C. Nelson, "Metal Detection and Classification Technologies," *Johns Hopkins APL technical Digest*, vol. 24, pp. 62-66, 2004.

[27] C. Nelson, "Wide-area metal detection system for crowd screening," in *Proceedings of SPIE Conference on AeroSense, Sensors and Command, Control, Communication, and Intelligence (C3T) Technologies for Homeland Defense and Law Enforcemnt II*, pp. 380-387, 2003.

[28] A. Maradudin, A. Shchegrov, and T. Leskova, "Resonant scattering of electromagnetic waves from a rectangular groove on a perfectly conducting surface," *Optics Communications,* vol. 135, pp. 352-360, 1997.

[29] A. Hunt, "Demonstration of a concealed weapons detection system using electromagnetic resonances, Final report," *National Institute of Justice, US Department of Justice, NCJ Number: 190134,* 2001.

[30] D. Novak, R. Waterhouse, and A. Farnham, "Millimeter-wave weapons detection system," in *Applied Imagery and Pattern Recognition Workshop*, pp. 6 -20, 2005.

[31] N. Bowring, J. Baker, N. Rezgui, M. Southgate, and J. Alder, "Active millimeter wave detection of concealed layers of dielectric material," in *Optics and Photonics in Global Homeland Security III*, USA, pp. 1-10, 2007.

[32] N. Bowring, J. Baker, N. Rezgui, and J. Alder, "A sensor for the detection and measurement of thin dielectric layers using reflection of frequency scanned millimetric waves," *Measurement Science and Technology*, vol. 19, pp. 1-7, 2008.

[33] A. Ibrahim, K. Liu, D. Novak, and R. Waterhouse, "A subspace signal processing technique for concealed weapons detection," in *IEEE International Conference on Acoustics, Speech and Signal Processing*, pp. II-401 - II-404, 2007.

[34] J. Hausner, "A radar-based concealed threat detector," *Microwave Journal,* vol. 50, pp. 26-40, 2007.

[35] Y. Li and G. Y. Tian, "A radio-frequency measurement system for metallic object detection using pulse modulation excitation," *Proceedings of 17th World Conference on Nondestructive Testing*, pp. 1-9, 2008.
[36] Y. Li, G. Y. Tian, N. Bowring, and N. Rezgui, "A microwave measurement system for metallic object detection using swept-frequency radar," in *SPIE proceeding on Millimetre Wave and Terahertz Sensors and Technology*, 2008.
[37] Y. L. a. G. Y. Tian, "A radar system for detection and characterisation of guns and knives," *Proceedings of the 47th Annual British Conference on NDT,* pp. 1-12, 2008.
[38] V. Lubecke, O. Boric-Lubecke, A. Host-Madsen, and A. Fathy, "Through-the-Wall Radar Life Detection and Monitoring," in *IEEE/MTT-S International, Microwave Symposium*, pp. 769-772, 2007.
[39] M. Shaw, S. Millard, T. Molyneaux, M. Taylor, and J. Bungey, "Location of steel reinforcement in concrete using ground penetrating radar and neural networks," *NDT & E International,* vol. 38, pp. 203-212, 2005.
[40] L. Douglas, M. David, H. Collins, E. Thomas, and H. Ronald, "Wideband millimeter-wave holographic weapons surveillance systems," in *SPIE proceedings on Law Enforcement Technologies: Identification Technologies and Traffic Safety*, pp. 131-141, 1995.
[41] M. David, L. Douglas, H. Collins, E. Thomas, and H. Ronald, "Concealed explosive detection on personnel using a wideband holographic millimeter-wave imaging system," in *SPIE Proceeding on Signal Processing, Sensor Fusion, and Target Recognition*, pp. 503-513, 1996.
[42] L. Douglas, M. David, E. Thomas, and H. Ronald, "Cylindrical holographic radar camera," in *SPIE Proceeding on Enforcement and Security Technologies*, pp. 79-88, 1998.
[43] C. Hua-Mei, L. Seungsin, R. M. Rao, M. A. Slamani, and P. K. Varshney, "Imaging for concealed weapon detection: a tutorial overview of development in imaging sensors and processing," *Signal Processing Magazine, IEEE,* vol. 22, pp. 52-61, 2005.
[44] D. Kozakoff and V. Tripp, "Antennas for concealed weapon detection," in *5th International Conference on Antenna Theory and Techniques*, pp. 65-69, 2005.
[45] L. Douglas, E. Thomas, and M. David, "Holographic radar imaging privacy techniques utilizing dual-frequency implementation," in *SPIE Proceeding on Sensors and Command, Control, Communications, and Intelligence, Technologies for Homeland Security and Homeland Defense*, p. 69430P, 2008.
[46] D. Sheen, D. McMakin, and T. Hall, "Three-dimensional millimeter-wave imaging for concealed weapon detection," *IEEE Transactions on Microwave Theory and Techniques,* vol. 49, pp. 1581-1592, 2001.
[47] H. Essen, H. Fuchs, M. Hagelen, S. Stanko, D. Notel, S. Erukulla, J. Huck, M. Schlechtweg, and A. Tessmann, "Concealed weapon detection with active and passive millimeter-wave sensors, two approaches," presented at the German Microwave Conference, Karlsruhe, Germany, 2006.
[48] R. Appleby, "Passive millimetre-wave imaging and how it differs from terahertz imaging," *The Royal Society,* vol. 362, pp. 379- 393, 2004.
[49] L. Yujiri, M. Shoucri, and P. Moffa, "Passive millimeter wave imaging," *IEEE Microwave Magazine,* vol. 4, pp. 39-50, 2003.
[50] R. McMillan, N. Currie, D. Ferris, and M. Wicks, "Concealed weapon detection using microwave and millimeter wave sensors," in *IEEE Proceedings on Microwave and Millimeter Wave Technology,* pp. 1-4, 1998.
[51] A. Luukanen, "Bolometer and Thz imaging," *Millimetre-wave Laboratory of Finland -MilliLab-Microsensing seminar,* 2008.

[52] S. Harmer, N. Bowring, D. Andrews, N. Rezgui, M. Southgate, and S. Smith, "A review of nonimaging stand-off concealed threat detection with millimeter-wave radar," *IEEE Microwave Magazine*, vol. 13, pp. 160-167, 2012.

[53] D. Sheen, D. McMakin, T. Hall, and R. Severtsen, "Active millimeter-wave standoff and portal imaging techniques for personnel screening," in *IEEE Conference on Technologies for Homeland Security*, pp. 440-447, 2009.

[54] G. Wang, D. Xu, and J. Yao, "Review of explosive detection using terahertz spectroscopy technique," in *Electronics and Optoelectronics (ICEOE), 2011 International Conference on*, pp. V4-22-V4-25, 2011.

[55] A. Burnett, J. Cunningham, A. Davies, P. Dean, and E. Linfield, "Terahertz frequency spectroscopy and its potential for security applications," in *Infrared and Raman Spectroscopy in Forensic Science*, ed: John Wiley & Sons, Ltd, pp. 295-314, 2012.

[56] J. Federici, R. Barat, D. Gary, and D. Zimdars, "THz standoff detection and imaging of explosives and weapons," *Proceeding SPIE*, vol. 5781, 2005.

[57] R. Jennifer and D. Woolard, "Terahertz for military and security applications," *Proceedings of the SPIE*, vol. 6212, 2006

[58] R. Mcmillan, "Terahertz imaging, milimeter-wave radar," presented at the Conference on surveillance and assessment technologies for law, Alabama, USA, 2004.

[59] G. P. Gallerano. (2004). *Tera-Hertz radiation in Biological Research, Investigations on Diagnostics and study on potential Genotoxic Effects: Final Report*. Available: http://www.frascati.enea.it/THz-BRIDGE/reports/THz-BRIDGE

[60] Q. Song, Y. Zhao, A. Redo-Sanchez, C. Zhang, and X. Liu, "Fast continuous terahertz wave imaging system for security," *Optics Communications*, vol. 282, pp. 2019-2022, 2009.

[61] R. Willardson, D. Skatrud, and P. Kruse, *Uncooled Infrared Imaging Arrays and Systems in Semiconductors and Semimetals*: Academic Press, New York, 1997.

[62] C. Siu-Yeung and T. Nanda-Pwint, "Using infrared imaging technology for concealed weapons detection and visualization," in *TENCON 2010 - 2010 IEEE Region 10 Conference*, pp. 228-233, 2010.

[63] J. Duchateau and M. Hinders, "Using ultrasound in concealed weapons detection," *NDE Lab, Department of Applied Science, College of William and Mary*, pp. 1-59, 2005.

[64] A. Achanta, M. McKenna, and J. Heyman, "Nonlinear acoustic concealed weapons detection," presented at the Applied Imagery and Pattern Recognition Workshop, 2005.

[65] M. Hamilton and D. Blackstock, *Nonlinear acoustics*. Boston: Academic Press, 1998.

[66] E. Knott, J. Shaeffer, and M. Tuley, *Radar cross section*. SciTech Publishing, 2004.

[67] A. Hunt, R. Hogg, and W. Foreman, "Concealed weapons detection using electromagnetic resonances," *SPIE Proceeding, The International Society for Optical Engineering, Conference on Enforcement and Security Technolog* vol. 3575, pp. 62-67, 1998.

[68] Z. Liu, T. Macuda, Z. Xue, D. Forsyth, and R. Laganiére, "Concealed Weapon Detection: A Data Fusion Perspective," *Journal of Aerospace Computing Information and Communication*, vol. 6, pp. 1-29, 2009.

[69] L. Collins and P. Torrione, "Comparison of pattern recognition approaches for multi-sensor detection and discrimination of anti-personnel and anti-tank

landmines," presented at the SPIE Conf. Detection and Remediation Technologies for Mines and Minelike Targets, 2006.
[70] Department of Homland security. (2008). *Privacy Impact Assessment for the Future Attribute Screening Technology (FAST) Project*. Available: http://www.dhs.gov/xlibrary/assets/privacy/privacy_pia_st_fast.pdf
[71] C. Hua-Mei, L. Seungsin, R. Rao, M. Slamani, and P. Varshney, "Imaging for concealed weapon detection: a tutorial overview of development in imaging sensors and processing," *IEEE Signal Processing Magazine,* vol. 22, pp. 52-61, 2005.
[72] K. Dale, G. Lyle, and E. Robert, "Detection and classification of concealed weapons using a magnetometer-based portal," in *SPIE Proceeding, Sensors and Command, Control, Communications, and Intelligence (C3I) Technologies for Homeland Defense and Law Enforcement*, pp. 145-155, 2002.
[73] L. Seungsin, R. Rao, and M. Slamani, "Noise reduction and object enhancement in passive millimeter wave concealed weapon detection," in *Proceedings of International Conference on Image Processing*, vol.1, pp. I-509-I-512, 2002.
[74] C. Liane, K. Mucahit, K. Pramod, G. Mark, D. David, and J. Ferris, "Morphological filters and wavelet-based image fusion for concealed weapons detection," in *SPIE Proceding, Sensor Fusion: Architectures, Algorithms, and Applications II*, pp. 110-119, 1998.
[75] S. Xilin, C. R. Dietlein, E. Grossman, Z. Popovic, and F. G. Meyer, "Detection and Segmentation of Concealed Objects in Terahertz Images," *Image Processing, IEEE Transactions on,* vol. 17, pp. 2465-2475, 2008.
[76] M. Slamani, M. Alford, and D. Ferris, "Setting thresholds in infrared images for the detection of concealed weapons," in *Proceedig SPIE, Applications of Digital Image Processing XXI*, pp. 630-639, 1998.
[77] R. C. Gonzalez, *Digital Image Processing* Second ed.: Prentice-Hall Inc., 2003.
[78] M. Tran, C. Lim, C. Abeynayake, and L. Jain, "Feature extraction and classification of metal detector signals using the wavelet transform and the fuzzy ARTMAP neural network," *Journal of Intelligent and Fuzzy Systems,* vol. 21, pp. 89-99, 2010.
[79] K. Hendrik and E. Hartmut, "Signal processing and pattern recognition for eddy current sensors, used for effective land-mine detection," in *Proceedings of the Second international conference on Autonomous and intelligent systems*, Burnaby, Canada, pp. 294-302, 2011.
[80] G. Turhan-Sayan, "Real time electromagnetic target classification using a novel feature extraction technique with PCA-based fusion," *IEEE Transactions on Antennas and Propagation,* vol. 53, pp. 766-776, 2005.
[81] S. Pal and M. Mitra, "Detection of ECG characteristic points using Multiresolution Wavelet Analysis based Selective Coefficient Method," *Measurement*, vol. 43, pp. 255-261, 2010.
[82] Z. Qibin and Z. Liqing, "ECG feature extraction and classification using wavelet transform and support vector machines," in *International Conference on Neural Networks and Brain*, pp. 1089-1092, 2005.
[83] F. Zhang and M. Li, "Wavelet analysis method of harmonics and electromagnetic interference in coal mines," *Mining Science and Technology,* vol. 20, pp. 576-580, 2010.
[84] M. Tran and C. Abeynayake, "Evaluation of the continuous wavelet transform for feature extraction of metal detector signals in automated target detection: New advances in intelligent decision technologies." vol. 199, K. Nakamatsu, G. Phillips-Wren, L. Jain, and R. Howlett, Eds., ed: Springer Berlin/Heidelberg, pp. 245-253, 2009.

[85] M. Nixon and A. S. Aguado, *Feature Extraction & Image Processing*. : Elsevier Ltd, Second edition, 2008.
[86] M. Hu, "Visual pattern recognition by moment invariants," *IRE Transactions on Information Theory*, vol. 8, pp. 179-187, 1962.
[87] M. Rizon, H. Yazid, P. Saad, A. Shakaff, A. Saad, M. Mamat, S. Yaacob, H. Desa, and M. Karthigayan, "Object detection using geometric invariant moment," *American Journal of Applied Sciences*, vol. 2, pp. 1876-1878, 2006.
[88] H. Pourghassem, O. Sharifi-Tehrani, and M. Nejati, "A novel weapon detection algorithm in X-ray dual-energy images based on connected component analysis and shape features," *Australian Journal of Basic and Applied Sciences*, vol. 5, pp. 300-307, 2011.
[89] Air Force Research Laboratory. (2001). *Final Technical Report: Sensor fusion algorithms and performance limits*. Available: http://www.dtic.mil/cgi-bin/GetTRDoc?AD=ADA391935
[90] A. Sophian, G. Y. Tian, D. Taylor, and J. Rudlin, "A feature extraction technique based on principal component analysis for pulsed Eddy current NDT," *NDT and E International*, vol. 36, pp. 37-41, 2003.
[91] S. Yeom, D. Lee, Y. Jang, M. Lee, and S. Jung, "Real-time concealed-object detection and recognition with passive millimeter wave imaging," *Optical Society of America, Opt. Express*, vol. 20, pp. 9371-9381, 2012.
[92] W. Chin-Hsiung and H. Shi-Jinn, "Run-length chain coding and scalable computation of a shape's moments using reconfigurable optical buses," *IEEE Transactions on Systems, Man, and Cybernetics, Part B: Cybernetics*, vol. 34, pp. 845-855, 2004.
[93] D. Xiaolong and S. Khorram, "A feature-based image registration algorithm using improved chain-code representation combined with invariant moments," *IEEE Transactions on Geoscience and Remote Sensing*, vol. 37, pp. 2351-2362, 1999.
[94] A. R. Al-Qubaa, G. Y. Tian, J. Wilson, W. L. Woo, and S. Dlay, "Feature extraction using normalized cross-correlation for pulsed eddy current thermographic images," *Measurement Science and Technology*, vol. 21, pp. 115501-115511, 2010.
[95] A. R. Al-Qubaa, G. Y. Tian, and J. Wilson, "Electromagnetic Imaging System for Weapon Detection and Classification," presented at the Fifth International Conference on Sensor Technologies and Applications, France,pp.317-321, 2011.
[96] S. Mehmet, K. Gulay, B. Melih, and B. Yildirim, "Buried metalic object identification by EMI sensor," in *SPIE Proceedings on Detection and Remediation Technologies for Mines and Minelike Targets XII*, p. 65530C, 2007.
[97] H. Haoping, F. Bill San, N. Steve, and I. J. Won, "Identification of buried landmines using electromagnetic induction spectroscopy: evaluation of a blind test against ground truth," in *SPIE Proceeding on Detection and Remediation Technologies for Mines and Minelike Targets X*, pp. 233-241, 2005.
[98] C. Abeynayake, I. J. Chant, and G. Nash, "Modified Kalman target detection algorithm applied to metal detection," in *SPIE Proceeding on Detection and Remediation Technologies for Mines and Minelike Targets VII*, Orlando, FL, USA, pp. 836-846, 2002.
[99] H. Krüger and H. Ewald, "New approach of signal processing for classification problems using a-priori information," in *IEEE Sensores conference*, pp. 1459-1462, 2009.
[100] M. Paliwal and U. Kumar, "Neural networks and statistical techniques: A review of applications," *Expert Systems with Applications*, vol. 36, pp. 2-17, 2009.

[101] S. Kamruzzaman and A. Sarkar, "A new data mining scheme using artificial neural networks," *Sensors*, vol. 11, pp. 4622-4647, 2011.
[102] M. Xi, M. Azimi-Sadjadi, T. Bin, A. Dubey, and N. Witherspoon, "Detection of mines and minelike targets using principal component and neural-network methods," *IEEE Transactions on Neural Networks*, , vol. 9, pp. 454-463, 1998.
[103] A. David, B. Nicholas, D. Nacer, S. Matthew, G. Elizabeth, H. Stuart, and A. Ali, "A multifaceted active swept millimetre-wave approach to the detection of concealed weapons," in *SPIE Proceeding on Millimetre Wave and Terahertz Sensors and Technology*, pp. 711707, 2008.
[104] D. Andrews, N. Rezgui, S. Smith, N. Bowring, M. Southgate, and J. Baker, "Detection of concealed explosives at stand-off distances using wide band swept millimetre waves " in *SPIE Proceeding on Millimetre Wave and Terahertz Sensors and Technology*, 2008.
[105] C. Chang and C. Lin, "LIBSVM: A Library for support vector machines," *ACM Transactions on Intelligent Systems and Technology*, vol. 2, pp. 1-27, 2011.
[106] J. Fernandez, B. Barrowes, K. O'Neill, K. Paulsen, I. Shamatava, F. Shubitidze, and K. Sun, "Evaluation of SVM classification of metallic objects based on a magneticdipole representation," presented at the Detection and Remediation Technologies for Mines and Minelike Targets XI, 2006.
[107] Z. Beijia, K. O'Neill, K. Jin Au, and T. M. Grzegorczyk, "Support Vector Machine and Neural Network Classification of Metallic Objects Using Coefficients of the Spheroidal MQS Response Modes," *Geoscience and Remote Sensing, IEEE Transactions on*, vol. 46, pp. 159-171, 2008.
[108] F. Juan Pablo, ndez, S. Fridon, S. Irma, E. B. Benjamin, and O. N. Kevin, "Realistic subsurface anomaly discrimination using electromagnetic induction and an SVM classifier," *EURASIP J. Adv. Signal Process*, vol. 2010, pp. 1-11, 2010.
[109] G¨. Lehner, *Electromagnetic Field Theory for Engineers and Physicists*. Springer-Verlag, Berlin Heidelberg, 2010.
[110] John E. Nelson, "Coil assembly for electronic article surveillance system," U.S.A. Patent, No:5440296, Aug 8, 1995.
[111] K. T. Mcdonald. (2003). *A parallelogram loop antenna, Joseph Henry Laboratories, Princeton University, Princeton, NJ 08544*. Available: http://physics.princeton.edu/~mcdonald/examples/loopantenna.pdf
[112] M. Baibich, J. Broto, A. Fert, F. Van Dau, F. Petroff, P. Etienne, G. Creuzet, A. Friederich, and J. Chazelas, "Giant Magnetoresistance of (001)Fe/(001)Cr Magnetic Superlattices," *Physical Review Letters*, vol. 61, pp. 2472-2475, 1988.
[113] S. Yamada, K. Chomsuwan, T. Hagino, H. Tian, K. Minamide, and M. Iwahara, "Conductive microbead array detection by high-frequency eddy-current testing technique with SV-GMR sensor," *IEEE Transactions on Magnetics*, vol. 41, pp. 3622-3624, 2005.
[114] C. Smith, R. Schneider, T. Dogaru, and S. Smith, "Eddy-current testing with GMR magnetic sensor arrays," *Review of Progress in Quantitative Nondestructive Evaluation*, vol. 23, pp. 406-413, 2003.
[115] Y. Guang, A. Tamburrino, L. Udpa, S. Udpa, Z. Zhiwei, D. Yiming, and Q. Peiwen, "Pulsed eddy-current based giant magnetoresistive system for the inspection of aircraft structures," *IEEE Transactions on Magnetics*, vol. 46, pp. 910-917, 2010.
[116] K. Thiyagarajan, B. Maxfield, K. Balasubramaniam, and C. Krishnamurthy, "Pulsed eddy current digital imaging of corrosion pits," *Journal of Nondestructive Testing & Evaluation*, vol. 7, pp. 32-36, 2008.

[117] G. Y. Tian and A. Sophian, "Study of magnetic sensors for pulsed eddy current techniques," *INSIGHT*, vol. 47, pp. 277-280, 2005.
[118] F. Thollon, B. Lebrun, N. Burais, and Y. Jayet, "Numerical and experimental study of eddy current probes in NDT of structures with deep flaws," *NDT & E International*, vol. 28, pp. 97-102, 1995.
[119] G.Y. Tian and A. Sophian, "Pulsed eddy current sensor," in *Encyclopedia of Sensors*. vol. 8, ed, pp. 347-366, 2006,.
[120] L. Shu, H. Songling, and Z. Wei, "Development of differential probes in pulsed eddy current testing for noise suppression," *Sensors and Actuators A: Physical*, vol. 135, pp. 675-679, 2007.
[121] NVE Corporation. (2011). *GMR sensor catalogue* Available: www.nve.com/Downloads/catalog.pdf
[122] J. Lenz and S. Edelstein, "Magnetic sensors and their applications," *Sensors Journal, IEEE*, vol. 6, pp. 631-649, 2006.
[123] J. Pelegrí , J. Alberola , and J. Lajara "Signal conditioning for GMR magnetic sensors: Applied to traffic speed monitoring GMR sensors," *Sensors and Actuators A: Physical*, vol. 137, pp. 230-235, 2007.
[124] Agilent 33250A. *Function Generator*. Available: http://cp.literature.agilent.com/litweb/pdf/5968-8807EN.pdf
[125] Kepco BOP 36-12ML bipolar power amplifier. Available: http://www.kepcopower.com/1461965.pdf
[126] National instruments PXI PC. Available: http://www.ni.com/pxi/
[127] NI PXI-6251 data acquisition card. Available: http://sine.ni.com/nips/cds/view/p/lang/en/nid/14125
[128] INA111 instrumentation amplifier datasheet. Available: http://www.farnell.com/datasheets/80119.pdf
[129] V. Vapnik, *Estimation of Dependences Based on Empirical Data*. Springer Verlag, New York, 1982.
[130] J. Flusser, T. Suk, and B. Zitová, *Moments and Moment Invariants in Pattern Recognition*: John Wiley & Sons, 2009.
[131] Air Force Research Laboratory, "Sensor fusion algorithms and performance limits," Final Technical Report, 2001, Available: http://www.dtic.mil/cgi-bin/GetTRDoc?AD=ADA391935,2001.
[132] R. Smid, A. Docekal, and M. Kreidl, "Automated classification of eddy current signatures during manual inspection," *NDT & E International*, vol. 38, pp. 462-470, 2005.
[133] Y. Li, G. Tian, N. Bowring, and N. Rezgui, "A microwave measurement system for metallic object detection using swept frequency radar," in *SPIE Proceeding on Millimetre Wave and Terahertz Sensors and Technology*, 2008.
[134] A. Savitzky and M. Golay, "Smoothing and differentiation of data by simplified least squares procedures," *Analytical Chemistry*, vol. 36, pp. 1627-1639, 1964.
[135] S. J. Orfanidis, *Introduction to Signal Processing*: Prentice-Hall, Englewood Cliffs, NJ, 2010.
[136] F. Herbert, "Computer processing of line-drawing images," *ACM Computing Surveys*, vol. 6, pp. 57-97, 1974.
[137] E. Micheli-Tzanakou, *Invariant moments: supervised and unsupervised pattern recognition*: CRC Press, 2000.
[138] Y. Yin and G. Tian, "Feature extraction and optimisation for X-ray weld image classification," presented at the 17th World Conference on Non-Destructive Testing, Shanghai, China, 2008.
[139] Computing Fourier Series and Power Spectrum with MATLAB. Available: http://faculty.olin.edu/bstorey/Notes/Fourier.pdf

[140] H. G. Stark, *Wavelets and Signal Processing: An Application-based Introduction*: Springer, Heidelberg, 2005.

[141] E. Tamil, N. Kamarudin, R. Salleh, and A. Tamil, "A review on feature extraction & classification techniques for biosignal processing " in *(Part I: Electrocardiogram) 4th Kuala Lumpur International Conference on Biomedical Engineering 2008*. vol. 21, N. Abu Osman, F. Ibrahim, W. Wan Abas, H. Abdul Rahman, H. Ting, and R. Magjarevic, Eds., ed: Springer Berlin Heidelberg, pp. 107-112, 2008.

[142] C. Torrence and G. Compo, "A practical guide to wavelet analysis," *American Meteorological Society* vol. 79, pp. 61–78, 1998.

[143] A. Al-Qubaa, G. Tian, and J. Wilson, "Object identification using feature extraction for electromagnetic images," presented at the Electrical and Electronic Conference of Postgraduate Research Newcastle University, 2011.

[144] G. Y. Tian, A. Al-Qubaa, and J. Wilson, "Design of an electromagnetic imaging system for weapon detection based on GMR sensor arrays," *Sensors and Actuators A: Physical,* vol. 174, pp. 75-84, 2012.

[145] K. Anil, P. Robert, and M. Jianchang, "Statistical pattern recognition: A review," *IEEE Transactions on Pattern Analysis and Machine Intelligence,* vol. 22, pp. 4-37, 2000.

[146] M. Egmont-Petersen, D. Deridder, and H. Handels, "Image processing with neural networks- A review," *Pattern Recognition,* vol. 35, pp. 2279-2301, 2002.

[147] N. Bowring, D. Andrews, N. Rezgui, M. Southgate, S. Smith, S. Harmer, and A. and Atiah, "A multifaceted active swept millimeter-wave approach to the standoff detection on concealed weapons," presented at the SPIE Proceeding on Millimetre Wave and Terahertz Sensors and Technology, 2008.

[148] Y. Zheng, J. Greenleaf, and J. Gisvold, "Reduction of breast biopsies with a modified self-organizing map," *IEEE Transactions on Neural Networks* vol. 8, pp. 1386-1396, 1997.

[149] Z. Zhigang, Y. Shiqiang, X. Guangyou, L. Xueyin, and S. Dingji, "Fast road classification and orientation estimation using omni-view images and neural networks," *IEEE Transactions on Image Processing,* vol. 7, pp. 1182-1197, 1998.

[150] Y. Park, "A comparison of neural net classifiers and linear tree classifiers: Their similarities and differences," *Pattern Recognition,* vol. 27, pp. 1493-1503, 1994.

[151] T. Ziemke, "Radar image segmentation using recurrent artificial neural networks," *Pattern Recognition Letters,* vol. 17, pp. 319-334, 1996.

[152] S. Marinai, M. Gori, and G. Soda, "Artificial neural networks for document analysis and recognition," *IEEE Transactions on Pattern Analysis and Machine Intelligence,* vol. 27, pp. 23-35, 2005.

[153] F. Chen, "Back-propagation neural networks for nonlinear self-tuning adaptive control," *IEEE Control Systems Magazine,* vol. 10, pp. 44-48, 1990.

[154] G. Cybenko, "Approximation by superpositions of a sigmoidal function," *Mathematics of Control, Signals, and Systems (MCSS),* vol. 5, pp. 455-455, 1992.

[155] R. Hecht-Nielsen, "Neurocomputing: picking the human brain," *IEEE Spectrum* vol. 25, pp. 36-41, 1988.

[156] G. Onkal-Engin, I. Demir, and S. Engin, "Determination of the relationship between sewage odour and BOD by neural networks," *Environmental Modelling & Software,* vol. 20, pp. 843-850, 2005.

[157] J. Christopher, "A tutorial on support vector machines for pattern recognition," *Data Mining and Knowledge Discovery,* vol. 2, pp. 121-167, 1998.

[158] R. Duda, P. Hart, and D. Stork, *Pattern Classification*. USA: John Wiley&Sons, 2001.
[159] K. Wang, Y. Xie, and L. Sun, "Study on nonlinear compensation of eddy current sensor based on support vector machine," in *IEEE International Symposium on Industrial Electronics*, pp. 133-137, 2009.
[160] S. Keerthi and C.-J. Lin, "Asymptotic Behaviors of Support Vector Machines with Gaussian Kernel," *Neural Computation*, vol. 15, pp. 1667-1689, 2003.
[161] A. Bernieri, L. Ferrigno, M. Laracca, and M. Molinara, "Crack shape reconstruction in eddy current testing using machine learning systems for regression," *IEEE Transactions on Instrumentation and Measurement,* vol. 57, pp. 1958-1968, 2008.
[162] M. Curilem, M. Chacón, G. Acuña, S. Member, S. Ulloa, C. Pardo, C. Defilippi, and A. Madrid "Comparison of artificial neural networks an support vector machines for feature selection in electrogastrography signal processing," presented at the IEEE International Conference of the Engineering in Medicine and Biology Society, 2010.
[163] D. Mcmakin, D. Sheen, H. Collins, T. Hall, and R. Severtsen, "Wideband millimetre-wave holographic weapons surveillance systems," in *SPIE Proceedings on Law Enforcement Technologies: Identification Technologies and Traffic Safety*, pp. 131-141, 1995.
[164] D. Mcmakin, D. Sheen, T. Hall, and R. Severtsen, "Cylindrical holographic radar camera," in *SPIE Proceedings on Enforcement and Security Technologies*, pp. 79-88, 1998.
[165] W. Zhijun, D. Ziou, C. Armenakis, D. Li, and L. Qingquan, "A comparative analysis of image fusion methods," *IEEE Transactions on Geoscience and Remote Sensing,* vol. 43, pp. 1391-1402, 2005.
[166] C. Pohl and J. Van-Genderen, "Review Article: Multisensor image fusion in remote sensing: concepts, methods and applications," *International Journal of Remote Sensing*, vol. 19, pp. 823-854, 1998.
[167] Z. Liu, T. Macuda, Z. Xue, D. Forsyth, and R. Laganière, "Concealed weapon detection: A data fusion perspective," Journal of Aerospace Computing, Information, and Communication, vol. 6, pp. 1-13, 2009.

Appendix A: System Manual

A.1 Equipment Connection and Functions:

- **Agilent 33250A function generator**– provides excitation waveform to power amplifier.
- **Kepco BOP 36-12ML bipolar power amplifier** – provides excitation to the coil where the excitation current is proportional to the excitation voltage from the function generator.
- **National instruments data acquisition system:**
  - PC equipped with a PXI bus to accommodate multiple data acquisition cards.
  - 5 x NI PXI-6251, 16 input data acquisition cards. Allows acquisition of 80 channels of data at a sample rate of 125kHz.
  - 5x breakout boxes and cables to allow us to establish a connection to the data acquisition cards.
- **Sensor boards** – Each board contains 8 x NVE AAL002-02 giant magneto-resistive sensors.
- **Amplifier boards** – Each board contains 16 circuits based on the INA111 instrumentation amplifier, to allow connections from two 8-channel sensor boards.
- **CEIA walk-through metal detector and control box** – We provide our own pulsed excitation to the coils in the metal detector panel through a connection in the control box.

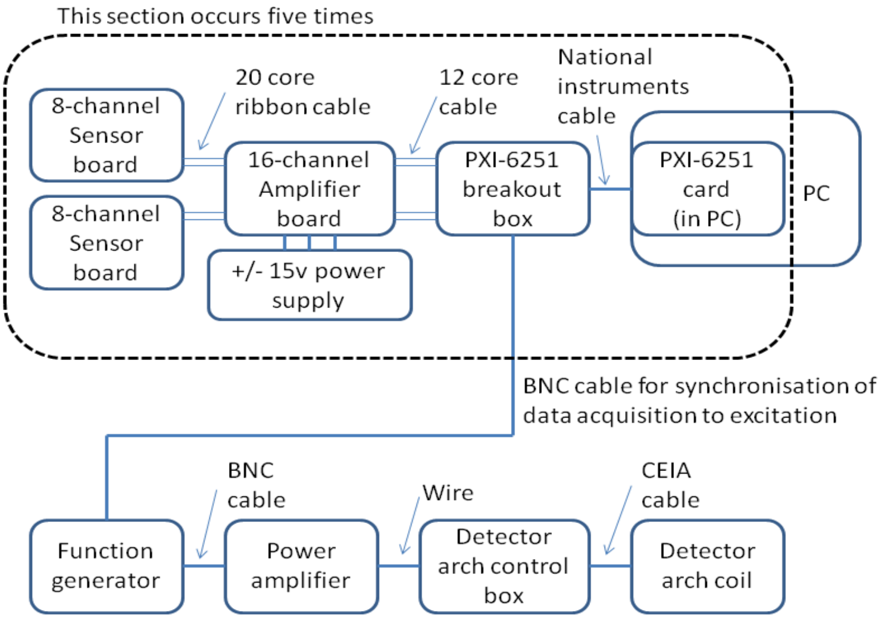

Figure A.01: System connection diagram

Figure A.01 shows the system connection diagram. The upper part of the diagram is duplicated five times to make 80 channels (16 channels on each card x 5 cards). Two 8-channel sensor boards are connected to each of the 16-channel amplifier boards via 20-core ribbon cable. The INA instrumentation amplifiers provide differential termination and amplification for the sensor outputs (see Figure A.02). The amplifier circuits are powered by a +/-15v power supply. The outputs from the amplifier boards are connected to the data acquisition boards in the PC via the breakout boxes. An additional connection is established to the data acquisition board from the function generator. This allows the data acquisition to be synchronised to excitation waveform.

A function generator supplies the excitation waveform. The Bipolar power amplifier is set to produce an output CURRENT that is proportional to the input VOLTAGE supplied by the function generator. The output from the function generator must be connected to the ***current programming input*** on the amplifier to achieve this. The output from the power amplifier is connected to the coil in the detector board via the arch control box. Note – none of the electronics in the control box are used in the test, it is just there to establish a connection to the detector panel.

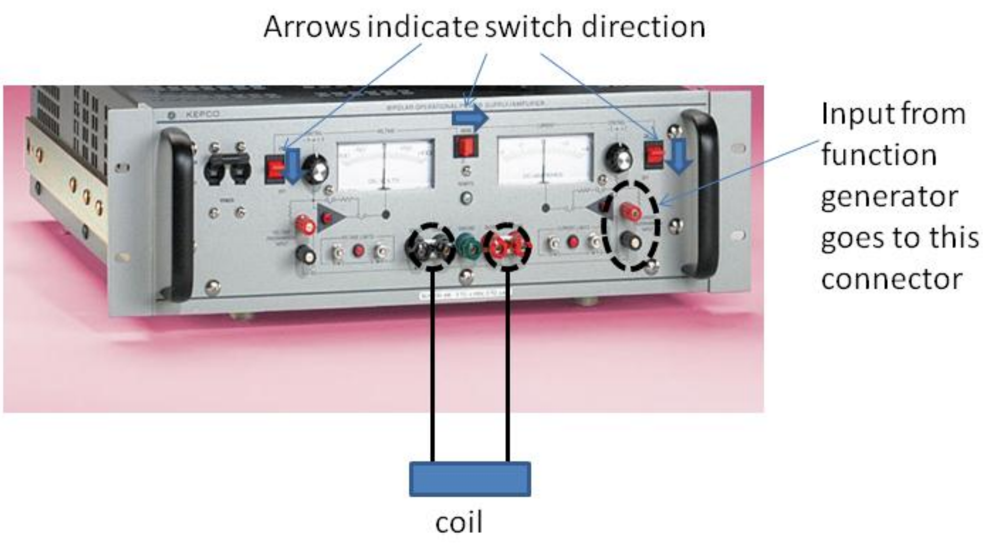

Figure A.02: BOP connections

A.2 System Operation

The following steps are required to either image the EM field from objects passing through the system or to acquire data using the system.

A.2.1 Start-up

1. Turn on the computer and monitor.

2. Turn on the lab power supply; check the red lights just above the power connectors. If any of these are lighted up, turn off the power supply and check for short circuits.

3. Turn on the function generator (FG) and recall setting #2 from the function generator memory. This should result in a waveform with the following parameters:

- Frequency = 500Hz.
- Waveform = square wave.
- Amplitude = 1v.
- Offset = 500mv.
- Duty = 50%.

4. Check that the function generator output is ON.

5. Turn on the Kepco BOP power amplifier. Check the VU meters on the front. If either of the needles are at maximum, turn off the BOP and check; i) that the FG output is on and outputting the right signal, ii) that the signal is reaching the BOP (use oscilloscope), iii) that the connection to the arch is OK (check resistance), and iv) that the settings on the BOP match those in the previous section.

Note: The function generator must always be ON and outputting the right waveform if the BOP is on, otherwise a large current could be applied to the arch and damage it. So always turn the BOP off BEFORE the FG.

A.2.2 Data acquisition / scanning

1. Open the file "plotter_02" in the following directory (see Figure A. 3)

(C:\MATLAB_FILES\ NEW_GUI_FULL_ARRAY\plotter_02)

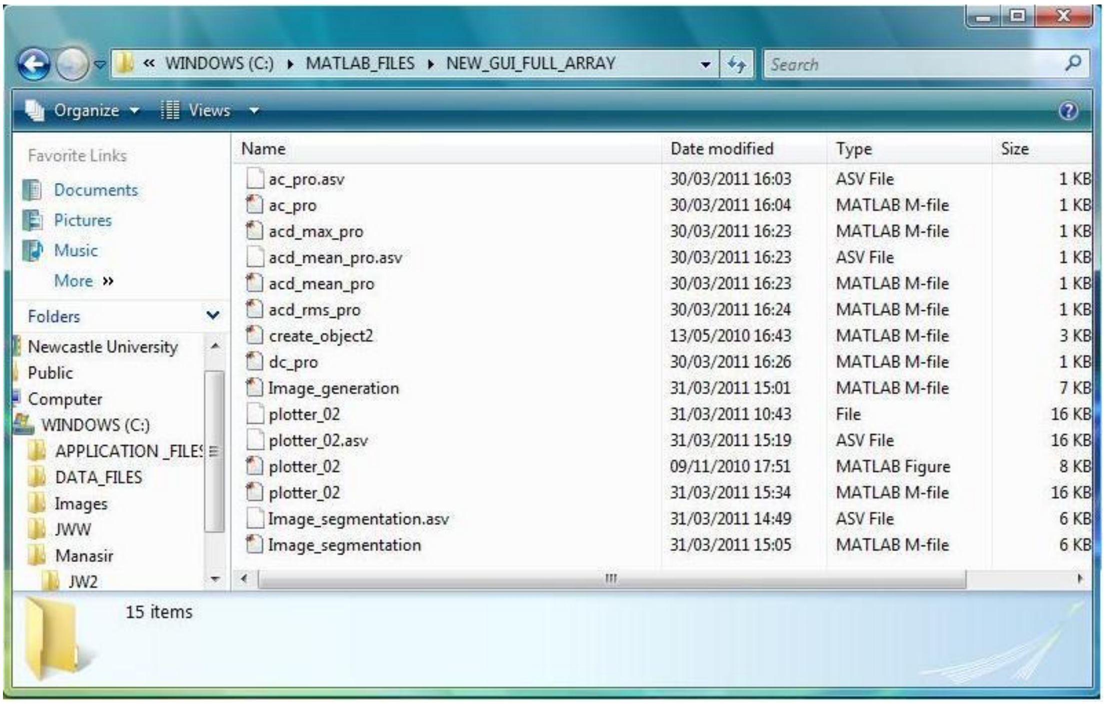

Figure A. 3: The paths and the files used to capture data and process it.

2. Check the user input section of the file; different settings are required for different array configurations; see the annotation in the file for details.

3. Enter a location to save the generated data. See the annotation in the file for details.

4. Run the file (F5) and change directory when prompted. The GUI will appear as shown in Figure A.04.

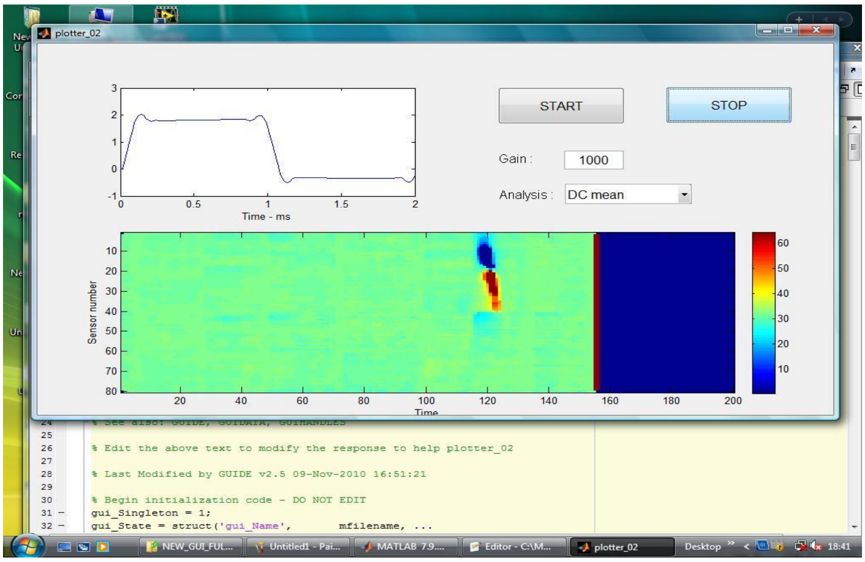

Figure A.04: The GUI for the system

5. Set the gain and the analysis type. Gain = 1000, Analysis type = DC mean is a good starting point for most tests. But smaller / more distant objects may require more gain.

6. Press the START button to start acquisition / scanning.

Note: The system must be clear of any metallic objects during the first 6 readings after the START button is pressed, as these readings are taken as a measurement of the background field.

7. Move the object under test through the arch. Slower movement will results in a better resolution in the final images.

8. The GUI saves the first “K” (currently set at 140) readings after the start button is pressed. The file is saved on pressing the STOP button or the data acquisition loop in the GUI file reaching its end.

Note: The saved file will be overwritten if the save location is not changed before the next time the START button is pressed.

A.2.3 Data processing

The saved data file “IMAGE.mat” contains the following:

- IM2 – matrix representing the image shown in the GUI at the end of the data acquisition period.
- KEEP – matrix containing the raw unprocessed data collected by the system during the test, in the form WP x CH x K (see “plotter_02” for definitions), i.e. (number of samples acquired for each reading) x (number of sensors in the array) x (number of readings).
- TIME – time vector for the data acquisition period.
- PARAMS – structure storing all the user input parameters.

The data can be processed using the following files:

- Image_generation – outputs a number of images that correspond to different processing techniques, see functions called for definitions of processing techniques. This file will generate the data V_{DC} and V_{AC} from the original “IMAGE.mat” file. Each of them related with different signal processing methods.

- Image_segmentation – outputs segmented, ‘time slot’ images. This file will generate the 14 frames for same objects captured by the sensor-array through the time.
- These two files will be in the same directory (Image_generation Image_segmentation):

  (C:\MATLAB_FILES\ NEW_GUI_FULL_ARRAY\)

The files require the user to enter the locations of the files to be processed – see file annotation for details. As an example, the final generated data will be appearing as shown in Figure A.05.

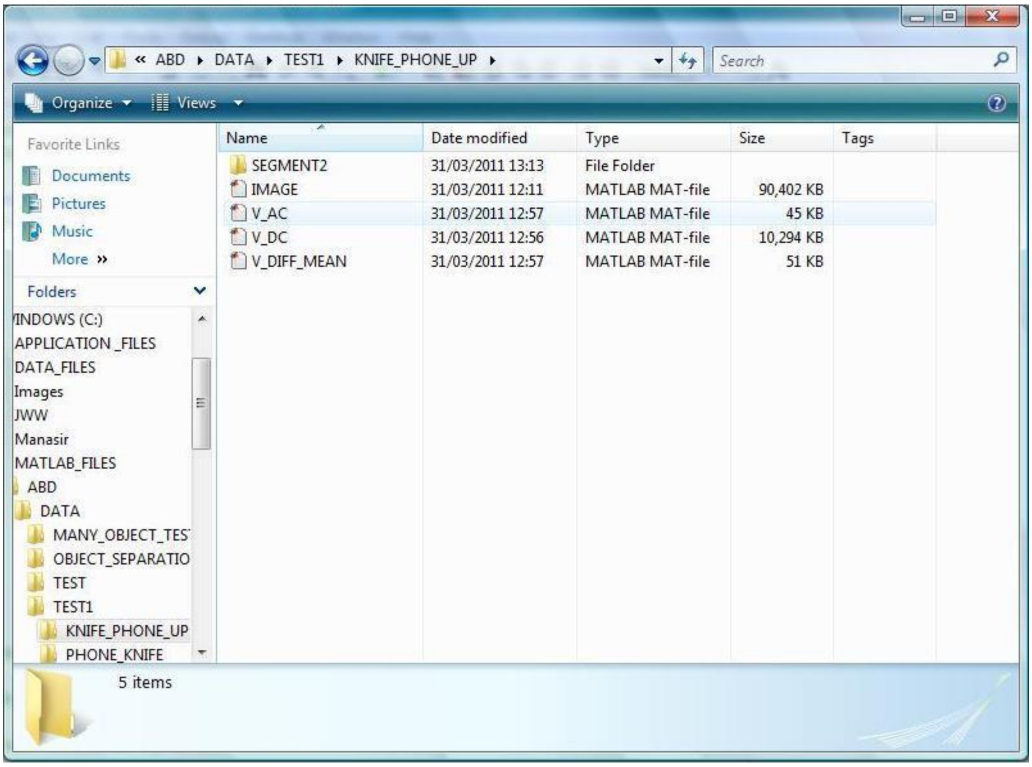

Figure A.05: The final appearance of the data

Appendix B: Police Test Report

A test was carried out in the Metropolitan Police office in London in the beginning of the project which all the system equipment were moved to the location of the test. A report was written for this test as follows.

B.1 Sample Summary

Six weapons (Table B.0.1) were provided by the Metropolitan Police for the tests. The samples represent common weapons seized by the police; of particular interest is sample #5 – the blank firer, converted to fire real bullets by welding another barrel to existing mechanism and the replica hand gun (sample #6), commonly used by armed robbers, etc., as a threat.

Table B.0.1: Summary of samples used in tests

No.	Type	Model	Notes	Weight	Length
1	Small revolver	Brocock .22”	Not many of this type in circulation	516g	150mm
2	Small semi-automatic	Walther PP - 7.65mm	Used as personal protection by a few people – quite rare	637g	175mm
3	Medium revolver	Brocock .22”	Converted from firing air capsules, common modification	937g	215mm
4	Medium semi-automatic	Glock	Used by police, light, lots of plastic, not many used by criminals	689g	205mm
5	Converted blank firer	BBM GAP, 8mm	Barrel replaced by welding, common modification	800g	200mm
6	Replica	Bruni 8mm	Replica, commonly used by armed robbers, etc. as a threat	1140g	215mm

B.2 Test Set-up

Tests were carried out using the apparatus shown in Figure B.01. The apparatus consists of:

- The array; fixed to the Tx or Rx panel in the optimal position with respect to the excitation coil, ascertained by previous tests.

- The sample holder: holds the sample in a constant position as it is moved past the array.
- The platform; fixed between the panels to ensure that the sample maintains a constant horizontal position with respect to the array and the panel.
- The ramp; the sample is moved down the ramp (in the holder) past the array.

The apparatus is designed so the sample can move past the array in 10cm increments with respect to the panel.

Figure B.2a shows the array configuration and the relationship between the array and the samples. Two 80-elemet arrays were built into one framework:

- Array 1; 80-element array with a 7.5mm x 42 mm pitch.
- Array 2: 80-element array with a 7.5mm x 10 mm pitch.

A multiplexing circuit is used to switch between the two arrays configurations, as shown in Figure B.2b.

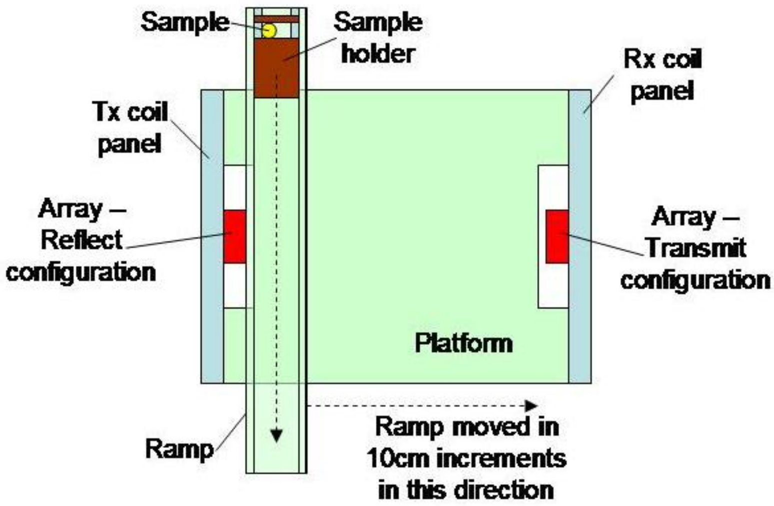

Figure B.01: Test set-up – top view

Two set of tests were carried out, as shown in Figure B.03:

- **Dynamic tests;** samples moved through the arch in one pass, data taken with the sample moving. Separate data sets taken in positions 1, 2, 3 ….10. Sample rate = 62.5 kHz, pulse repetition rate 100 kHz. .
- **Static tests;** samples moved through the arch in 10cm increments, data taken with the sample stationary. Separate data sets taken in positions 1, 2, 3 ….10, sample rate = 250 kHz, pulse repetition rate = 1 kHz.

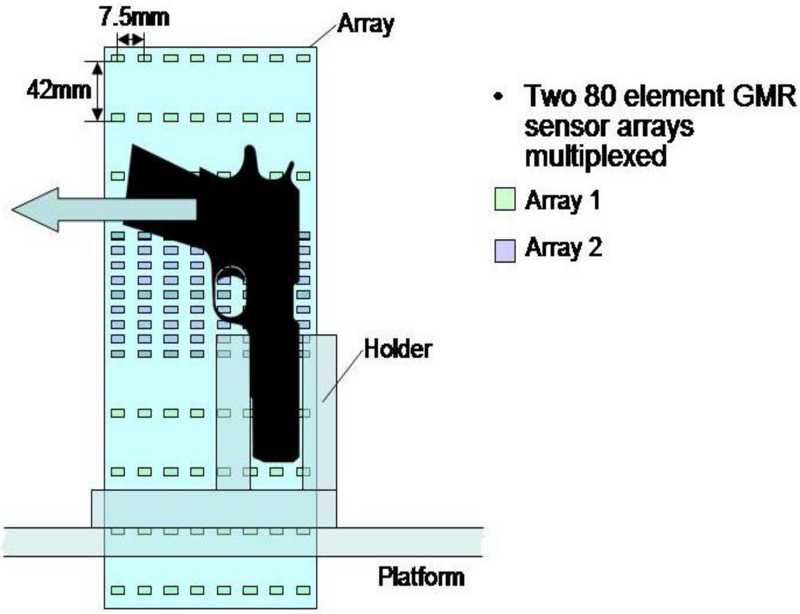

a)

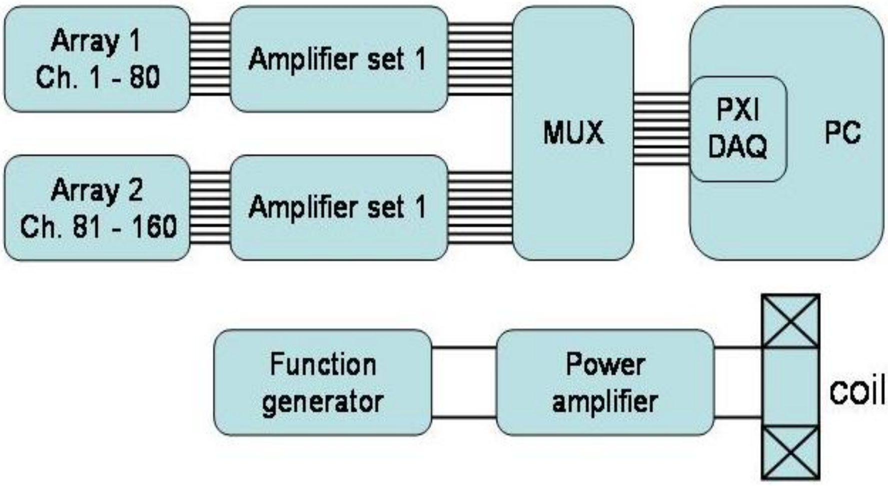

b)

Figure B.2: Test set-up: a) Test set-up side view b) System setup

B.3 Test Results

In this section the dynamic tests results with the sample moving through the arch are shown. The low sample rate and lack of data for averaging meant that processing of the raw data (Figure B.04a) did not yield useful results. For this reason, the following steps were taken:

1. Up-sampling of the raw signal (x10), as shown in Figure B.04b.
2. Calculation of a moving average (20 pulse responses).
3. Calculation of the difference signal (signal with object – signal without object) for each sensor.

4. Calculation of mean and RMS amplitude of difference signal (see Figure B.04c and Figure B.04d) for all sensors and interpolation to produce sample image.

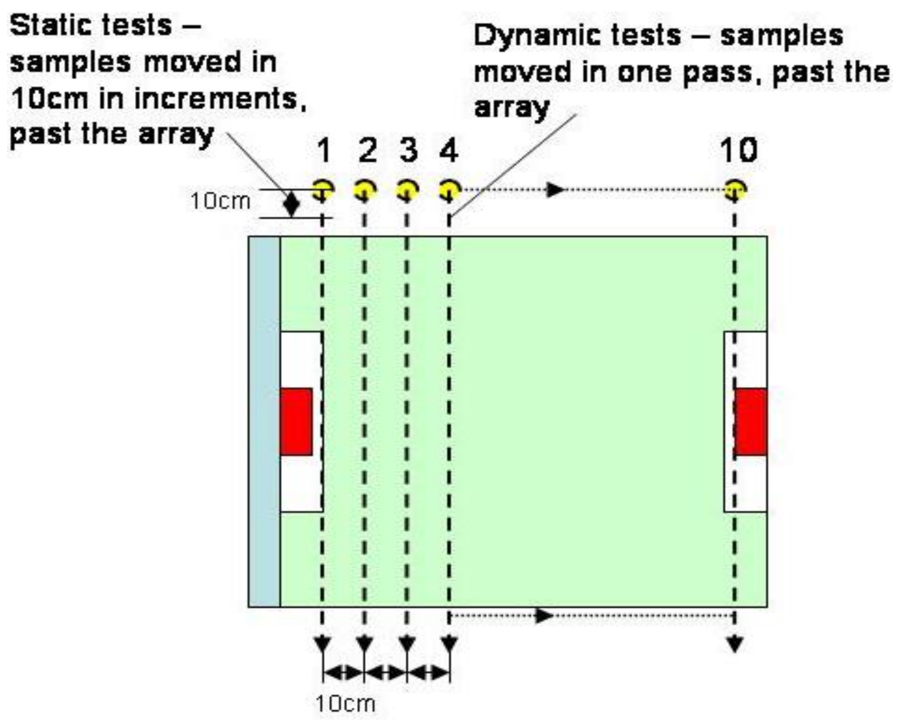

Figure B.03: Sample position increments.

The moving average process allowed 20 pulse responses to be averaged to increase the effective SNR while retaining the response to the presence of the object.

The data from only one column of sensors (see Figure B.5) was used in order to produce the images shown in Figure B.6, with the sample passing by the column of sensors, and data plotted with respect to time.

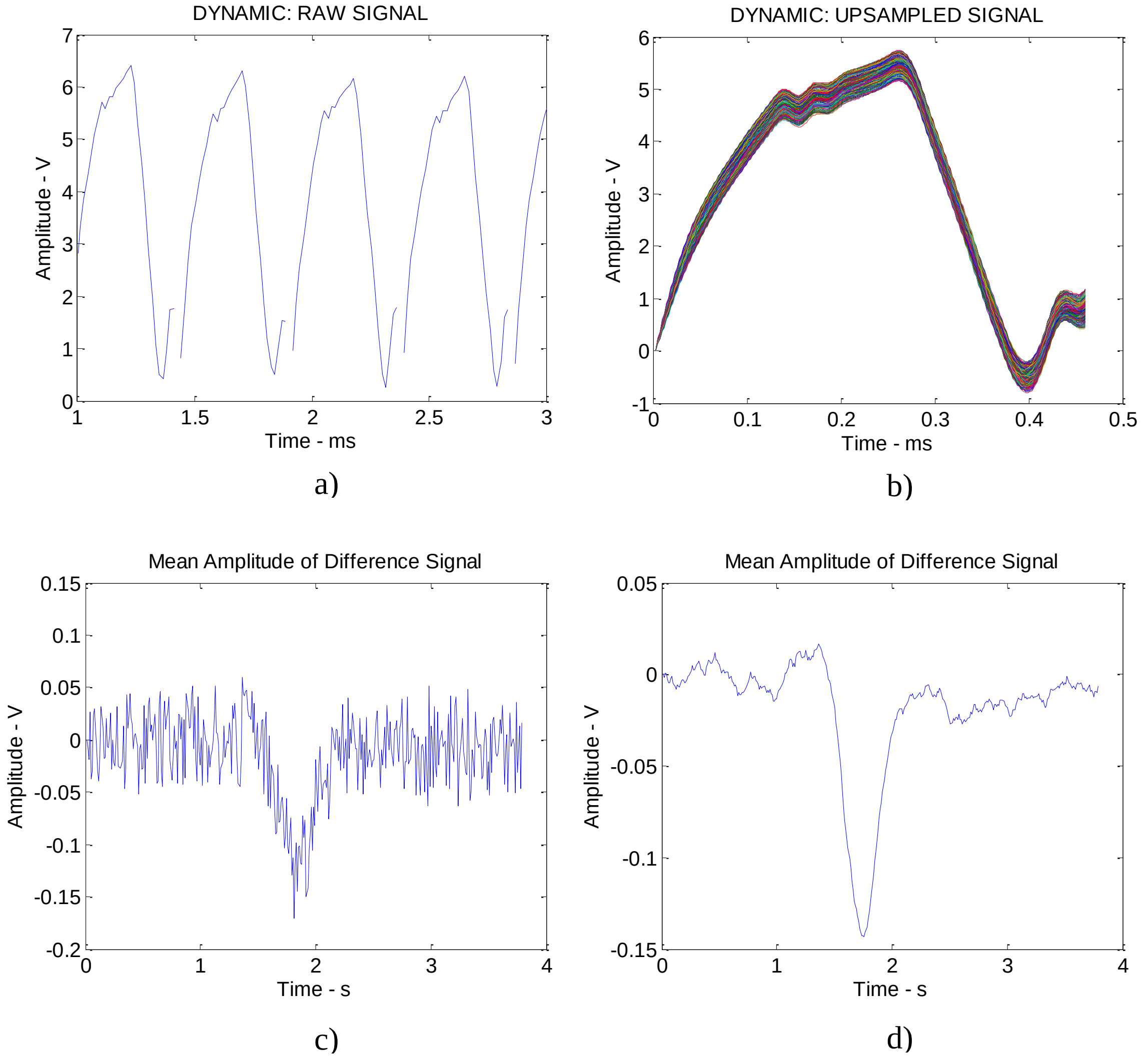

Figure B.04: a) Raw sensor signal for one sensor, b) Up-sampled (x10) signal for all sensors, c) Mean amplitude of raw signal with object passing through the arch, d) Mean amplitude of up-sampled and averaged signal with object moving through the arch

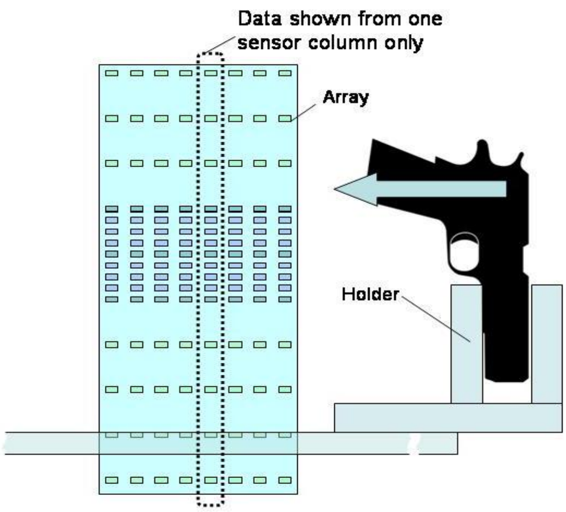

Figure B.5: One column of sensors used to produce the images

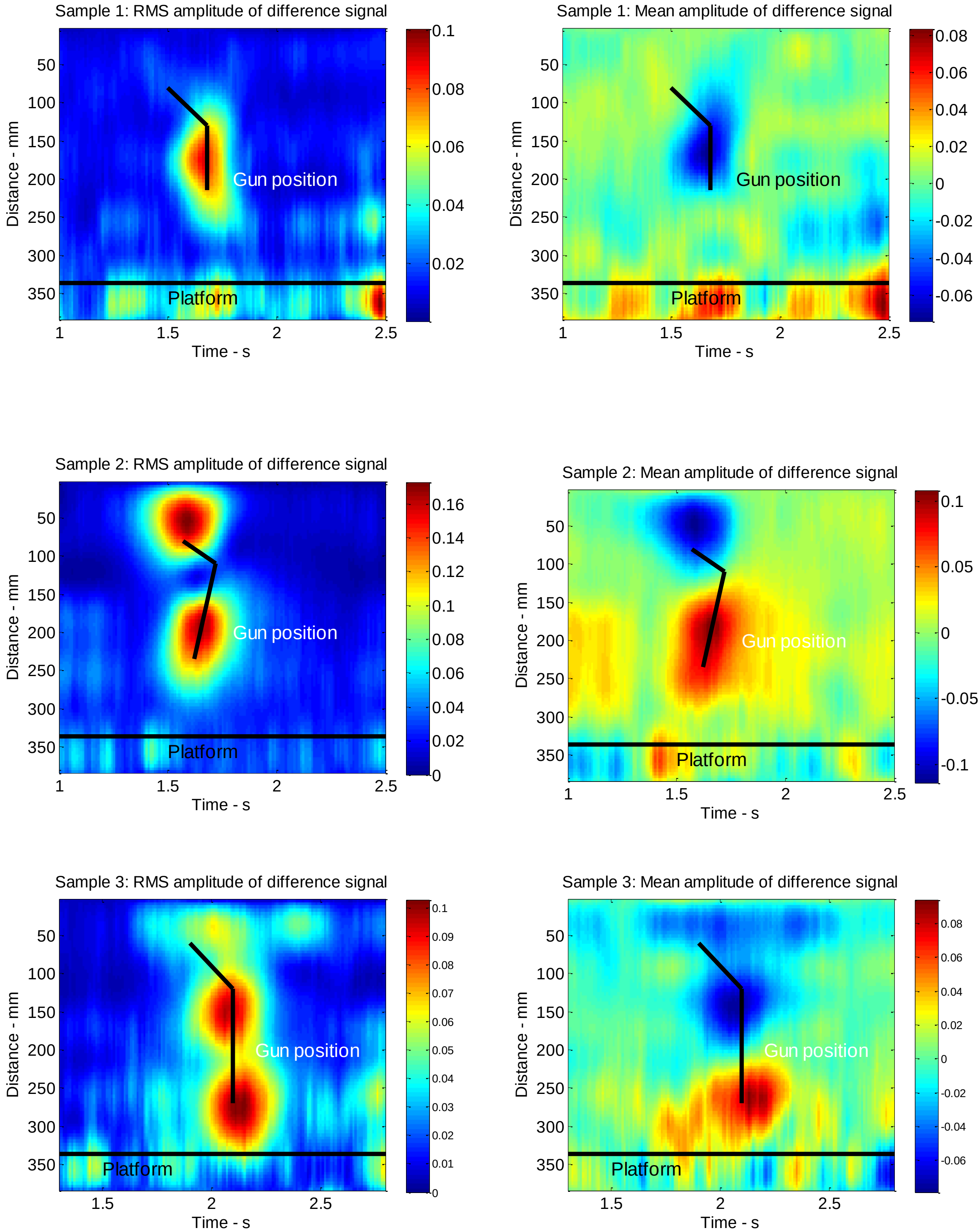
Sample 1: RMS amplitude of difference signal
Sample 1: Mean amplitude of difference signal
Sample 2: RMS amplitude of difference signal
Sample 2: Mean amplitude of difference signal
Sample 3: RMS amplitude of difference signal
Sample 3: Mean amplitude of difference signal
Distance - mm
Time - s
Gun position
Platform

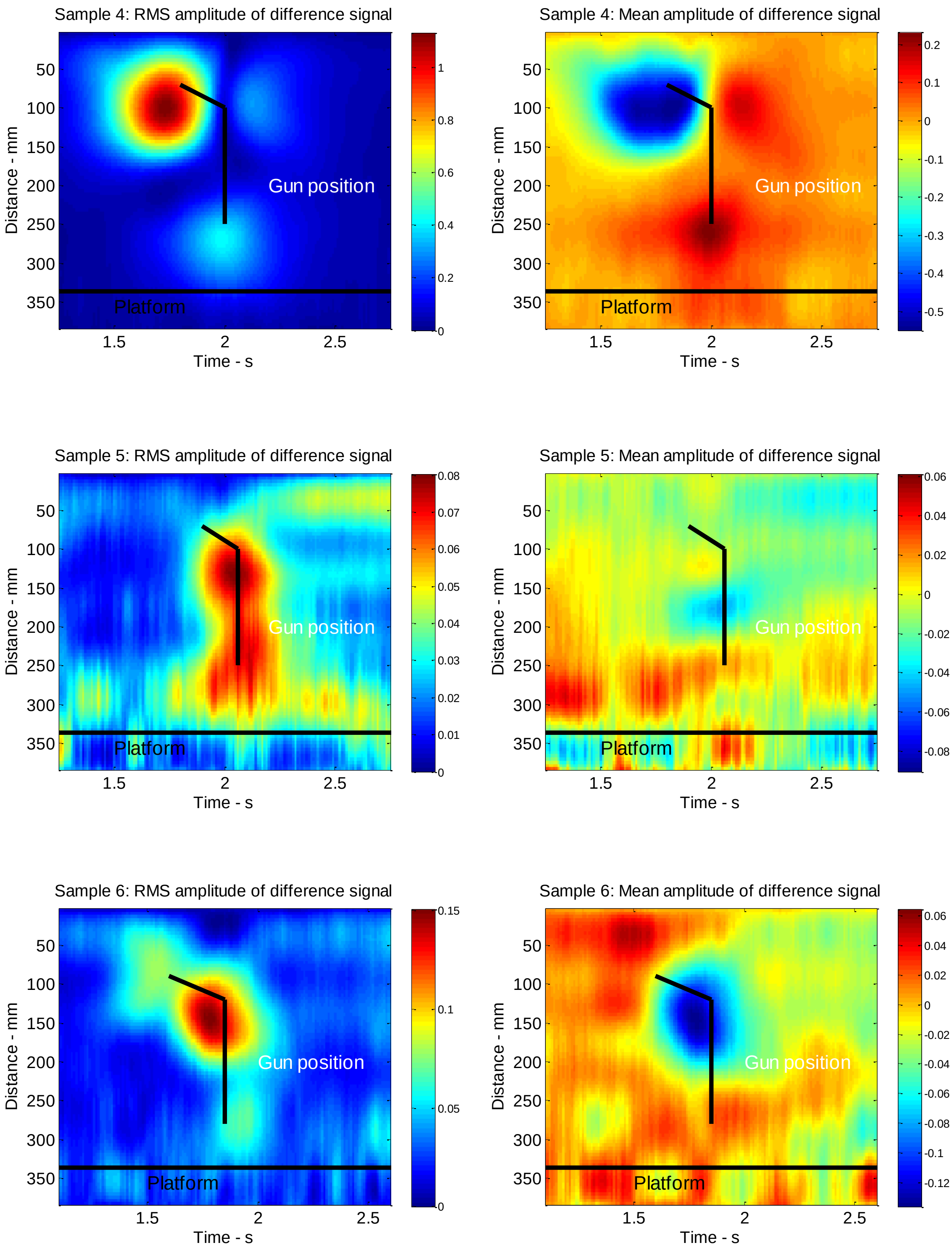

Figure B.6: Maps of RMS and mean amplitude of difference signals for a single column of sensors over time as object passes through the arch for all samples

Figure B.7 shows another test of the maps of RMS of difference signals for a single column of sensors over time as object passes through the arch, for sample 2 only with 10, 20, 30, and 40 cm distance from array changing as shown in Figure B.03.

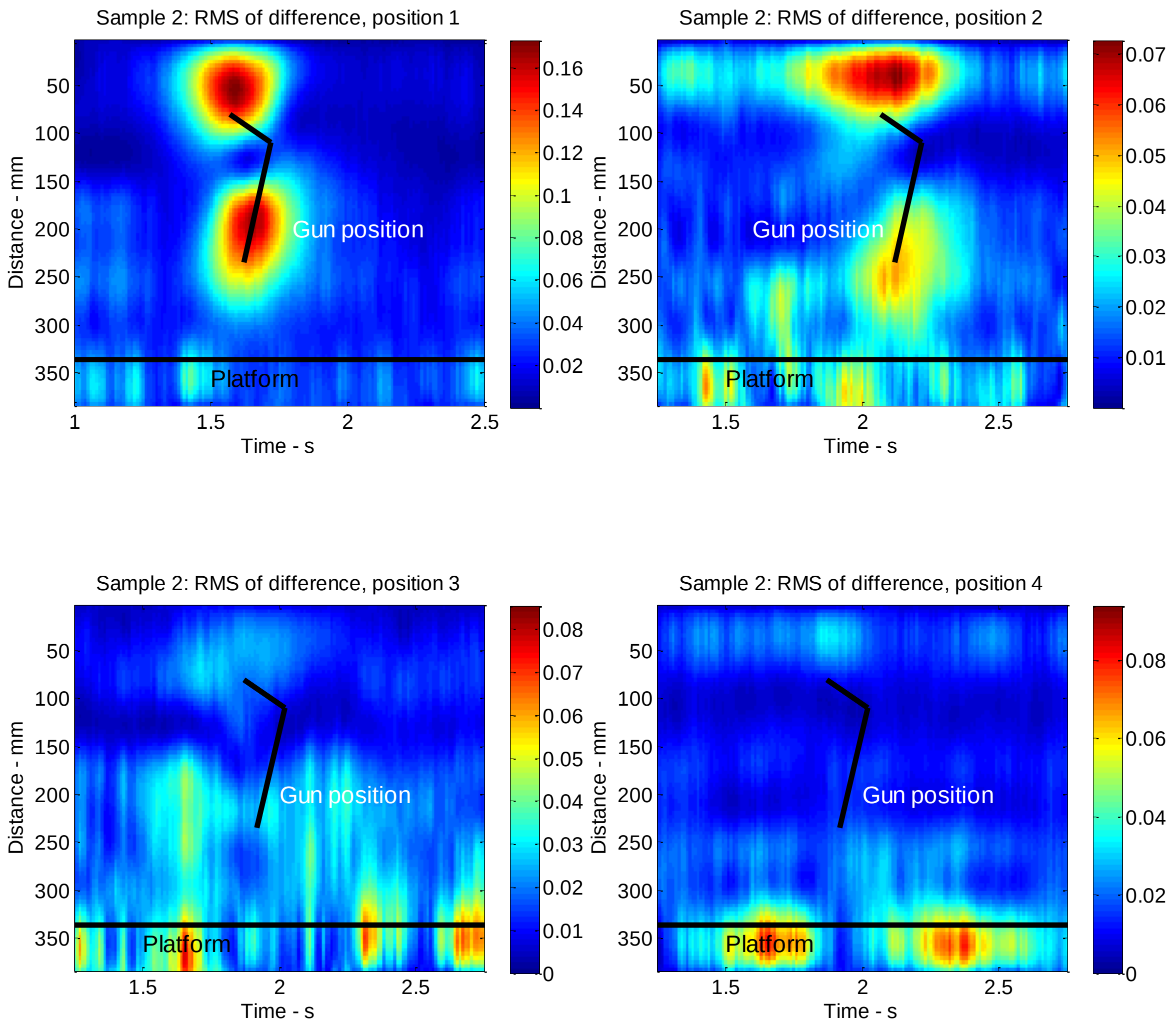

Figure B.7: Maps of RMS of difference signals for a single column of sensors over time as object passes through the arch, for sample 2 only with distance from array changing as shown in Figure B.03.

B.4 Conclusions

The results show that:

- Figure B.6 shows that there is some correlation between the position and shape of the object and the signal from the array (at least at short distances).
- Figure B.7 shows that the correlation is retained as the distance between the array and the object is increased up to a limit of around 400mm, this is still not good enough.
- A single column of sensors (10 sensors rather than 80 sensors) can be used to create an image of the object passing through the arch.

Appendix C: Image Fusion

Several fusion attempts have been tested using different image fusion techniques through the system developing stages to visualize the object under test. Pixel-based image fusion approaches were investigated and tested: Average approaches, principle component analysis and contrast enhancement techniques. All the three methods are single resolution methods. The source images for all methods were greyscale images.

C.1 Average Algorithm

Image averaging is the most simply and commonly used example of fusion methods. In this case, the fused signal is evaluated as the average value between the inputs, however, despite being significantly more computationally efficient than most other fusion systems, image averaging, does not achieve enviable performance. The main reason for this is the loss of contrast, a result of destructive superposition when input signals are added. So it does not give the exact small defect in NDE application.

C.2 Principal Component Analysis (PCA)

PCA is a powerful tool used for merging different sensors images. It is a statistical technique that transforms a set of correlated variables into a set of new uncorrelated linear combinations of the original variables. Evaluation of principal components (PCs) of an image signal also involves calculations of covariance and eigenvalues (vectors). An inverse PCA, transforms the data back to the original image space.

PCA are produced in our system by performing a PCA of the covariance matrix of input intensities, the weightings for each input frame are obtained from the eigenvector corresponding to the largest eigenvalues then multiply the first eigenvalues by the first image and the second one by the second image then adding the results to form the fused images.

C.3 Contrast Enhancement

Image fusion using contrast enhancement as Equation below:

New Image=255*((img1/255)^(img2/255)).

Figure C.1 below shows the original images and the results of the fusion methods used [165-167].

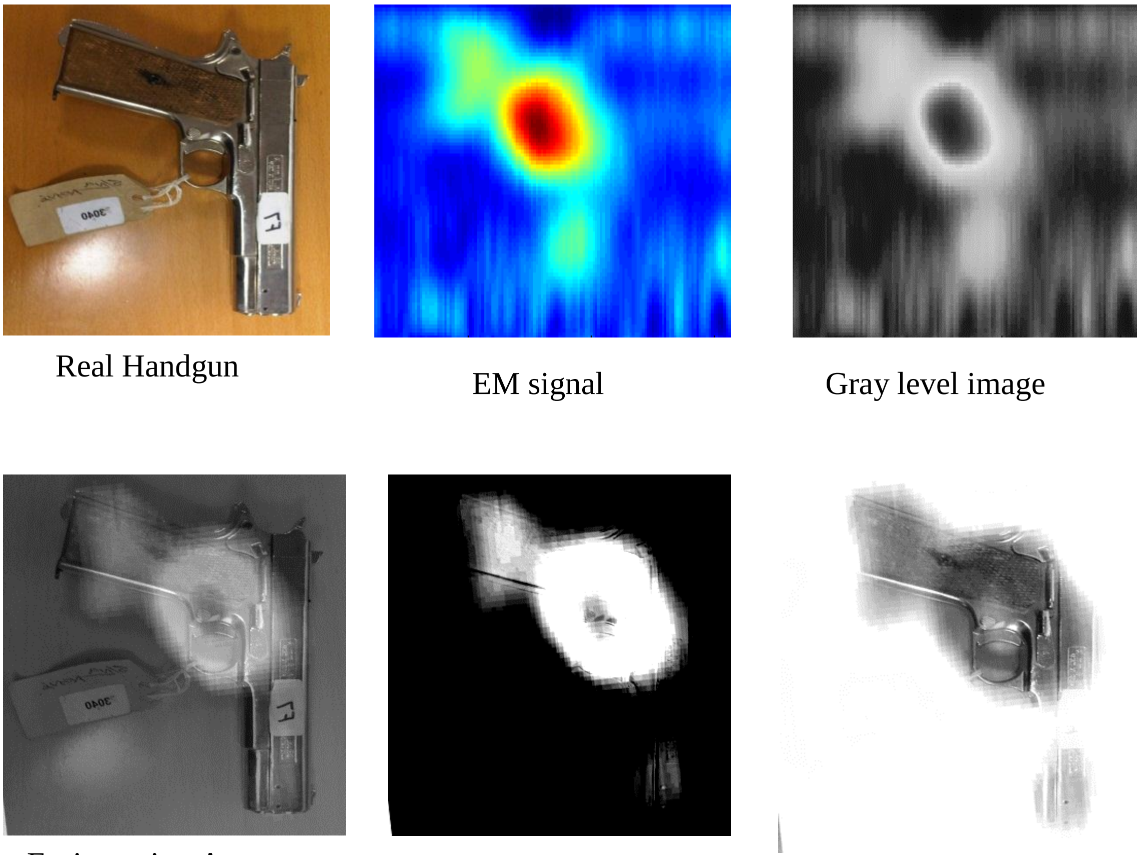

Real Handgun
EM signal
Gray level image
Fusion using Average
Fusion using PCA
Fusion using Enhancement

Figure C.1: Different fusion methods deployed to help visual of the EM images and a certainty of the threat objects (especially for the operator).

Appendix D: Cross Correlation

A novel research was developed by the researcher, and used later in this project, to investigate the transient temperature distribution inside material using cross-correlation (CC) technique. Defects can be characterized by tracking the diffusion of heat in a sample through the analysis of a sequence of PEC thermography images. The CC technique is based on finding the statistical correlation between two images.

This novel technique has been used in Chapter 4 for classify the type of targeted object material. The technique has been demonstrated below [97]:

Cross Correlation (CC):

The CC technique is based on finding the statistical correlation between two images. The basic principle of the CC method is to search for the maximum correlation between small zones in the two images from which the displacement at different positions in the zone of interest can be obtained. The simplest form of image-matching can be obtained using cross-correlation, which determines the in-plane displacement field by matching different zones of two images.

CC is one of the methods used to measure the degree of similarity between two images. It is used to determine the location of a certain pattern in a two dimensional image function based on a template-matching algorithm. To match a template to an image, where the template is a sub-image that contains the shape to be found, the template will be centred on an image point and the number of points in the template which match those in the image will be calculated. The procedure is repeated for the entire image, and the point that leads to the best match (the maximum count) is considered to be the point where the shape (given by the template) lies within the image. For two images F(t0) and F(t0+ Δt) in a video sequence to be correlated, where Δt is the difference in time between consequent frames, two sub-images of spatial coincident pixel positions are placed in both images (Figure D.1). A name template will be called to the sup-image of $F(t_0)$ and a search area to the sup-image of $F(t_0+\Delta t)$. $f(x, y)$ are image intensity value of the search area f with a size of $Mx \times My$ at the pixel position (x, y) , $x \in \{0, . . ., Mx - 1\}$, $y \in \{0, . . ., My - 1\}$. Similarly, let $t(x, y)$ be the intensity value of the template t at pixel (x, y) with a size of $Nx \times Ny$ where $Nx \leq Mx$ and $Ny \leq My$. CC is evaluated at every point (u, v) for f and t, which has been shifted over the original image $f(x, y)$ by u-steps in the x-direction and v-steps in the y-direction. All the CC coefficients are stored in a correlation matrix $\gamma(u, v)$ defined in Eq. 1 shown below [94]:

$$\gamma(u, v) = \frac{\sum_{x,y}\,[f(x,y)-\bar{f}_{u,v}][t(x-u,y-v)-\bar{t}]}{\left\{\sum_{x,y}[f(x,y)-\bar{f}_{u,v}]^2\,\sum_{x,y}\,[t(x-u,y-v)-\bar{t}]^2\right\}^{0.5}} \tag{1}$$

where $u \in \{0, 1, 2, . . ., Mx-Nx\}$ and $v \in \{0, 1, 2, ...,My-Ny\}$, and $\bar{f}_{u,v}\bar{f}_{u,v}$ denotes the mean value of $f(x, y)$ within the area of the template t shifted by (u, v) steps. $\bar{t}$ denotes the mean value of the template t.

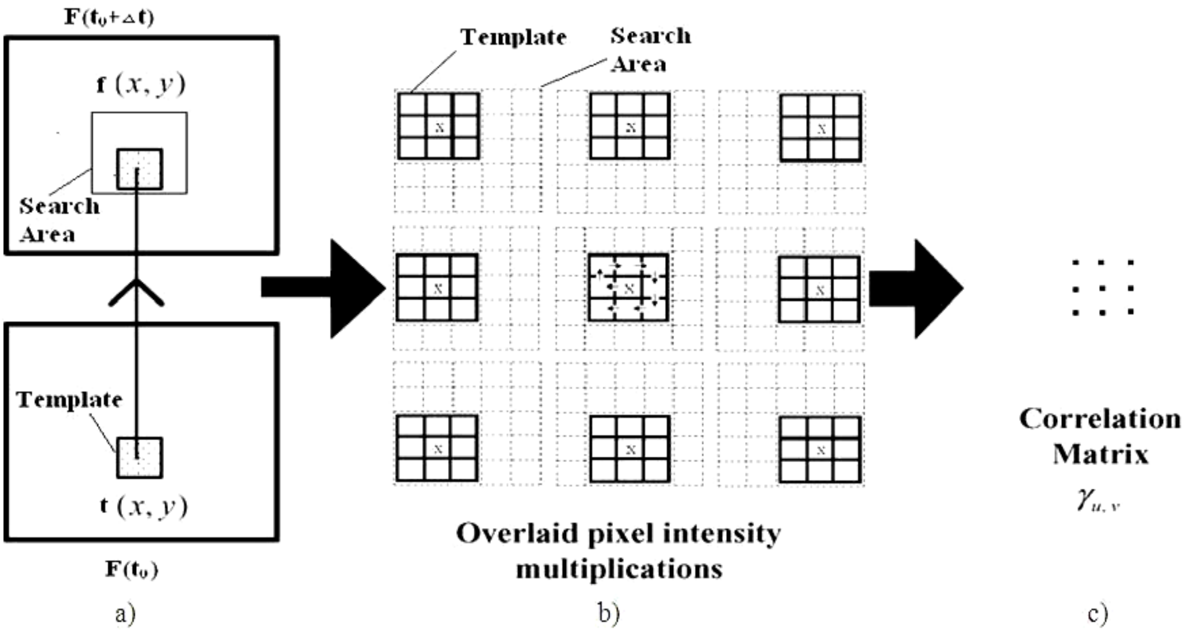

Figure D.1: Formation of cross-correlating: a) The two images. b) Template dimension=3×3 and search area dimension=5×5 pixels. c) Resulting 9 coefficient matrix.

Features derived from CC techniques in conjunction with appropriate templates and ROIs, including the size and direction of heat propagation, have been considered as quantitative defect characterizations for the angular defects. The CC technique has been developed to track the heat diffusion through tracking the changes in pixel intensity caused by heat transformation. Experimental studies have been carried out to demonstrate the influence of the defect geometry on the thermographic distribution. Thus, the work shows that the identification of the defect angle is necessary to evaluate the other geometrical features such as the length and depth of a defect.

The results have been used to extract the features of defects including characterize the length and depth of defects.

List of Publications

In the course of completing this thesis, the contents of a number of chapters have already been published by the author. These are:

- **Refereed Journal Papers**

[1] A. Al-Qubaa, G. Y. Tian, "An Evaluation of the Feature Extraction and Classification Methods for a Novel Electromagnetic Weapon Detection System", *Submitted to IEEE sensors Journal*, 2012.

[2] A. Al-Qubaa, G. Y. Tian, "Weapon Detection and Classification Based on Time-Frequency Analysis of Electromagnetic Transient Images", Accepted in *International Journal on Advances in Systems and Measurements*, 2012.

[3] G. Tian, A. Al-Qubaa, and J. Wilson, "Design of an electromagnetic imaging system for weapon detection based on GMR sensor arrays", *Sensors and Actuators A: Physical*, vol. 174, pp. 75-84, 2012.

[4] A. R. Al-Qubaa, G. Y. Tian, J. Wilson, W. L. Woo, and S. Dlay, "Feature Extraction using Normalized Cross-Correlation for Pulsed Eddy Current Thermographic Images", *Measurement Science and Technology*, vol. 21, pp. 115501-115511, 2010.

- **Refereed Chapter in book**

[1] J. Wilson, G. Tian, M. Morozov and A. Al-Qubaa, "Sensor Fusion for Electromagnetic Stress Measurement and Material Characterisation", book Chapter in "Sensor Fusion and Its Applications", edited by C. Thomas, ISBN 978-953-307-101-5, SCIYO Publishers, September, 2010.

- **Refereed Conference Papers**

[1] A. R. Al-Qubaa and G. Y. Tian, "Automatic Threat Object Classification Based on Extracted Features From Electromagnetic Imaging System", in *Proceeding of the IEEE International conference on Imaging System and Techniques-IST*, UK, pp. 164-169, 2012.

[2] A. Al-Qubaa, G. Y. Tian, "Automatic Threat Object Classification Based on Electromagnetic Imaging System", *Annual research conference ARC2012,* Newcastle University, 2012. (Awarded one of the best paper)

[3] A. Al-Qubaa, G. Y. Tian, and J. Wilson, "Electromagnetic Imaging System for Weapon Detection and Classification", in *Proceeding of the Fifth International Conference on Sensor Technologies and Applications*, France, pp. 317-321, 2011. (Awarded the best paper)

[4] A. Al-Qubaa, G. Y. Tian, and J. Wilson, "Object Identification using Feature Extraction for Electromagnetic Images", *Postgraduate Conference PGC2011*, Newcastle University, 2011.

[5] A. Al-Qubaa, G. Y. Tian, "Feature Extraction for Object Identification and Classification using Electromagnetic Imaging", *Conference of Engineering Sciences*, London, 2011.

[6] A. Al-Qubaa, G. Y. Tian, and J. Wilson, I. Adewale, "Object Identification and Classification using Feature Extraction from Electromagnetic Images", *accepted in the 53th IEEE International Symposium ELMAR-2011*, Croatia, 2011.

- **Refereed Posters**

[1] A. R. Al-Qubaa and G. Y. Tian, "People Screening for Threats with Automatic Detection and Localization", *Products and Processes Postgraduate Research Awareness Event*, Newcastle University, March, 2012.(Awarded the best research poster in that event)

[2] A. R. Al-Qubaa, G. Y. Tian, and J. Wilson, "Electromagnetic Imaging System for Threat Object Detection and Classification", *Communication and Dissemination Event, Newcastle Institute for Research on Sustainability (NIReS), Newcastle University*, November, 2012.

[3] A. R. Al-Qubaa and G. Y. Tian, "Design a New Sensor-Array Detection System using GMR sensors", *Sensors Design and Applications workshop*, Newcastle University, September, Newcastle, 2012.

[4] A. R. Al-Qubaa, G. Y. Tian, J. Wilson and S. Crichton, "People Screening for Threats with Automatic Detection and Localization", *Show case of the Innovative Research Call (IRC)2007(Home Office)*, London, November, 2011.

[5] A. R. Al-Qubaa, G. Y. Tian, J. Wilson, W. L. Woo, and S. Dlay, "Visible and Thermal Image Fusion for NDT", *Postgraduate Conference PGC2010*, Newcastle University, January, 2010.

[6] O. Bouzid, K. Li, G. Tian, and A. Al-Qubaa, "Integration of Acoustic Emission and Wireless Sensor Networks for Intelligent Wind Turbine Blade Structural Health

Monitoring”, *Sustainable Control of Offshore Wind Turbines Workshop,* Hull University, September, 2012.

[7] O. Bouzid, K. Li, G. Tian, and A. Al-Qubaa, “Integration of Acoustic Emission and Wireless Sensor Networks for Intelligent Wind Turbine Blade Structural Health Monitoring”, *Sensors Design and Applications workshop*, Great North Museum, Newcastle, September, 2012.